INFORMATION TO USERS

This manuscript has been reproduced from the microfilm master. UMI films the text directly from the original or copy submitted. Thus, some thesis and dissertation copies are in typewriter face, while others may be from any type of computer printer.

The quality of this reproduction is dependent upon the quality of the copy submitted. Broken or indistinct print, colored or poor quality illustrations and photographs, print bleedthrough, substandard margins, and improper alignment can adversely affect reproduction.

In the unlikely event that the author did not send UMI a complete manuscript and there are missing pages, these will be noted. Also, if unauthorized copyright material had to be removed, a note will indicate the deletion.

Oversize materials (e.g., maps, drawings, charts) are reproduced by sectioning the original, beginning at the upper left-hand corner and continuing from left to right in equal sections with small overlaps.

ProQuest Information and Learning
300 North Zeeb Road, Ann Arbor, MI 48106-1346 USA
800-521-0600

THE STRUCTURES AND DYNAMICS OF ORGANOMETALLIC-ARENE COMPLEXES AND BIMETALLIC CLUSTERS

By

PHILIPPA EDLYNE LOCK, B. Sc.

A Thesis

Submitted to the School of Graduate Studies

In Partial Fulfillment of the Requirements

for the Degree

Doctor of Philosophy

McMaster University

STRUCTURES AND DYNAMICS OF ARENE-METAL AND CLUSTER COMPLEXES

DOCTOR OF PHILOSOPHY (2001) McMaster University

(Chemistry) Hamilton, Ontario

TITLE: The Structures and Dynamics of Organometallic-Arene Complexes and Bimetallic Clusters

AUTHOR: Philippa Edlyne Lock, B. Sc. (McMaster University)

SUPERVISOR: Dr. Michael J. McGlinchey

NUMBER OF PAGES: xix, 259

Abstract

This thesis describes the synthesis, characterisation and molecular dynamics of several series of new arene-metal and cationic organometallic complexes, and the potential utility of these systems in synthesis.

The first characterised organometallic complexes of trindane (the condensation trimer of cyclopentanone, and a potential synthetic precursor to the unknown molecule sumanene), are reported, and the possibility of derivatising trindane at the benzylic sites is discussed. The X-ray crystal structures of three trindane complexes reveal that sterically demanding groups affect the conformations of the cyclopentene rings.

A series of hexaethylbenzene (HEB)-Ru complexes was investigated with respect to their HEB ligand conformations and dynamics in solution. The conformational versatility of HEB allowed a means of probing the stereochemistry and dynamics of these complexes, which were characterised by NMR spectroscopy and X-ray crystallography. A by-product of one reaction, the known complex *trans*-$RuCl_2(PMe_3)_4$, was found; the previously unreported X-ray crystal structure of this compound is described.

The ideas of Bürgi and Dunitz (that a succession of static X-ray structures can provide information about the dynamics of a reaction) have been applied to finding the migration pathway of a CR_2^+ moiety in a series of bimetallic cluster cations, $[Cp_2Mo_2(CO)_4(HC{\equiv}C{-}CR_2)]^+$, from one molybdenum vertex to the other. The construction of an energy hypersurface for the migration of a $C{=}CH_2$ fragment over a $[Cp_2Mo_2(CO)_4CH]^+$ triangular base reveals that the structure whereby the CH_2 group is

oriented directly over a metal vertex lies at the bottom of the potential energy well. The calculated migration trajectory between vertices is beautifully paralleled by a series of X-ray crystal structures of cations $[Cp_2Mo_2(CO)_4(RC{\equiv}C{-}CR'R'')]^+$.

In dicobalt clusters, the preference of an alkynyl dicobalt hexacarbonyl moiety to occupy an equatorial position in ring systems has been extended to several alkynylcyclohexanols. The alkynol conformations are compared with the structures of the corresponding $Co_2(CO)_6$ complexes, including structures where the Co_2 cluster competes with a *tert*-butyl group for an equatorial site. A mechanism involving migration of a carbocationic centre between cobalt vertices in a cluster is rationalised in light of these results.

THE LABORATORY MIDNIGHT

Science is what the world is, earth and water.
And what its seasons do. And what space fountained it.
It is forges hidden underground. It is the dawn's slow salvo.
It is the closed retort. And it is not yet.

It looks up and counts the Perseids in August,
A fire from nowhere like signals overhead
And it looks for portents, as redmen on a hill,
In the white stream where Altair swims with the Andromedid.

Now you who know what to believe, who have God with you
By desk and bed, blue fire in the stove;
Whom the rains from the northeast alter but perfect
Into new powers, and new pities, and new love;

Go look in lava flows for newer elements,
And dismantle the electric shape of matter like a house;
And weigh the mountains in small sensitive scales;
Break buds; and test the senses of a mouse;

And if you are unpanicked, tell me what you find
On how the sun flies and the snow is spent,
What blasts and bessemers we live in, that dissolve
All the loam loaned to spine and ligament.

Reuel Denney

Acknowledgements

I would like to thank my supervisor, Dr. M. J. McGlinchey ("MJM"), for his guidance, and for the many opportunities he has provided for me during my time with his group. He, above all others, has understood my love for "*d* electrons" and fostered my passion for teaching. He has also encouraged and supported me in the pursuit of studies in music throughout my time here. Without this combination of influences, and without his patience and understanding, I would not have adequately survived some of the difficult times I encountered, and emerged with my sanity and sense of humour intact. For you I have one word: "liff".

I would like to thank the members of my supervisory committee, Dr. Paul Harrison, Dr. Alex Bain, and also Dr. Lijuan Li, for their support, ideas and questions, and their endurance!

Many aspects of research in this department would not be bearable without the outstanding support of the many technical support staff. I gratefully acknowledge the expertise of Don Hughes and Brian Sayer, as well as George Timmins, and thank them for all their help with answering my NMR questions, and always coming to the rescue when needed. Thanks also to Richard Smith and the many people who have been part of the mass spectrometry facility over the years. A special "thank you" I send to Jim Britten, who has given me invaluable advice about X-ray crystallography, and from whom I have learned much of what I know in this field. Thank you, Jim, for also extending your friendship to me. Thanks also to Mike Malott, computer expert par excellence, and to all

of the ladies who have graced ABB 156, particularly Carol Dada, for all of their help, and for sharing many a laugh. I would also like to acknowledge McMaster University, OGS and NSERC for providing funding.

One of the great things about graduate school is the opportunity to meet many people, as they come and go with great frequency. In ABB 357, it has been my pleasure to get to know Luc, Hari, Lisa, Suzie, Ralph, Jamie, Mark, Stacey, John, Nada, Laura and Frank, as well as numerous thesis students and visitors. Luc, thank you for showing me some of the ropes, including "how to do a column"; Hari, thank you for making beautiful molecules, and showing me how to grow even more beautiful crystals. Suzie, I can definitely say that there was never a dull moment with you around! Jamie, I thank you for all the conversations we had side by side over the years, it was a pleasure to work near you. I will never forget the "Ralph and Jamie" years in the lab; thank you Lisa for giving some balance to the craziness, and sharing your wisdom. Ralph, thank you for being a good friend, one of the longstanding buddies of undergraduate days; thank you also for teaching how to *really* cook pasta. John, what can I say, except that you have many moments of great charm! Nada, I have enjoyed the growth of our friendship, through shared experiences and laughter. Laura, I greatly admire your zeal for chemistry! Frank, I have greatly appreciated experiencing your very sincere nature. Mark and Stacey, while it was a pleasure to be your TA, it has been an even better experience learning from both of you, and to count you both among the best friends I have. Mark ("Dr. Rock"), I still say you are a "Hanson" brother in disguise. Stacey, you are a guiding light, and a person of truly exceptional spirit and spirituality. Thank you for being there for me on many occasions.

It would be impossible to do justice to the many others who have been great friends during my time here. For fear of leaving someone out, let me say that I had a great time with you all, whether it was playing softball, soccer or basketball, or simply enjoying the Phoenix patio. My experience at McMaster is coloured with happy memories that I will cherish because of the many exceptional people I encountered here. There are some extra special people I need to mention, because they are among the ones who have put up with me longest; thank you John and Kereen, no one could ask for better friends. Thanks also to Russell Bell, Alan Guest and Ed Hileman for their friendship and support and for sharing their non-chemistry interests with me. I also thank friends from Centenary and the world of music; your kind thoughts and support have been my strength and shield.

Well, you save the best for last...I thank my family, who have seen me through more stress, white hair, laughter and tears than I thought were possible: finally, here it is! Mum, Nicola, Ben, Gordon and Kate, I love you all. Thank you all for sharing in our unique brand of humour, and giving me a haven in times of need. Thanks also to Mel, for welcoming me and giving me your warm support, and for the many interesting discussions of things academic. Finally, thank you to Erick and Ryan; I love you and I am so glad you are both a part of my life. Erick, you have supported me so strongly as my partner, soul mate and friend, and I look forward to loving you for many more special years to come.

Dad, I know you're not here to read this, so I hope you will forgive any grammatical mistakes that may get past the many eyes that look over this document. I appreciate the support that you offered in so many ways. I hope you are looking on with approval. Sláinte.

Table of Contents

List of Figures

List of Tables

List of Schemes

List of Abbreviations and Symbols

Å	Ångstrom
Ar	Aryl
benz	benzylic
^{13}C NMR	Carbon-13 Nuclear Magnetic Resonance Spectroscopy
CACAO	Computer Assisted Composition of Atomic Orbitals
CI	Chemical Ionisation Mass Spectrometry
Cp	Cyclopentadienyl
cod	cyclo-octadiene
cot	cyclo-octatetraene
COSY	Correlated spectroscopy
2D	Two-dimensional
3D	Three-dimensional
δ	Chemical Shift
d	Doublet (^{1}H NMR)
DEI	Direct Electron Impact Mass Spectrometry
DEPT	Distortionless Enhancement by Polarisation Transfer
DMSO-*d6*	Hexadeuterated dimethylsulfoxide
EHMO	Extended Hückel Molecular Orbital
Et	Ethyl
Et_2O	Diethyl ether
EtOH	Ethanol
EV	Electron volt
FID	Free Induction Decay
FVP	Flash Vacuum Pyrolysis
g	Gram
GOF	Goodness of fit
^{1}H NMR	Proton Nuclear Magnetic Resonance Spectroscopy
h	Hours
hν	light
HEB	Hexaethylbenzene
HMBC	Heteronuclear Multiple Bond Correlation
HOMO	Highest Occupied Molecular Orbital
HSQC	Heteronuclear Single Quantum Coherence
Hz	Hertz
IR	Infrared Spectroscopy

J	Spin-spin coupling constant
K	Temperature, degrees Kelvin
kcal	Kilocalories
L, L′, L″	Ligand
LDA	Lithium diisopropylamide
LUMO	Lowest Unoccupied Molecular Orbital
m	Multiplet (^{1}H NMR)
M	Metal
$[M]^+$	Parent ion mass (mass spectrometry)
mg	Milligram
Me	Methyl
MHz	Megahertz
mL	Millilitre
ML_n	Organometallic fragment
mmol	Millimole
mol	Mole
mp	Melting point
MS	Mass Spectrometry
m/z	mass/charge ratio (mass spectrometry)
NBS	*N*-Bromosuccinimide
NMR	Nuclear Magnetic Resonance
nOe	Nuclear Overhauser Enhancement
OAc	Acetate
p	para
PAH	Polycyclic Aromatic Hydrocarbon
PCC	Pyridinium Chlorochromate
PECH	Phenylethynylcyclohexanol
ppm	Parts per million
R, R′, R″	Alkyl group
t	Triplet (^{1}H NMR)
t-BuOK	Potassium tertiary-butoxide
tert	Tertiary
THF	Tetrahydrofuran
TMS	Trimethylsilyl
wing	Wingtip

Chapter 1

Introduction

1.1 Prelude

While the field of organometallic chemistry continues to bloom and expand in new directions, one must not underestimate the continued exploration of both new and familiar compounds in order to discern fully their chemical behaviour and how they may be of further utility to the scientist. In particular, the use of organometallic compounds (those compounds having at least one metal-carbon covalent bond) as aids for organic synthesis has received much attention, with more recent focus on the use of cationic organometallic complexes as useful synthons. The chemistry of several new cationic organometallic complexes related to arene-transition metal chemistry and transition metal cluster chemistry, and the rationales for the investigation of them, is presented herein.

1.2 Goals of the Project

The carbon framework of the proposed molecule *sumanene*, $C_{21}H_{12}$, is found on the surface of buckminsterfullerene, C_{60}; this C_{21} molecule remains as yet unsynthesised. One goal of this project is to begin the development of a potential synthetic route for the total synthesis of sumanene that avoids a flash vacuum pyrolysis step, and to investigate how cationic organometallic complexes may be of use in the synthesis. In particular, the focus on ruthenium-arene complexes stems from the idea that they may serve as reactive 18

electron metal(II) precursors for the synthesis of molecules through substitution at sites where one has carbon-hydrogen bond activation. This idea stimulated the investigation of the chemistry of ruthenium complexes of the arenes trindane and hexaethylbenzene.

Another part of this project focuses on the molecular dynamics and structures of complexes that involve cations stabilized on metal clusters. The investigation of the migration of a carbocationic centre between metal vertices in a bimetallic cluster is reported herein. Further, developing the use of bimetallic clusters for conformational control of ring systems is explored. With regard to structural characterisation and molecular dynamics studies, the use of nuclear magnetic resonance (NMR) spectroscopic and X-ray diffraction techniques have been of primary importance.

In this thesis, synthetic, structural and molecular dynamics studies of metal complexes of the arenes trindane and hexaethylbenzene are presented. Subsequently, the use of metal clusters to stabilize cationic centres is discussed. Further background material is included with each chapter.

1.3 Transition Metal-Arene Complexes

An arene (a ring comprising six sp^2 hybridized carbon atoms) may serve as a two, four, or six-electron donor ligand when forming a π-interaction with a metal in an organometallic complex. If an arene were functioning as a six electron donor, it would be considered to be bonded to a metal moiety through all six of its carbon atoms, and would

bear the label "η^6".[a] Following the "18 electron" rule, which governs much of organometallic chemistry,[b] a neutral complex having an η^6-arene ligand should also incorporate a 12-electron metallic moiety. Typical examples of such moieties would be $M(CO)_3$ fragments (M = group 6 metal, Cr, Mo, W). One could also envision a moiety bearing a 1+ charge (for M = group 7, e.g. Mn), or a 2+ charged fragment (for M = group 8, e.g. Fe, Ru), to generate cationic organometallic species.

1.3.1 Cationic Metal-Arene Complexes

It has been demonstrated that cationic transition metal-arene complexes promote activation of certain sites on the arene, which allow the arene to be functionalised in a programmed fashion. This allows a building up of more complicated target molecules that would not be accessible either with the same ease, or by a different route.

An example of this idea is seen in the syntheses of polyaromatic ethers reported by Abd-El-Aziz.[1] In order to overcome problems such as low yields and elevated temperatures encountered for some of the traditional routes to polyaromatic ethers, Abd-El-Aziz devised an alternative synthetic route that made use of relatively inexpensive starting materials and also circumvented problems of poor solubility. In this case, the complexation of a chloroarene to a metal moiety ($CpFe^+$) was used to activate the ring towards nucleophilic aromatic substitution, which allowed the preparation of

---

[a] This notation reads as "hexahapto", and signifies that the ligand has a *hapticity* of six; this designates that all six carbon atoms in the ring are bonded to a metal atom.

[b] The electronic structures of many organometallic compounds are based on the 18-electron rule, also referred to as the effective atomic number (EAN) rule. A total valence electron count of 18 at the central metal atom, based on a full complement of s, p and d electrons, is favoured, in order to achieve a noble gas electron configuration.

poly(cyclopentadienyliron) cations of polyaromatic ethers. This method allowed for the tailored design of a large number of oligomeric systems containing a variety of functional groups. An example of this work is shown in Reaction 1.1, which illustrates the reaction of a dihydroxy-aromatic complex with chloroarene complexes in a molar ratio of 1:2 to yield a tris[$CpFe^+$] complex. It is possible to continue building in this fashion to give larger oligomers, and removal of the iron moieties is readily accomplished by use of ultraviolet radiation.

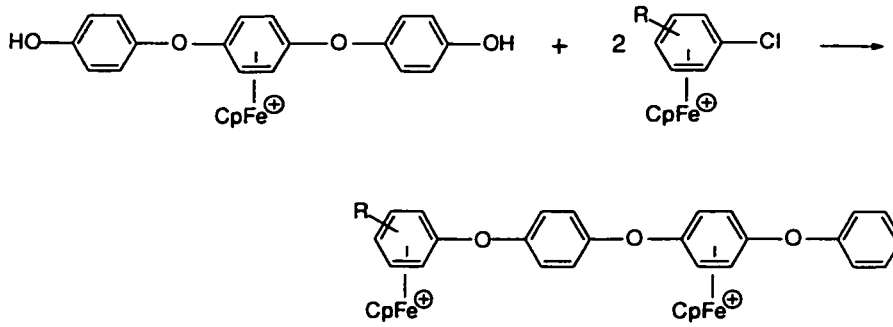

1.1

1.3.2 Synthesis of Transition Metal-Arene Compounds

The chemistry of many transition metal-arene complexes is well documented.[2] In particular, the chemistry of ruthenium-arene complexes[3] is the main focus of Chapters 3 and 4 of this thesis. There are several known preparative methods, although one of the preferred routes is *via* reaction of a transition metal trihalide with an arene or with a cyclohexadiene derivative, as shown for a ruthenium complex in Reaction 1.2.[3]

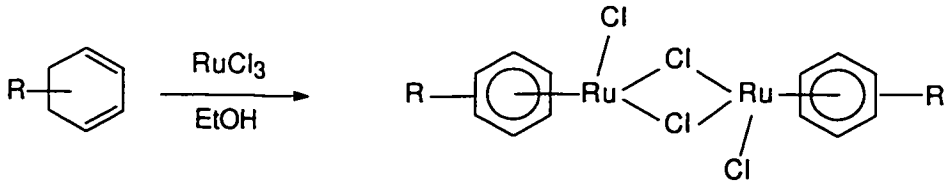

1.2

The dichloro-bridged species that is formed in such a step can undergo subsequent reactions such as arene exchange and ligand addition. In the former instance, fusion of the original complex with a different arene will lead to exchange of both of the arene ligands in the starting dimer (Reaction 1.3).[3]

$$[RuCl_2(\textit{para}\text{-cymene})]_2 \xrightarrow[\text{heat}]{\text{arene, e.g. } C_6Me_6} [RuCl_2(\text{arene})]_2 \qquad \textbf{1.3}$$

It is then possible to add a variety of two-electron donor ligands to the dimer, in order to effect cleavage of the chloro bridge (Reaction 1.4).[3]

$$[RuCl_2(\text{arene})]_2 \xrightarrow[\text{e.g. L} = PR_3,\ P(OR)_3]{2\ L} 2\ RuCl_2(L)(\text{arene}) \qquad \textbf{1.4}$$

The utility of such reactions is explored in greater detail in Chapters 3 and 4.

1.4 Buckminsterfullerene – C_{60}

C_{60} (**1**), the allotrope of carbon known as "buckyball", has received worldwide attention since it was first reported in 1985,[4] and the molecule has since sparked intense interest as researchers have attempted to explore its chemistry. Some have made successful attempts to form derivatives of it (Figure 1.1),[5,6] and even to encapsulate other species within it; others have shown interest in developing a classical synthetic route to this famous soccer-ball like species. The molecule, and related species, e.g. C_{70}, (collectively known as the fullerenes), were detected in vaporized graphite. Vaporization of carbon remains to date the method of choice for the formation of C_{60}

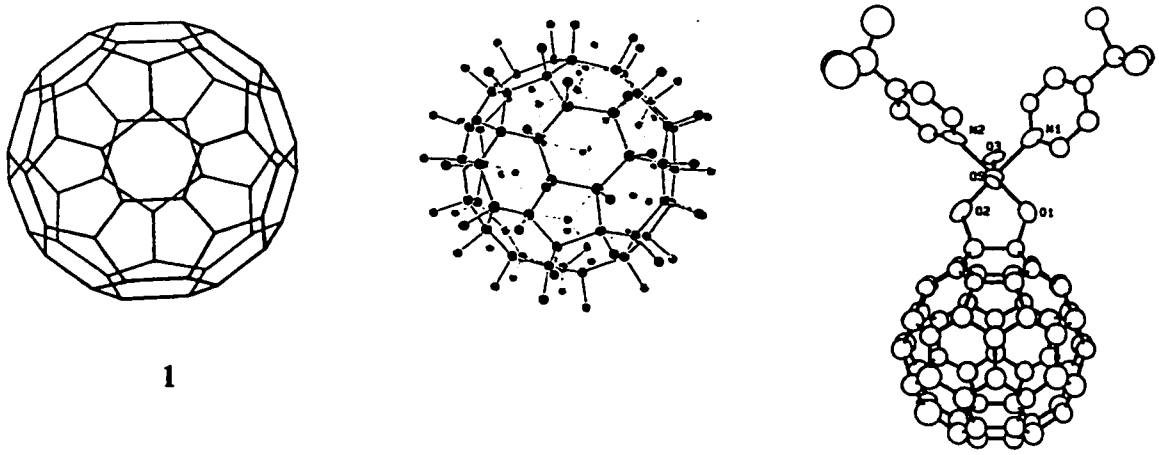

1

Figure 1.1: C_{60} (**1**), $C_{60}H_{60}$ ("fuzzyball"), and the adduct $C_{60}(OsO_4)$(4-*tert*-butylpyridine)$_2$ ("bunnyball").

and other fullerenes. A particular disadvantage of this method is that the yield of any given fullerene is very small, and hence to realise any reasonable quantity of product is an

expensive proposition. The possibility that one may be able to synthesise C_{60} by traditional solution-phase synthetic methods remains to be explored.

1.4.1 Fragments of C_{60}

One approach to the synthesis of C_{60} is based on a retrosynthetic idea that begins by breaking the molecular framework down in a symmetrical fashion into smaller fragments found within the C_{60} structure. This idea, as delineated by Mehta,[7,8] is illustrated in Figure 1.2.

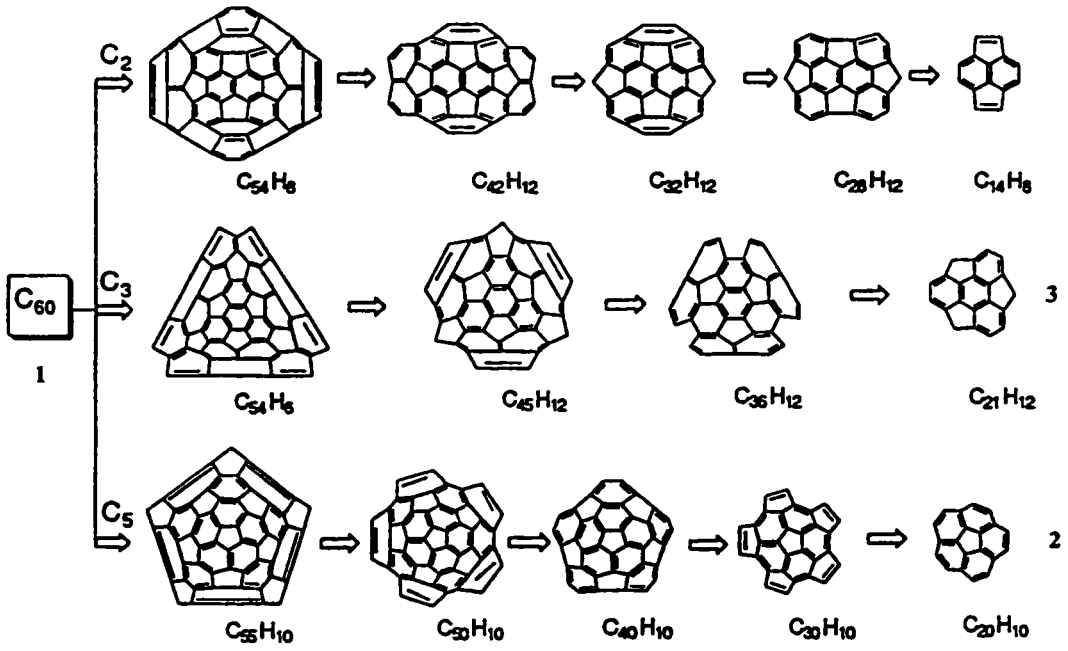

Figure 1.2: Retrosynthetic scheme showing three routes to C_{60}, *via* fragments that maintain C_5, C_3 or C_2 symmetry.

The synthesis of certain of these, and related, fragments (so-called "buckybowls") has attracted much attention in recent years, and several groups have had great success in this area. Barth and Lawton first reported corannulene (**2**),[9] the $C_{20}H_{10}$ fragment of C_5 symmetry, but the rigorous 17-step synthesis impeded others from fully investigating its chemistry. Synthetic routes developed by Scott[10] led to the use of a flash vacuum pyrolysis (FVP) step, which has rendered corannulene more readily accessible, and this method is now widely used as the final step in the syntheses of many of these polynuclear aromatic hydrocarbons. These syntheses are more fully explored in Chapter 2.

The buckybowl fragments, ranging in size from approximately $C_{20} - C_{30}$, possess some degree of curvature (hence the "bowl" nomenclature). The incorporation of this curvature (or strain) into the polynuclear aromatic hydrocarbons is a particular synthetic challenge. One of the fragments which has been identified on the C_{60} surface is a C_{21} fragment; the proposed isolated molecule, of formula $C_{21}H_{12}$, (**3**), has been given the name *sumanene*. The sumanene motif is shown on the C_{60} framework in Figure 1.3.

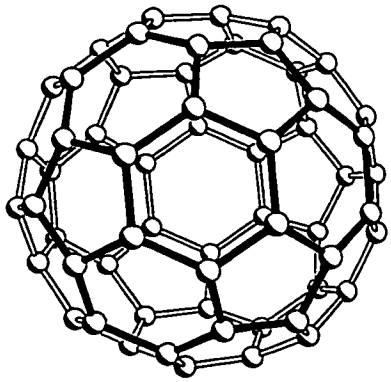

Figure 1.3: The C_{21} sumanene skeleton outlined on C_{60}.

1.5 Towards Sumanene

The synthesis of sumanene, **3**, has not yet been achieved, although the potential precursor **4** has been reported. It is obtained in low yield by FVP, starting from a precursor of three-fold symmetry, in which the six-membered rings are already in place, and one is attempting to close the five-membered rings. It appears, however, under the given experimental conditions, that the degree of strain associated with closing all three of the five-membered rings is too much to overcome in the final step of the synthesis.

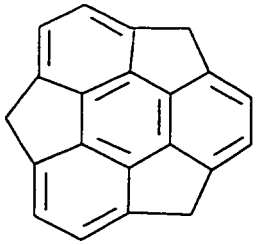

3

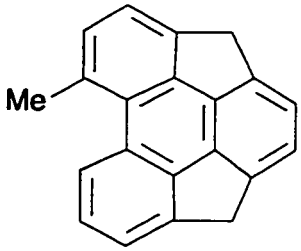

4

1.5.1 The Starting Point - Trindane

To circumvent the problem posed by incorporating strain into the sumanene framework, it may be possible to start instead with the five-membered rings in place, and derivatise the benzylic sites in order to build up the six-membered rings. This approach would allow the strain associated with the five-membered rings to be incorporated from the start of the synthesis. A logical starting molecule would be trindane ($C_{15}H_{18}$), **5**, which could then be derivatised at the benzylic hydrogen sites to build the six-membered rings.

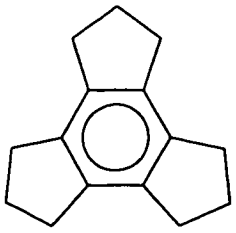

5

1.5.2 The Organometallic Approach

Replacement of the hydrogen atoms by alkyl groups at these benzylic sites can be accomplished by base-catalyzed exchange. Further, it has been demonstrated in many examples that this type of exchange at the benzylic sites can be enhanced by the presence of a metal moiety adjacent to the benzylic positions. For example, in the steroidal complex shown in Scheme 1.1, a hydrogen atom at position 6 is replaced by -CH_2OH, the whole exchange being catalyzed by the presence of amide base, and promoted by the presence of the chromium tricarbonyl moiety complexed to the A-ring of the steroid. In particular, it is the hydrogen atom *exo* to the metal moiety that is replaced. The *exo* hydrogen atom is the one that points away from the metal moiety; *i.e.*, hydroxymethylation occurs on the face *anti* to the π-bonded metal atom.[11]

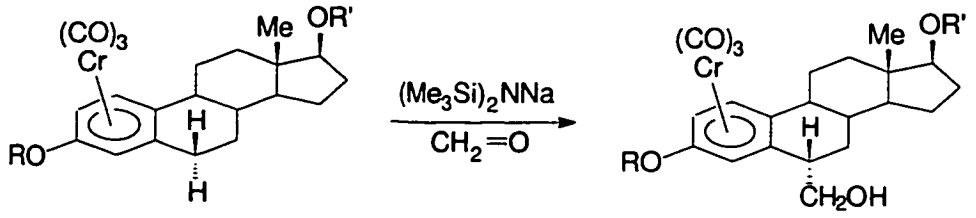

Scheme 1.1: Metal-promoted functionalisation at an *exo*-benzylic position.

A further example, which makes use of a cationic metal moiety, is seen in the conversion of a hexamethylbenzene ligand to a hexaethylbenzene ligand under mild conditions, as seen in Scheme 1.2.[12] The crucial factor is the presumed stabilisation of the zwitterion **6** as an η^5-complex in which no formal charges are required.

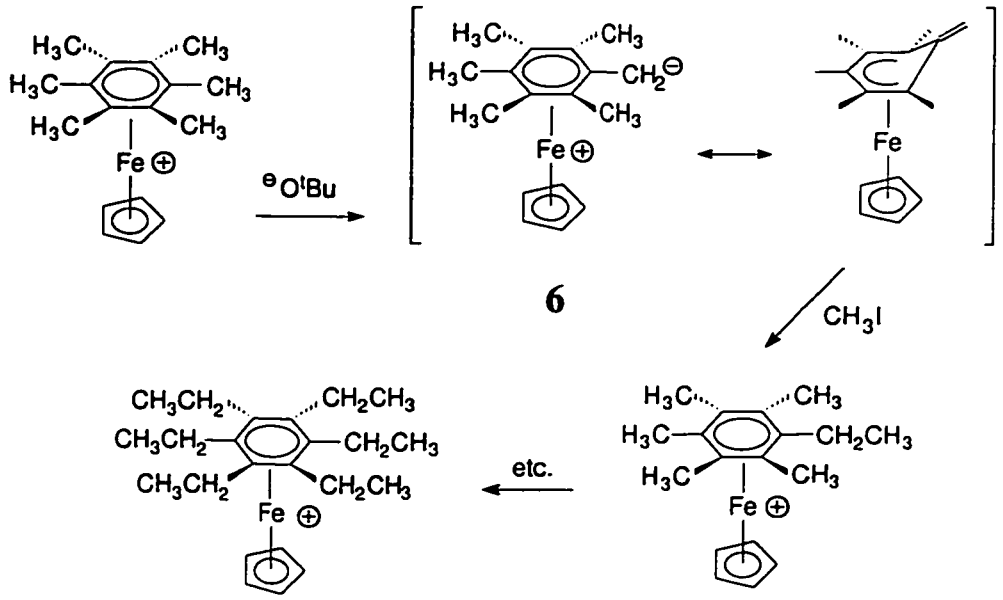

Scheme 1.2: Metal-promoted conversion of a C_6Me_6 ligand into a C_6Et_6 ligand.

1.5.3 Hexaethylbenzene

Hexaethylbenzene (HEB), **7**, is a ligand that adopts a wide variety of conformations when it forms metal complexes. The six ethyl groups are able to rotate

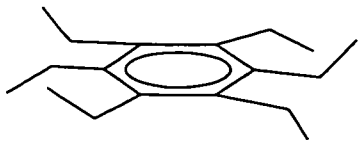

7

freely, and in an organometallic complex these groups may be oriented in a *proximal* fashion with respect to the metal moiety (meaning that they are directed towards the metal) or a *distal* fashion (meaning that they are pointing away). Calculations on HEB have shown that the lowest energy conformation has D_{3d} symmetry whereby the six ethyl groups alternate in proximal and distal orientations; the highest energy conformation has all six of the ethyl groups oriented distal, giving rise to a molecule of local C_{6v} symmetry.

Hexaethylbenzene may be considered to be like an "unrestricted trindane" molecule; that is to say, there are several gross features that are similar for the two systems. Both have a central arene ring, and adjacent to the central six carbon atoms are six CH_2 groups. In trindane (**5**), these CH_2 groups are tethered together in pairs by a further CH_2 linker, while in hexaethylbenzene (**7**) the CH_2 groups are free to rotate, and are capped by terminal methyl groups. The possibility of derivatising the benzylic sites of HEB remains an interesting possibility, particularly as a comparison for the extent of substitution possible at trindane *versus* at HEB.

1.6 Transition Metal Clusters

A cluster, as opposed to the monometallic or dimeric complexes discussed thus far, may be defined as a group of two or more metal atoms in which there are substantial and direct bonds between the metal atoms.[13] Organometallic clusters, by extension, must possess metal-carbon bonds, as well as metal-metal bonds. There exist numerous examples of organometallic clusters, containing two or more metal atoms and varying numbers of other atoms, e.g. carbon, boron. One class of clusters is based on a

tetrahedrally shaped core, such as that observed in the Group 9 homoleptic carbonyl compounds $M_4(CO)_{12}$ (M = Rh, Ir).

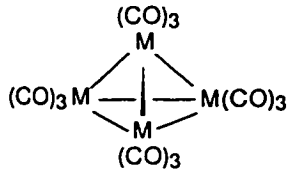

Derivatives of these species may be formed by isolobal replacement of an $M(CO)_3$ vertex with a –CR group; the theory supporting this idea is presented in section 1.6.1. If one performs two such vertex replacements, a cluster with an M_2C_2 core is formed. It is the class of tetrahedral clusters with an M_2C_2 core that are the focus of this particular project.

1.6.1 The Isolobal Analogy

Hoffmann has defined molecular fragments to be isolobal "...if the number, symmetry properties, approximate energy, and shape of the frontier orbitals and the number of electrons in them are similar – not identical, but similar".[14] Hoffmann, who calculated the bonding characteristics of cluster fragments ML_n in the frontier orbital region, compared them, for example, with CH_x fragments. In particular, he demonstrated that an $M(CO)_3$ fragment has three frontier orbitals, with (d^n + 6)-12 electrons available in the frontier orbitals. Thus, for a $Co(CO)_3$ fragment, there are three frontier orbitals, and (9+6)-12 = 3 electrons in the frontier orbitals. The 12-electron count is that required for bonding of the three carbonyl ligands to the metal. Similarly, a -CH fragment also has

three frontier orbitals, and a total of (4+1)-2 = 3 electrons available in those orbitals (the other two being used for the C-H σ bond). The $Co(CO)_3$ and CH fragments, both having three frontier orbitals of similar symmetry, and three electrons in these frontier orbitals, are said to be isolobal. Thus, one can envision how it might be possible in theory to successively replace $Co(CO)_3$ vertices in $Co_4(CO)_{12}$ with CH vertices, and end up at C_4H_4, as shown below. In practice, there are many examples of these mixed Co/C clusters, reported as early as 1956.[15]

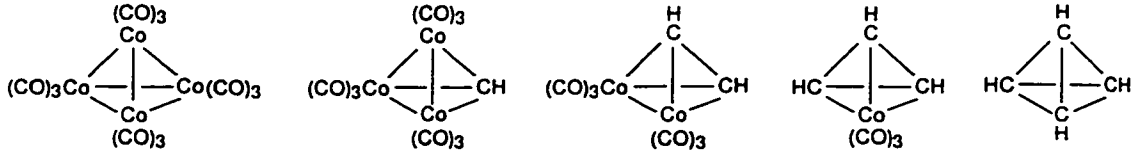

1.6.2 Synthetic Routes to Alkynyl Transition Metal Clusters

There are a variety of known methods for synthesising organometallic clusters, including the tetrahedral M_2C_2 clusters. The technique for generating these clusters is based on the addition of an alkyne to a bimetallic reagent that may be considered to contain a metal-metal triple bond. The synthesis of a dicobalt μ-alkyne cluster is illustrated below in Reaction 1.5;[15] addition of an alkyne to dicobalt octacarbonyl in a suitable solvent readily gives the dicobalt cluster **8**.

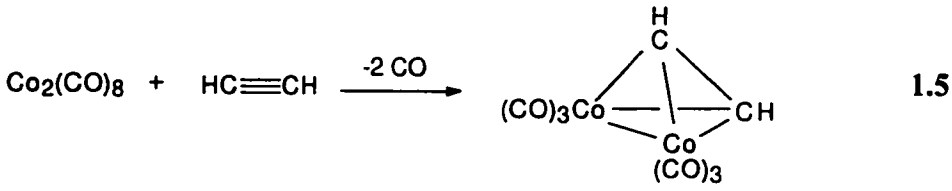

1.5

8

These dicobalt clusters may also act as precursors to other clusters, including mixed metal M_2C_2 clusters, and also M_3C clusters. For example, the cluster **8** may be treated with acid to give a cluster with a Co_3C core, as shown in Reaction 1.6.[16]

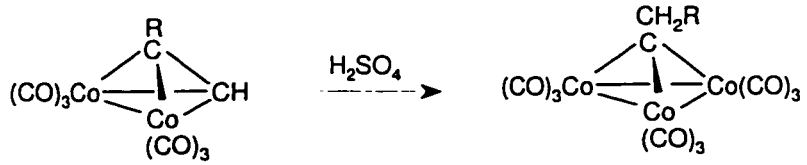

8 **9** **1.6**

Heterobimetallic clusters may be formed also from the dicobalt precursor by isolobal substitution of another organometallic vertex into an alkyne-dicobalt cluster, as shown in Reaction 1.7.[17] Since the starting cluster now has only a single mirror plane (C_s symmetry), substitution of one cobalt vertex by an isolobal group leads to a racemic mixture.

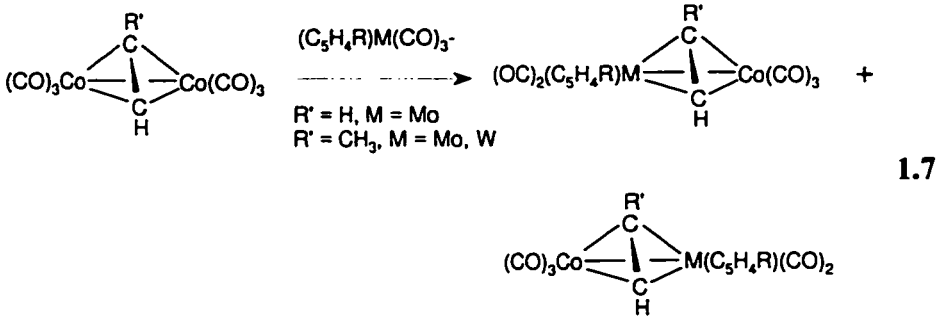

1.7

1.6.3 Cations Stabilized on Transition Metal Clusters

It has long been known that transition metal clusters can be used to effect intramolecular stabilisation of a charged fragment in a molecule. In particular, much of the early work in this field was pioneered by Seyferth in his explorations of tetrahedral Co_3C

clusters, and cationic derivatives of these clusters.[18] Schilling and Hoffmann performed calculations on cationic clusters such as $[Co_3(CO)_9C{=}CH_2]^+$ [19] and elucidated the maximum and minimum energy conformations of this cationic cluster. The energy maximum occurs when the charge is localized entirely at the methylene carbon atom, as in Figure 1.4(a). In this configuration the CH_2^+ is upright with respect to the basal plane of three cobalt atoms. The energy minimum is found when the CH_2 group is bent towards one of the $Co(CO)_3$ vertices, as shown in Figure 1.4(b). The observed stabilisation is explained as a consequence of the interaction of a vacant p_z orbital on the CH_2 group with a filled d_z^2 orbital on the Co atom, as shown in Figure 1.4(b), whereby the metal atom alleviates the electron deficiency at the cationic site. It is also possible to view this interaction as the resonance structure shown in Figure 1.4(c), in which the metal bears the positive charge, and the carbon atoms are depicted as an alkene coordinating to the metal atom.[20,21]

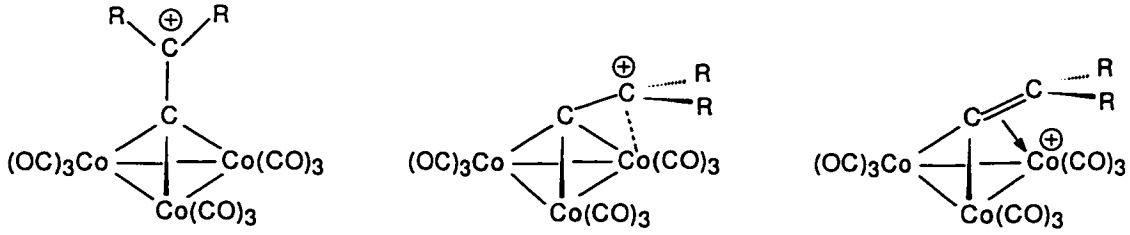

Figure 1.4: Stabilisation of a carbocation at a transition metal vertex.

It has also been demonstrated by calculations that, in mixed-metal clusters, the cationic fragment will exhibit a preference for a given organometallic vertex. For

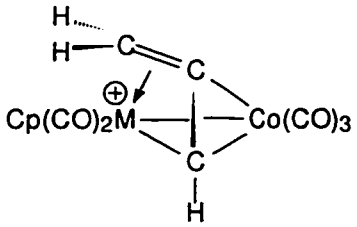

M = Mo, W

10

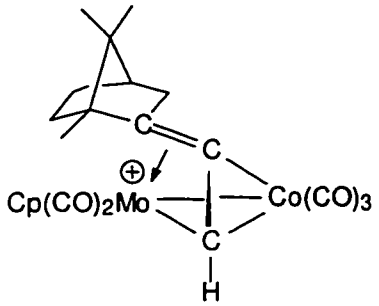

11

example, in the mixed metal cluster (**10**), the vinylidene moiety lies preferentially over the molybdenum atom or tungsten atom, as opposed to the cobalt vertex; this preference is also exhibited by the 2-bornyl cation represented by **11**.[22]

1.6.3.1 Synthesis of Cluster Cations

Protonation of μ-alkynol bimetallic clusters leads to the elimination of water from the cluster molecule, and gives straightforward access to cationic clusters. An example for a dimolybdenum (or ditungsten) cluster is shown in Reaction 1.8.

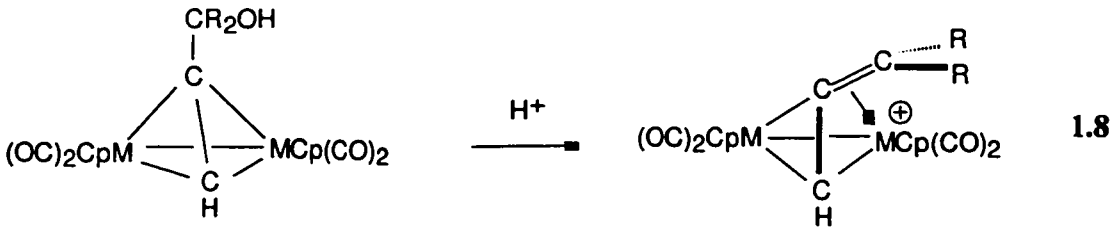

1.8

M = Mo, W

This idea may also be applied to dicobalt clusters, so that cluster cations may be prepared from the alkynol precursors $Co_2(CO)_6(RC{\equiv}C\text{-}CR_2OH)$.[23]

1.6.4 Dynamics of Cationic Cluster Complexes

It has been shown in bi- and tri-metallic cationic clusters that a positively charged fragment is stabilized by being bent towards a metal centre, and the cationic fragment may also migrate between different metal centres within a cluster. Variable-temperature NMR experiments have been used to study the dynamics of certain systems, and it has been possible to determine barriers to the movement from one metal atom to another. Examples of the type of migrations observed for a cationic Co_2C_2 cluster are outlined in Figure 1.5.[20]

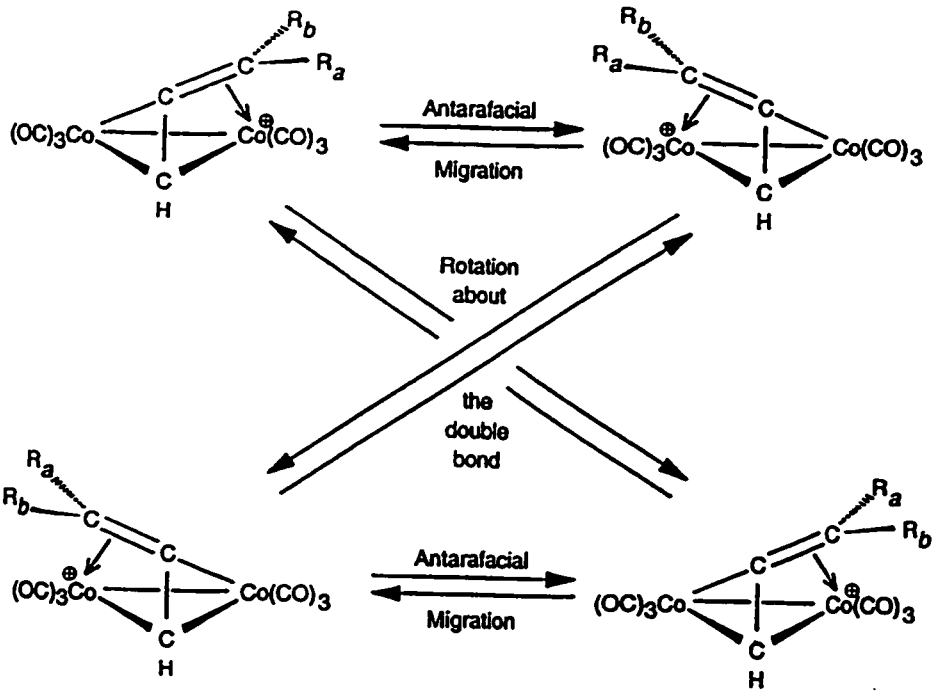

Figure 1.5: Two distinct migration processes of a cationic carbon site in a tetrahedral Co_2C_2 cationic cluster complex: An antarafacial migration that maintains the identity of the R_a and R_b substituents, and rotation about the double bond, which interconverts the R_a and R_b environments.

These fluxional processes are also observed in systems of the type $[Cp_2Mo_2(CO)_4(HC{\equiv}C\text{-}CR_2)]^+$, in which case a further probe for use in NMR experiments is provided by the presence of the cyclopentadienyl rings.

The activation barriers determined for these fluxional processes can give valuable information with regard to the nature of the interaction between the CR_2^+ fragment and the metal vertex. In the dimolybdenum systems, for example, the barrier for the antarafacial migration of CR_2^+ between Mo vertices increases from ~10 kcal mol^{-1} for tertiary cations to ~18 kcal mol^{-1} for primary cations.[20] This is seen as an indication that tertiary cations have less need for electronic assistance from the metal vertex than do secondary or primary cations, and thus the barrier to migration is lower.

The calculated barrier to antarafacial migration, and migration trajectory of a carbocationic site between two molybdenum vertices in a bimetallic cluster compound, are the subjects of Chapter 5.

1.6.5 Structural Analogies for Cationic Cluster Complexes

Until very recently, cationic dicobalt cluster complexes have not yielded X-ray quality crystals. Thus, the ability to study the ground state structures of these species has been restricted. Other approaches to modeling the ground state structures have been taken. The use of isolobality to solve this problem was advanced by McGlinchey *et al.* when they effected an isolobal replacement of a cationic cobalt vertex with a neutral iron vertex in such a cluster.[24] The neutral complex proved to be amenable to the formation of single crystals suitable for an X-ray structure determination; in the original example a CO group

was also replaced by a triphenylphosphine ligand in order to promote crystallization, as shown in Figure 1.6. Since that time, several other Fe-Co clusters that model cobalt-stabilized cations have been structurally characterised.[25,26]

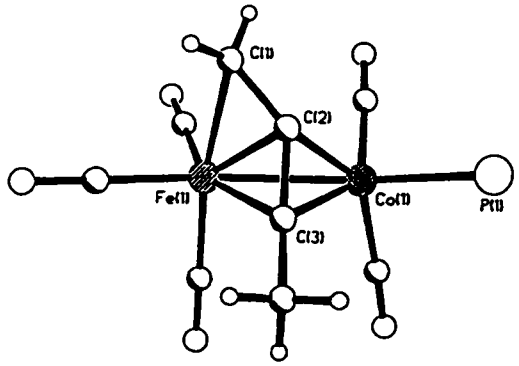

Figure 1.6: X-Ray crystal structure of $[MeC{\equiv}C{-}CH_2]FeCo(CO)_5PPh_3$; phenyl groups have been removed for clarity.

Recently, the first X-ray structure of a cationic cobalt cluster, **12**, was reported.[27] However, the cationic centre appears to be bridging between two tetrahedral Co_2C_2 cluster moieties (Figure 1.7); thus it is doubly stabilized in an attempt to enhance the

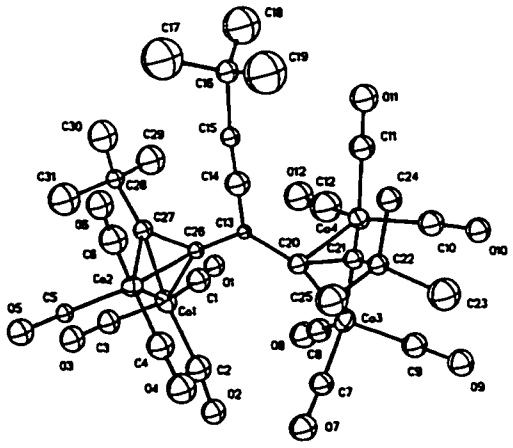

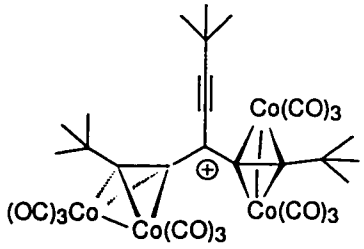

12

Figure 1.7: X-ray crystal structure of **12**, a carbocation stabilized by two dicobalt clusters.

thermal stability of the target cation. The structural characterisation of a carbocation stabilized by a single dicobalt cluster remains, as yet, unaccomplished.

It should be noted that cations stabilized on dimolybdenum clusters are highly amenable to study by X-ray diffraction. There are numerous examples of such systems,[20] which are discussed in Chapter 5.

1.6.6 Uses of Bimetallic Clusters

Much of the study of bimetallic clusters and their corresponding cationic complexes has focused on their fluxional processes and the energy barriers associated therewith. The interest in these systems, however, goes far beyond this topic.

Dicobalt hexacarbonyl complexes have been found to be very useful in synthetic organic chemistry. As discussed above, dicobalt clusters may be prepared by the straightforward addition of $Co_2(CO)_8$ to an alkyne moiety, and thus a cluster may serve as a protecting group for an alkynyl site within a molecule.[28] Some other examples where dicobalt clusters have proved useful in organic synthetic strategies include (i) in the rearrangement of 1-(1-alkynyl)cyclopropanols to 2-cyclopentenones,[29] (ii) the epimerisation of alkynyl sugars,[30] and (iii) the use of $Co_2(CO)_6$ as a "conformational switch" in a cyclopentylalkynol complex.[31] This latter idea is discussed in Chapter 6 of this thesis.

1.7 Goals of the Project - Revisited

1.7.1 The Organometallic Approach to Sumanene

Polycyclic aromatic hydrocarbon (PAH) buckybowl fragments have received a significant amount of attention because of the prevalence of C_{60} chemistry, especially over the past fifteen years. There are many interests in these molecules, quite apart from the synthetic challenge they provide. Some of the systems have demonstrated intriguing molecular dynamics, such as the bowl inversion observed for corannulene.[10] These hydrocarbons also have the potential to act as synthetic intermediates of fullerenes, as discussed above, and as end-caps for carbon nanotubes. With regard to their syntheses, development of the flash vacuum pyrolysis method has led to routes for previously unobtainable PAH. More recently, researchers have begun to find success in the development of synthetic routes that avoid the FVP step.

The focus of part of this project has been to develop a traditional synthetic route to the proposed C_{21} molecule *sumanene*, with the use of organometallic fragments to aid the synthesis. The starting materials used are the arenes trindane and hexaethylbenzene. As introduced in section 1.5.2, a cationic metal moiety, when bonded to an arene, can promote enhanced benzylic substitution. The syntheses, structures, and molecular dynamics of neutral and cationic trindane and hexaethylbenzene complexes are explored in Chapters 2 through 4.

1.7.2 Cations Stabilized on Organometallic Clusters

The theme of cations is continued in Chapter 5, but the systems under investigation are bimetallic clusters containing a tetrahedrally shaped core, rather than monometallic complexes. A series of dimolybdenum clusters is examined with the use of Bürgi-Dunitz analysis. This approach is taken in order to discern the migration trajectory and barrier to migration of a carbocationic site between metal vertices in a series of these clusters.

1.7.3 Organometallic Clusters as Conformational Switches

An introduction to a different use of bimetallic clusters is considered in Chapter 6. The idea of a bimetallic cluster as an agent for controlling the conformation of a cyclohexyl ring is discussed, along with the potential uses for such a system.

Chapter 2

Organometallic Chemistry of Trindane

2.1 Prelude

The majority of the material presented in the following two chapters has been published in the refereed ACS journal *Organometallics*.[32,33] The material is presented here in the overall context of the thesis, and includes discussion of some pertinent literature references that have appeared since the time of publication. The contributions of this author to the published work include the synthesis of trindane, full crystallographic characterisation of compounds, analysis and interpretation of NMR spectroscopic and mass spectral data and other characterisation data for all compounds, and writing significant portions of the manuscripts.

2.2 Introduction

2.2.1 C_{60} and Fragments of C_{60}

While the burgeoning chemistry of C_{60} continues to attract almost frantic world-wide attention,[34] rational attempts to synthesise fragments of the fullerene skeleton proceed at a more measured pace. Corannulene ($C_{20}H_{10}$), **2**, which represents the five-fold symmetric polar cap of C_{60}, was first obtained by Lawton and Barth in a now classic 17-step synthesis.[35] Since that time, shorter routes have been developed by Scott,[36] Siegel,[37] and Zimmermann;[38]

nevertheless, since the final cyclisation step requires Flash Vacuum Pyrolysis (FVP), these routes do not yield corannulene in quantities sufficient for the investigation of its organometallic chemistry.[39] Two of the more recent syntheses of corannulene by Scott[10] and Siegel[37] are represented in Scheme 2.1.[39]

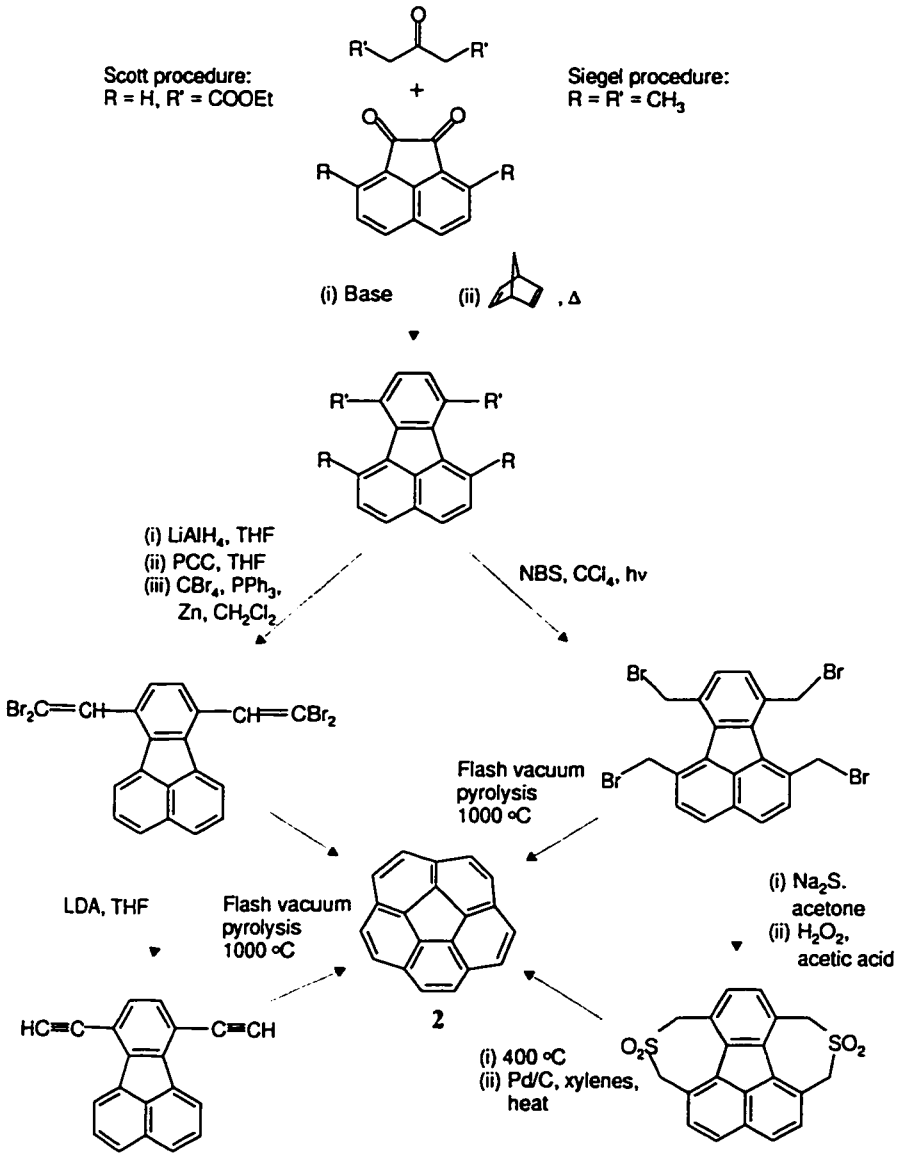

Scheme 2.1: Syntheses of corannulene, involving a flash vacuum pyrolysis step.

Recently, Rabideau[40] has employed flash vacuum pyrolysis to achieve the first synthesis of two $C_{30}H_{12}$ hydrocarbons, the carbon frameworks of which are represented on the buckminsterfullerene surface. These C_{30} molecules are known as the semibuckminsterfullerenes. Rabideau first reported **13**,[41] and then a second molecule, **14**,[42] which is of more synthetic interest, as it results from "halving" C_{60} to produce two isomeric bowl-shaped units. Both syntheses contain a FVP step, and are outlined in Schemes 2.2(a) and 2.2(b).

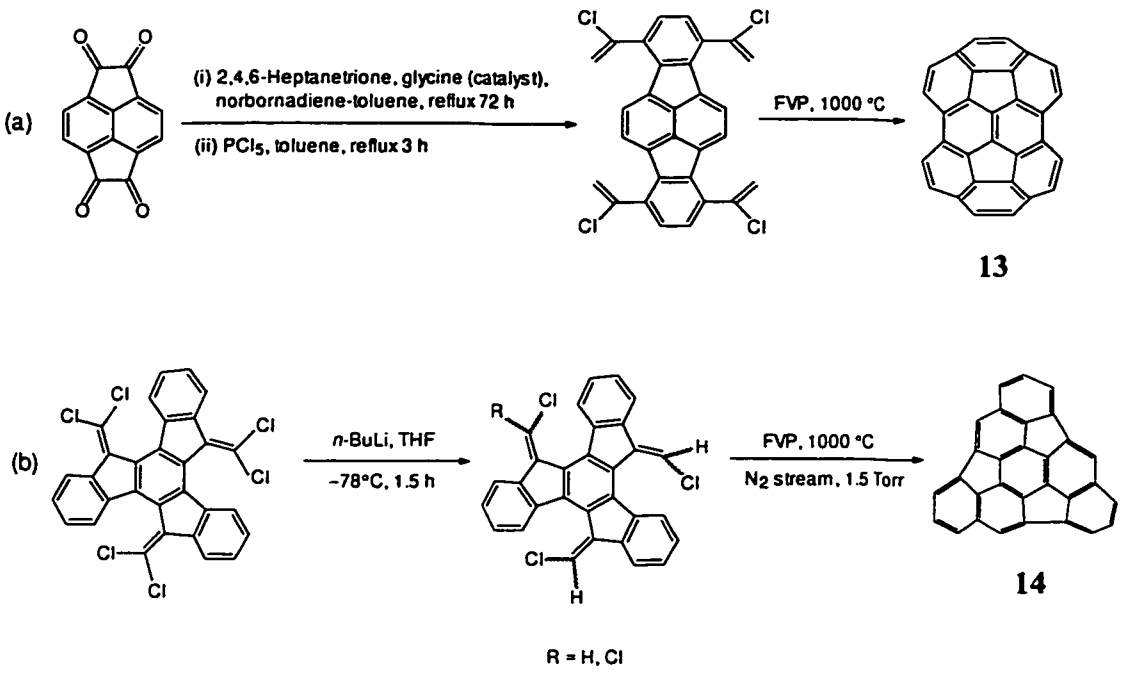

Scheme 2.2: Syntheses of semibuckminsterfullerenes, $C_{30}H_{12}$, (a) **13**, (b), **14**.

Once again, the final cyclisation involves FVP, and the products are available only in minimal quantities.

Further to this work, Rabideau[43,44] and Siegel[45] recently have managed to show that the FVP step can be avoided for corannulene, and related molecules, including Rabideau's semibuckminsterfullerenes. The nonpyrolytic syntheses rely on a reductive coupling between brominated sites to form the "rim" bonds of, for example, corannulene. In particular, homocoupling of benzylic and allylic halide groups with a low-valent vanadium[44] or titanium[45] reagent has been employed by these groups to achieve the non-pyrolytic synthesis of corannulene with yields (on the gram scale) of 70% and 80%, respectively. The final step of Rabideau's synthesis is shown in Scheme 2.3.

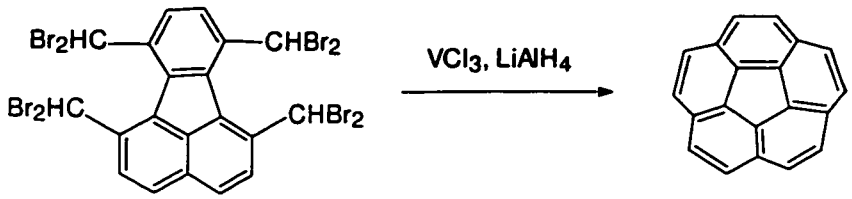

2

Scheme 2.3: Coupling of benzylic bromide sites to complete the rim bonds of corannulene.

2.2.2 En Route to Sumanene

Any synthetic route to C_{60} necessitates the introduction of some degree of strain, and a number of approaches have been analysed by Jemmis, Mehta and their colleagues.[7] They concluded that a viable concave intermediate would be the three-fold symmetric molecule $C_{21}H_{12}$, **3**, for which the name *sumanene* was proposed.[46] Attempts to synthesise sumanene have thus far proved unsuccessful, although the potential precursor **4** has been obtained in low yield by FVP and characterised by X-ray crystallography.[47]

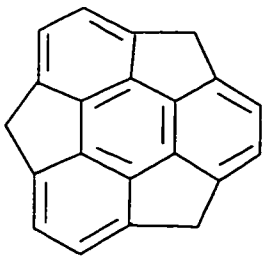

3

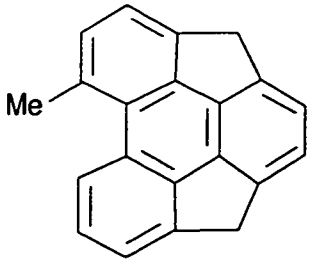

4

The final steps of the attempted syntheses of sumanene are shown in Scheme 2.4. So far, these attempts to thermally induce multiple cyclo-dehydrogenations have produced only the singly and doubly bridged products.

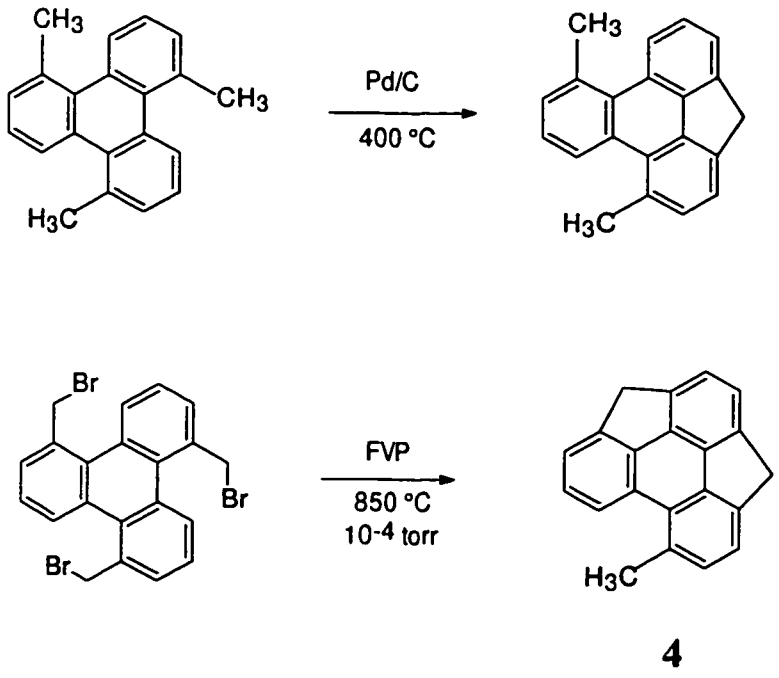

4

Scheme 2.4: Mehta's attempted syntheses of sumanene.

2.2.3 Trindane

Tris(cyclopenteno)benzene (*trindane*), **5**, is readily prepared by acid-catalysed condensation of three molecules of cyclopentanone.[48] There are few reports that discuss the chemistry of trindane. Those of note include a report by Katz and Slusarek[49] who prepared a hexabromo derivative, according to Reaction 2.1.

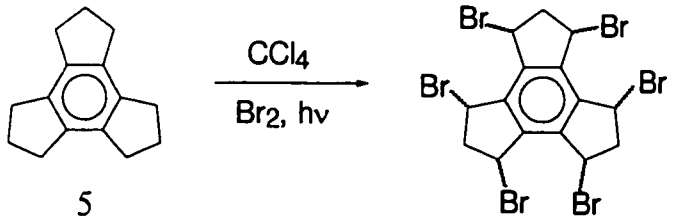

5 **2.1**

It was reported further by Katz and Slusarek that subsequent debromination yields dihydro-1*H*-trindene, the trianion of which can be complexed by a variety of organometallic fragments.[49,50] More recently, truxene (the tribenzo analogue of trindene),[51] has been investigated by Lynch, and the migration of $Mn(CO)_3$ or $Re(CO)_3$ units across this polycyclic surface has been unequivocally demonstrated.[52]

In another report, oxidation of the benzene ring in trindane was accomplished with a Ru(VIII) species generated *in situ*. The reaction is depicted in Reaction 2.2, and the product was characterised by single crystal X-ray crystallography.[53]

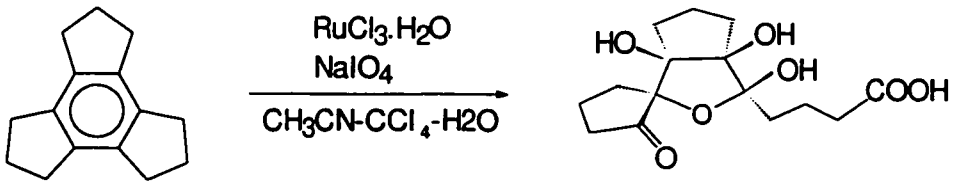

5 **2.2**

There is a recent report of a hexacarboxylic acid derivative of trindane, although the molecule is synthesised from the reaction of hexakis(bromomethyl)benzene with the sodium salt of diethyl malonate (as shown in Reaction 2.3).[54] Subsequent workup yielded the hexa-carboxylic acid derivative that contains the trindane framework; this compound was characterised by X-ray crystallography.[55]

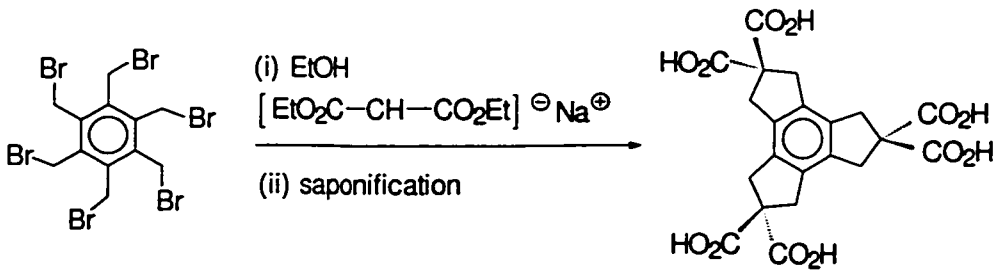

2.3

There are various other reports of molecules that contain the essential C_{15} trindane framework. The molecule that most closely resembles trindane is found in an account by Siegel, wherein the X-ray crystal structure of tris(bicyclo[2.1.1]hexeno)benzene is reported.[56] This molecule is synthesised by the trimerisation of 2-chlorobicyclo[2.1.1]hex-2-ene.

There is only one previous reference to an organometallic derivative of trindane.[57] In that case, a series of cationic complexes of the type $^{99m}Tc(arene)_2^+$ was prepared where the arene was C_6H_6, C_6Me_6, C_6Et_6, indane, trindane, *etc.* These materials were injected into rats to study the biodistribution of radioactive technetium to test their viability as myocardial imaging agents. These studies were, of necessity, carried out on trace quantities of material and no analytical nor spectroscopic data were reported for $[(trindane)_2Tc]^+ PF_6^-$.

2.3 Goals of the project

Herein are described the preliminary steps that have been taken toward developing an organometallic synthetic route to sumanene which does not require a low yield FVP step. This approach introduces the three cyclopentene moieties early in the synthesis rather than trying to make a five-membered ring in the final cyclisation step, and a retrosynthetic analysis is presented in Scheme 2.5.

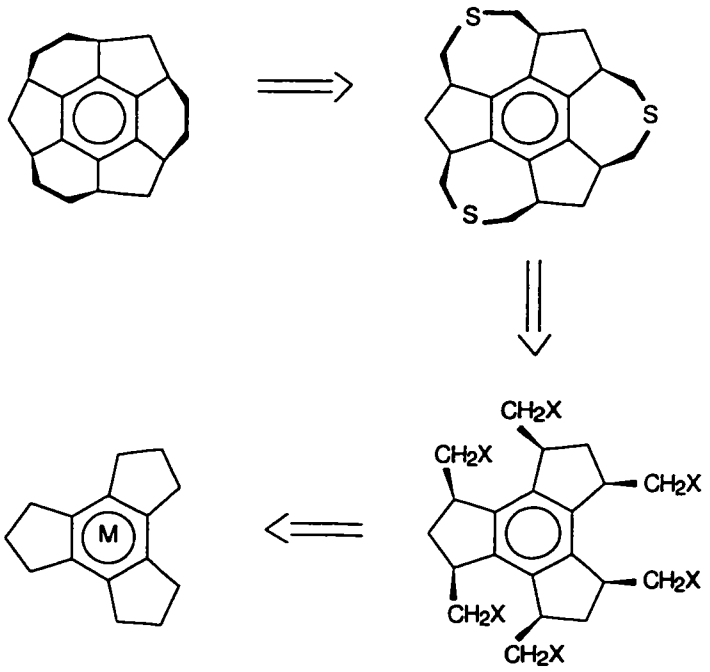

Scheme 2.5: Proposed retrosynthetic route to sumanene skeleton.

The results presented in this Chapter describe the efforts directed at obtaining the organometallic starting material used in this scheme, and performing the first step; namely, substitution at the benzylic hydrogen sites of trindane. The first characterised organometallic complexes of trindane are reported.

2.4 Results and Discussion

2.4.1 Synthetic and Structural Aspects

Trindane reacts with $Cr(CO)_6$ under standard conditions (dibutyl ether/THF/130º) to give yellow crystals of (η^6-trindane)$Cr(CO)_3$, **15**, which was characterised by X-ray crystallography. As shown in Figure 2.1, the tripodal moiety is oriented such that the three carbonyl ligands are staggered with respect to the cyclopentenyl rings. The observed bond lengths within the aromatic ring range from 1.376(6) to 1.401(6) Å; it is evident that there is no marked bond fixation, indicating that Mills-Nixon effects are not significant in this system.[58] It is, however, noticeable that the five-membered rings adopt envelope conformations such that the three central methylene "wingtips" (C(2), C(5), C(8)) are directed in an *endo* fashion with respect to the metal (Figure 2.2). An early X-ray study of the free ligand **5** was based on film data and indicated some disorder in these regions of the molecule.[59]

This type of bending may be compared with that observed in other arene complexes. Notably, the hydrogen atoms in $[(\mu\text{-}Cl)_3\text{-}\{(\eta^6\text{-}C_6H_6)Ru\}_2]^+$ and the methyl groups in $[(\mu\text{-}Cl)_3\text{-}\{(\eta^6\text{-}C_6H_5Me)Ru\}_2]^+$ are found to bend significantly towards the ruthenium atoms from the plane defined by the C_6 rings.[60] Extended Hückel calculations have been used to study the bonding interaction between the metals and the arene fragments. The results of these calculations show that a 6° bend is required in order to optimise the overlap between the $(\mu\text{-}Cl)_3Ru_2$ fragment and the arenes. The overall explanation is that there is increased overlap

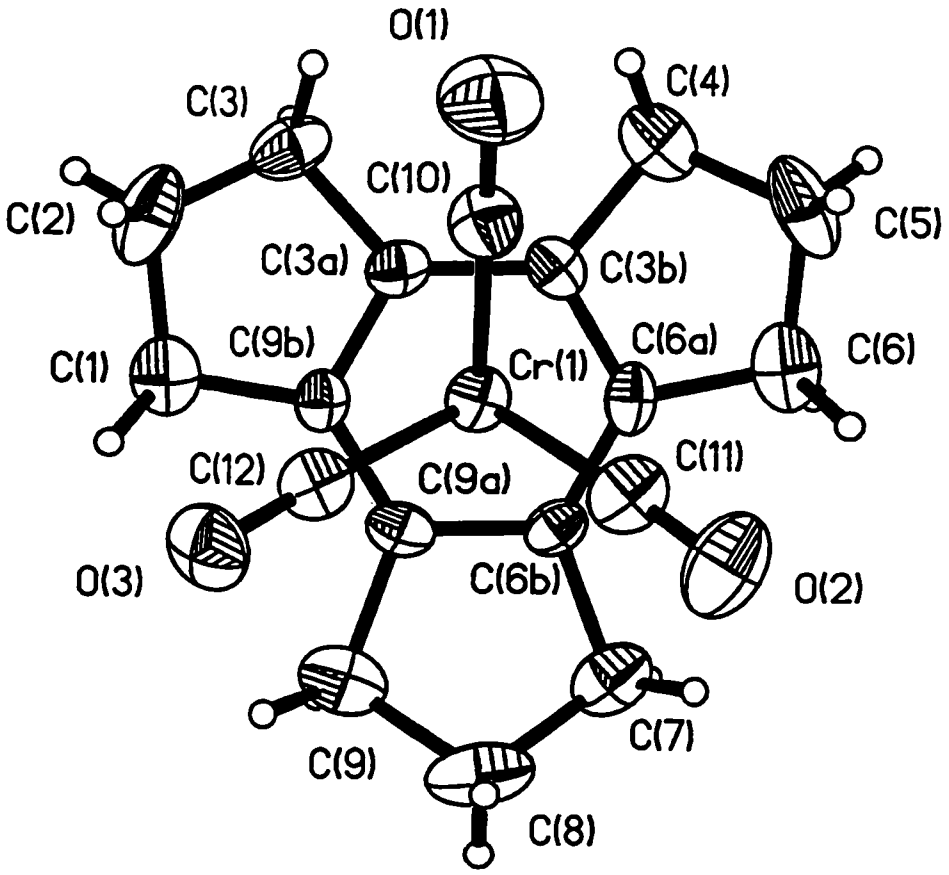

Figure 2.1: Molecular structure of $[(C_{15}H_{18})Cr(CO)_3]$ (**15**) showing the staggered orientation of the tripodal $Cr(CO)_3$ moiety. Thermal ellipsoids are shown at the 30% probability level, and hydrogen atoms are drawn at an arbitrarily selected size.

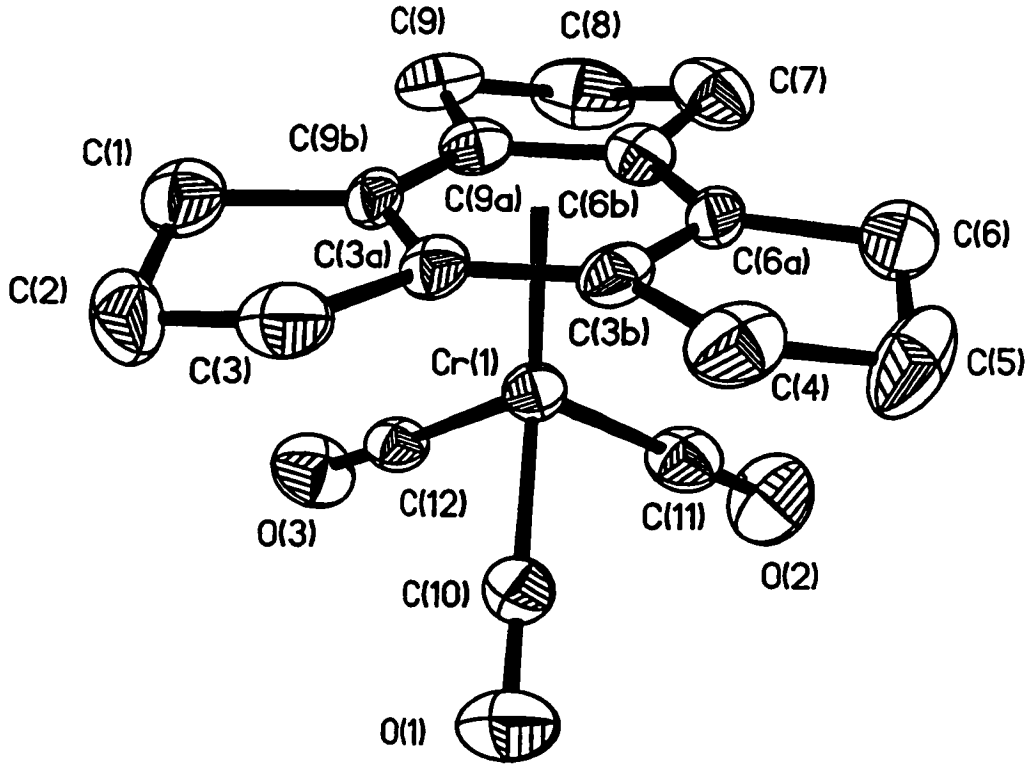

Figure 2.2: Molecular structure of $[(C_{15}H_{18})Cr(CO)_3]$ (**15**) showing the envelope conformation of the peripheral rings. Thermal ellipsoids are shown at the 30% probability level, and hydrogen atoms are removed for clarity.

between certain arene and metal orbitals; this results in the molecular orbitals having more bonding character, and a consequent lowering of their energy. Truly, it is a balance between the stabilisation and destabilisation of certain orbitals. With regard to the structure of **15**, one can apply the same reasoning, and surmise that the wingtip CH_2 groups are bent towards the Cr atom in order to allow better interaction of the π orbitals from the arene C atoms with those of the Cr atom.

The structure of **15** may be profitably compared with that of the known molecules [tris(cyclohexeno)benzene]$M(CO)_3$, M = Cr, **16a**, or Mn^+, **16b**, which also crystallise in a staggered orientation; in those cases, the peripheral six-membered rings exhibit conventional half-chair conformations.[61]

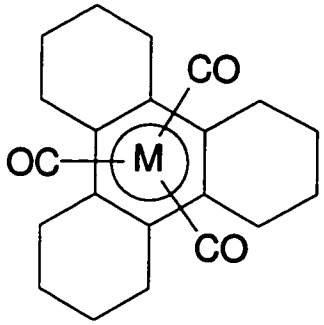

M = Cr **16a**

M = Mn^+ **16b**

In an analogous fashion, trindane reacts with $Mo(CO)_6$, $BrMn(CO)_5$ / $AgBF_4$, $(\eta^5\text{-}C_5H_5)Fe(CO)_2I$ / $AlCl_3$ / $AgBF_4$, or ferrocene / $AlCl_3$ / NH_4PF_6 to yield $(\eta^6\text{-}$trindane$)Mo(CO)_3$, **17**, $[(\eta^6\text{-}$trindane$)Mn(CO)_3]^+$ $[BF_4]^-$, **18**, $[(\eta^6\text{-}$trindane$)Fe(\eta^5\text{-}C_5H_5)]^+$ $[BF_4]^-$, **19a**, or $[(\eta^6\text{-}$trindane$)Fe(\eta^5\text{-}C_5H_5)]^+$ $[PF_6]^-$, **19b**, respectively. These complexes were readily identified by mass spectrometric and infrared spectroscopic techniques, as well as by their ^1H and ^{13}C NMR spectra.

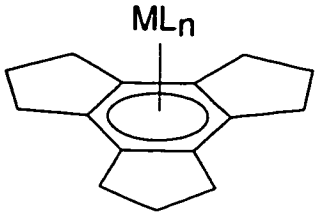

$ML_n = Cr(CO)_3$ **15**

$ML_n = Mo(CO)_3$ **17**

$ML_n = [Mn(CO)_3]^+$ **18**

$ML_n = [Fe(C_5H_5)]^+$ **19a, 19b**

2.4.2 NMR Spectroscopy

Trindane itself exhibits a very simple ^1H NMR spectrum, *i.e.*, a triplet (12H) for the benzylic protons, and a quintet (6H) for the central methylene groups, as shown in Figure 2.3. The incorporation of a π-complexed organometallic fragment renders inequivalent the faces of the trindane ligand and thus there are four ^1H NMR environments in the molecules **15** and **17** through **19b**. The benzylic proton environments (each 6H) are easily distinguished from the two resonances for the central methylenes (each 3H) by their relative intensities, but the assignment to *exo* or *endo* positions is less trivial. One is tempted to attribute the peaks on the basis of the different anisotropies of the ML_n fragments,[62] but such an approach is not always unequivocal. Fortunately, the X-ray data for the chromium complex **15** provide a rational means of assigning these resonances. Figure 2.4 illustrates the dihedral angles between a pair of benzylic protons and those of the neighbouring central methylene group in a five-membered ring. The ring conformations are not identical, but the dihedral angles differ only slightly and, in all cases, the *endo*-benzylic proton and its adjacent *exo*-wingtip methylene hydrogen make a dihedral angle of approximately 90°. The Karplus relationship suggests that the corresponding $^3J_{H\text{-}H}$ value between these particular protons should be rather

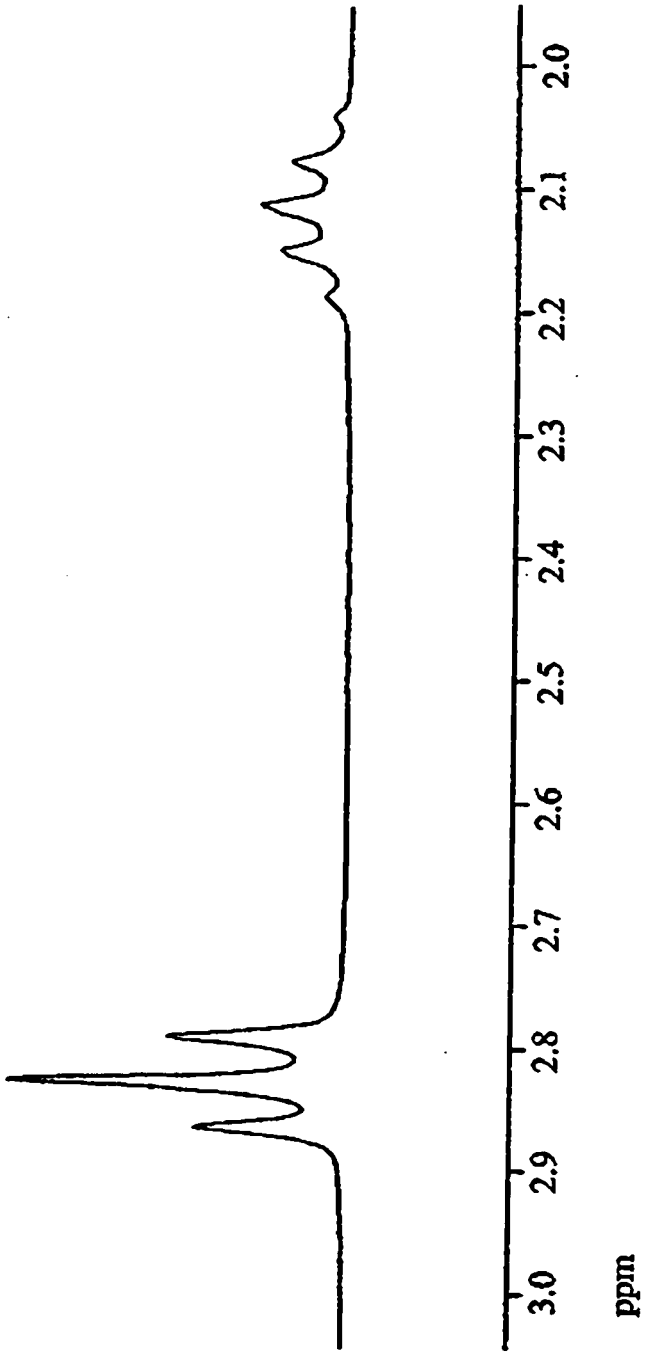

Figure 2.3: 200 MHz ^{1}H NMR spectrum of trindane, **5**, in $CDCl_3$.

small.[63] This is particularly evident in a series of ruthenium complexes of trindane, discussed in Chapter 3. These complexes show that, where coupling constants are clearly resolvable in the ^{1}H NMR spectrum, one can assign the *exo* and *endo* positions definitively.

For example, the 500 MHz ^{1}H NMR spectrum of (trindane)Mo(CO)$_3$, **17**, exhibits three multiplets in the intensity ratio 12:3:3. Although the *exo* and *endo* benzylic environments are severely overlapped for this particular complex, the wingtip protons can be differentiated. The value of the coupling constant, $^3J_{H\text{-}H}$, for the *exo*-benzylic / *endo*-wingtip protons (a diaxial interaction) is 12.2 Hz, while the coupling constant between the *endo*-benzylic / *exo*-wingtip protons (which are di-equatorially disposed) is too small to be resolved. The other two coupling constants of 4.4 Hz (*exo*-benzylic / *exo*-wingtip) and 9.6 Hz (*endo*-benzylic / *endo*-wingtip) are typical for axial-equatorial interactions. It is a reasonable assumption that the Cr (**15**) and Mo (**17**) complexes will have similar structures in the solution and solid states, and the assignment of the NMR spectrum of **17** is justified on the basis of the solid state structure of **15**. The ^{1}H NMR spectral data for molecules **15**, and **17** through **19b** are collected in Chapter 8, and their overall similarities suggest that all of these trindane complexes adopt analogous conformations.

2.4.3 Mass Spectral Observations

In the course of the mass spectrometric characterisation of the neutral complexes (trindane)M(CO)$_3$, **15** M = Cr, **17** M = Mo, a series of peaks at *m/z* values much higher than the parent peak for **15** or **17**, respectively, were consistently observed in the routine electron impact spectra. These peaks corresponded to $[(\text{trindane})_2M_2(CO)_3]^+$ and subsequent

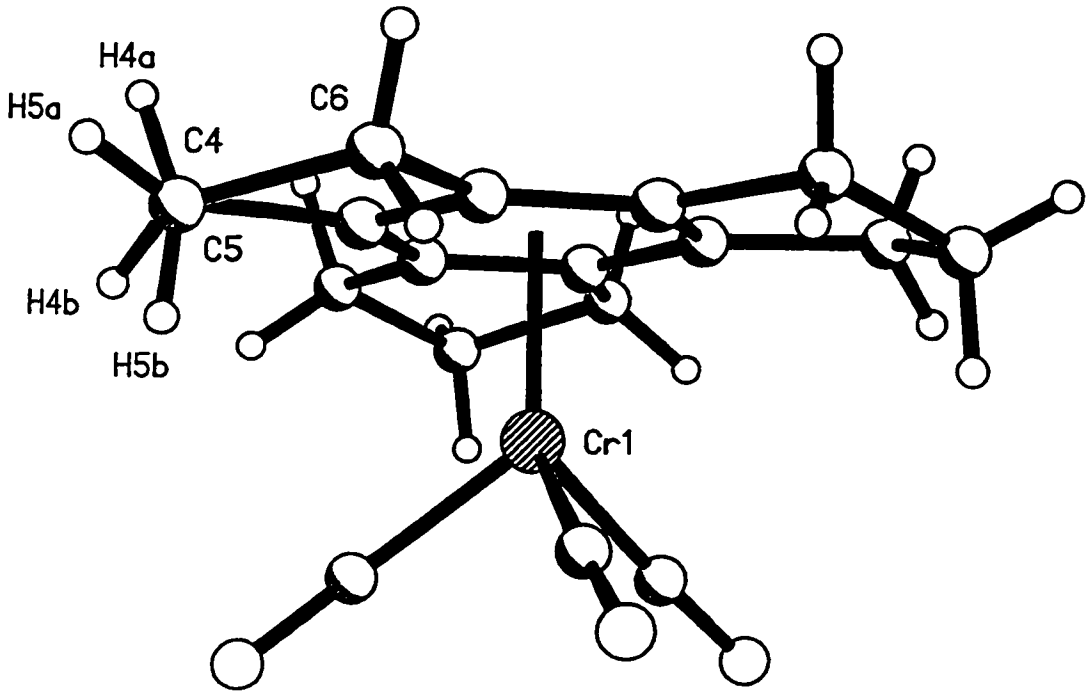

Figure 2.4: View of $[(C_{15}H_{18})Cr(CO)_3]$ (**15**) showing the dihedral angle between H5a (wingtip *exo*) and H4b (benzylic *endo*) to be approximately 90°.

fragmentation; this ion was also clearly detected in the chemical ionisation spectra. One can speculate about the structure of such a species: one viable candidate is the triple-decker system (η^6-trindane)M(μ-CO)$_3$M(η^6-trindane), **20**, entirely analogous to the known 30-electron complexes (η^5-C_5Me_5)Re(μ-CO)$_3$Re(η^5-C_5Me_5),[64] $[(\eta^5\text{-}C_5Me_5)_3Ru_2]^+$,[65] or ($\eta^6$-mesitylene)$_3Cr_2$,[66] in which the large surface area of the trindane ligands could provide steric protection at the outer layers of the sandwich.

Since a number of triple-decker complexes first observed mass spectrometrically have subsequently been isolated on a macro-scale, for example $[Cp_3Ni_2]^+$,[67] future work with this project may include exploring rational routes to molecules of the type [(trindane)$_2M_2(CO)_3$].

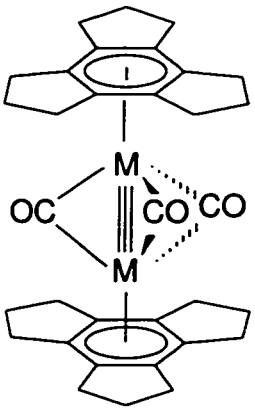

20 M = Cr, Mo

2.4.4 Deuterium Exchange Studies

It has been reported that base-catalysed hydrogen/deuterium exchange occurs upon treatment of (indane)Cr(CO)$_3$ with DMSO-d_6 and sodium methoxide.[68] Moreover, it has been

demonstrated conclusively that alkylation of (3-*O*-benzyl-17β-*O*-(*tert*-butyl-dimethylsilyl)estradiol)$Cr(CO)_3$ occurs on the face anti to the π-bonded metal atom.[69] It was reasoned that one could introduce deuterium atoms (or other substituents) only at the six *exo*-benzylic sites in (trindane)$Cr(CO)_3$, **15**. When **15** was allowed to react with *t*-BuOK in DMSO-d_6, however, multiple (zero to twelve) deuterium incorporation at the benzylic H sites was observed, as confirmed by mass spectrometry.

The use of a metal moiety to generate a cationic transition metal-arene complex was then attempted. In recent years, many examples of arene activation by the $(C_5H_5)M^+$ moiety, where M = Fe or Ru, have been reported.[70,71] Typically, as was shown in Scheme 1.2, Astruc has shown that treatment of $[(C_6Me_6)Fe(C_5H_5)]^+$ with *t*-BuOK and excess methyl iodide leads to ready formation of the cation $[(C_6Et_6)Fe(C_5H_5)]^+$,[12] presumably *via* successive reactions of zwitterionic intermediates such as **6**.[72,73]

To test the viability of functionalising all the *exo*-benzylic sites in a (trindane)ML_n system, the iron cation **19b** was stirred with *t*-BuOK in DMSO-d_6. Remarkably, the product isolated was not the anticipated hexa-deuterated product; instead, the ^{13}C NMR spectrum indicated that all twelve benzylic protons in (trindane)$Fe(\eta^5\text{-}C_5H_5)]^+$ $[PF_6]^-$, **19b**, had been replaced by deuterons. This result was confirmed by mass spectrometry, which revealed the exclusive formation of **19b**-d_{12}. Such an observation is reminiscent of the reaction of (η^5-indenyl)$Rh(C_2H_4)_2$, **21**, with CF_3CO_2D which shows not merely that Rh has undergone a haptotropic shift but also reveals incorporation of deuterium into the ethene ligands to give $[(\eta^6\text{-indene-}d_2)Rh(C_2D_4)_2]^+$, **22**. This presumably occurs through D^+ attack at the rhodium centre with subsequent scrambling via an ethyl intermediate.[74]

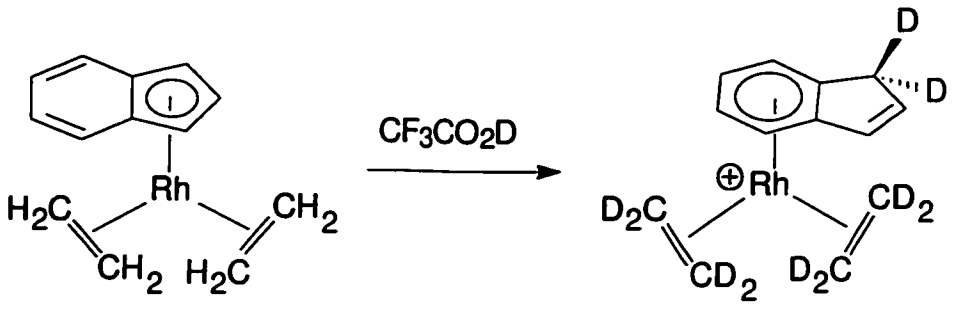

21 **22**

One is led to the conclusion that, although deprotonation of (trindane)Fe(η^5-C_5H_5)]$^+$ presumably occurs on the *exo* face, the incoming deuteron can attack at the metal centre and then migrate to an *endo* position, as indicated in Scheme 2.6. A similar mechanism has previously been invoked by Treichel to account for the sites of deuteration in the (indenyl)$_2$Fe system (Scheme 2.7).[75]

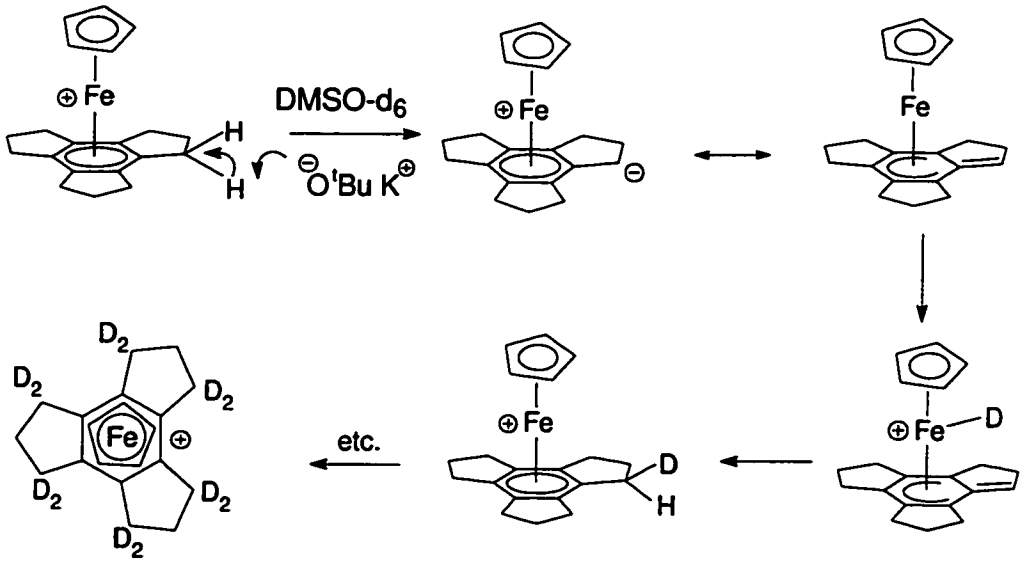

Scheme 2.6: Proposed mechanism for deuteration of CpFe(trindane)$^+$.

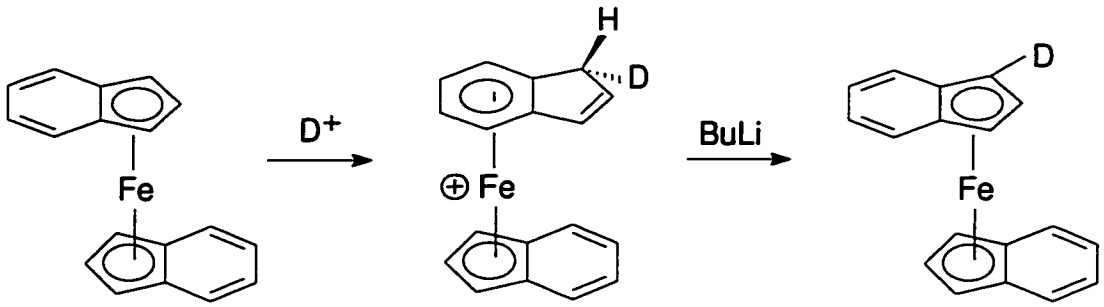

Scheme 2.7: Proposed deuteration in $(indenyl)_2Fe$.

2.5 Continuation of this work

It was thought that electrophiles larger than H^+ might, because of size restrictions, substitute only at the *exo* benzylic positions of trindane. This could provide, for example, a straightforward route to [(*all-cis*-hexamethyltrindane)Fe(C_5H_5)]$^+$. Experiments towards the realisation of this goal are being continued by another researcher. Preliminary results indicate, however, that substitution with benzyl groups can lead to incorporation of ten such groups! The question remains, how can this substitution process be made more selective?

In principle, it may be possible to achieve enhanced activation of an aromatic ring by incorporating a dicationic metallic fragment, as in $[(trindane)_2Ru]^{2+}$ $2BF_4^-$. The syntheses, structures and NMR spectra of this compound, and several related molecules, are the subject of Chapter 3.

Chapter 3

Ruthenium Complexes of Trindane

3.1 Prelude

Triscyclopentenobenzene (or *trindane*), $C_{15}H_{18}$, the condensation trimer of cyclopentanone, forms a series of organometallic complexes described in Chapter 2,[32] whereby the central aromatic ring is coordinated to a $Cr(CO)_3$, $Mo(CO)_3$, $Mn(CO)_3^+$, or $Fe(C_5H_5)^+$ fragment. It has been suggested in Chapter 2 that these compounds might serve as intermediates en route to *sumanene*, $C_{21}H_{12}$, **3**, which possesses an important structural motif present in C_{60}.

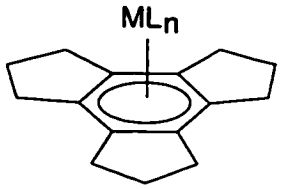

$ML_n = Cr(CO)_3$ **15**

$ML_n = Mo(CO)_3$ **17**

$ML_n = [Mn(CO)_3]^+$ **18**

$ML_n = [Fe(C_5H_5)]^+$ **19a, 19b**

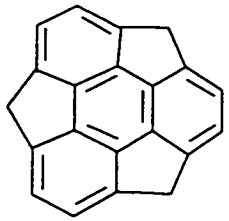

3

A crucial requirement of this synthesis is that the metal should activate the *exo*-benzylic hydrogens towards base-catalysed replacement by alkyl groups.

3.2 Goals of the Project

Since *mono*-cationic complexes, such as $[(C_6(CH_3)_6)Fe(C_5H_5)]^+$, are known to yield the corresponding hexakis substituted $[(C_6(CH_2R)_6)Fe(C_5H_5)]^+$ systems under mild

conditions,[76] the preparation of the *di*-cationic sandwich complex $[(trindane)_2Ru]^{2+}$, **23**, was undertaken in the hope that all twelve *exo*-benzylic sites on the arene ligands could be functionalised. The most convenient route to bis(arene)ruthenium dications proceeds *via* the corresponding dimer $[(arene)RuCl_2]_2$; herein are reported the synthesis and structural characterisation of $[(trindane)RuCl_2]_2$, **25**, and its subsequent conversion to **23**.[33]

3.3 Introduction

3.3.1 Chemistry of Ru-Arene Complexes

There is a rich chemistry of ruthenium-arene complexes,[3] including the class of chloro-bridged diruthenium arene complexes. The parent complex from which all subsequent products are derived is $[(arene)RuCl_2]_2$. This complex was first reported for the arene benzene; it was produced from the reaction of ruthenium(III) chloride with cyclohexa-1,3-diene in ethanol solvent.[77] It has been found since then that many dihydroarenes will react under similar conditions to give the corresponding arene derivatives.[78] The following two sections introduce some of the reactions that are of interest in this and the succeeding Chapter.

3.3.2 Bis-arene Sandwich Complexes

Treatment of a $[RuCl_2(arene)]_2$ dimer with a silver salt (e.g. $AgBF_4$) in a weakly coordinating solvent such as acetone or acetonitrile gives a cationic intermediate in which three solvent molecules are coordinated to ruthenium, giving a system of the general type

$[(arene)Ru(solvent)_3]^{2+}(BF_4^-)_2$. This complex may, in turn, react with a variety of nucleophiles, including a different arene. When the complex is heated with an excess amount of a second arene in the presence of an acid (HX), a mixed-arene cationic complex of the general form $[(arene')Ru(arene'')]^{2+}(X^-)_2$ is obtained (Reaction 3.1).[3]

$$[RuCl_2(arene')]_2 \xrightarrow[AgBF_4]{\text{acetone}} \xrightarrow[\text{heating}]{\text{arene''/HX}} Ru(arene')(arene'')^{2+}(X^-)_2 \qquad \textbf{3.1}$$

3.3.3 $[(Arene)Ru(\mu\text{–}X)_3(Arene)]^+$ Cations

The $[RuCl_2(arene)]_2$ dimer can also be used as the starting material for the formation of a cationic triply chloro-bridged binuclear ruthenium complex of the type depicted in Reaction 3.2 (e.g. arene = C_6H_6, C_6Me_6).[3]

$$[RuCl_2(\eta^6\text{-arene})]_2 \xrightarrow[2.\ NH_4PF_6]{1.\ H_2O/\text{heating}} \left[(\eta^6\text{-arene})Ru\begin{matrix}\diagup Cl \\ — Cl — \\ \diagdown Cl\end{matrix}Ru(\eta^6\text{-arene})\right]^{\oplus} \qquad \textbf{3.2}$$

3.4 Results and Discussion

3.4.1 Synthetic and Spectroscopic Aspects

As a prelude to the goal of the synthesis of the sandwich dication $Ru(trindane)_2^{2+}$, $[(p\text{-cymene})RuCl_2]_2$ was converted to its tris-acetone derivative which, upon treatment with trindane, yielded the mixed sandwich $[(trindane)Ru(cymene)]^{2+}$ $2BF_4^-$, **24**, as shown in Scheme 3.1. *Para*-cymene (4-isopropyltoluene) is a commonly used arene in such sandwich

molecules[79] because [(*p*-cymene)$RuCl_2$]$_2$ is readily available from the redox reaction of ruthenium trichloride with α-phellandrene (5-isopropyl-2-methyl-1,3-cyclohexadiene), an inexpensive diene.[80]

[(Trindane)Ru(cymene)]$^{2+}$ $2BF_4^-$, **24**, was readily identified by its mass spectrum, in particular the intense peak at *m/z* 217 (the doubly-charged ion corresponding to the sandwich dication [$^{102}RuC_{25}H_{32}$]$^{2+}$ of mass 434). Another peak was seen at an *m/z* value of 453 which corresponds to [(trindane)Ru(cymene)F]$^+$. Moreover, the ^1H and ^{13}C NMR spectra clearly indicated the presence of the cymene ligand. Of more immediate interest were the resonances associated with the η^6-bonded trindane ligand. As seen previously in the ^1H NMR spectra of molecules **15** and **17** through **19b**, complexation to a metal renders inequivalent the *exo* and *endo* faces of the $C_{15}H_{18}$ moiety, and gives rise to four proton environments. The *exo* and *endo* benzylic proton absorptions are, as expected, twice as intense as the central methylene (wingtip) peaks.

In Chapter 2 the X-ray crystal structure of (trindane)$Cr(CO)_3$, **15**, was discussed; in this structure all three five-membered rings adopt an envelope conformation such that the central methylene unit is folded towards the metal. This molecular geometry places the *exo*-benzylic and *endo*-wingtip hydrogens in a pseudo-*trans*-diaxial relationship, and in the structurally analogous (trindane)$Mo(CO)_3$ complex a $^3J_{H\text{-}H}$ coupling of 12.2 Hz is observed. Consequently, the *endo*-benzylic and *exo*-wingtip hydrogens occupy pseudo-equatorial sites and, since the dihedral angle between them is approximately 90°, the $^3J_{H\text{-}H}$ value is small (~1.5 Hz).[81] The same pattern of coupling constants is observed for the trindane moiety in

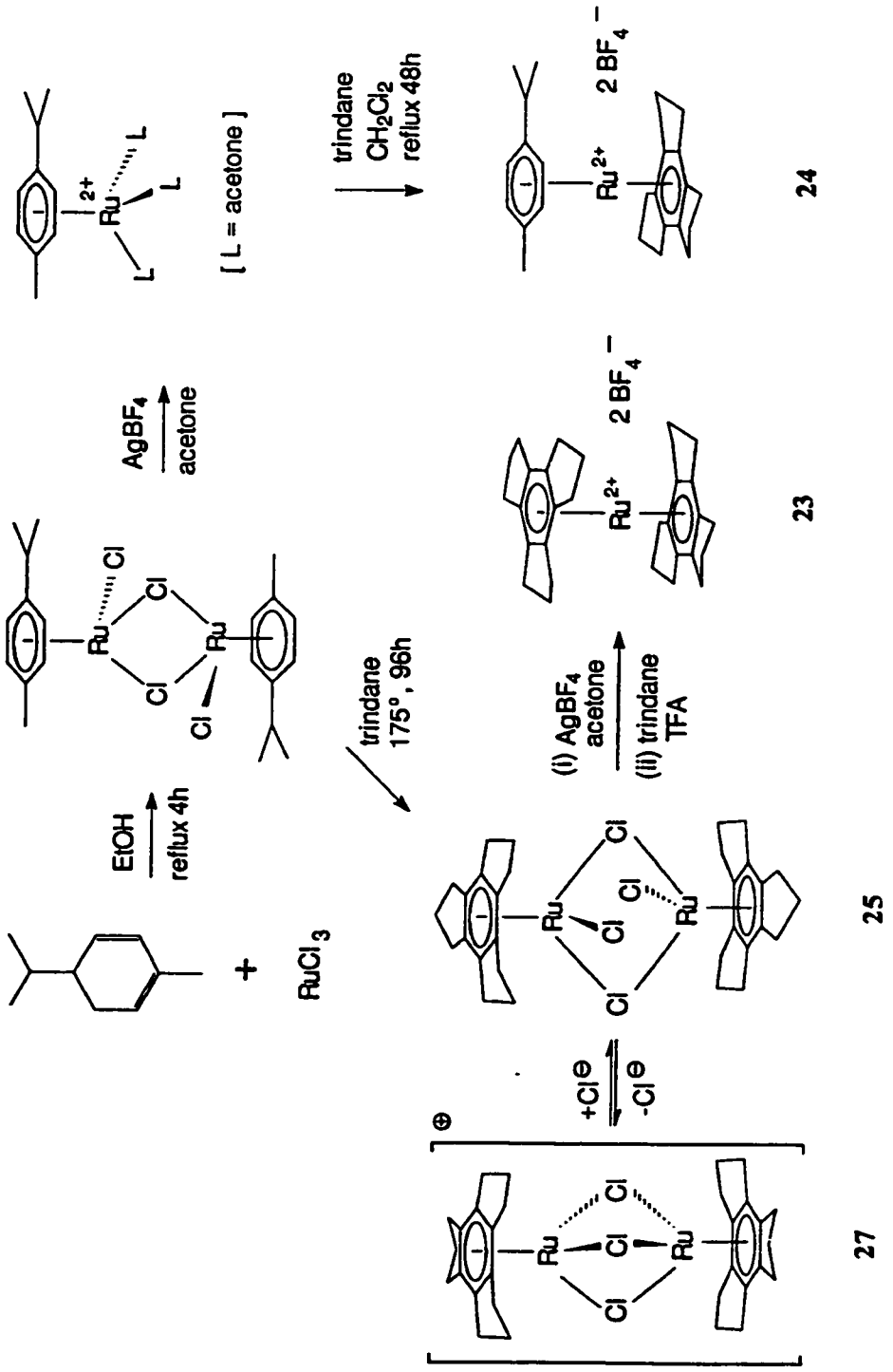

Scheme 3.1: Synthetic routes to trindane-ruthenium complexes.

[(trindane)Ru(cymene)]$^{2+}$ 2BF_4^-, **24**, and so one can presume a similar *endo:endo:endo* conformation for the wingtip methylene groups, as depicted in Scheme 3.1.

In the absence of an appropriate commercially available cyclohexadiene precursor to trindane, it was decided to attempt an arene exchange reaction by heating [(*p*-cymene)$RuCl_2$]$_2$ in a large excess of molten trindane at 150 °C.[82] Encouragingly, it was possible to obtain [(trindane)$RuCl_2$]$_2$, **25**, in 85% yield. The NMR spectra and X-ray crystal structure of **25** are discussed below, but it is noted initially that treatment with excess trindane in the presence of $AgBF_4$ did indeed yield the hoped-for symmetrical sandwich dication [(trindane)$_2$Ru]$^{2+}$ 2BF_4^-, **23**. Figure 3.1 shows the beautifully resolved 500 MHz ^{1}H NMR spectrum of **23** in which coupling between all four proton environments is clearly evident. Each benzylic methylene proton appears as a doublet of doublets of doublets, while the central methylene protons (the wingtips) both exhibit the expected 18-line pattern for a doublet of triplets of triplets. The chemical shifts and coupling constants are collected in Table 3.1, and again are entirely consistent with a D_{3d} structure in which the five-membered rings adopt envelope conformations such that the wingtips are all folded inwards, *i.e.* towards the ruthenium atom.

3.4.2 NMR Spectra and X-ray Crystal Structures of [(Trindane)$RuCl_2$]$_2$, 25, and (Trindane)$RuCl_2$[$P(OMe)_3$], 28.

As discussed above, the trindane ligands in the organometallic complexes **15**, **17** through **19b**, **23**, and **24** have been shown, either by X-ray crystallography or from their NMR data, to adopt a three-fold symmetric structure in which the five-membered ring

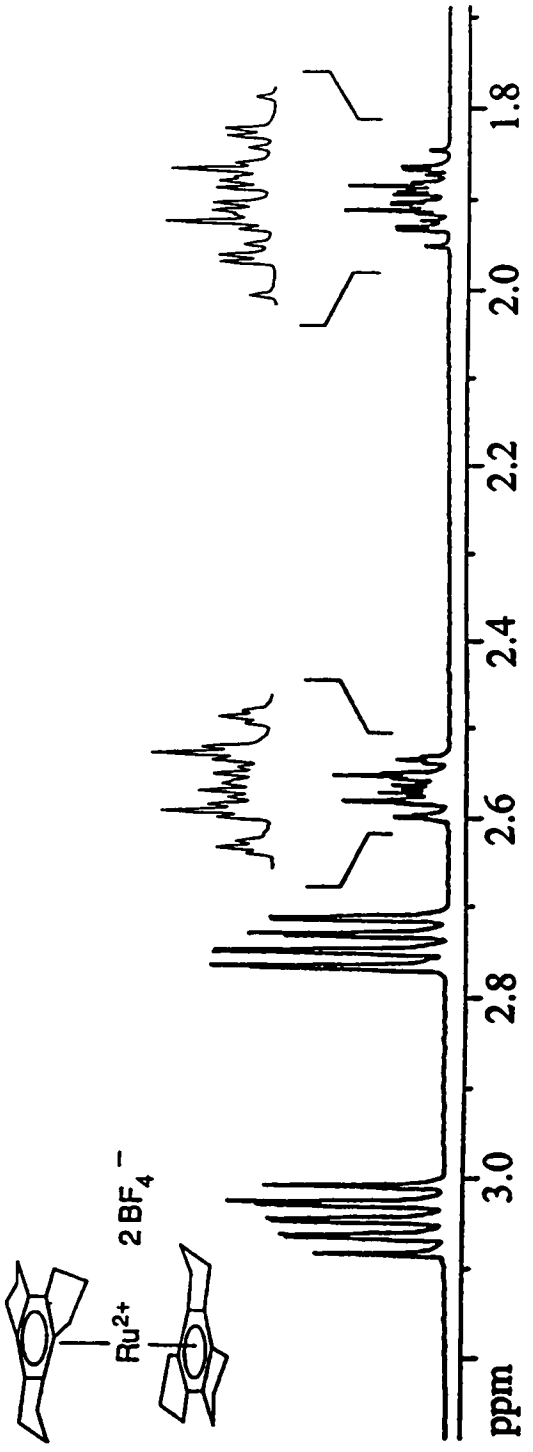

Figure 3.1: Proton NMR spectrum of (trindane)$_2$Ru^{2+}2BF$_4^-$, (**23**), (500 MHz, in $CDCl_3$).

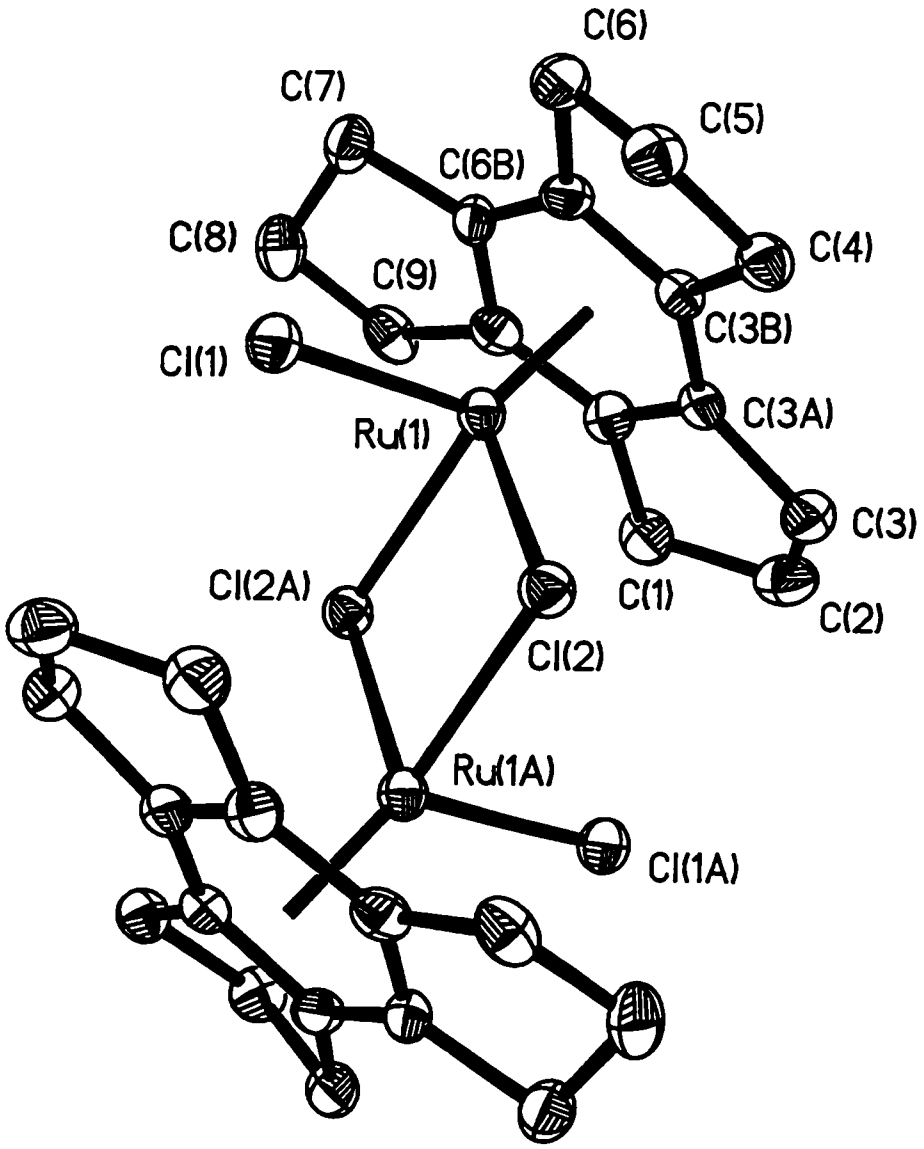

Figure 3.2: View of $[(C_{15}H_{18})RuCl_2]_2$ (**25**), showing the atomic numbering scheme. Thermal ellipsoids are shown at the 30% probability level and hydrogen atoms are removed for clarity. Salient bond lengths (Å) and angles (deg): Ru–(trindane centroid) 1.640, Ru(1)–Cl(1) 2.389(2), Ru(1)–Cl(2) 2.451(2), Ru(1)–Cl(2A) 2.451(2), Cl(2)–Ru(1A) 2.451(2); Cl(2)–Ru(1)–Cl(2A) 81.44(7), Ru(1)–Cl(2)–Ru(1A) 98.56(7).

envelopes are folded towards the metal. However, this conformation is not maintained in [(trindane)$RuCl_2$]$_2$, **25**, as illustrated in the X-ray crystal structure depicted in Figure 3.2.

The general features of the molecule resemble those previously reported for the [(*p*-cymene)$OsCl_2$]$_2$ analogue, **26**.[83] The two metals and the bridging chlorines are coplanar with average Ru–Cl distances of 2.451 Å; the Ru···Ru distance of 3.715 Å is too long to be considered a bond. A crystallographic inversion centre relates the two halves of the molecule; thus the two trindane ligands lie in parallel planes, and the Ru–trindane

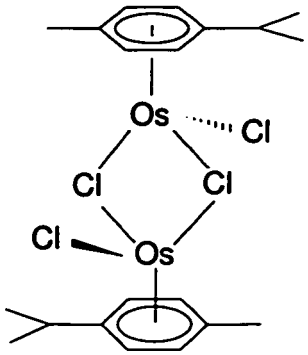

26

(centroid) distance is 1.640 Å. The most interesting structural feature is the intrusion of each terminal chlorine atom into the space occupied by the trindane *in the other half of the dimer.* This steric interaction causes one of the cyclopentene rings in each trindane ligand to fold away from the ruthenium atom giving rise to an *endo:endo:exo* conformation for the wingtip methylene units. The space-filling representation in Figure 3.3 emphasises the degree of molecular crowding in **25**.

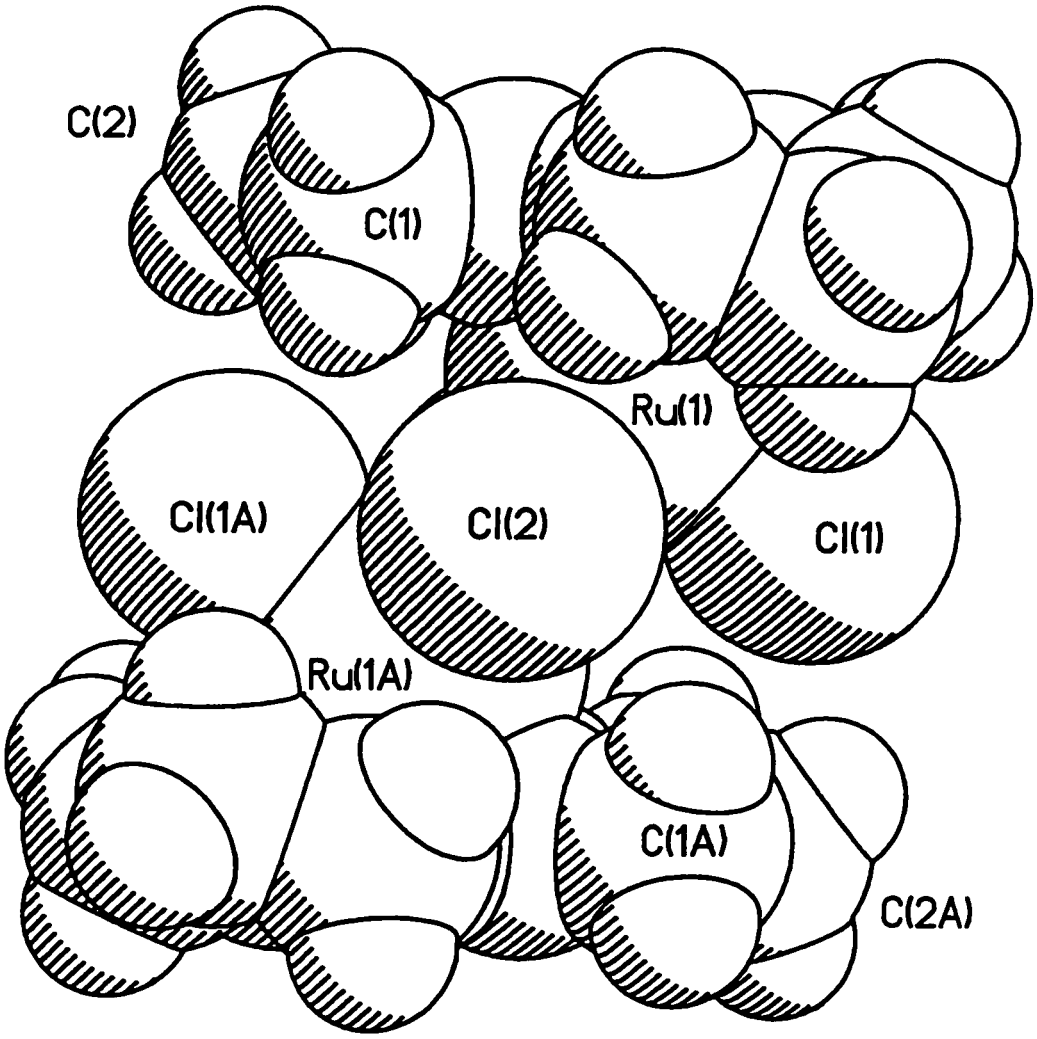

Figure 3.3: Crystallographic space-filling view of **25**, emphasising the degree of crowding caused by the nonbridging chlorine atoms, Cl(1) and Cl(1A).

Surprisingly, the room temperature ^{1}H NMR spectrum of [(trindane)$RuCl_2$]$_2$, **25**, in CD_2Cl_2 showed not four, but eight proton environments, in the approximate ratio 4:4:2:2:2:2:1:1. Likewise, in the ^{13}C regime, the aromatic ring carbons gave rise to two resonances, while the methylene carbons exhibited a four peak pattern. The initial thought was that the molecule adopted C_s symmetry, as in the solid state structure. Moreover, these data suggested that one should consider the possibility of slowed arene rotation; such a phenomenon has been unequivocally demonstrated for a number of (arene)CrLL'L" systems,[84] and also in [1,4-bis(*t*-butyl)benzene]Ru(CO)($SiCl_3$)$_2$.[85]

However, such a hypothesis is not valid in the case of [(trindane)$RuCl_2$]$_2$, **25**. Instead the results can be more readily explained in terms of ionisation to form [{(trindane)Ru}$_2$(μ-Cl)$_3$]$^+$ Cl^-, **27**. When the sample was cooled in either toluene-d_8 or CD_2Cl_2, the relative intensities of the proton resonances and of the carbon peaks gradually changed, suggesting an equilibrium between the doubly-bridged neutral molecule **25** and the triply-bridged ion **27**; the ratio of **25**:**27** is 30:70 in CD_2Cl_2 at -50 °C. Even more dramatically, use of CD_3NO_2 (which would surely favour the ionised species) resulted in almost complete conversion to only one of the isomers; at room temperature, the ratio of **25** to **27** is approximately 1:10. The ^{1}H-^{1}H COSY (correlation spectroscopy) and ^{1}H-^{13}C shift-correlated spectra, Figures 3.4 and 3.5, respectively, led to the assignments collected in Table 3.1.

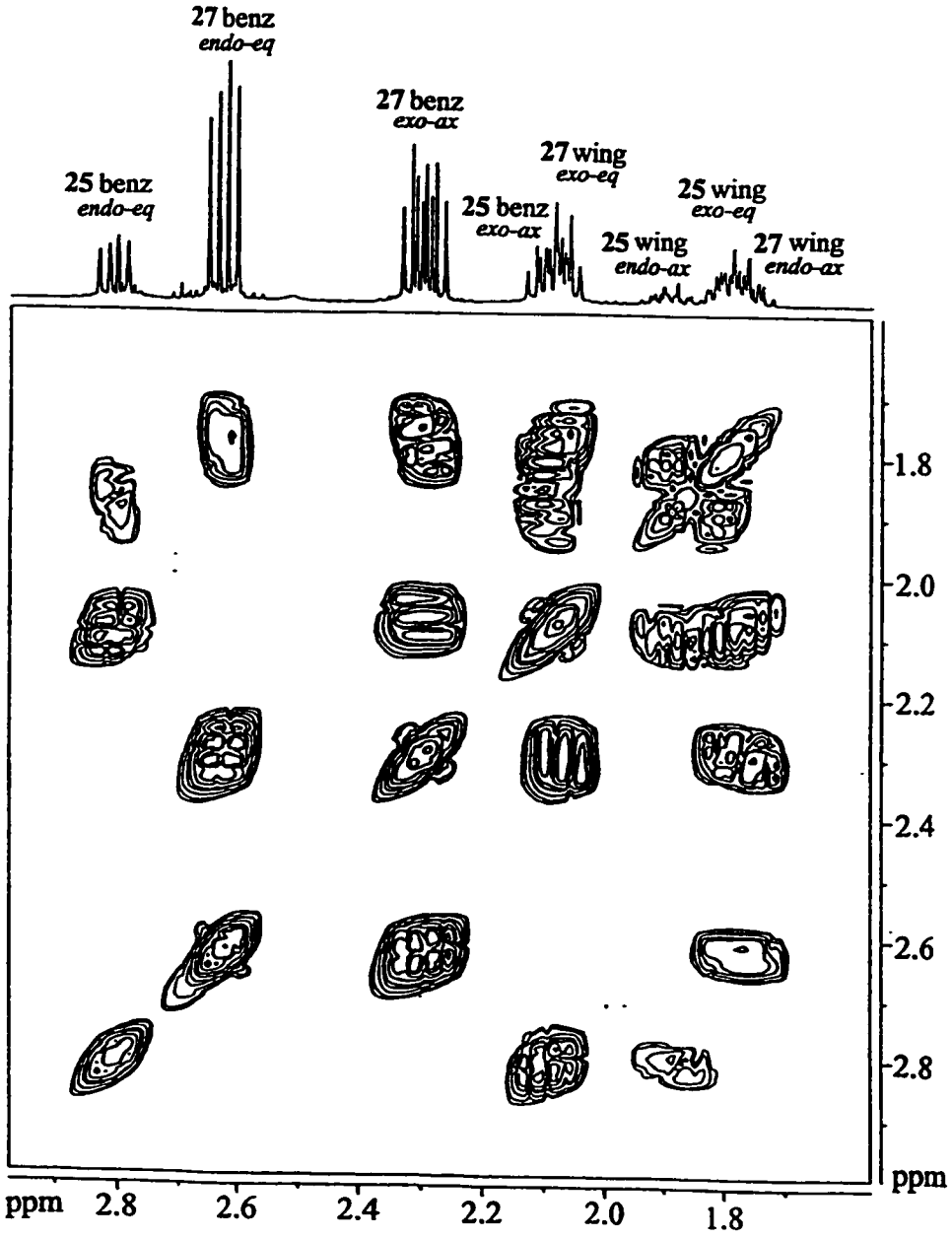

Figure 3.4: ^1H–^1H COSY spectrum of **25** and **27** (500 MHz, in CD_2Cl_2); benz = benzylic CH_2, wing = wingtip CH_2.

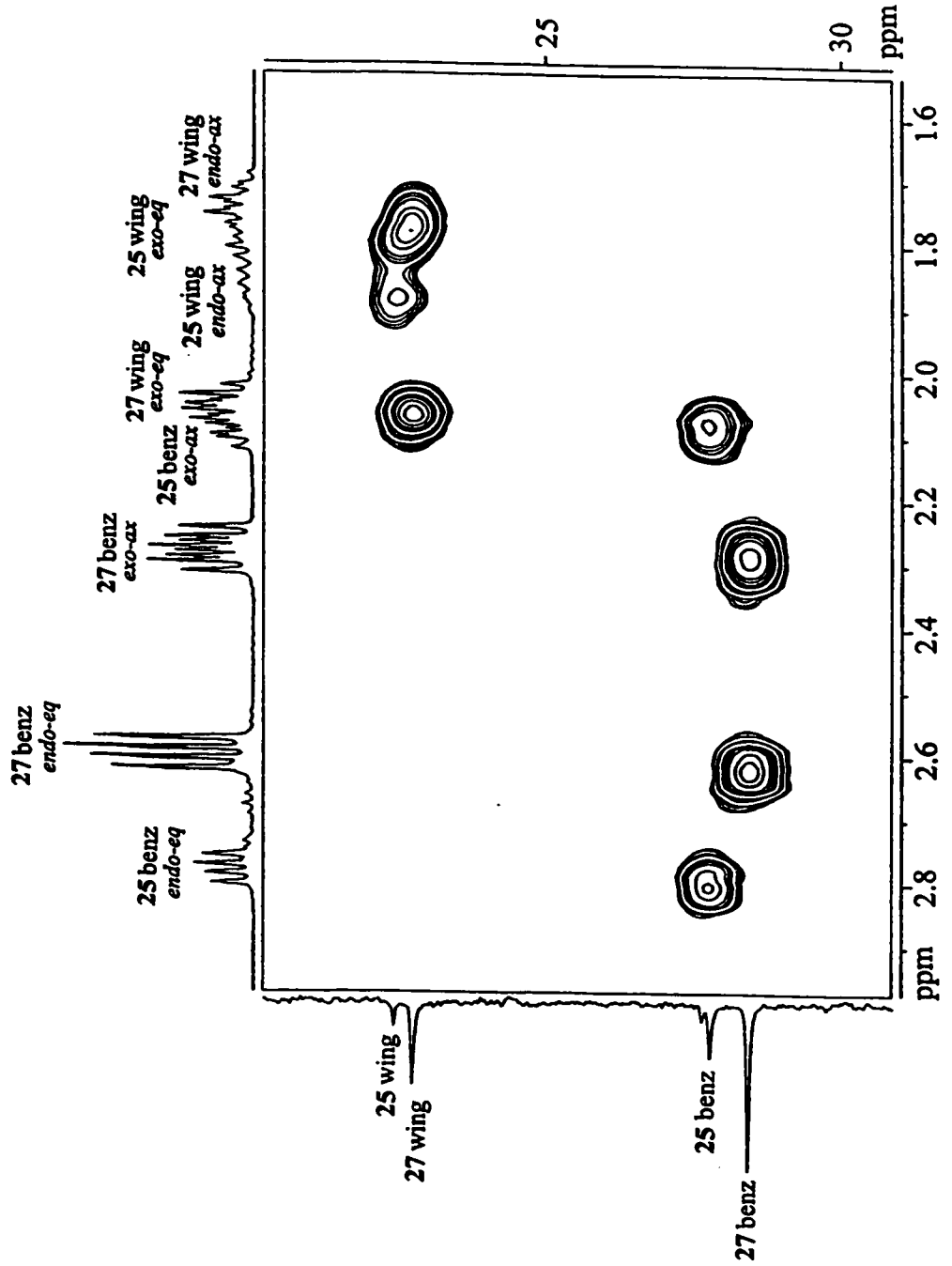

Figure 3.5: $^{1}H-^{13}C$ shift-correlated spectrum of **25** and **27** (500 MHz, 125 MHz in CD_2Cl_2); benz = benzylic CH_2, wing = wingtip CH_2.

Table 3.1 500 MHz ^{1}H NMR Chemical Shifts and Coupling Constants (trindane region) for **23**, **24**, **25**, **27** and **28**.

	δ, ppm				
^{1}H	**23**[a]	**24**[a,b]	**25**[c]	**27**[c]	**28**[c,d]
benzylic, *exo* (axial)	3.05	3.08	2.30	2.09	2.36
benzylic, *endo* (equatorial)	2.74	3.06	2.63	2.81	2.77
wingtip, *exo* (equatorial)	2.57	2.55	2.07	1.80	1.88
wingtip, *endo* (axial)	1.90	2.17	1.78	1.90	1.88
$^2J(benz_{exo}$ - $benz_{endo})$	-18.0	*e*	-15.6	-14.6	-15.3
$^2J(wing_{exo}$ - $wing_{endo})$	-13.7	-13.7	-11.2	*e*	-12.5
$^3J(benz_{exo}$ - $wing_{exo})$	8.9	7.6	7.7	*e*	8.3
$^3J(benz_{exo}$ - $wing_{endo})$	10.6	*e*	11.2	*e*	10.1
$^3J(benz_{endo}$ - $wing_{exo})$	1.5	*e*	~1	*e*	1.8
$^3J(benz_{endo}$ - $wing_{endo})$	8.8	9.4	7.9	7.5	8.6

[a] Solvent CD_3NO_2

[b] Cymene resonances: δ 2.97 (septet, 6.9 Hz, 1H, Me_2CH); 1.24 (d, 6.9 Hz, 6H, $(CH_3)_2CH$); 2.46 (s, 3H, CH_3); 6.61 (d, 6.7 Hz, 2H, *CH* (aromatic)); 6.67 (d, 6.7 Hz, *CH* (aromatic)).

[c] Solvent CD_2Cl_2

[d] Methoxy resonance: δ 3.78 (d, 9H, OCH_3); $^3J(^1H\text{-}^{31}P)$ = 10 Hz

[e] Coupling constant not resolved because of overlapping multiplets

It is well established that dimeric complexes of the type $[(arene)RuCl_2]_2$ can be dechlorinated by $AgBF_4$ or HBF_4 to give the cationic species $[\{(arene)Ru\}_2(\mu\text{-}Cl)_3]^+$.[8,12] In light of the crystallographic data for **25**, one can now rationalise the facile ionisation of **25** to give **27**, especially in solvents of high dielectric constant. The steric hindrance between each terminal chlorine in **25** and the trindane in the other half of the dimer is readily alleviated by loss of a chloride ion, formation of a third bridge, and adoption of a D_{3h} structure. The stability of $[\{(arene)Ru\}_2(\mu\text{-}Cl)_3]^+$ cations is evidenced not merely by X-ray crystallographic data and molecular orbital analyses,[86] but also by the magnitude of the $[M\text{-}Cl]^+$ ion peak in the mass spectrum of **25**.

To verify that ionisation of **25** is indeed promoted by steric hindrance from a chlorine in the other half of the dimer, **25** was treated with trimethyl phosphite in the expectation that the monomeric species $(trindane)RuCl_2[P(OMe)_3]$, **28**, would be formed.

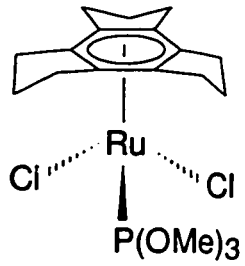

28

Figure 3.6 shows the X-ray crystal structure of **28**; overall, there is a close resemblance to the previously reported structures of $(arene)RuCl_2(PMePh_2)$, where the arene is benzene or cymene.[87] In particular, the $RuCl_2P$ tripod is staggered with respect to the three 5-membered rings. As with the $PMePh_2$ complexes, the ruthenium-carbon distances vary such that the two

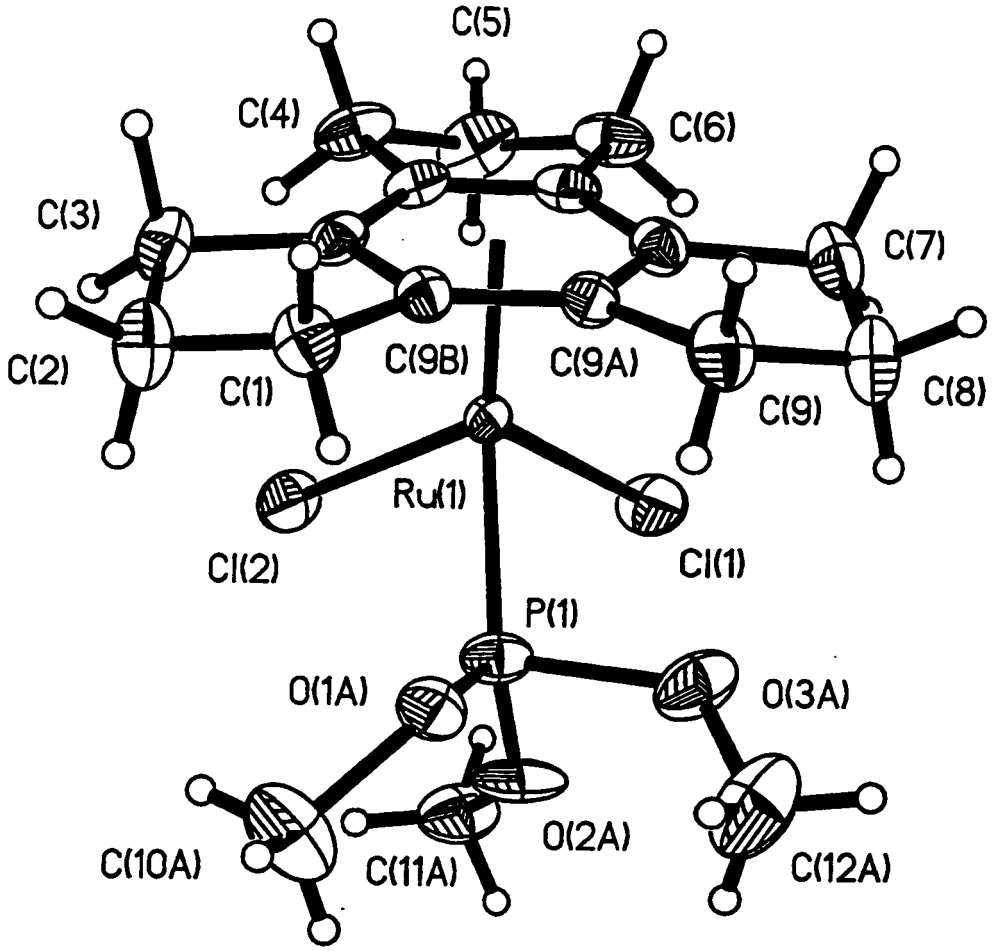

Figure 3.6: View of (trindane)$RuCl_2[P(OMe)_3]$ (**28**), showing the atomic numbering scheme. Thermal ellipsoids are shown at the 30% probability level, and hydrogen atoms are shown at an arbitrarily selected size. Only one part of the disorder in the methoxy region is drawn. Salient bond lengths (Å) and angles (deg): Ru–(trindane centroid) 1.719, Ru(1)–C(3A) 2.208(4), Ru(1)–C(3B) 2.250(4), Ru(1)–C(6A) 2.256(4), Ru(1)–C(6B) 2.209(4), Ru(1)–C(9A) 2.221(4), Ru(1)–C(9B) 2.220(4), Ru(1)–Cl(1) 2.402(1), Ru(1)–Cl(2) 2.415(1), Ru(1)–P(1) 2.278(1); P(1)–Ru(1)–Cl(1) 85.78(5), P(1)–Ru(1)–Cl(2) 86.93(5), Cl(1)–Ru(1)–Cl(2) 87.56(7).

lengths opposite the PR_3 ligand are significantly longer than the others (in this case, for **28**, Ru-C(3B) 2.250(4) Å and Ru-C(6A) 2.256(4) Å). It does not appear, however, that there is asymmetric bonding of the arene ligand, as none of the ring carbon atoms deviate significantly from a mean plane taken through them. For our present purposes, the most important feature is that the "normal" *endo:endo:endo* trindane conformation has been recovered. The Ru–trindane (centroid) distance is 1.719 Å (*cf.* 1.640 Å in **25**), and there appear to be no serious steric problems between the trindane wingtips and the methyls of the $P(OMe)_3$ ligand. However, the crystal packing diagram shows a weak intermolecular interaction (2.771 Å) between terminal chlorine Cl(1) and H(3a) of a neighbouring trindane; the same chlorine also shows a weak interaction (2.823 Å) with H(12d), a hydrogen atom in the methoxy region of yet another molecule. The former is reminiscent of the situation in $[\{(toluene)Ru\}_2Cl_3]BF_4$.[86]

Nevertheless, the NMR spectra of **28** are not without their interesting features. The ^1H NMR spectrum of the trindane portion of **28** appears as Figure 3.7 and reveals that the ^{31}P nucleus clearly couples to the benzylic protons; $^4J_{P\text{-}H(exo)}$ = 3.8 Hz and $^4J_{P\text{-}H(endo)}$ = 1.5 Hz. Phosphorus decoupling of the ^1H spectrum yields a "conventional" trindane spectrum in which the *exo* and *endo* protons are readily assignable. The fully coupled ^{31}P spectrum is broad and featureless; presumably it is a 490 line multiplet made up of septets of septets of decets. Selective irradiation of the *exo*-benzylic protons removes the $^4J_{P\text{-}H}$ 3.8 Hz coupling but leaves the smaller 1.5 Hz septet; the net result (Figure 3.8) is a slightly broadened 1:9:36:84:126:126:84:36:9:1 decet attributable to coupling to the three equivalent methyl groups.

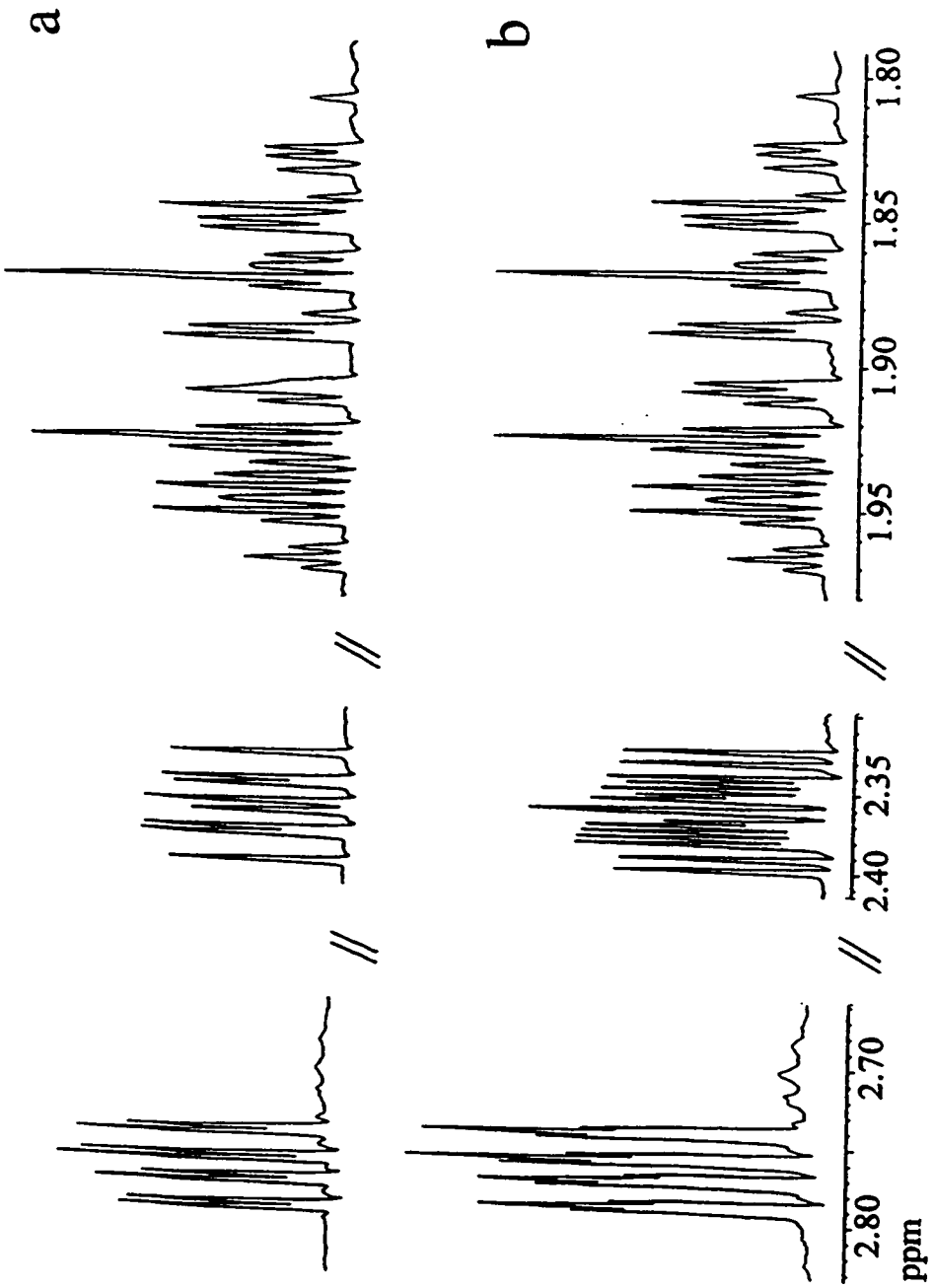

Figure 3.7: Proton NMR (500 MHz, CD_2Cl_2) spectrum of the trindane region of **28**: (a) ^{31}P decoupled and (b) ^{31}P coupled.

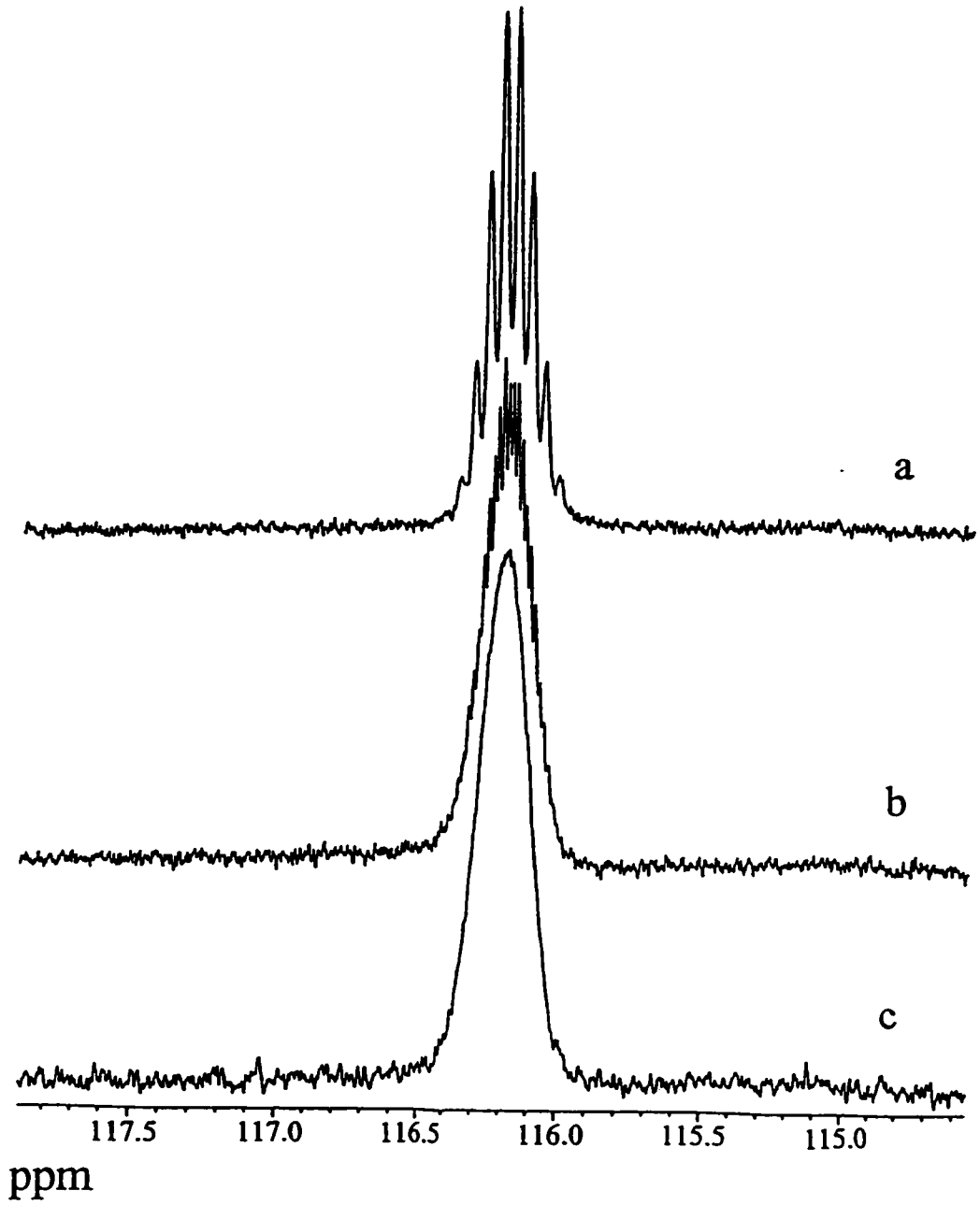

Figure 3.8: 202 MHz ^{31}P NMR spectrum of **28** in CD_2Cl_2 with selective decoupling of (a) the *endo* equatorial benzylic protons, (b) the *exo* axial benzylic protons, and (c) fully coupled.

3.5 Summary and Continuation of This Work

In conclusion, $[(\text{trindane})RuCl_2]_2$, **25**, readily ionises to alleviate the steric crowding caused by the proximity of a terminal chlorine in the other half of the dimer. Cleavage of the chloro-bridge with trimethyl phosphite gives $(\text{trindane})RuCl_2[P(OMe)_3]$, **28**. Treatment of **25** with excess trindane in the presence of $AgBF_4$ yields the dicationic sandwich compound $[(\text{trindane})_2Ru]^{2+}\ 2BF_4^-$, **3**. The chemistry of this molecule, with respect to derivatisation at the benzylic sites, remains to be investigated.

Other experiments with regard to the chemistry of trindane and its possible use as the backbone of a starting material to larger hydrocarbons, e.g. C_{30} molecules, are currently under investigation by another member of this research group.

Chapter 4

Ruthenium Complexes of Hexaethylbenzene

4.1 Prelude

In a continuation of the investigation of ruthenium-arene chemistry, this section provides the results of an examination of the structure and solution dynamics of several new ruthenium-hexaethylbenzene (HEB) complexes.[88] The use of the combination of their NMR spectra and X-ray crystal structures provides an intriguing picture of the behaviour of these fluxional systems. The contributions of the author to this work include the characterisation of these complexes and writing portions of the manuscript in preparation.

4.2 Goals of the Project

As previously mentioned, molecules of the type $[(arene)RuCl_2]_2$ are generally prepared by the replacement of cymene in $[(cymene)RuCl_2]_2$;[3] this latter system is readily available by reaction of $RuCl_3$ with dipentene, an inexpensive diene.[80] In Chapter 3 the synthesis, X-ray crystal structure and variable-temperature NMR data of $[(trindane)RuCl_2]_2$, **25**, which appears to dissociate in polar solvents into $[(trindane)_2Ru_2(\mu\text{-}Cl)_3]^+ Cl^-$, **27**,[33] were discussed. Although trindane is a hexa-alkylated arene, and bears a superficial resemblance to hexaethylbenzene, it lacks the subtle stereochemical probes for molecular symmetry that HEB can, in principle, provide.

The objective was to synthesise a number of ruthenium-hexaethylbenzene complexes in order to study their solid state structures, and discern how differing ligands might affect (i) hexaethylbenzene conformation and (ii) dynamic processes within each molecule. In this chapter the syntheses, NMR spectra and X-ray crystal structures of a series of $(C_6Et_6)RuCl_2L$ complexes are described, and a discussion of how the ^1H and ^{13}C NMR spectra of the HEB ligands correlate with the solid state structures of these molecules is presented.

4.3 Introduction

4.3.1 Conformations and Dynamics of Hexaethylbenzene

Hexaethylbenzene (HEB), **7**, is a conformationally versatile ligand. When bonded to organometallic fragments, such as $Cr(CO)_3$,[89] $Fe(C_5H_5)^+$,[90] or $Mo(CO)_3Cl^+$,[91] the ethyl groups can adopt a variety of conformational patterns.[92] The favoured structure – and the one found for the free ligand[93,94] – is the 1,3,5-*distal*-2,4,6-*proximal* isomer exemplified by $[(HEB)Cr(CO)(CS)NO]^+$, **29**, shown in Figure 4.1.

This particular system, which possesses a chiral tripod, was specifically designed to probe the molecular dynamics of both the HEB ligand and also the ML_3 fragment.[95] In the series (HEB)Cr(CO)L′L″, where L′ and L″ are CO, CS or NO^+, the ethyl groups exhibit uncorrelated *proximal-distal* exchange with a $\Delta G^{\ddagger}$ (free energy) value of ≈11.5 kcal mol^{-1}.[94-96] In contrast, tripodal rotation has a markedly lower barrier (≈ 9.5 kcal mol^{-1}).[95,96] These studies are complemented by previous work on (pentaethylacetophenone)$Cr(CO)_3$,[97] and also by an elegant series of experiments by Siegel, who independently measured the alkyl and

tripodal rotation barriers in 1,4-bis(4,4-dimethyl-3-oxopentyl)-2,3,5,6-tetraethylbenzene and its tricarbonylchromium complex.[98]

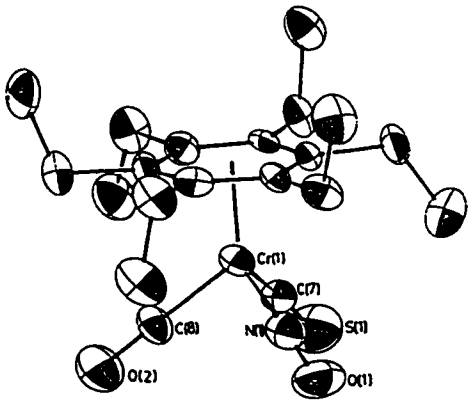

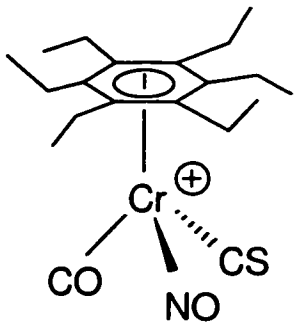

Figure 4.1: Representation of $[(HEB)Cr(CO)(CS)NO]^+$, **29**, showing the alternating distal and proximal ethyl groups.

The relative energies of the conformations of hexaethylbenzene have been computed; these are depicted in Figure 4.2 together with the labelling scheme originally used by Mislow *et al.*[94] These differing conformations are observed in many complexes. It has been shown, for example, that in the molecules $(HEB)Cr(CO)_2(PR_3)$, there is a clear correlation between the size of the phosphine and the ratio of *distal* to *proximal* ethyl substituents, such that as phosphine size increases, there is an increasing number of distal substituents. Thus, X-ray crystallographic data for the complexes $(HEB)Cr(CO)_2(PMe_3)$,[99] $(HEB)Cr(CO)_2(PEt_3)$,[100] and $(HEB)Cr(CO)_2(PPh_3)$[94] yield structures **(c)**, **(e)** and **(h)**, respectively.

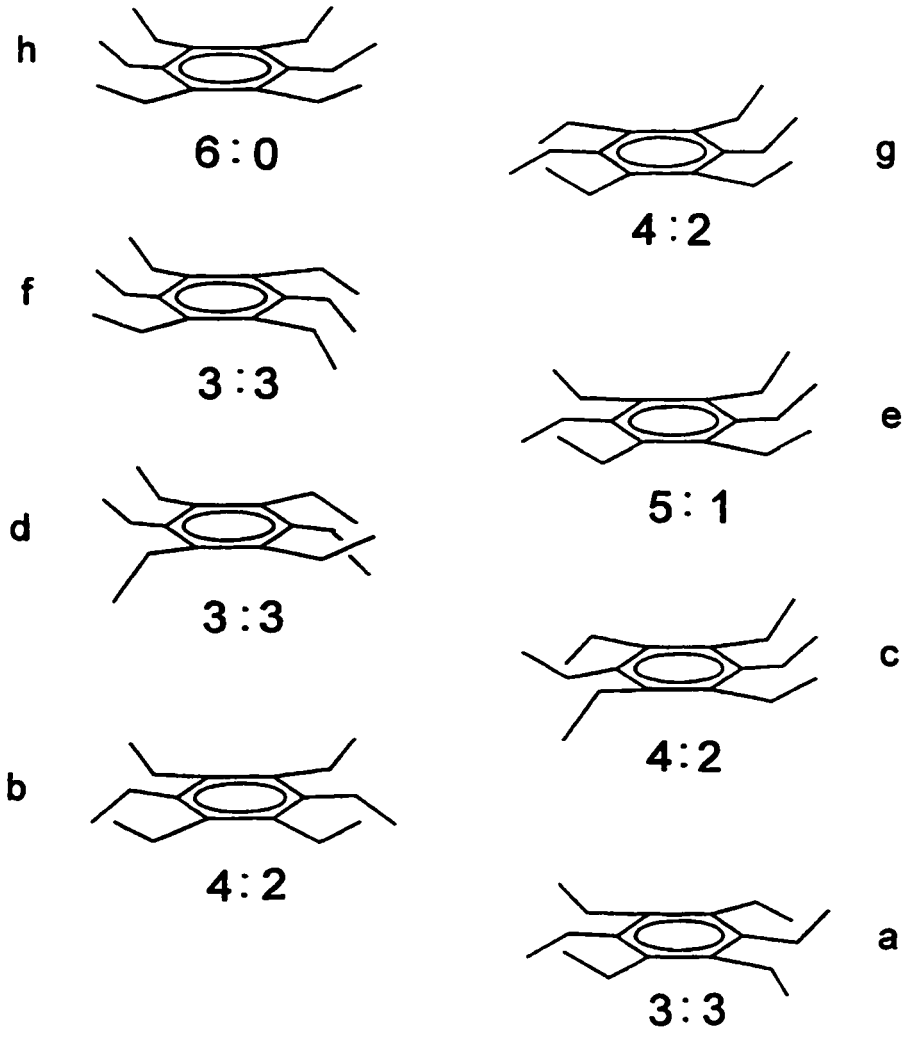

Figure 4.2: The eight isomers of hexaethylbenzene (7), arranged in order of increasing relative energy (as calculated by Mislow *et al.*).

4.3.2 The Use of NMR Spectroscopy and X-Ray Crystallography for Determining Conformations

Nuclear magnetic resonance spectroscopy (both ^{1}H and ^{13}C) provides a convenient probe for the symmetry of (HEB)ML_n complexes. For example, Flood's low-temperature NMR measurements have shown that protonation of a series of (arene)$Cr(CO)_2PR_3$ complexes leads to a square-based pyramidal structure for the corresponding $[(arene)Cr(CO)_2(PR_3)H]^+$ systems;[101] likewise, protonation of $(C_6H_5OMe)Cr(CO)_3$ yields a 2:1 pattern for the ^{13}CO resonances.[102] Since the X-ray crystal structure of $[(HEB)Mo(CO)_3Cl]^+$ $[MoCl_6]^-$, **30**, reveals that the ML_4 moiety is square pyramidal and that the hexaethylbenzene ligand adopts conformer **(b)**,[91] one might have anticipated a similar arrangement of ethyls for $[(HEB)Cr(CO)_3H]^+$, **31**. However, the ^{1}H and ^{13}C NMR data for **31** show unambiguously that the ethyls adopt the 1,3,5-*distal*-2,4,6-*proximal* conformation **(a)** of Fig. 4.2, indicating that the proton has attacked along the three-fold axis of the molecule.[103] For example, the ^{13}C NMR spectra show that the singlets observed for the arene ring, methylene and methyl carbon atoms in the room temperature spectra are each split into two equally intense environments at low temperature.

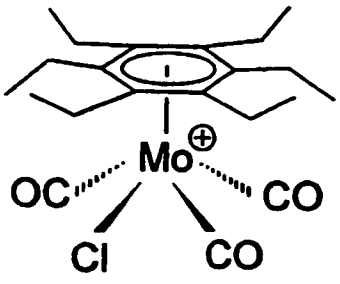

30

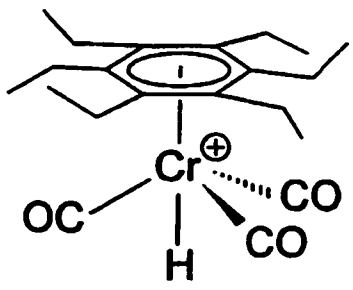

31

4.4 Results and Discussion

4.4.1 $[(HEB)RuCl_2]_2$

When $[(cymene)RuCl_2]_2$ and hexaethylbenzene were melted together at 170 °C, a product **32**, with empirical formula $(C_6Et_6)RuCl_2$, was obtained. Despite numerous attempts to acquire an acceptable X-ray data set, the only available crystals of **32** were of marginal quality, and it has not yet proven possible to solve the structure. Consequently, the identity of **32** as $[(HEB)RuCl_2]_2$, or as $[(HEB)_2Ru_2(\mu\text{-}Cl)_3]^+$ Cl^-, in the solid state remains an open question. However, the ^1H and ^{13}C NMR spectra of **32** in CD_2Cl_2 reveal the presence of two equally populated ethyl environments at low temperature (Figures 4.3 and 4.4). The ^1H NMR spectra show that the quartet at 2.53 ppm, and triplet at 1.42 ppm, observed in the 30°C spectrum, are split, respectively, into broad singlets at (2.57, 2.27) ppm and (1.40, 1.22) ppm at –90°C. The ^{13}C spectra show that singlets observed for the arene (94.23 ppm), methylene (20.47 ppm) and methyl (14.12 ppm) carbon atoms are each split into two environments

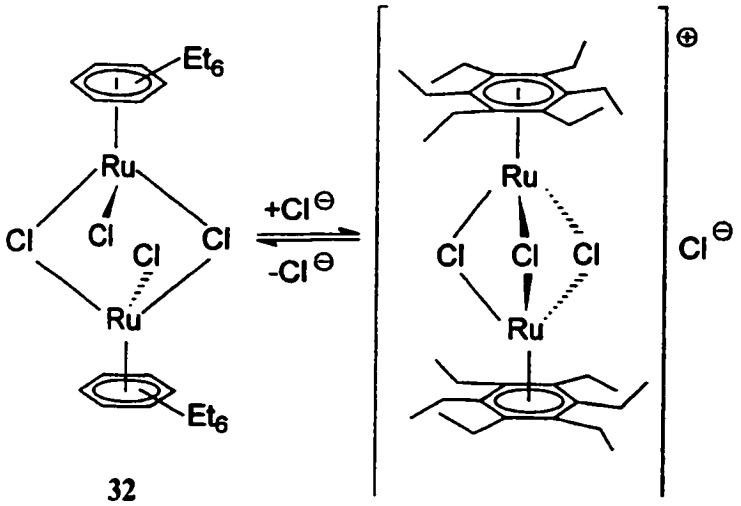

32

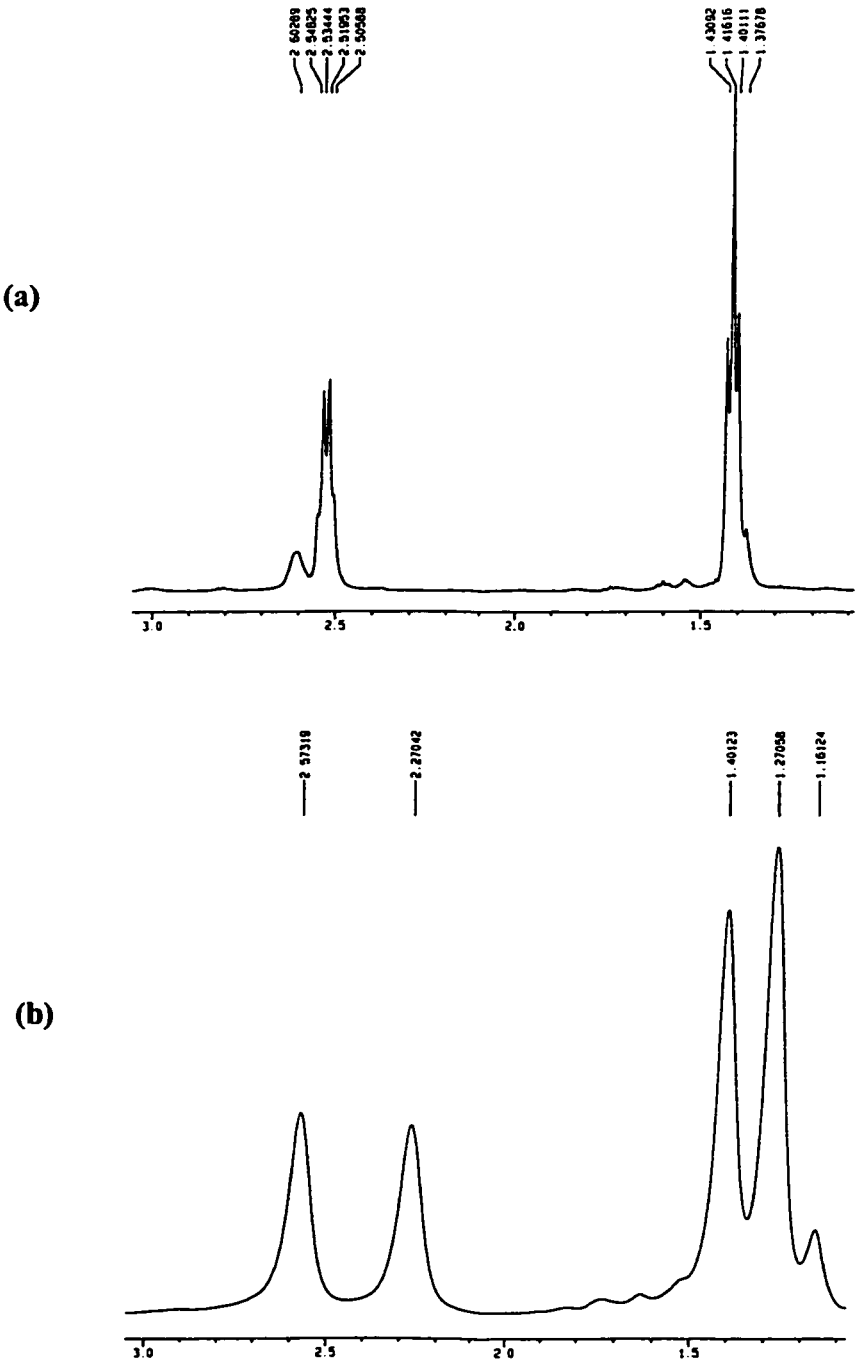

Figure 4.3: Proton NMR spectrum of **32**, at (a) 30°C and (b) –90°C, showing the two equally populated ethyl environments.

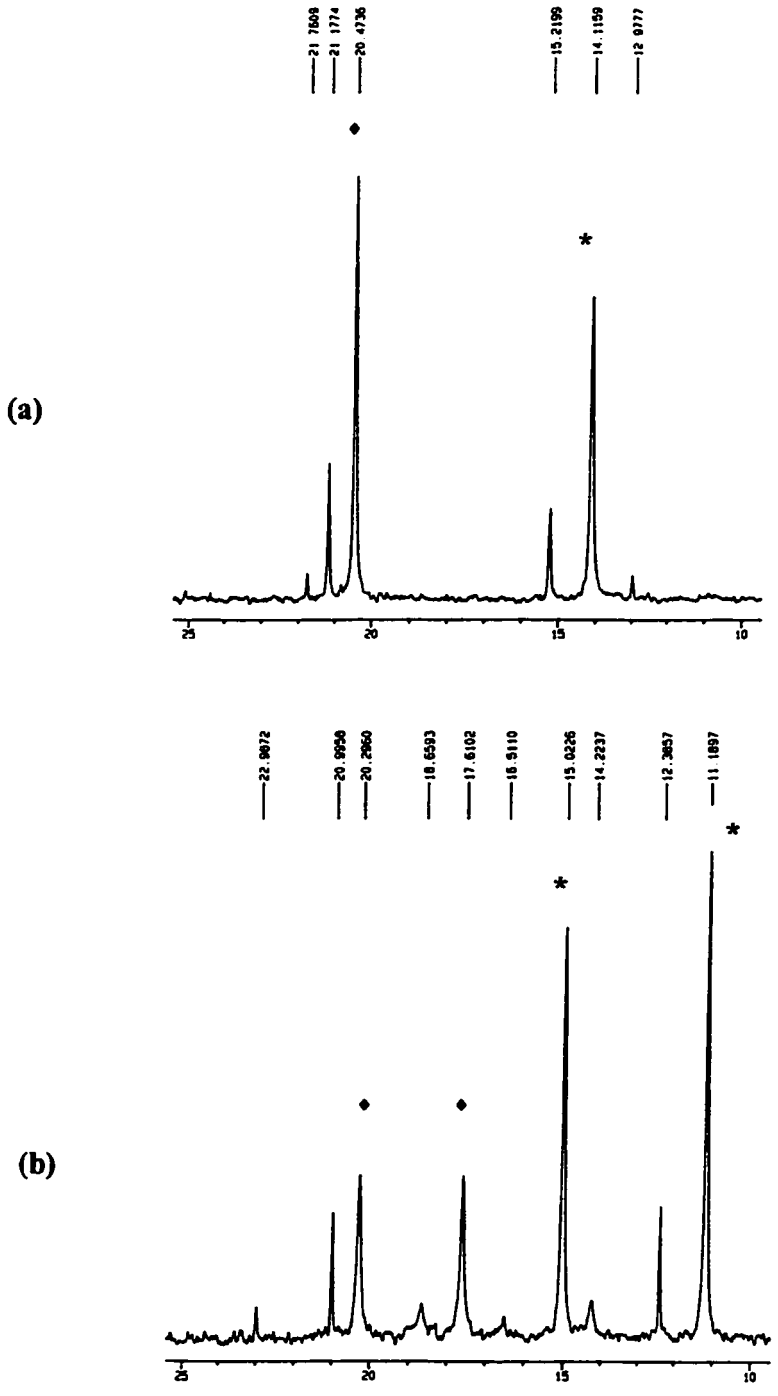

Figure 4.4 Carbon-13 NMR spectrum (ethyl region) of **32**, at (a) 30°C and (b) –90°C, showing the split of the ethyl CH_2 (♦) and CH_3(*) carbon signals into two equally populated environments.

(99.11, 85.09; 20.29, 17.61; 15.02, 11.19 ppm, respectively) at –90°C. The coalescence behaviour of these HEB resonances is entirely reminiscent of the previously discussed systems that adopt the 1,3,5-*distal*-2,4,6-*proximal* conformation; the calculated $\Delta G^{\ddagger}$ value of 11.5 ± 0.4 kcal mol^{-1} is in the normal range for such ethyl rotation barriers. It is therefore concluded that **32** exists in solution as $[(HEB)_2Ru_2(\mu\text{-}Cl)_3]^+Cl^-$, and that the arene adopts conformation **(a)**.

4.4.2 $[(HEB)_2Ru_2(\mu\text{-}Cl)_3]^+ [C_5(CO_2Me)_5]^-$

To determine whether this same structure could be found in the solid state, **32** was treated with the potassium salt of penta(carbomethoxy)cyclopentadienide, $K[C_5(CO_2Me)_5]$.[104] Removal of KCl and recrystallisation from hexane yielded X-ray quality crystals of $[(HEB)_2Ru_2(\mu\text{-}Cl)_3]^+ [C_5(CO_2Me)_5]^-$, **33**. The NMR spectra of **33** in the ethyl region parallel exactly the behaviour of **32**, confirming the presence of the triply-bridged species in solution in both cases. The X-ray crystal structure of the cation of **32** appears as

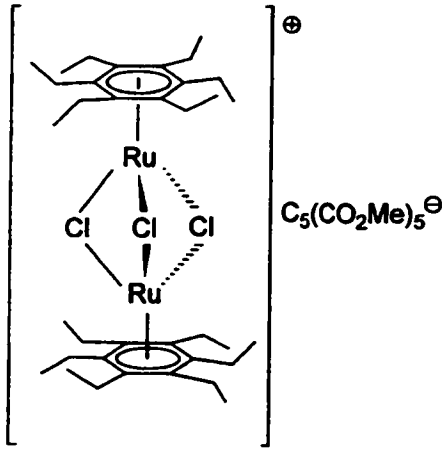

33

Figure 4.5. The cation has effective D_{3h} symmetry in which each HEB ligand adopts the alternating *proximal-distal* arrangement of ethyls such that the three bridging chlorines eclipse *distal* substituents and so minimise steric interactions. Figure 4.6 shows the eclipsed orientation of the chlorine tripod with respect to the distal ethyl groups in the hexaethylbenzene rings. The ruthenium–arene centroid distance of 1.648 Å is comparable to that observed in systems such as $[(arene)_2Ru_2(\mu\text{-}Cl)_3]^+$, where the arene is benzene, toluene or cymene.[105] Interestingly, in $[(\eta^6\text{-benzene})_2Ru_2(\mu\text{-}Cl)_3]^+$ the $RuCl_3$ tripod is staggered with respect to the benzene ligand, while in $[(\eta^6\text{-cymene})_2Ru_2(\mu\text{-}Cl)_3]^+$ the Cl atoms eclipse arene C atoms. As predicted by molecular orbital calculations at the extended Hückel level,[105a] the methylene substituents are bent slightly towards the metal atoms (an average of 2.5° for distal ethyl and 0.5° for proximal ethyl groups); this enhances the overlap between the arene π-manifold and the ruthenium *d* orbitals. The bend is not as significant as the 6° bend observed in $[(\eta^6\text{-benzene})_2Ru_2(\mu\text{-}Cl)_3]^+$.[105a] The average Ru-Cl distance in **33** is 2.442 Å, and the average Ru-C(arene) distance is 2.183 Å; these distances are similar to those observed, for example, for $[(trindane)RuCl_2]_2$, **25**. The average Ru-Cl distance is similar to that observed for the other arene systems mentioned above, however the average Ru-C(arene) distance is slightly longer than the average distance observed in $[(\eta^6\text{-benzene})_2Ru_2(\mu\text{-}Cl)_3]^+$ (2.163 Å, 2.160 Å) and $[(\eta^6\text{-cymene})_2Ru_2(\mu\text{-}Cl)_3]^+$ (2.168 Å).[105]

The carboxylate anion in the structure of **33** is highly disordered, as is sometimes the case for this isolated anion in crystal structures,[106] and it has not proved possible to determine its rigid conformation in the solid state structure. In the packing diagram shown in Figure 4.7, however, it is possible to see that the anions and cations form alternating layers, as is seen for

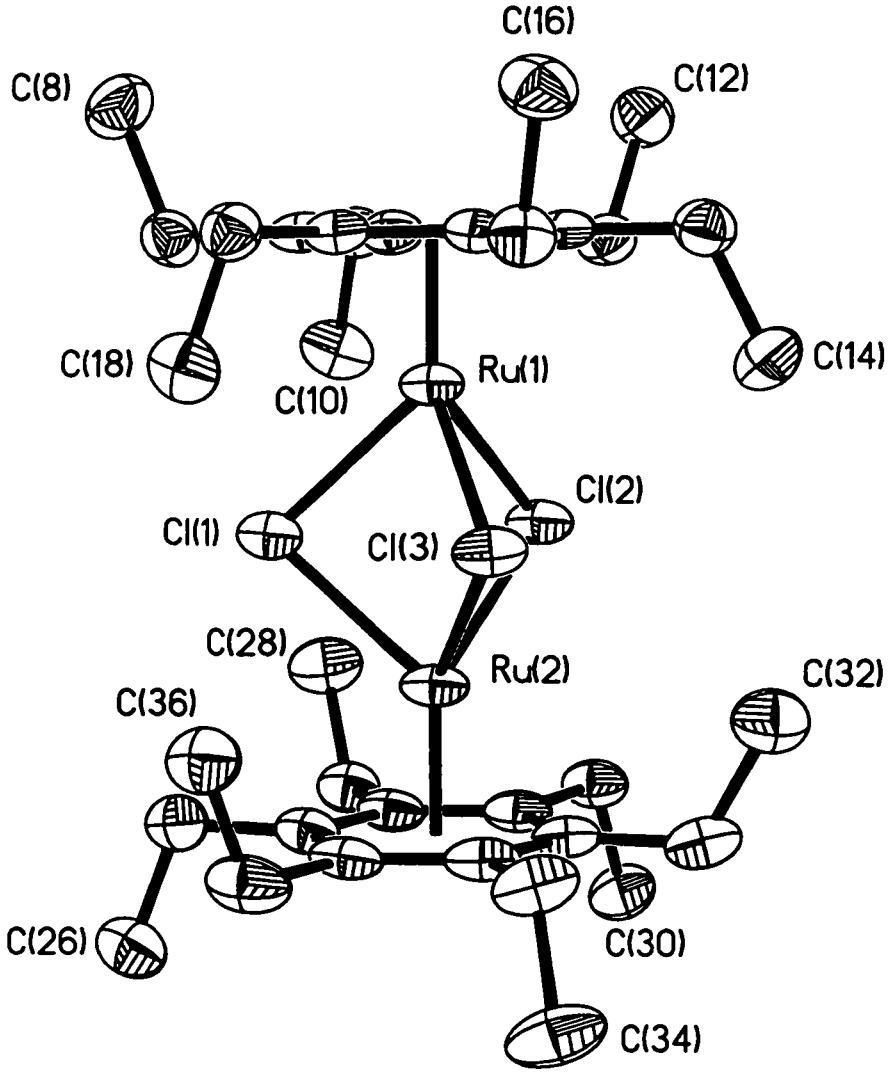

Figure 4.5: Molecular structure of **33**, showing the alternating proximal and distal ethyl groups. Thermal ellipsoids are shown at the 50% probability level. Hydrogen atoms are omitted for clarity.

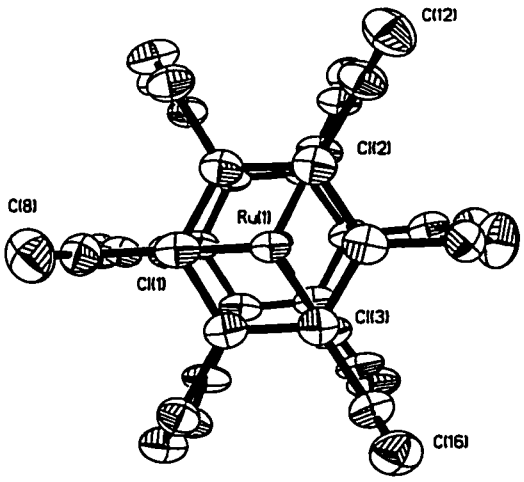

Figure 4.6 Eclipsed tripod of Cl atoms with respect to distal ethyl groups, labelled, for one HEB ring, by C(8), C(12) and C(16), for **33**. Hydrogen atoms are omitted for clarity.

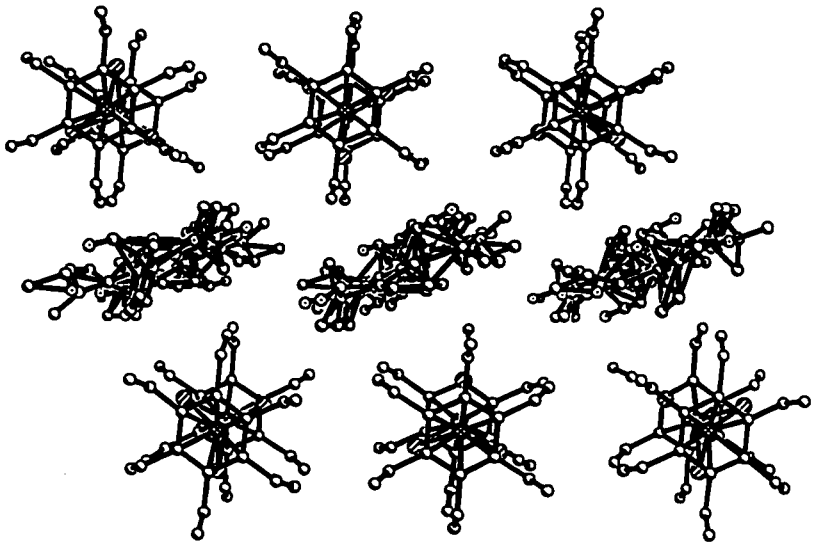

Figure 4.7: Crystal packing diagram for **33**, showing the alternating layers of [(HEB)Ru-μCl_3-Ru(HEB)]$^+$ cations with disordered $[C_5(CO_2Me)_5]^-$ anions. Hydrogen atoms are omitted for clarity.

$[C_7H_7]^+[C_5(CO_2Me)_5]^-$.[106] The program PLATON[107] was used to subtract the averaged diffractional contribution of the disordered $[C_5(CO_2Me)_5]^-$ anion from the X-ray intensity data collected for **33**. This allowed a more accurate determination of the structure of the $[(HEB)Ru\text{-}\mu Cl_3\text{-}Ru(HEB)]^{2+}$ cation. The crystal packing of the cations also shows that they are arranged in layers such that intermolecular contacts between the *distal* ethyls are minimised (as shown in Figure A1, Appendix 2).

4.4.3 $[(HEB)Ru(H_2O)_3][BF_4]_2 \cdot H_2O$

As discussed in Chapter 3, the sandwich cation $[(trindane)_2Ru]^{2+}$, **23**, was prepared by treatment of $[(trindane)RuCl_2]_2$ (**25**) with $AgBF_4$ in acetone; the presumed intermediate, $[(trindane)Ru(acetone)_3]^{2+}$, reacted with excess trindane to yield the bis(arene)Ru dication. Interestingly, the $[(arene)Ru(solvent)_3]^{2+}$ structure type is rare. One such molecule for which a crystal structure has been reported is $[(1,3,5\text{-}C_6H_3Me_3)Ru(acetone)_3][BF_4]_2$ in which two of the acetone molecules have coupled.[108]

In an attempt to prepare $[(HEB)_2Ru]^{2+}$, "$(C_6Et_6)RuCl_2$", **32**, was treated with $AgBF_4$ in acetone. The reaction yielded a crystalline material, **34**, whose ^1H and ^{13}C NMR spectra are entirely consistent with a molecule possessing three-fold symmetry; once again, at low temperature the familiar pattern of alternating *proximal* and *distal* ethyls is apparent. As shown in Figure 4.8, the product was characterised by X-ray crystallography as $[(C_6Et_6)Ru(H_2O)_3][BF_4]_2 \cdot H_2O$. In **34**, the cation possesses an almost ideal C_{3v} symmetry in which the HEB ligand adopts conformation **(a)** of Figure 4.2 – the 1,3,5-*distal*-2,4,6-*proximal* arrangement – where each water ligand is partially encapsulated by two ethyl

groups. Figure 4.9 shows the cation, with the alternating distal and proximal ethyl groups, while Figure 4.10 shows the eclipsed tripod of oxygen atoms with respect to the distal ethyl groups. In the closely related structure of $[(\eta^6\text{-benzene})Ru(H_2O)_3^{2+}]$ the RuO_3 tripod is staggered with respect to the benzene ligand.[109]

The ruthenium–arene centroid distance of 1.650 Å in **34** is in the expected range, and while the average Ru-C(arene) distance of 2.183 Å is very similar to that seen in **33**, it is slightly longer than that observed in $[(\eta^6\text{-benzene})Ru(H_2O)_3^{2+}]$ (2.164 Å). The average Ru-O distance of 2.145 Å in **34** is also longer than the 2.127 Å observed in $[(\eta^6\text{-benzene})Ru(H_2O)_3]^{2+}$.

There is extensive hydrogen bonding observed in the packing diagram for **34**, such that H_2O ligands bonded to Ru have contacts to F atoms of BF_4^- anions, and also to lattice H_2O molecules. The lone H_2O of crystallisation also has contacts to BF_4^- anions. For example, in one layer, one lattice solvent H_2O has contacts through its H atoms to two neighbouring BF_4^- anions, such that "O-H_a" = 0.966 Å, and "H_a---F_1" = 1.889 Å, while the contact O-F_1 is 2.742 Å. For the other H, O-H_b = 0.822 Å, H_b---F_2 = 1.934 Å, such that the O-F_2 contact is 2.733 Å. This oxygen atom also shows contact to a closeby H_2O bonded to a ruthenium atom, with O---H' = 1.748 Å, and an O---O' contact of 2.616 Å. Some BF_4^- anions also show a long contact to an H atom of a CH_2 from a neighbouring distal ethyl group (e.g. F---H = 2.539 Å). Layers of the contacts described above persist throughout the structure. A partial picture of these interactions is given in Figure A2 (Appendix 2).

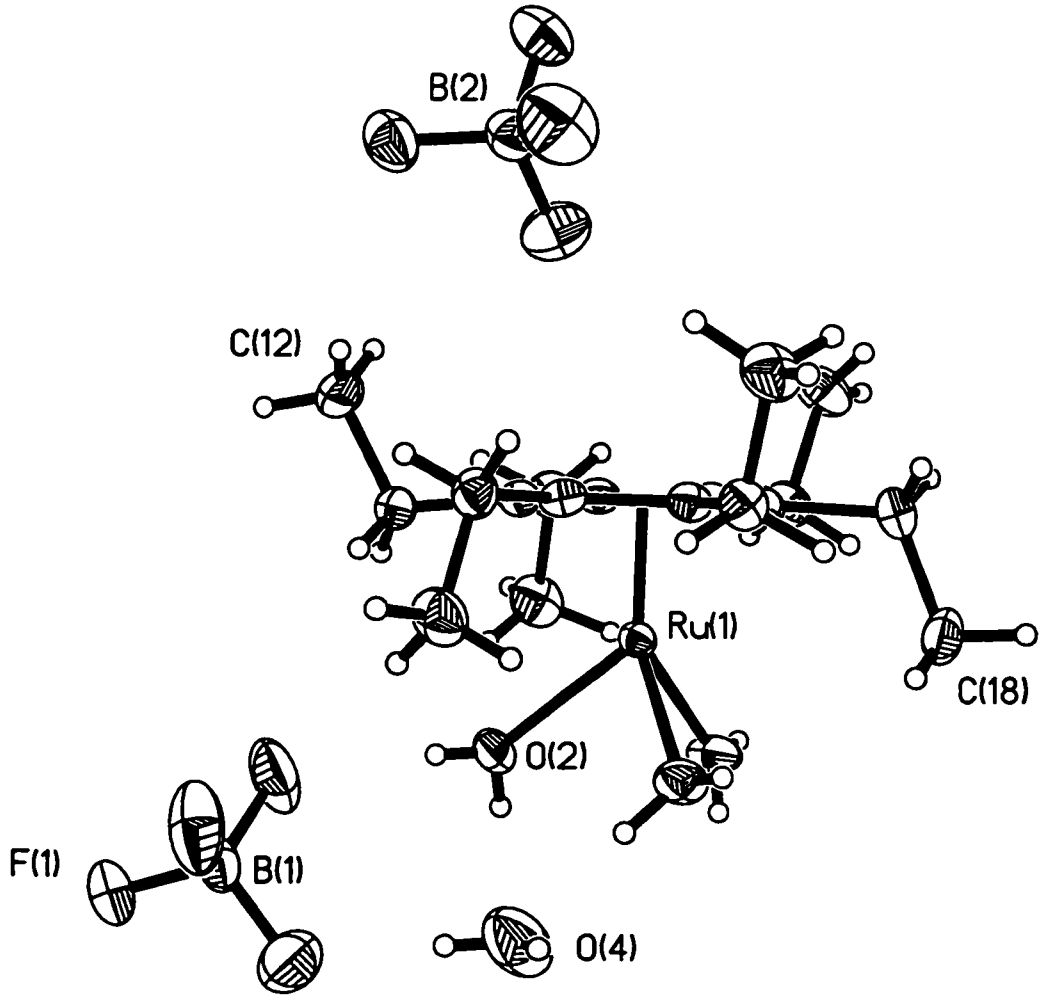

Figure 4.8: X-ray crystal structure of $[(C_6Et_6)Ru(H_2O)_3][BF_4]_2 \cdot H_2O$, **34**. Thermal ellipsoids are shown at the 50% probability level. Hydrogen atoms are shown at an arbitrarily selected size.

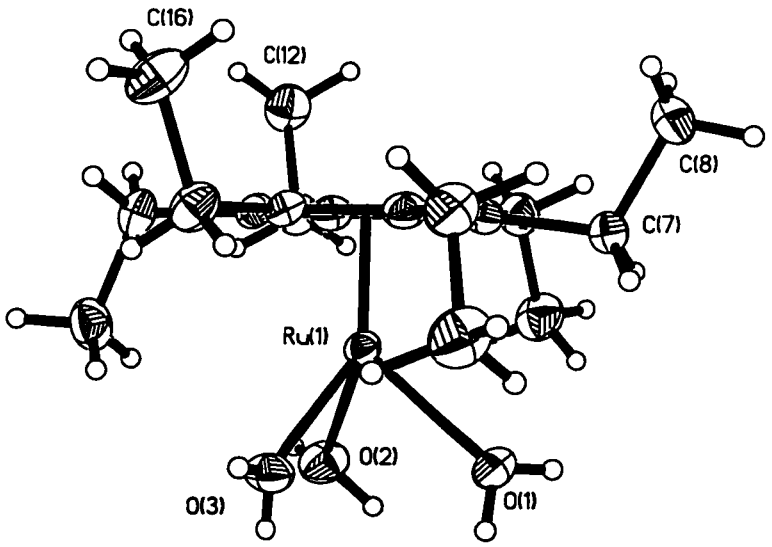

Figure 4.9: View of the $[(HEB)Ru(H_2O)_3]^{2+}$ cation of **34**, showing the 3 : 3 distal : proximal ethyl group configuration of the HEB ligand.

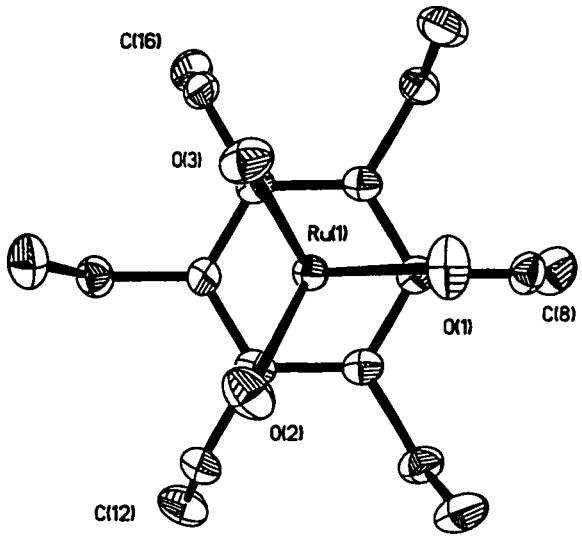

Figure 4.10: View of the $[(HEB)Ru(H_2O)_3]^{2+}$ cation of **34**, showing the tripod of O atoms eclipsing the distal ethyl groups (the distal CH_3 groups labelled as C(8), C(12) and C(16)). Hydrogen atoms are omitted for clarity.

4.4.4 Synthesis and Characterisation of Phosphine Derivatives

To test the steric limits of the (HEB)RuL_n system, **32** was treated with trimethyl phosphite and trimethylphosphine to give (HEB)$RuCl_2[P(OMe)_3]$, **35**, and (HEB)-$RuCl_2(PMe_3)$, **36**, respectively. The ^1H and ^{13}C NMR spectra of both complexes exhibited only a single ethyl environment, even at low temperature. This result suggested that neither molecule possessed the alternating *proximal-distal* arrangement **(a)**. On the basis of the relative cone angles of $P(OMe)_3$ (107°) and PMe_3 (118°),[110] one might have predicted that the phosphine complex, **36**, would tend to have the greater number of *distal* ethyl substituents, and this is indeed the case. As shown in Figure 4.11, (HEB)$RuCl_2[P(OMe)_3]$, **35**, prefers isomer **(e)**, in which there is a single *proximal* ethyl substituent. For (HEB)$RuCl_2(PMe_3)$, **36**, a satisfactorily complete refinement of the crystal data has not yet proved possible, however, a preliminary picture of the structure shows that the HEB ligand adopts the "all-*distal*" conformer **(h)**, as seen in Figure 4.12.

The single *proximal* ethyl in (HEB)$RuCl_2[P(OMe)_3]$, **35**, is the one furthest from the relatively bulky phosphite ligand; the structure is analogous to that of $(C_6Et_6)Cr(CO)_2(PEt_3)$, which likewise exhibits the 5:1 *distal*-to-*proximal* ratio.[100] The ruthenium-arene centroid distance is 1.717 Å, with an average Ru-C(arene) distance of 2.233 Å; the average Ru-Cl distance is 2.414 Å, while the Ru-P distance is 2.270 Å. These values agree very closely with those observed for the structure of (trindane)$RuCl_2[P(OMe)_3]$, **28**.

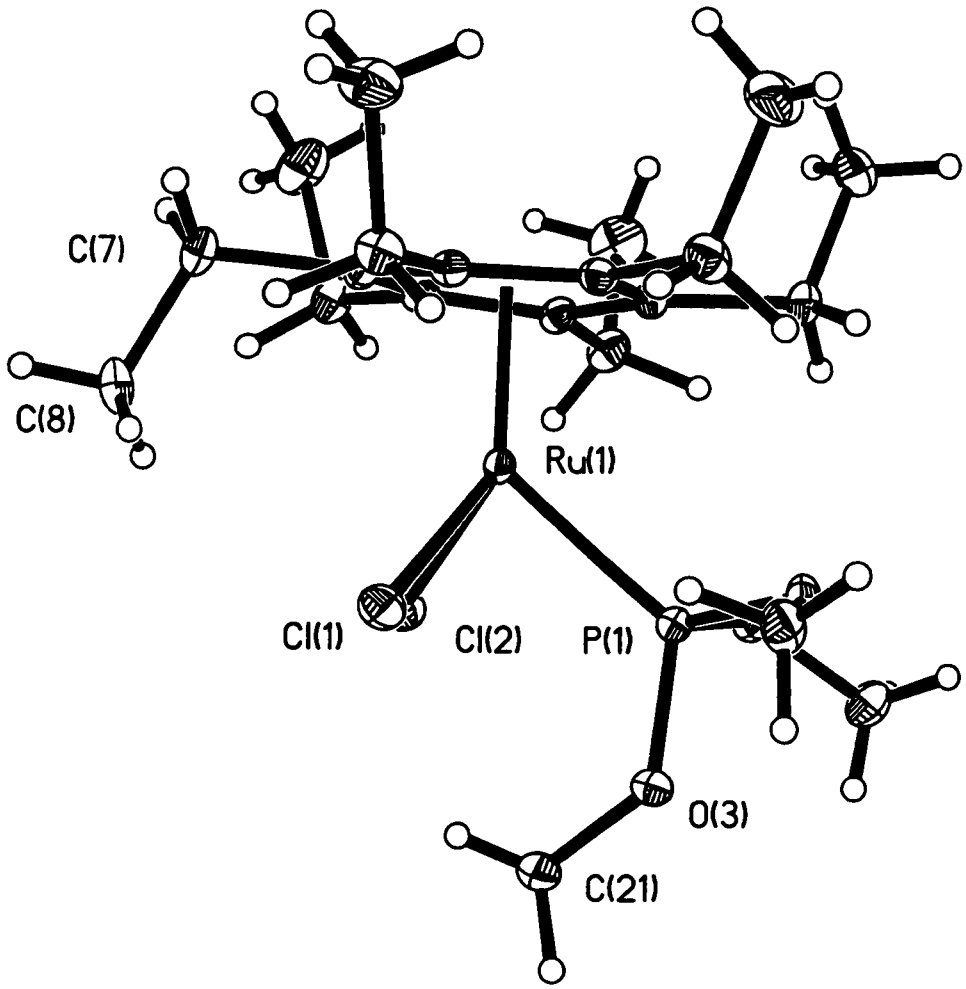

Figure 4.11: X-ray crystal structure of **35**; the ethyl groups are oriented in a 5 : 1 distal : proximal ratio. Thermal ellipsoids are shown at the 50% probability level, and hydrogen atoms are shown at an arbitrarily selected size.

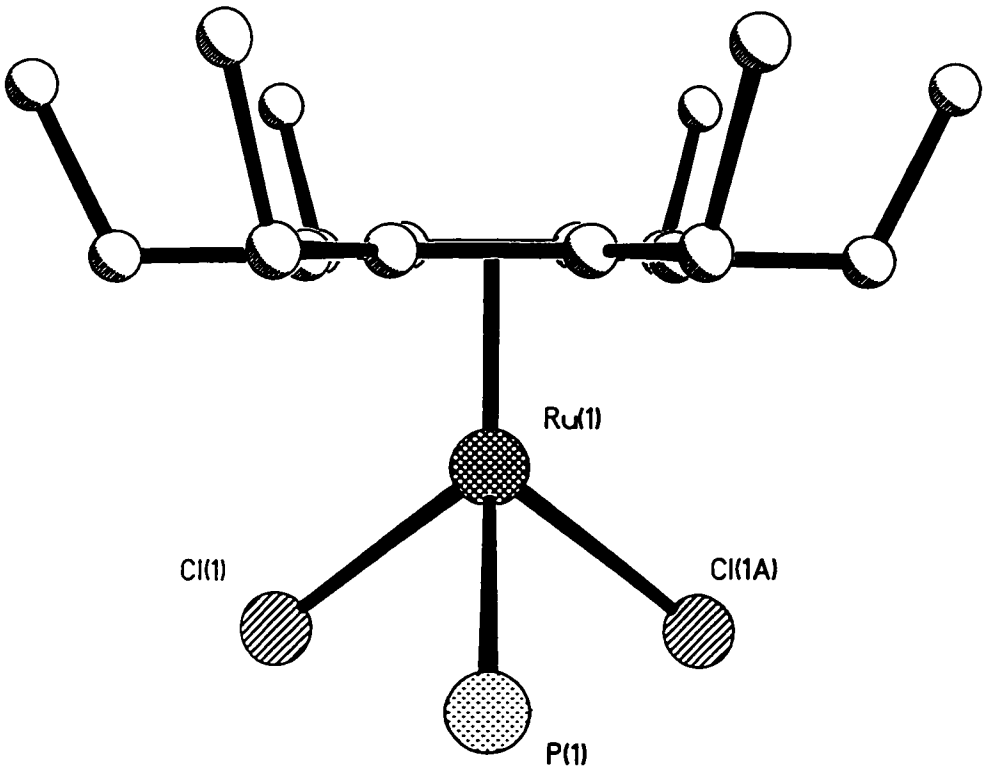

Figure 4.12: Preliminary picture of the molecular structure of **36** showing the HEB ligand and the $RuCl_2P$ tripod; all ethyl groups are distal to the metal moiety.

In **36**, the preliminary data suggest that the $RuCl_2(PMe_3)$ tripod is staggered with respect to the HEB ring, like the pattern found in $(C_6Et_6)Cr(CO)_2(PPh_3)$, which also adopts conformation (h).[94] The orientations of the $RuCl_2(PR_3)$ tripods with respect to the HEB ligands are illustrated in Figures 4.13 and 4.14. Interestingly, the trimethyl phosphite ligand in **35** crystallises in a propeller conformation rendering the molecule chiral; in contrast, in $(C_6Et_6)Cr(CO)_2(PEt_3)$ the Et_3P ligand lies in a molecular mirror plane.[100] The preliminary structural features of **36** are similar to those reported for other (arene)$RuCl_2PR_3$ systems.[111] Interest in related systems of the type (*p*-cymene)$RuCl_2PR_3$ stems from their use as efficient catalyst precursors.[112]

The reaction of **32** with trimethylphosphine yielded a small quantity of a second crystalline product that was shown to be the known compound *trans*-dichloro-tetrakis(trimethylphosphine)ruthenium(II), **37**.[113] A search of the Cambridge Crystallographic Database revealed that structures containing a *trans* isomer of the type $(Me_3P)_4RuXY$ are rare, although a number of *cis* complexes have been reported.[114] Since suitable crystals were obtained, the structure was determined and appears as Figure 4.15. While the structure solves to give two independent half molecules in the asymmetric unit, the symmetry operator of the space group completes the full molecules, and the successful structure solution gives the *trans* isomer. The steric problems that arise with four equatorially disposed trimethylphosphines are immediately evident. The PMe_3 ligands undergo a tetragonal distortion such that they are displaced alternately above and below their mean plane. This type of distortion is not uncommon in phosphine complexes. The P-Ru-P angles found in each molecule are 165.86(2)° and 165.38(11) °. The non-linearity is, however,

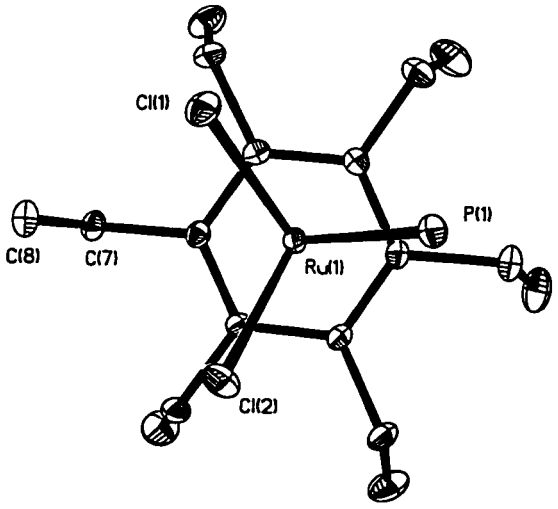

Figure 4.13: Orientation of HEB ligand with respect to $RuCl_2[P(OMe)_3]$ tripod in 35. Atoms labelled C(7) and C(8) denote the lone distal ethyl group.

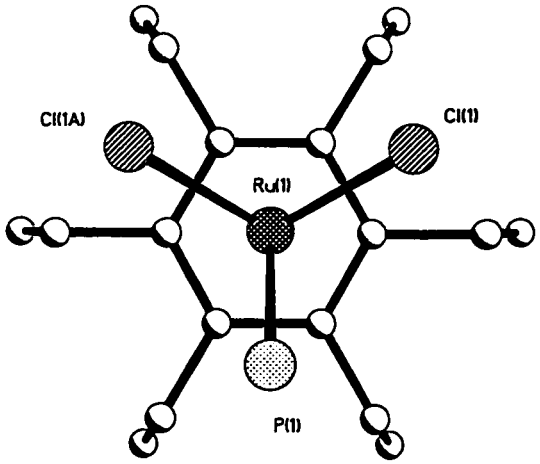

Figure 4.14: Preliminary picture of the orientation of HEB ligand with respect to $RuCl_2[P(Me)_3]$ tripod in 36.

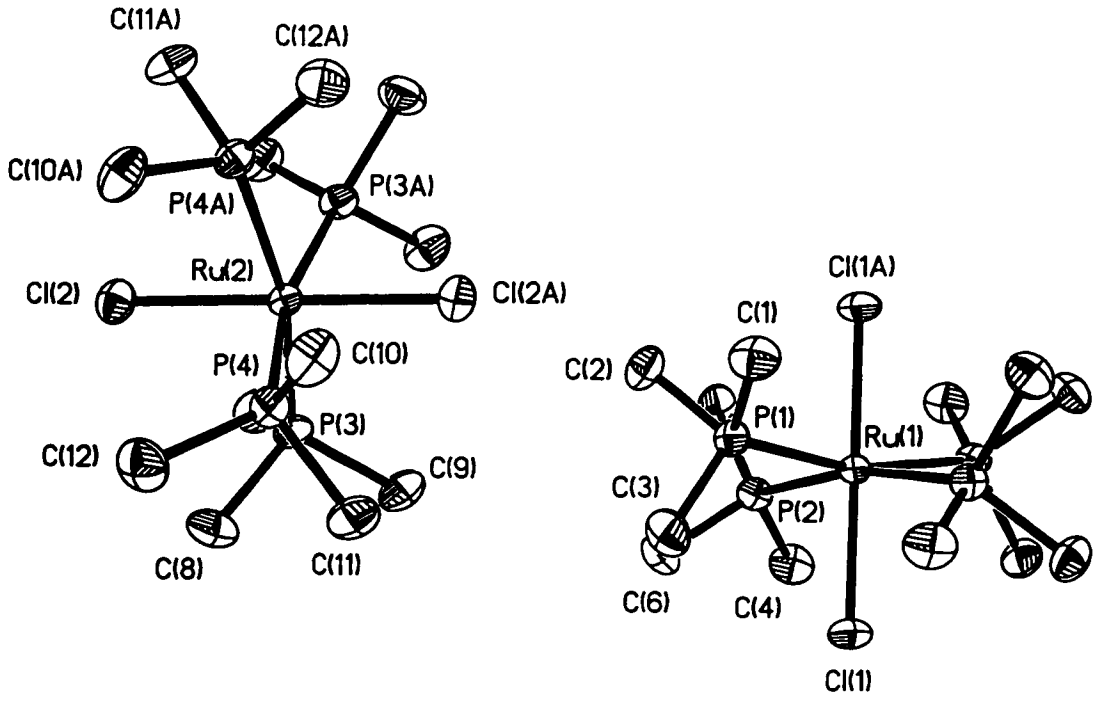

Figure 4.15: Molecular structure of **37**, showing the two independent molecules in the asymmetric unit (atoms marked "A" are generated by symmetry from the two independent half-molecules). Thermal ellipsoids are shown at the 50% probability level, and hydrogen atoms are omitted for clarity. The distortion of the opposing phosphine ligands away from 180° is visible, for example, for P(4A)-Ru(2)-P(3).

somewhat less than the corresponding P-Rh-P angles (151.46°(5) and 148.29(5)°) found in $[(Me_3P)_4Rh]^+(Cl^-)$[113], and the P-Ru-P angle (161.41°) found in *trans*-$RuH_2[(C_6H_5)P(OC_2H_5)_2]_4$[115]. Apparently, the out-of-plane distortion of the phosphines in *trans*-$(Me_3P)_4RuCl_2$, **37**, is limited by the presence of the two axial chlorine ligands. The *cis* P-Ru-P angles are close to 90° (with a range of 90.05(3) – 92.11(4)°).

In a closely related system, *trans*-$(PMe_3)_4Ru(N_3)_2$, the molecule crystallises in a lower symmetry space group. All four phosphine ligands are located individually, and there is no ambiguity between the assignment as a *cis* or *trans* isomer, since it is clearly a *trans* system. However, the P–Ru–P angles between *trans* phosphines (163.1° and 163.4°) agree very closely with those found in **37**, a fact that reinforces the structure determination presented here.

Finally, since the completion of this study, a comprehensive review of Ru-arene compounds by Bennett[116] makes passing mention of a few of the (HEB)Ru complexes mentioned herein. It will be interesting to compare the data from the compounds reported here with theirs, when they become available in the primary literature.

Attempts to determine a satisfactorily refined crystal structure solution for **36**, (HEB)$RuCl_2[P(Me)_3]$, continue.

Chapter 5

The Rearrangement Pathway in $[Cp_2Mo_2(CO)_4(RC{\equiv}C\text{-}CR_2)]^+$ Cations

5.1 Prelude

The body of this chapter first appeared as a publication in the Journal of Organometallic Chemistry.[117] It was a collaborative effort, which served to introduce this author to concepts of cluster chemistry, organometallic cations and molecular dynamics. The author's contributions include work with the X-ray crystallographic section, both database searching and correlation of X-ray structures with NMR barriers, as well as manuscript preparation. The text of the manuscript has been modified and adapted to suit the flow of this document.

5.2 Goals of the Project

The fluxional behaviour of cluster cations of the type $[Cp_2Mo_2(CO)_4(RC{\equiv}C\text{-}CR'R'')]^+$ has been widely studied by variable-temperature NMR techniques; the objective was to determine a proposed mechanism involving migration of the carbocationic centre between the organometallic vertices. The suggested mechanism has been investigated by means of extended Hückel molecular orbital (EHMO) calculations, which have allowed the evaluation of the lowest energy pathway by which this process may occur. These computations are supplemented by a Bürgi-Dunitz trajectory analysis of 11 X-ray crystal structures of such cations which yields a series of "snapshots" of the migration process. The

use of a combination of NMR, EHMO and Bürgi-Dunitz trajectory data allows one to obtain a relatively complete picture of the mechanism of migration of a vinylidene moiety over the surface of a Mo_2C triangle; these results are described herein.

5.3 Introduction

5.3.1 Criteria for the Characterisation of Fluxional Processes

Nowadays, the complete elucidation of a fluxional process generally requires: (a) an X-ray crystal structure to establish the ground-state molecular geometry; (b) the unambiguous attribution of the NMR resonances in the limiting low-temperature spectrum; (c) the identification of the nuclei which undergo site exchange – often achieved directly by means of magnetisation transfer techniques; (d) evaluation of the activation energy barrier(s) for the exchange process(es) either by simulating the peak coalescence pattern or by 2D-exchange experiments; and (e) comparison of the experimental activation energies with calculated values of the steric and/or electronic contributions to the barrier obtained by means of molecular modelling and molecular orbital methods, respectively. Such computational approaches towards evaluating the energy requirements of fluxional processes require that one select a geometrically viable mechanistic pathway through which the rearrangement can occur. Clearly, it would be advantageous if one could establish experimentally the actual trajectory followed by the migrating group.

5.3.2 The Bürgi-Dunitz Trajectory Model

In recent years, the powerful concepts developed by Bürgi and Dunitz[118] have proven to be valuable additions to the arsenal of those who wish to gain an understanding of molecular dynamics. It has been demonstrated that a succession of static X-ray structures of related molecules can give information about the dynamics of a reaction. In their now classic studies Bürgi and Dunitz showed, for example, that a series of crystal structures of systems containing both a nucleophile and an organic carbonyl group could be used to obtain the trajectory of approach of the two reagents.[119] It is clear from these data not only that the nucleophile attacks along a line making an angle of approximately 105° to the C=O bond but also that the trigonal planar sp^2 carbon atom is gradually transformed into a tetrahedral centre. The significance of these observations for mechanistic organic chemistry is profound, and it was soon exploited by Baldwin to rationalise the favourable or unfavourable nature of many ring-closure processes.[120]

Another beautiful result from Dunitz's laboratory[121] showed how the distribution of crystal structures of more than sixty $(C_6H_5)_3P$-X fragments in many different environments can be related to the "two-ring flip" mechanism by which these chiral propeller-like moieties can undergo racemisation. In this process all three phenyl rings do not rotate at the same rate nor in the same direction, and this phenomenon should be reflected in the crystallographic results which capture a series of snapshots of the Ph_3P fragment in different environments. This crystallographically derived picture of the stereoisomerisation pathway is complemented by force field calculations and variable-temperature NMR data on related Ar_3CH systems which also favour the "two-ring flip" mechanism.[122]

The ideas of Bürgi and Dunitz have been extended elegantly into the organometallic arena by Crabtree and Lavin.[123] In their study it was shown that carbonyl migration between two metal atoms proceeds *via* a trajectory in which a linear terminal carbonyl ligand proceeds through a series of increasingly more bent semi-bridging structures to a symmetrically bridging situation (Figure 5.1).

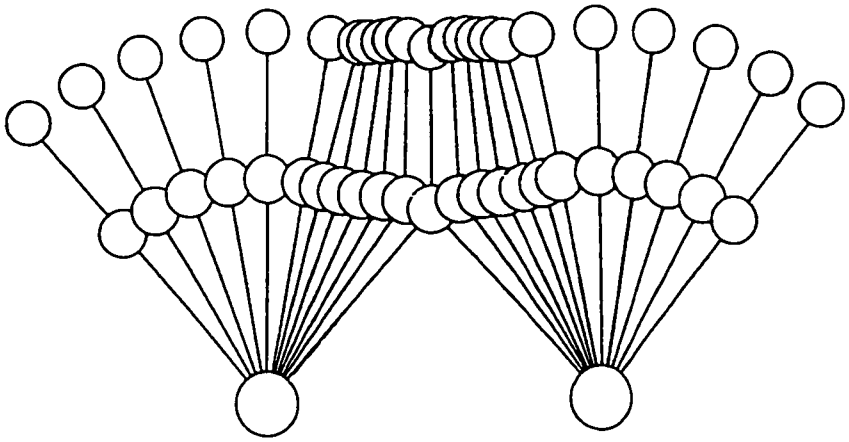

Figure 5.1: Reaction trajectory for the terminal-bridge-terminal carbonyl exchange between two iron atoms.

5.4 Results and Discussion

5.4.1 The Fluxional Behaviour of Cluster Cations, $[M_2L_n(H-C\equiv C-CH_2)]^+$

The original impetus for these studies was Seyferth's work on $[Co_3(CO)_9C-CR_2]^+$ cations for which the bent structure **38a** was proposed rather than the more symmetrical isomer **38b** with its pseudo-threefold axis.[124]

Extended Hückel molecular orbital calculations by Schilling and Hoffmann[19] provided a rationale for the favoured structure **38a**; they examined the frontier orbital interactions between a $[Co_3(CO)_9]^{3+}$ triangle and a vinylidene fragment, $[C{=}CH_2]^{2-}$,

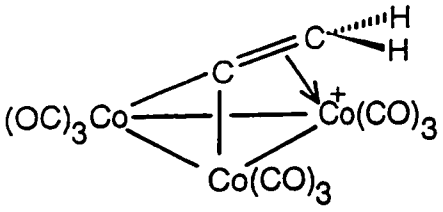

38a

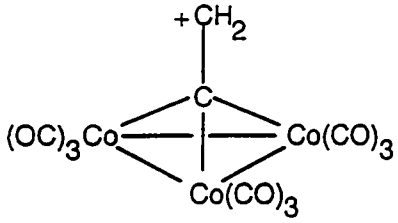

38b

and were able to show that the C_s isomer **38a** is energetically markedly preferred over the pseudo-C_{3v} structure **38b**. One can readily envisage that, by allowing the sp^2-hybridized α-carbon to lean towards a cobalt vertex, the vacant *p* orbital on carbon can accept electron density from a filled metal *d* orbital. The net result is not only enhanced stabilisation of the cationic centre, *via* delocalisation of the positive charge onto the metal vertex, but also a larger energy gap between the highest occupied molecular orbital (HOMO) and the lowest unoccupied molecular orbital (LUMO).[125] Presumably the carbocation can lean towards any of the cobalt verteices and may migrate between them. Schilling and Hoffmann suggested that the favoured pathway is the antarafacial migration depicted for a bimetallic cluster in Figure 5.2; this route stabilises the transition state by interaction of the *p* orbital on the migrating methylene with an out-of-phase combination of metal d_{z2} orbitals.[19]

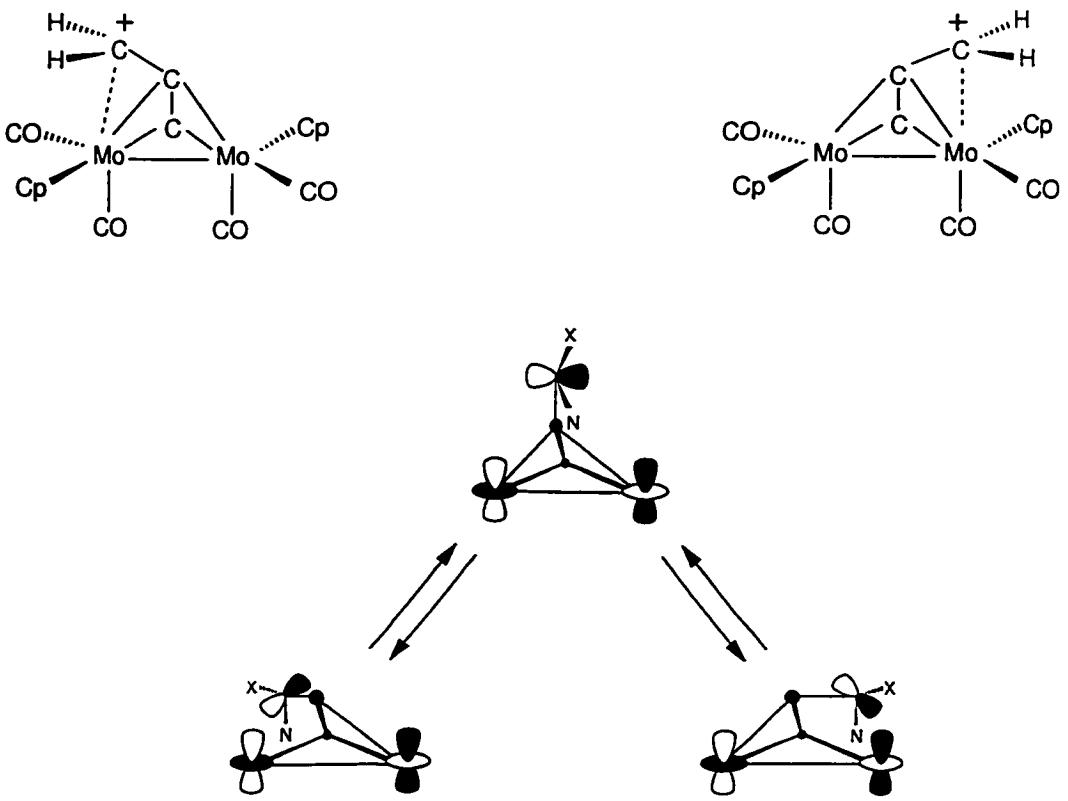

Figure 5.2: Antarafacial migration of an α–methylene group between metal centres in a tetrahedral cluster; note how the exo (X) and endo (N) substituents maintain their relative position.

These concepts have been extended to the closely analogous $[Co_2(CO)_6(RC{\equiv}C{-}CR'R'')]^+$ cations, **39**, whose synthetic potential has been cleverly exploited by Nicholas[126] and Schreiber.[127] Although no crystallographic data have been reported on these cobalt-stabilised cations, Edidin, Norton and Mislow[128] have provided compelling NMR evidence in favour of the C_s isomer **38a**. Moreover, the mixed-metal cluster **40b**, which is the isolobal analogue of **39**, has been crystallographically characterised

recently.[24] The mixed metal cluster **40b** is derived from the precursor **40a**; **40a** proved to be an oil, which upon addition of PPh_3 yielded suitable crystals of **40b**.

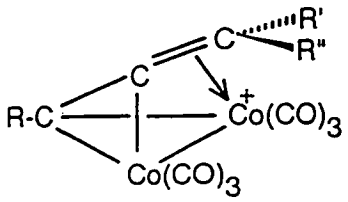

39

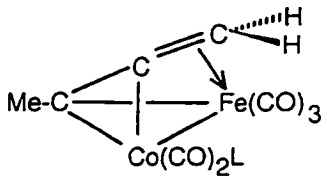

40a, L = CO
40b, L = PPh_3

It is noteworthy that the antarafacial migration process shown in Figure 5.2 maintains the identity of the *exo* and *endo* substituents at C_α but equilibrates the metal sites. This latter aspect is beautifully illustrated in the $[(C_5H_4Me)_2Mo_2(CO)_4(HC{\equiv}C{-}CH_2)]^+$ cation, **41**, where

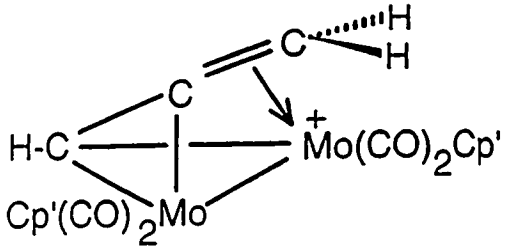

41

the tricarbonylcobalt moieties in **39** have been replaced by isolobal (cyclopentadienyl)-dicarbonylmolybdenum vertices.[129] Curtis demonstrated that the cyclopentadienyl ligands in **41** are equilibrated via a process with an activation energy of 17 kcal mol^{-1}; in contrast, the barrier for interconversion of the *exo* and *endo* α-CH_2 protons is considerably higher.[129]

These data are entirely in accord with the antarafacial mechanism depicted in Figure 5.2. Subsequent investigations have revealed that the barrier to these antarafacial migrations of α-CR_2^+ fragments from one metal vertex to the other is critically dependent on the primary, secondary or tertiary character[c] of the carbocationic centre.[130] The activation energy for such a process in molybdenum-, tungsten- or cobalt-stabilised α-CR_2^+ moieties falls from ≈18 kcal mol^{-1} for 1° cations to ≈10 kcal mol^{-1} for 3° cations, a fact which indicates that the more stable tertiary centres have much less need for anchimeric assistance from the metal than do primary cations. This apparent weakening of the metal-to-carbocation interaction is also reflected in the increasing Mo ..C^+ distances which range from 2.44 Å to 2.74 Å in the series M–CH_2^+, M–CHR^+, M–CR_2^+ [131]. The available X-ray crystallographic data on the molybdenum cations were assembled, not only to carry out a Bürgi-Dunitz trajectory analysis but also to complement the detailed EHMO investigation of the reaction pathway.

5.4.2 Extended Hückel Molecular Orbital Calculations on Mo_2C_2 Cluster Cations

A complicating factor in any calculatory approach to understanding the mechanism of carbocation rearrangement in the $[Cp_2Mo_2(CO)_4(HC{\equiv}C{-}CH_2)]^+$ system is the conformational variability of the $CpMo(CO)_2$ groups as well as the propensity of the carbonyl ligands to adopt semi-bridging positions.[132] The question of the favoured orientations of (cyclopentadienyl)dicarbonylmolybdenum vertices has been discussed elsewhere.[133] These difficulties are forestalled by taking advantage of Vollhardt's report of

[c] The label *primary* denotes that the carbon atom in question is bonded to two H atoms and one alkyl group; *secondary* indicates bonded to one H and two alkyl groups, and *tertiary* indicates bonded to three alkyl groups.

the fulvalene complex $[\eta^5:\eta^5\text{-}(C_5H_4\text{-}C_5H_4)Mo_2(CO)_4(MeC{\equiv}C{-}CH_2)]^+$, **42**.[131c] In this relatively rigid bridged bis-cyclopentadienyl system, the carbonyls are clearly terminal and the structure justifiably can be idealised to the C_s structure. It is this model which has been used for these calculations.

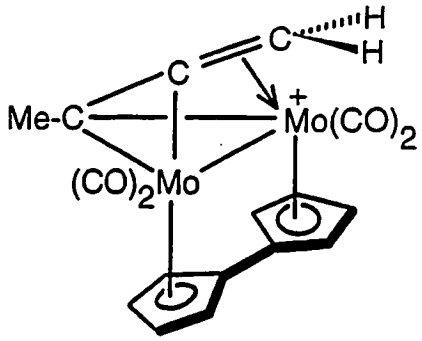

42

In order to define the geometry of the cationic cluster which undergoes rearrangement (see Figure 5.3), the origin, ⊙, of the co-ordinate system is placed at the centroid of the Mo(1)-Mo(2)-C(3) basal triangle. The capping carbynyl atom C(2) is defined by a vector starting at the origin and which makes an angle of 71° with the line C(3)-⊙. The distance C(3)-C(2) was taken as 1.369 Å, as in **5**. The coordinates of the α-CH_2 unit are defined in terms of the C(2)-C(1) distance (1.475 Å) and the three angles θ, ϕ and ω. As shown in Figure 5.3, θ is the angle ⊙-C(2)-C(1) which decreases from 180° as the methylene unit is allowed to lean towards the Mo(1)-Mo(2) bond.

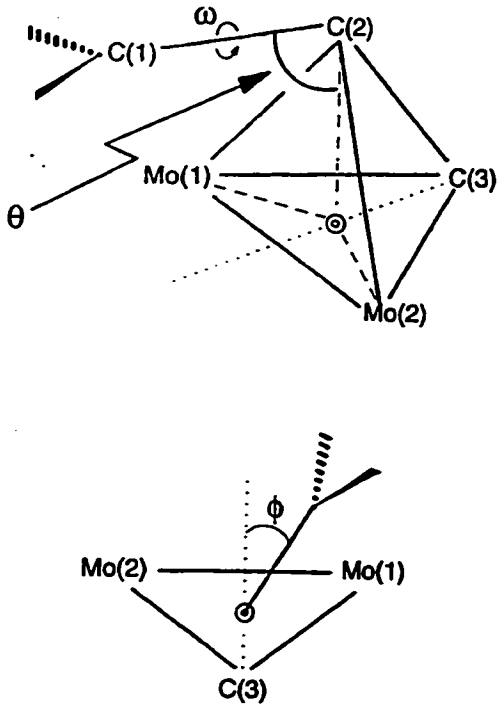

Figure 5.3: Definition of the angles θ, ϕ and ω which define C(1) and C(2).

As the methylene group swivels away from the mirror plane, which contains C(3) and C(2), the dihedral angle ϕ opens up from 0° towards 70° at which point the C(2)-C(1) bond eclipses the C(2)-Mo(1) vector. The third degree of freedom, the twist angle ω, defines the positions of the hydrogen atoms attached to C(1). When all three components of the CH_2 unit lie in the molecular mirror plane (ϕ = 0°) the ω values are 0° for H_{endo} and 180° for H_{exo}. As the methylene fragment swivels towards Mo(1), one might anticipate that the values ω(H_{endo}) and ω(H_{exo}) would gradually evolve towards 90° and -90°, respectively. To generate the hypersurface shown in Figure 5.4, the angles θ and ϕ were incremented in units of 5° and 2°,

respectively. At each point the torsion angle ω was varied from 0° to 180° in 15° increments and the minimum energy ω value for each (θ,ϕ) position was plotted.

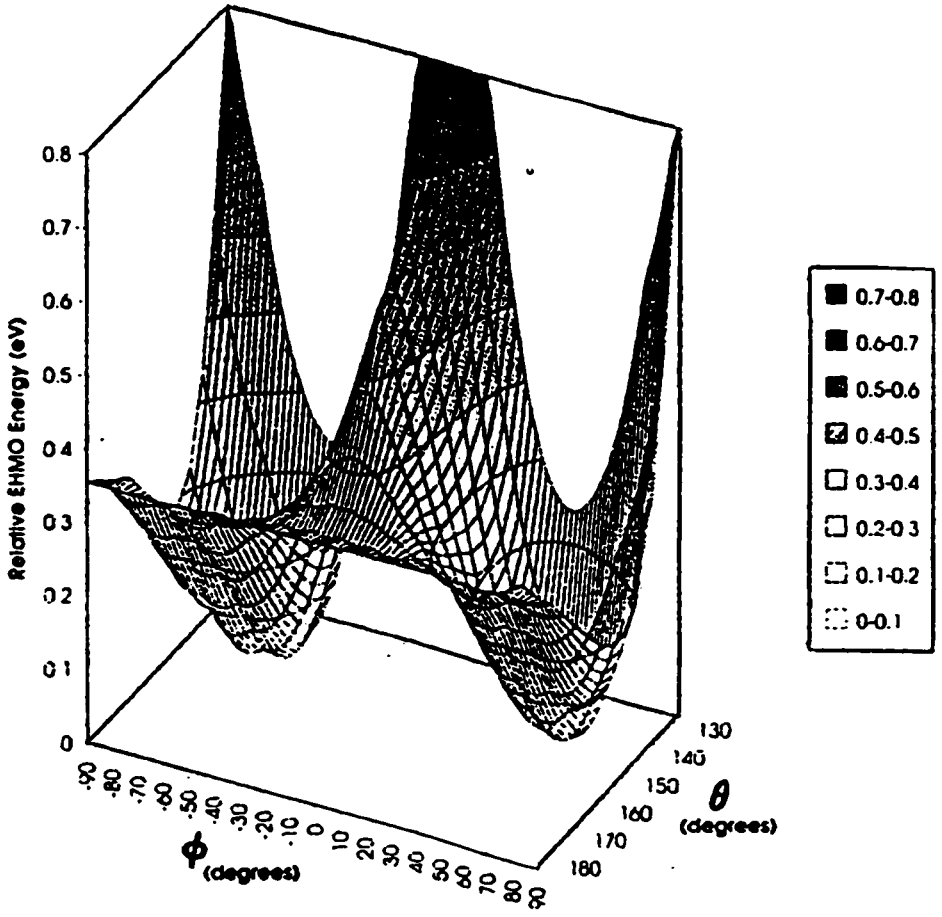

Figure 5.4: Energy hypersurface for the migration of the CH_2 group in $[\eta^5{:}\eta^5\text{-}(C_5H_4\text{-}C_5H_4)Mo_2(CO)_4(MeC{\equiv}C{-}CH_2)]^+$, **42**.

At $\phi = 0$ the molecule maintains C_s symmetry such that the p orbital at C(1) is oriented parallel to the Mo-Mo axis. This geometry optimises the overlap of the vacant orbital of the cationic carbon with the filled d_{z^2} orbitals on both metal atoms and so stabilises

the electron-deficient methylene centre during its transit from one molybdenum vertex to the other. The optimal value of the bend angle θ is 175°, *i.e.*, the CH_2 group leans only slightly towards the Mo-Mo vector. As ϕ increases to 20°, the initially relatively flat region of the hypersurface begins a precipitous drop into a potential well. This fall is accompanied by a sharp decrease in θ, the ⊙-C(2)-C(1) bend angle, which becomes 140° by the time ϕ reaches 28°. The value of θ remains essentially constant as one approaches the global minimum, and indeed is maintained briefly even after the C(2)-C(1) bond has passed the ϕ = 70° mark, corresponding to the eclipsing of the C(2)-Mo(1) vector.

The global minimum is located in the region ϕ = 50° to 70°, where the energy is virtually constant. Careful scrutiny of the potential well, shown in Figure 5.4, reveals a small fluctuation at the bottom of the well; this is reflected as the calculated global minimum at ϕ = 54°, with a subtly differentiated local minimum at ϕ = 62°. Of course, such observations may be attributable to artefacts of the EHMO calculation and may disappear at a higher level of approximation; however, as is seen in the discussion of the X-ray diffraction data, a number of cations of this type crystallise with two noticeably different structures in the same unit cell.

The orientation of the hydrogen atoms of the migrating group, as indicated by the torsion angle ω, was found to evolve with increasing ϕ so as to allow an optimal interaction of the carbon *p* orbital with the filled *d* orbital on the molybdenum atom towards which it is moving. In order to compute the lowest-energy pathway for migration of C(1) from Mo(1) to Mo(2), we used the data embedded in Figure 5.4 to seek out, for each value of ϕ, the optimal value of θ. The (θ,ϕ) coordinates thus obtained were then further refined in terms of ω, at a resolution of 2°, to reveal the pathway depicted in Figures 5.5 and 5.6. The former shows the

calculated trajectory followed by C(1), and the character of the rather steep descent into the potential well near each molybdenum is evident. The EHMO-calculated barrier for a methylene cation migrating from one molybdenum site to the other

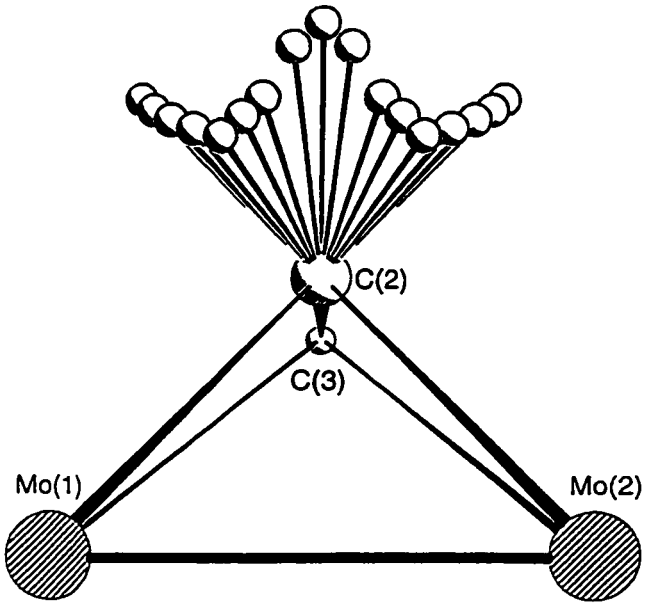

Figure 5.5: View of the EHMO-calculated trajectory of C(1) during the migration process.

is 9 kcal mol^{-1}, somewhat lower than the experimentally determined activation energy. However, we note that our chosen model, with its idealised C_s tetrahedral core and bridging η^5:η^5-(C_5H_4-C_5H_4) fragment, takes no account of the energy required to deform the relatively rigid fulvalene ligand. Nevertheless, calculations based on the linked bis-cyclopentadienyl system **42** avoid the complications of $CpMo(CO)_2$ vertex rotations and exchange of terminal and semi-bridging carbonyl ligands.

Figure 5.6 illustrates the evolution of the methylene twist angle ω as the migrating fragment seeks to maximize its orbital overlap with molybdenum as it approaches the metal centre. Thus, the plane containing C(1) and its attached hydrogen atoms rotates relative to the Mo(1)-Mo(2)-C(3) basal triangle such that, when $\phi = 0°$, these two planes are orthogonal but, at $\phi = 70°$, they are almost parallel.

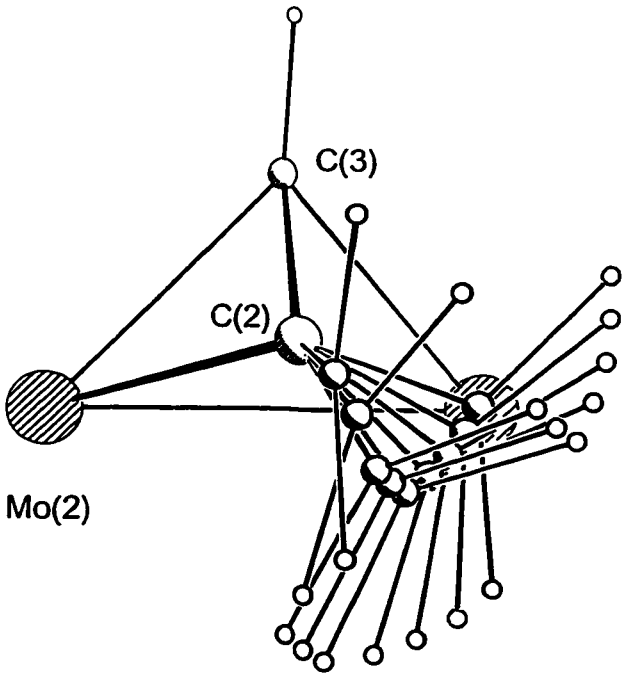

Figure 5.6: Bird's eye view of the EHMO-calculated twisting motion of the CH_2 fragment during the migration process.

5.4.3 Musical Interlude

The author digresses for one moment to draw attention to the observation that this pathway for methylene migration is remarkably similar to the trajectory followed by a conductor's baton during an orchestral performance. This phenomenon is dramatically and beautifully illustrated in Figure 5.7.

Figure 5.7: Multiple exposure flash photographs of Akira Endo conducting the Hamilton Philharmonic Orchestra in a performance of Tchaikovsky's 6th Symphony. The author thanks the Editor of the Hamilton Spectator for permission to reproduce Figure 5.7.

5.4.4 X-Ray Crystallographic Data for Mo_2C_2 Cluster Cations

The establishment of a trajectory for migration of the CR_2^+ moiety between metal vertices requires the compilation of a series of X-ray crystal structures of the $[Cp_2Mo_2(CO)_4(RC{\equiv}C{-}CR'R'')]^+$ type. Data are available for the cations listed in Table 5.1, and include such R′, R″ substituents as H [129, 131a-c], methyl [131d,e] and ferrocenyl [131f], as well as steroidal [131g] and terpenoid [131h] fragments. It can be seen from Table 5.1 that, as noted previously, the Mo•••C^+ distances lengthen as the character of C(1) changes from a primary carbon, to a secondary carbon, and finally to tertiary cationic centre. However, for the present purpose, one needs to know not only bond distances but also the experimental values of the bend angle θ, and the torsional parameters, ϕ and ω, for each cationic cluster. Analogously to the method used for the EHMO calculations, the origin, ⊙, was defined as the centroid of the Mo(1)-Mo(2)-C(3) triangle; the distances ⊙–C(2) and C(2)–C(1), and the angles C(3) –⊙–C(2), θ, ϕ, and ω, were evaluated from the X-ray crystallographic data. These measurements yielded cartesian coordinates for the C(2) and C(1) atoms, as well as for any non-hydrogen substituents attached to C(1). In Figure 5.8, the C(2) and C(1) positions for each of the eleven crystallographically determined structures are superimposed on the Mo_2C triangular base of **42**. This allows a direct comparison with the atomic positions for the EHMO-calculated minimum energy pathway shown in Figures 5.5 and 5.6.

Table 5.1 Crystallographic data for molybdenum cations.

Structure	*rMo(1)-C(1)* (Å)	*r⊙-C(2)* (Å)	*∠C(3)- ⊙ -C(2)* (°)	*rC(2)-C(1)* (Å)	θ ⊙-C(2)-C(1) (°)	ϕ *C(3)- ⊙ -C(2)- C(1)* (°)	*Ref.*
$[(C_5H_4–C_5H_4)Mo_2(CO)_4(MeC{\equiv}C–CH_2)]^+$	2.442	1.248	71.3	1.475	123	61	131c
$[(C_5H_5)_2Mo_2(CO)_4(HC{\equiv}C–CH_2)]^+$	2.444	1.315	68.3	1.379	122	58	131b
$[(C_5H_4Me)_2Mo_2(CO)_4(HC{\equiv}C–CH_2)]^+$	2.465	1.358	67.0	1.345	124	53	129
$[(C_5H_4Me)_2Mo_2(CO)_4(HC{\equiv}C–CH_2)]^+$	2.468	1.324	69.0	1.437	122	53	129
$[(C_5H_4–C_5H_4)Mo_2(CO)_4(MeC{\equiv}C–CH_2)]^+$	2.557	1.251	70.9	1.484	128	51	131c
$[(C_5H_5)_2Mo_2(CO)_4(HC{\equiv}C–CHMe)]^+$	2.613	1.354	70.7	1.380	132	72	131d
$[(C_5H_5)_2Mo_2(CO)_4(BuC{\equiv}C–CH(ferrocenyl))]^+$	2.630	1.316	68.4	1.424	123	54	131f
$[(C_5H_5)_2Mo_2(CO)_4(MeC{\equiv}C–bornyl)]^+$	2.737	1.350	65.1	1.397	136	50	131h
$[(C_5H_5)_2Mo_2(CO)_4(HC{\equiv}C–mestranyl)]^+$	2.738	1.368	66.5	1.364	127	53	131g
$[(C_5H_4–C_5H_4)Mo_2(CO)_4(HC{\equiv}C–CMe_2)]^+$	2.753	1.404	68.7	1.361	126	71	131e
$[(C_5H_5)Mo(CO)_2Co(CO)_3(MeC{\equiv}C–bornyl)]^+$	2.915	1.350	65.1	1.397	146	50	131h

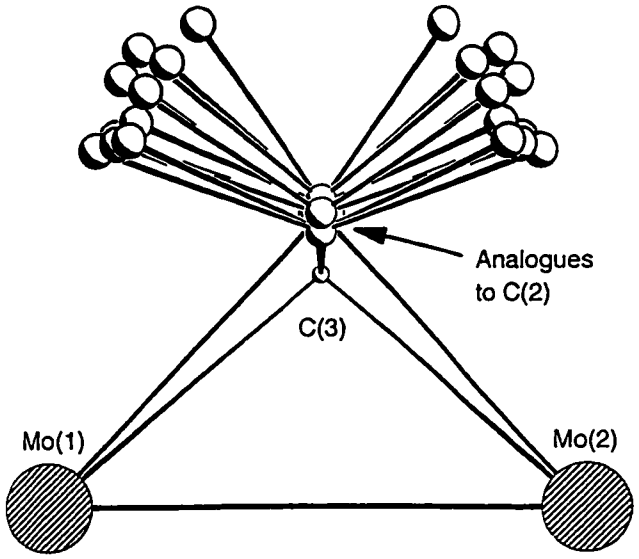

Figure 5.8: Superposition of the C(1) cationic centres in 11 different X-ray crystal structures, $[Cp_2Mo_2(CO)_4(RC{\equiv}C{-}CR'R'')]^+$.

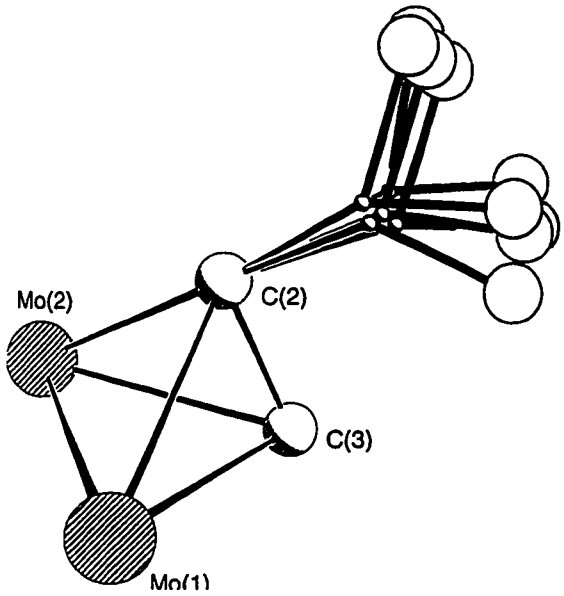

Figure 5.9: View of the twisting motion of the CR'R" fragment in a series of X-ray crystal structures.

It is immediately apparent from a comparison of Figures 5.5 and 5.6 with Figures 5.8 and 5.9, respectively, that there is a good correlation between the EHMO-calculated and X-ray determined series of structures. The crystallographically located positions of the C(2) capping carbons in the series of clusters, although very similar, are not identical. This observation shows that one can consider the whole vinylidene fragment to be capable of moving over the triangular base. Nevertheless, it is evident that the locus of the cationic site is readily defined in terms of the angles θ, and ϕ.

It is fortunate that the $[Cp_2Mo_2(CO)_4(RC{\equiv}C{-}CR'R'')]^+$ clusters for which structures have been reported cover a range of substituents with widely differing electronic and steric requirements, and so yield a data set with bend angles, θ, varying from 122° to 146° and with torsional angles, ϕ, covering the range 50° to 70°. These values encompass almost the entire domain of the deep potential well in the hypersurface depicted in Figure 5.4. Indeed, one can clearly see that the tertiary cationic centres have not merely lengthened the Mo $\cdot\cdot C^+$ distances relative to those found in CH_2^+ systems, but have also started to climb out of the potential well by rotating the C(2)-C(1) vector towards the mirror plane which bisects the two molybdenum vertices. Moreover, as illustrated in Figure 5.9, the twist angles ω gradually evolve such that the *exo* and *endo* substituents move towards their predicted vertical positions as the migration proceeds. We note also that, in those crystal structures where the substituents attached to C(1) are observable, the cationic centre is not planar in an ideal sp^2 fashion, but rather shows a tendency to pyramidalise. Of course, in those cases where the greatest pyramidalisation is to be expected, *i.e.*, the primary cations most firmly bonded to the metal centre, the α-hydrogens cannot be located unequivocally. Interestingly, the EHMO calculations suggest that, at the calculated global minimum energy for **5** (where

$\theta = 140°$ and $\phi = 54°$), the methylene hydrogens can each be bent away from the Mo atom by 8°; this stabilises the system by about 1.2 kcal mol^{-1}.

Finally, it is noteworthy that in two of the systems studied, namely $[(C_5H_4Me)_2Mo_2(CO)_4(HC{\equiv}C{-}CH_2)]^+$, **41**, and $[\eta^5{:}\eta^5\text{-}(C_5H_4\text{-}C_5H_4)Mo_2(CO)_4\text{-}(MeC{\equiv}C{-}CH_2)]^+$, **42**, there are two independent molecules of the cation in the unit cell. In each case, this effect manifests itself as a slightly different orientation of the methylene fragment with respect to the nearby molybdenum vertex. In **5**, the Mo $\cdot\cdot C^+$ distances in the two molecules are 2.44 Å and 2.56 Å and, while these may possibly be dismissed simply as crystal packing effects, one might also consider that this phenomenon reflects the observation of two calculated minima, as shown in Figure 5.4. Clearly, we are close to the limits of reliability of the EHMO approach but, nevertheless, it provides food for thought!

5.5 Conclusions

In summary, the remarkable similarity of the calculated lowest-energy pathway for cation migration between two metal vertices, and the trajectory indicated by a series of crystallographic "snapshots" of the process is manifest evidence of the power of the Bürgi-Dunitz approach towards understanding molecular dynamics. According to the basic assumptions of the structure correlation method,[118] there should be a concentration of sample points (*i.e.* crystal structures) in the low-energy regions of three-dimensional space. Moreover, there should be a gradual thinning-out of sample points along the reaction path as the energy rises. One may thus identify the transition state as lying in the least densely populated stretch of the reaction path. In the present case, this is when the angle ϕ

approaches 0° and the plane containing the CH_2 moiety is orthogonal to the basal plane of the tetrahedral cluster.

The complete characterisation of this fluxional process, observed for a series of related molecules, is aptly described not only by an NMR investigation, but also by molecular orbital calculations complemented by a trajectory analysis of the available crystallographic data.

5.6 Computational Methods

Molecular orbital calculations were performed within the extended Hückel formalism using weighted H_{ij}'s.[134] Computations were carried out by use of the program CACAO[135] on an EVERDATA 486-50 MHz IBM clone, which required 84 hours to generate the data from which the surface shown in Figure 5.4 was constructed. Microsoft EXCEL 4.0's "Chart Wizard" was used to generate the 3D surface as a mesh plot.

Chapter 6

Cobalt Complexes of Cyclohexylalkynol Ligands

6.1 Prelude

Cyclohexane, and structural derivatives that incorporate the cyclohexyl ring, are known to exhibit favoured ring geometries. The energetically favoured ring geometry in these six-membered ring systems is that of the "chair", while the "boat" geometry represents a higher energy conformation, and is approximately 6.9 kcal mol^{-1} less stable than the chair form.[136] These are represented for cyclohexane in Figure 6.1 (a) and (b). Two other common intermediate conformations shown in Figure 6.1 are (c) the "half-chair" (approximately 11 kcal mol^{-1} less stable than the chair) and (d) the "twist", 5.6 kcal mol^{-1} less stable than the chair. The boat and twist-boat conformations, being unstable with respect to the chair form, are thought of merely as intermediates between more stable conformations.

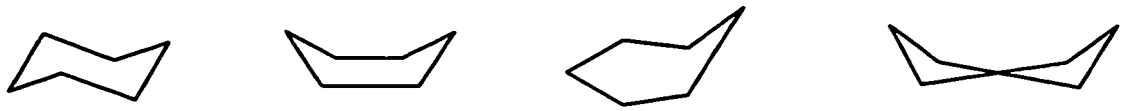

(a) (b) (c) (d)

Figure 6.1: Conformations observed for cyclohexane: (a) chair, (b) boat, (c) half-chair, (d) twist.

The goal of this project was to develop a series of molecular structures that would show cyclohexyl ring geometries intermediate between the energy-extreme chair (lowest energy) and boat (transition form) conformations. With such a series, one might be able to develop a Bürgi-Dunitz analysis (discussed in Chapter 5) of the pathway of interconversion between the two isomeric forms. The synthetic goal was to accomplish this interconversion with the use of a bimetallic dicobalt cluster as a "conformational switch". Several interesting results were obtained during the course of this investigation,[137] which was started by the author and continued by a senior thesis project student.[138] These results form the basis of this final chapter.

6.2 Introduction

6.2.1 Cycloalkynols

Cyclo-alkanols can be generated by nucleophilic attack of an acetylide ion on a given cyclo-alkanone molecule. Many researchers have investigated the direction of attack by alkynyl anions on alkyl-substituted 5- and 6-membered ring systems.[139] The experimentally observed stereoselectivities of nucleophilic additions to cyclic ketones have been rationalised by a torsional strain transition state model proposed by Felkin,[140] and subsequently supported by Anh and Eisenstein.[141] In this model, it is suggested that steric effects control the direction of nucleophilic attack, such that attack of the acetylide of choice occurs so as to prevent steric interference with ring substituents already present near the site of attack. Further, direction of attack is also controlled by the torsional strain imposed on the system in its transition state. In the case of cyclohexanones, this transition

state involves a distorted chair conformation whereby the axial transition state is perfectly staggered, whereas equatorial attack proceeds through a transition state in which partial eclipsing occurs.[142]

In a related example, it has been shown for substituted cyclopentanols that both *cis* and *trans* products can be observed and that the ratio of *cis:trans* products depends on many factors, including the nature of the nucleophile.[143] For example, bulky aryl/alkyl reagents will attack the opposite face of that occupied by substituents. However, alkynyl reagents, being more needle-like, may enter in a *cis* fashion to ring substituents. Further to this, interconversion of the *cis* and *trans* products may be observed in the presence of base.

The preparation of 2-methyl-1-(phenylethynyl)cyclopentanol reported by Malisza *et al.*[143] produced a 91:9 mixture of cyclopentanols from the addition of phenylacetylide to 2-methylcyclopentanone. This ratio describes the preference for the cyclopentanol product in which the alkyne occupies an axial position (91%), **43a**, versus an equatorial position (9%), **43b**. The relative orientations of the 2-methyl and 1-hydroxyl groups were determined by a series of NMR spectroscopic nuclear Overhauser effect (nOe) difference experiments. In these experiments it was shown for **43a** that irradiation of the hydroxyl proton produced nOe enhancements of the pseudo-axial hydrogen atoms at the two adjacent cyclopentyl ring positions (labeled C(2) and C(5) in Figure 6.2(a)). These data support a structure in which the alkynyl group occupies an axial position, and the methyl group is in an equatorial site. The structure determined by the NMR assignments was further supported by the single crystal X-ray structure reported for this molecule; the molecular connectivity is shown in Figure 6.2(a).[143]

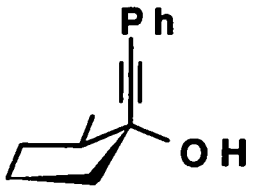

43a

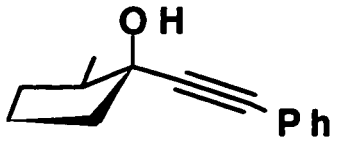

43b

6.2.2 A Dicobalt Cluster as a Conformational Switch

While the ability of the alkynyl dicobalt hexacarbonyl moiety to stabilise a neighbouring carbocationic site is well established,[144] its use as a stereocontrol element has been less widely explored. In their study of the $Mn(OAc)_3$-mediated oxidative cycloaddition of β-dicarbonyl compounds with $Co_2(CO)_6$-complexed 1-alken-3-ynes, Melikyan and Nicholas have rationalised the reaction in terms of a transition state whereby the bulky cluster unit is disposed pseudo-equatorially, which favours a pseudo-axial approach by the incoming nucleophile.[145] Similarly, the stereospecificity of the Friedel-Crafts cyclisation of cobalt-stabilised propargyl cations onto suitably activated arenes[146] has been accounted for by describing a transition state in which the $(-C{\equiv}CH)Co_2(CO)_6$ fragment adopts the less hindered pseudo-equatorial site.[147]

Malisza *et al.* reported the reaction of 2-methyl-1-(phenylethynyl)cyclopentanol (**43a**) with dicobalt octacarbonyl ($Co_2(CO)_8$), the product of which is a dicobalt complex with a dimetallatetrahedrane cluster core (**44**). There is a net addition of $Co_2(CO)_6$ across the alkyne group, and, with this addition, an interesting change in the orientation of the cyclopentyl ring substituents is observed. The X-ray crystal structure of the cluster was determined, and the molecular connectivity depicted in Figure 6.2(b) shows that the

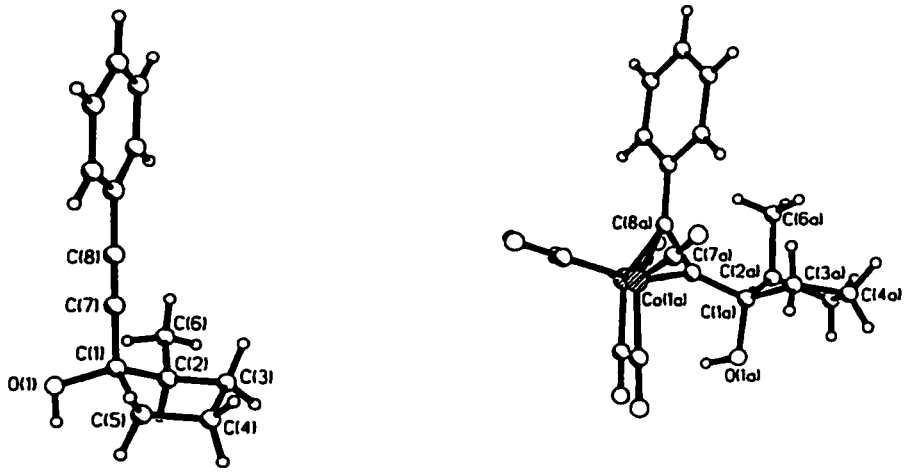

Figure 6.2: Views of (a) 2-methyl-1-(phenylethynyl)cyclopentanol, **43a**, and (b) [2-methyl-1-(phenylethynyl)cyclopentanol]$Co_2(CO)_6$, **44**.

relative arrangement of the hydroxyl and methyl groups is maintained. However, these groups are forced into pseudo-axial positions, and the bulky Co_2C_2 cluster occupies an equatorial site. The spatial preference of the cluster for the equatorial site far outweighs the ability of the methyl group to hold the equatorial position it has in the starting ligand. In a sense, the tetrahedral dicobalt cluster, with its proclivity for the equatorial site functions as a conformational 'switch', and is able to force a change in the conformation of the ring.

6.2.3 Ring Conformations in Cyclohexanes

As mentioned above, cyclohexyl rings are normally found preferentially with the lowest energy chair geometry. It has been shown that substituents on the cyclohexyl ring have varying effects on the ability of the ring to undergo conformational flips. For example, in methylcyclohexane the ring flips rapidly (about 10^6 times/second at 25°C)

from one chair form to another, through the intermediate unstable boat form.[148] The preferred conformation has the methyl substituent in an equatorial position, with a free energy difference of 1.7 kcal mol^{-1} for the equatorial methyl group (preferred) over axial. As bulkiness of the substituent is increased, it shows a more pronounced preference for the equatorial position. For example, the propensity of tertiary-butyl (*tert*-Bu) groups to prefer and maintain the occupancy of an equatorial site is well established.[148] For *tert*-Bu-cyclohexane, the *tert*-Bu group shows a preference of more than 5 kcal mol^{-1} for the equatorial position. Effectively, the incorporation of a bulky *tert*-Bu group can stop the flip from one chair form to another; it prefers to occupy an equatorial site on the cyclohexyl ring, and is not easily moved from such an orientation. Effectively, it serves as an anchor at one position of the cyclohexyl ring, and so interferes with the interconversion process.

6.3 Goals of the Project

It was thought that the ideas of conformational variability of cyclopentyl rings with the presence of a dicobalt cluster might prove applicable to six-membered rings, which show a more definite axial/equatorial disposition of substituents, as compared to five-membered ring systems. To depict the energy extreme points of this series, the "pure-chair" and "pure-boat" conformations would be required. It was anticipated that the known compound 1-(phenylethynyl)cyclohexanol (**45**) would prove to depict the chair geometry for the cyclohexyl ring. The previously unreported dicobalt complex of this ligand (**46**) was expected to show a conformational flip to put the alkyne cluster into an equatorial position, and thereby also give a chair structure, providing a picture of the

opposite end of the pathway. To find points between the two, it was thought that a *tert*-Bu group could be used to "anchor" one end of the chair. Subsequent formation of a dicobalt cluster at an alkyne function (located three carbon sites away from the *tert*-butyl group around the cyclohexyl ring) might induce a chair-to-boat interconversion. The premise for this argument was that the large cluster moiety would prefer, for stability, to adopt an equatorial position. Thus, the presence of two sterically demanding groups, a *tert*-Bu group and a dicobalt cluster, might cause distortion of the cyclohexyl ring in order to place both of these bulky groups into more energetically favoured positions.

With this in mind, a series of experiments involving cyclohexanone, and its 4-*tert*-butyl substituted derivatives, were undertaken. Where possible, both NMR spectroscopy and X-ray crystallography were used to determine unequivocally substituent and ring geometries. The results of these experiments, as well as related results involving derivatives of 1,4-cyclohexanedione, are discussed below.

6.4 Alkynylcyclohexanols and Derived Dicobalt Cluster Complexes: Results and Discussion

6.4.1 (1-Phenylethynyl)cyclohexan-1-ol, 45

The molecule selected to demonstrate the chair geometries was the known compound 1-(phenylethynyl)cyclohexan-1-ol, (herein referred to as 1-PECH-ol), **45**. This compound was synthesised according to the method reported by Hurd and Cohen.[149] The synthesis involves the attack of the MgBr salt of phenylacetylide on cyclohexanone, with subsequent quenching of the reaction with aqueous HCl. Alternatively, the molecule can

be synthesised with the use of *n*BuLi, instead of the Grignard reagent, to generate the acetylide.

The compound was initially identified by mass spectrometry, and subsequently characterised by NMR spectroscopy. Efforts to obtain a single crystal suitable for X-ray diffraction proved unsuccessful. The ^{1}H NMR spectrum of this compound in CD_2Cl_2 at 200 MHz is complex; acquisition of high-field (500 MHz) ^{1}H and ^{13}C spectra was necessary in order to characterise the compound. Standard ^{1}H-^{1}H COSY and ^{1}H-^{13}C shift-correlated techniques were used to identify the proton and carbon signals. NMR assignments are collected in Table 6.1. The atomic numbering scheme used for 1-PECH-1-ol, **45**, is shown below.

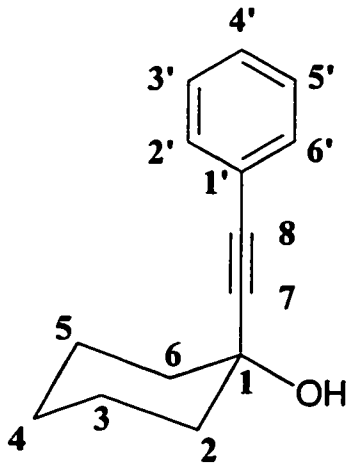

45

It was not possible to determine coupling constants even from the high-field spectra, since multiplets were severely overlapped or not sufficiently well resolved. It is assumed that the attack of the alkyne is axial, as is the case for the trimethylsilyl analogue of this compound discussed in Section 6.4.3.

6.4.2 [(1-Phenylethynyl)cyclohexan-1-ol]$Co_2(CO)_6$, 46

When 1-PECH-ol (**45**) was stirred with $Co_2(CO)_8$ in THF, the complex [1-(phenylethynyl)cyclohexanol]$Co_2(CO)_6$ (**46**) was obtained, after evaporation of solvent, as a dark red solid. The compound was identified by mass spectrometry; losses of 1, 2, 4, 5 and 6 carbonyl groups were observed (*m/z* 458, 430, 374, 346 and 318 respectively). Crystals suitable for X-ray diffraction were not obtained for this compound, and from the results gathered it was not possible to establish definitively that the cobalt-complexed phenylethynyl moiety sits, as expected, in the equatorial site, in a fashion analogous to the 2-methylcyclopentanol dicobalt complex reported by Malisza. It is reasonable to expect that the bulky cluster will prefer to lie in an equatorial position, and since there are no other substituents on the cyclohexyl ring, there is nothing to prevent the ring from flipping to the favoured conformation. This expectation is supported by the results obtained for the trimethylsilylethynyl analogue of this compound, the structure of which was determined by Deschamps, as discussed below in section 6.4.3.

6.4.3 (1-Trimethylsilylethynyl)cyclohexanol, 47, and [(1-Trimethylsilylethynyl)cyclohexanol]$Co_2(CO)_6$, 48

In a continuation of this investigation in our laboratory, Deschamps[138] synthesised the trimethylsilylethynyl analogue of 1-PECH-1-ol (**45**) in order to attempt to model the two expected chair geometries – before and after the formation of the dicobalt cluster at the alkyne site. Cyclohexanone was treated with (trimethylsilylethynyl)lithium, and then hydrolysed to yield the single alkynol product **47**.[150] Characterisation by NMR

spectroscopy revealed that attack of the acetylide occurred at the axial site; in particular, an nOe experiment was used to show that the OH group occupies an equatorial site, thus the alkyne substituent is axial, giving the result expected from the Felkin-Anh model.

Deschamps reported that the addition of $Co_2(CO)_6$ to **47** gave the cluster complex **48**. The single crystal X-ray crystal structure shows clearly that the cyclohexyl ring has flipped to place the dicobalt cluster in an equatorial position, as shown in Figure 6.3.[138]

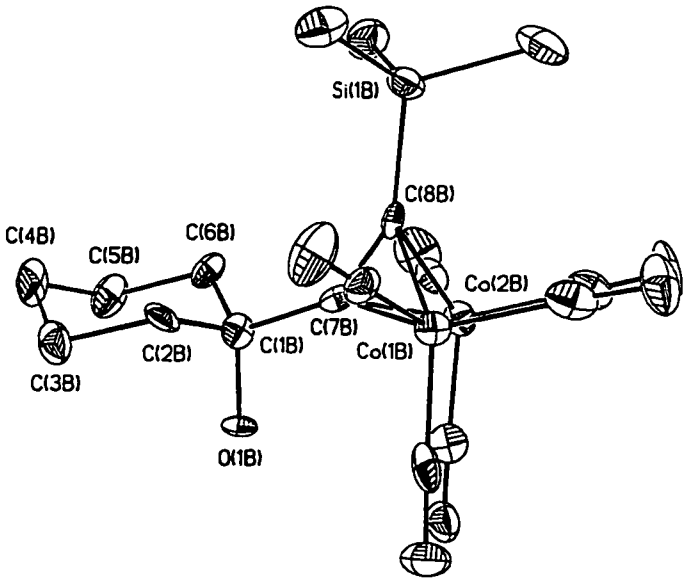

Figure 6.3: Molecular structure of **48**. Thermal ellipsoids shown at the 50% probability level. Hydrogen atoms omitted for clarity.

It should be noted that Braga *et al.*[151] have reported the X-ray crystal structures of 1-(*tert*-butylethynyl)cyclohexan-1-ol, **49**, and of its platinum and nickel complexes, **50a** and **50b**, as shown in Scheme 6.1. These molecules are of interest as they also demonstrate that the axial alkyne substituent prefers the equatorial site upon

complexation. The authors did not comment upon this observation, as the focus of the work was the intermolecular hydrogen bonding patterns in the crystal lattice.

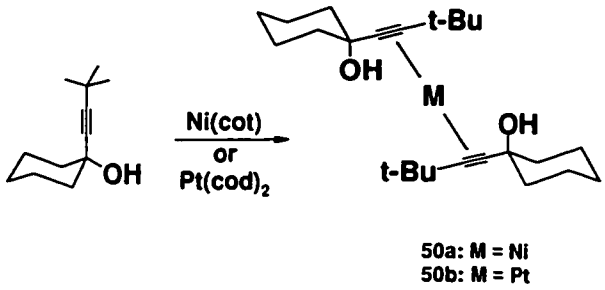

Scheme 6.1: Formation of dimers, giving rise to cyclohexyl ring flip.

6.4.4 Trans-4-*tert*-Butyl-1-(Phenylethynyl)cyclohexan-1-ol, 51

By a method analogous to that for 1-PECH-ol, the previously unreported 4-*tert*-butyl derivative of this ligand, 4-*tert*-butyl-1-(phenylethynyl)cyclohexan-1-ol (herein referred to as 4-*t*Bu-PECH-ol), **51**, was synthesised (Scheme 6.2).

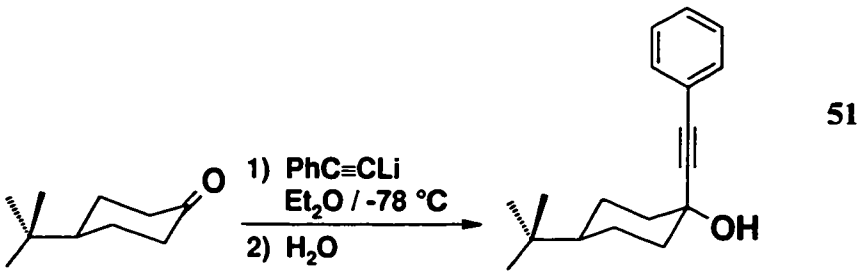

Scheme 6.2: Synthesis of *trans*-4-tert-butyl-1-(phenylethynyl)cyclohexan-1-ol.

There was no evidence for the formation of more than one product of the reaction. NMR spectroscopy was used to characterise the product, and shows that the alkynyl

substituent is in an axial site at position 1 of the cyclohexyl ring, as expected, while the *tert*-butyl group occupies an equatorial site at position 4, as discussed below. The molecular numbering scheme for **51** is shown below.

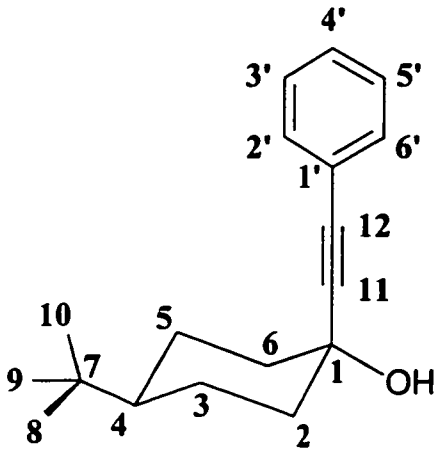

51

The compound was characterised by a series of one- and two-dimensional NMR experiments, including long distance correlation experiments, COSY, DEPT and nOe experiments. In the ^{1}H NMR spectrum, the *tert*-butyl protons were assigned based on chemical shift, integration, and lack of spin-spin coupling, to the peak at 0.84 ppm. Similarly, the OH proton appears at 5.47 ppm, and a multiplet corresponding to the phenyl protons occurs at 7.36 ppm.

In the cyclohexyl proton region, additional experiments were required in order to make definitive assignments. In the ^{1}H NMR spectrum, it is clear from integration that the lone proton at position 4 (axial) appears at δ 0.99 ppm. This signal appears as a well resolved triplet of triplets, which is what would be expected, again, based on the Karplus relationship - a large coupling to the neighbouring H3,5-axial protons, and a smaller coupling to the H3,5-equatorial protons. These couplings are observed as 11.6 Hz and 3.3

Hz, respectively. In the cyclohexyl proton region, experiments with ^{1}H-^{1}H spin decoupling were carried out at δ 1.95, 1.68 and 0.99 ppm. With proton spin decoupling at 1.68 ppm, the triplet of triplets (H4) signal at 0.99 ppm collapses to a triplet; the peaks are slightly broadened and show some fine structure. The coupling for the triplet that remains is approximately 11.7 Hz. This allows assignment of the multiplet at 1.68 ppm to the H3,5-axial protons. If spin decoupling is carried out at 1.95 ppm, then a splitting of 3.2 Hz observed in the multiplet at 1.38 ppm disappears. With the H3,5-equatorial protons already assigned, of the possible remaining couplings this corresponds to the coupling between H3,5-axial and H2,6-equatorial, and supports the assignment of H2,6-equatorial at 1.95 ppm and H3,5-axial at 1.38 ppm. Integration of the multiplet at 1.38 ppm indicates that two other protons contribute to this signal – namely the H2,6-axial protons. The simplified multiplet that remains at 1.38 ppm (after spin decoupling at 1.95 ppm) has slightly broadened signals, and it appears that the H2,6 and H3,5 geminal couplings and H2,6-axial – H3,5,-axial coupling give rise to overlapping lines in the multiplet.

The ^{1}H-^{1}H COSY experiment (spectrum shown in Figure 6.4) allows a further determination of related axial and equatorial protons at sites 2, 3, 5 and 6 on the cyclohexyl ring. The signal for H4 (0.99 ppm) does not show cross peaks to H2,6-equatorial peaks (1.95 ppm), nor does it show cross peaks to the H2,6-axial part of the multiplet at 1.38 ppm. The H4 signal does show cross peaks to H3,5-equatorial and H3,5-axial. In turn, the H3,5-equatorial and H3,5-axial signals show cross peaks not only to each other, but also (each) to the H2,6-equatorial and H2,6-axial signals. The characteristics of the multiplet centred at 1.38 ppm are distinct enough to allow further assignments to be made, and it appears that this multiplet arises from overlapping signals from H2,6-axial (1.41 ppm) and H3,5-axial

(1.35 ppm). Qualitatively, for H2,6-axial one would expect a geminal coupling of magnitude 10-12 Hz to H2,6-equatorial, a large coupling to H3,5-axial, and a smaller coupling to H3,5-equatorial. This would give rise to a pseudo-triplet with a further small splitting, as appears (with $^{3}JH_{2,6ax}\text{-}H_{3,5ax}$ = 3.06 Hz) at the higher frequency end of the multiplet. For H3,5-axial, three large couplings would be expected: a geminal coupling to H3,5-equatorial, trans coupling to H2,6-axial, and trans coupling to H4-axial. This would give rise to a pseudo-quartet, which would exhibit a further smaller splitting from coupling to H2,6-equatorial, which is resolvable at the lower frequency end of the mutiplet.

Assignment of the ^{13}C signals was possible by comparison of peak intensities, and comparison to known chemical shifts.[152] For example, in the phenyl region, the peaks at 130.9 and 1128.6 ppm are twice the intensity of the peak at 128.1 ppm. Thus it is possible to assign the signal at 128.1 ppm to the *para* carbon of the phenyl ring, while the peaks at 130.9 and 128.6 ppm (twice as intense) are the *ortho/meta* phenyl carbon atoms. Likewise, in the cyclohexyl region, the C3,5 and C2,6 signals have twice the intensity of the C4 and C1 peaks. The ^{13}C DEPT experiment was used to aid in the assignment of the ^{13}C signals, by showing which signals arose from CH/CH_3 groups or CH_2 groups. These data were then applied to the HMBC spectrum (shown in Figure 6.5) in order to determine correlation of proton and carbon sites, and allow the full assignment of all carbon signals.

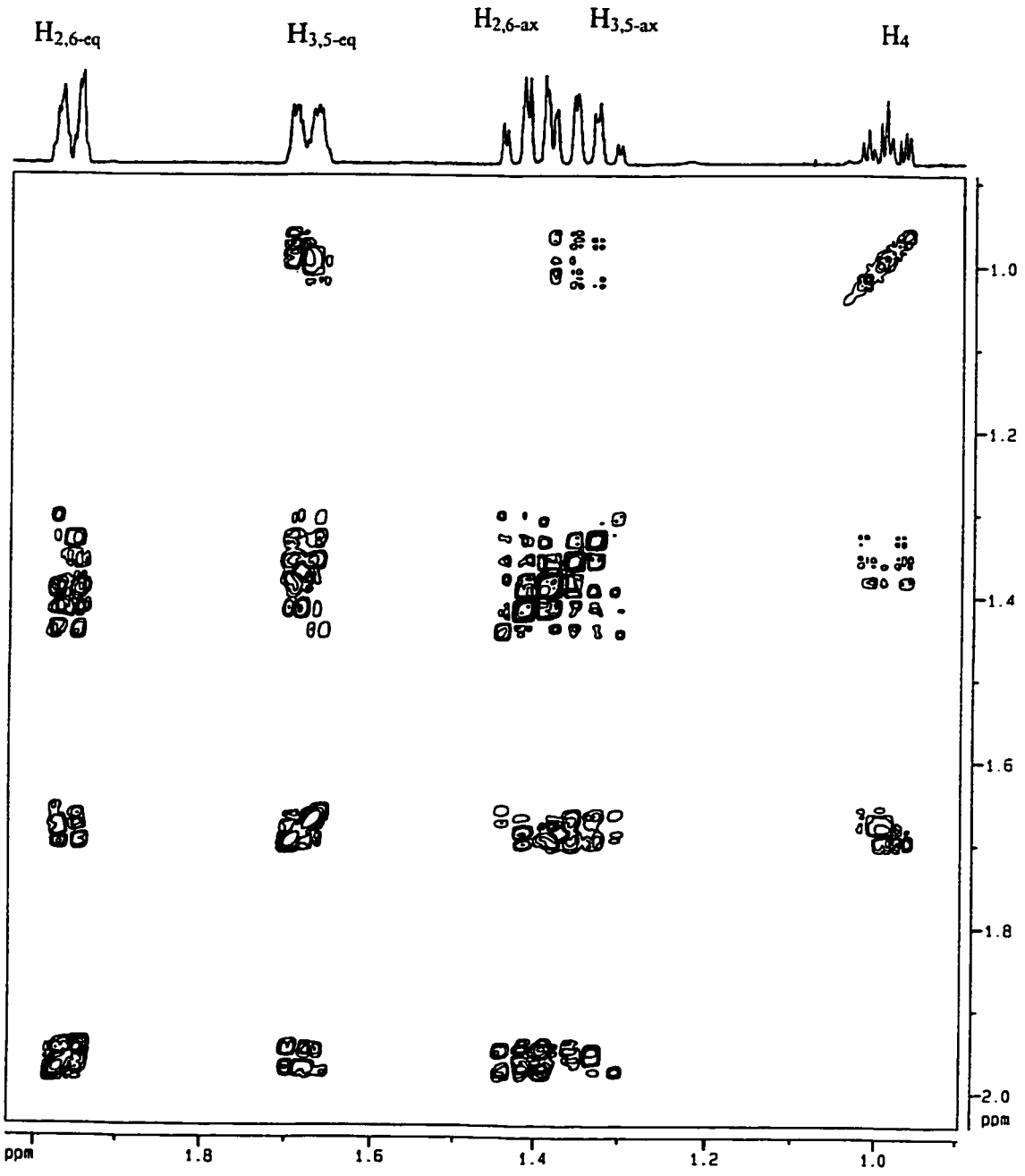

Figure 6.4: ^{1}H-^{1}H COSY spectrum in the cyclohexyl proton region for **51**.

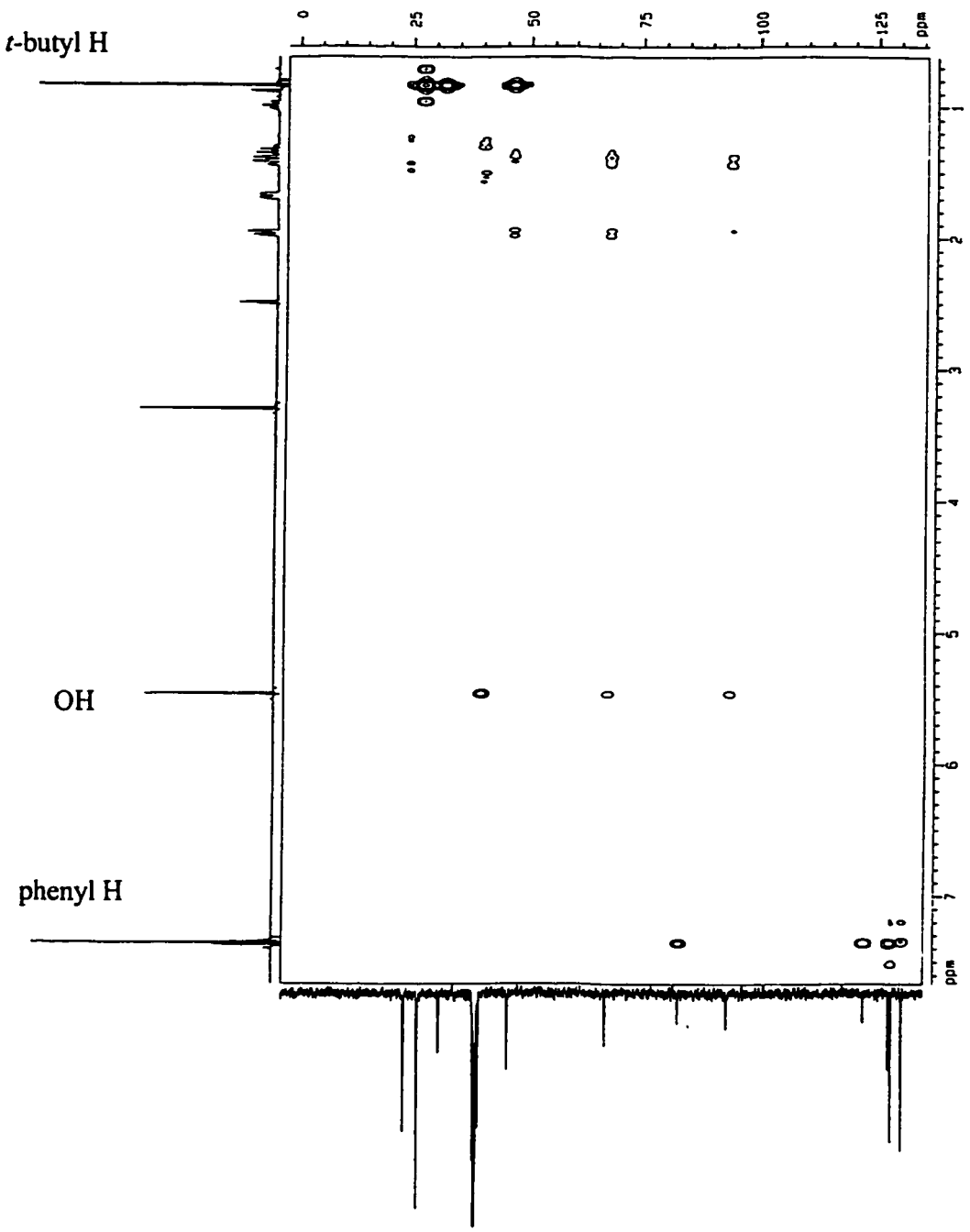

Figure 6.5: HMBC spectrum for **51**.

Table 6.1 Proton and ^{13}C NMR Chemical Shifts and Coupling Constants for **45**, **51** and **52**.

		δ, ppm	
^1H	**45**[a]	**51**[a]	**52**[b]
C_6H_5	7.36	7.36	7.43, 6.97
OH	5.38	5.47	4.30
$H_{2,6\text{-eq}}$	1.83	1.96	2.03
$H_{3,5\text{-eq}}$	1.64	1.68	}1.63 – 1.07
$H_{2,6\text{-ax}}$	}1.50	1.41	}1.63 – 1.07
$H_{3,5\text{-ax}}$	} 1.50	1.35	}1.63 – 1.07
H_{4eq}	}1.50	n/a	n/a
H_{4ax}	1.23	0.99	0.85
$C(CH_3)_3$	n/a	0.84	0.54
^{13}C			
CO	n/a	n/a	170.0[c]
ortho, meta-C	131.5, 128.9	130.9, 128.6	130.3
para-C	128.5	128.1	*d*
ipso-C	123.1	122.7	127.7
$C{\equiv}C\text{-}C_6H_5$	95.3	94.1	*d*
$C{\equiv}C\text{-}C_6H_5$	83.0	83.7	69.1
C_1	67.3	67.9	74.1
C_4	25.2	46.4	48.0
$C_{2,6}$	42.2[e]	40.2	43.2
$C(CH_3)_3$	n/a	31.9	32.2
$C(CH_3)_3$	n/a	27.4	27.5
$C_{3,5}$	23.1	24.3	24.3
		J, Hz	
$^3J(H_4 - H_{3,5ax})$	*f*	11.6	*f*
$^3J(H_4 - H_{3,5eq})$	*f*	3.3	*f*
$^3J(H_{2,6eq} - H_{3,5ax})$	*f*	3.2	*f*
$^3J(H_{2,6ax} - H_{3,5eq})$	*f*	3.1	*f*

[a] DMSO-d_6 (^1H NMR 500MHz, ^{13}C NMR 125 MHz)
[b] C_6D_6, (^1H NMR 300 MHz, , ^{13}C NMR 75 MHz)
[c] CD_2Cl_2, 75 MHz
d signal not observed
[e] CD_2Cl_2, 50 MHz
f Coupling constant not resolved

The nOe experiment showed enhancement of the H2 and H6 equatorial protons upon saturation of the OH signal. This evidence confirms that the OH group occupies an equatorial position, and thus the alkynyl group is situated in an axial position at carbon 1. The ^{1}H NMR spectrum and spectra from the DEPT and nOe experiments are collected in Appendix 2. NMR spectroscopic data are collected in Table 6.1.

6.4.5 [Trans-4-*tert*-Butyl-1-(Phenylethynyl)cyclohexan-1-ol]$Co_2(CO)_6$, 52

The reaction of 4-*t*Bu-PECH-ol, **51**, with $Co_2(CO)_8$ in THF gave [4-*t*Bu-1-(phenylethynyl)cyclohexanol]$Co_2(CO)_6$, **52**, as depicted in Scheme 6.3. Following evaporation of solvent, a red solid was obtained, and characterised initially by mass spectrometry. As is usual for many metal carbonyl compounds, the parent ion peak was not seen, however successive losses of six carbonyl groups were seen (*m/z* 514, 486, 458, 430, 402 and 374). A peak at *m/z* 525 $[M+H-H_2O]^+$ was observed also.

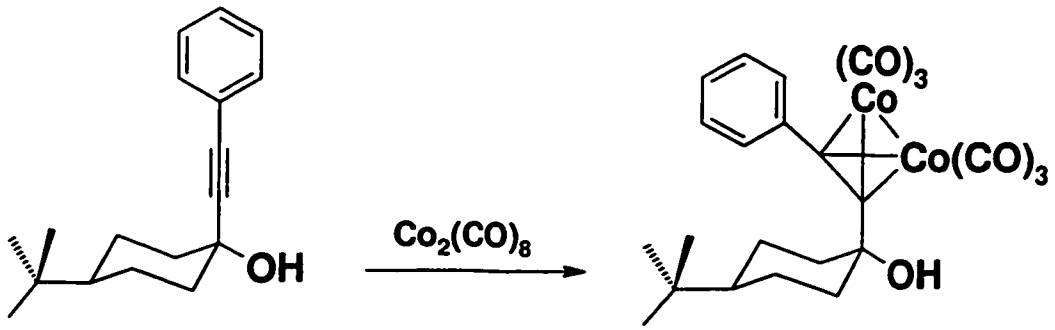

51 **52**

Scheme 6.3: Synthesis of dicobalt cluster complex, **52**.

Upon elution of the complex on silica gel in hexanes/diethyl ether, purple-red crystals of the complex (**52**) were obtained. These crystals proved to be suitable for X-ray diffraction, which was used to determine the structure of the complex. The structure shows that there are four independent (yet very similar) molecules observed in the unit cell; one of these molecules is depicted in Figure 6.6. The plane of the cyclohexyl ring defined by, for example, C2, C1 and C6, is bent only very slightly further away from the (C2, C3, C5, C6) plane than one would expect for a chair conformation. A complete list of bond lengths and angles for **52** is given in Appendix 1, and a packing diagram is shown in Appendix 2. What is apparent from the structure is that while the starting ligand (**51**) contains the alkyne moiety in an axial position (as shown by NMR experiments), the net addition of $Co_2(CO)_6$ across the alkyne has not had the desired effect of causing a flip of the alkyne cluster to an equatorial position. The alkyne is, however, bent away from its axial position by several degrees, and the cluster orients itself away from the cyclohexyl chair. The phenyl ring, at the end of the alkyne unit, is slightly bent back over the cyclohexyl chair and oriented so as to minimise interactions with the cyclohexyl ring. There is space to allow the bending of the phenyl group because there are no other cyclohexyl substituents that will interfere with the phenyl ring (which itself is relatively flat in nature). Thus, the substituents on the cluster moiety are not sufficiently sterically demanding to force a significant change in ring geometry, and the tert-butyl group continues to control the ring conformation. Given this result, the goal, then, was to synthesise a starting ligand such that addition of the dicobalt octacarbonyl to the ligand would cause sufficient steric interference of the cluster with the ligand to force the cluster moiety away from the axial position.

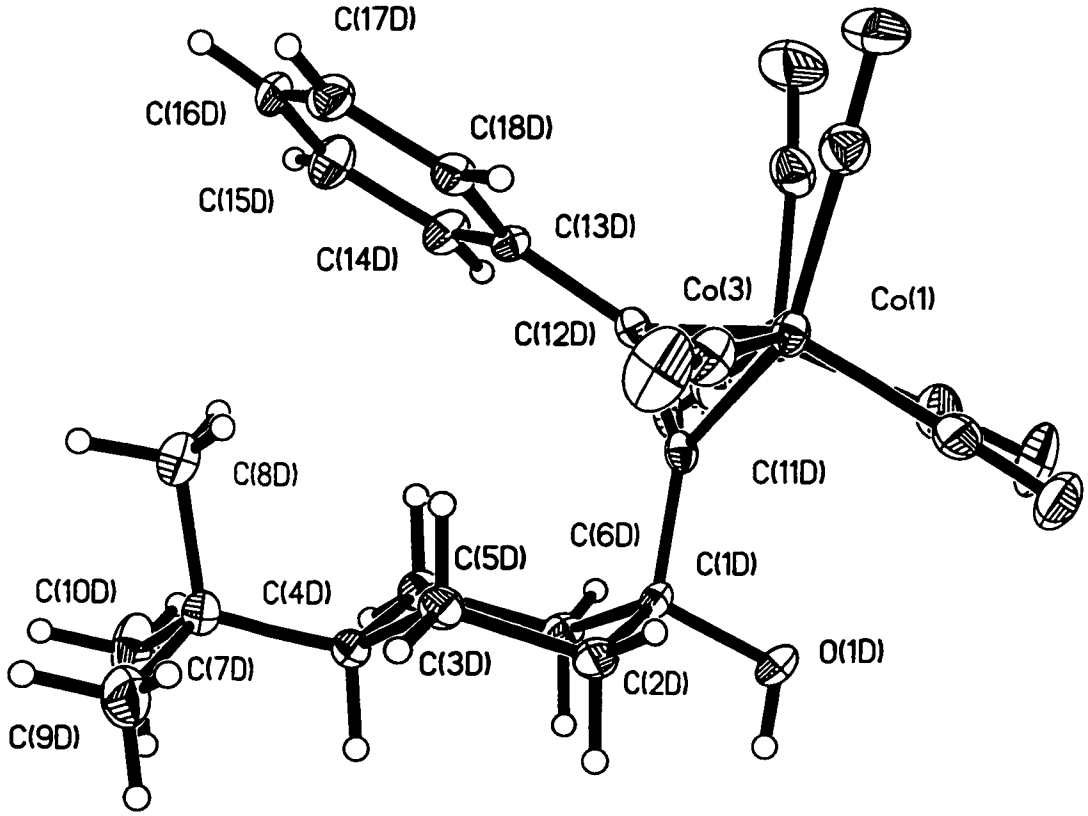

Figure 6.6: X-ray crystal structure of one of the four independent molecules of **52**. Thermal ellipsoids are shown at the 50% probability level. Hydrogen atoms are shown at an arbitrarily selected size.

6.4.6 Cis- and Trans-4-*tert*-Butyl-1-(Trimethylsilylethynyl)cyclohexan-1-ol

The next objective was to replace the phenyl moiety with larger groups in an attempt to force a change in the cyclohexyl ring geometry as it tries to accommodate the steric requirements of its substituents. The first idea was to use trimethylsilylacetylene in *lieu* of phenylacetylene: the trimethylsilyl (TMS) group being of a more "three-dimensional" nature, was expected to interact sterically to a greater extent with the cyclohexyl ring, and thus cause further displacement of the cluster from the axial position.

To test the steric requirements of the system, 4-*tert*-butylcyclohexanone was treated with (trimethylsilylethynyl)lithium, giving 4-*tert*-butyl-1-(trimethylsilylethynyl)cyclohexan-1-ol. The major product of the reaction was separated by flash column chromatography, and initially identified by mass spectrometry. Preliminary mass spectral data included a peak at *m/z* 235, which corresponded to $[M+H-H_2O]^+$. Compound **53a** crystallized in the freezer; however, the crystals were short-lived and melted very close to room temperature. The product was characterised by ^1H and ^{13}C NMR spectroscopy; NMR data are collected in Table 6.2. It was possible to determine from the ^{13}C shift of C_1 that the product isolated was the *trans* isomer, **53a**, (as discussed below).

Deschamps repeated this work in our laboratory, and found that two components were formed in a 5:2 ratio.[138] Deschamps identified the products by NMR spectroscopy, with the major component being the *trans* isomer, as discussed above, and the minor component being the *cis* (**53b**) isomer. For the *trans* isomer, the C_1 chemical shift occurs at 69.7 ppm, while for the *cis* isomer, (where the alkynyl substituent is equatorial) it is approximately 4 ppm more shielded, and occurs at 66.0 ppm. It appears that the increased bulk of the trimethylsilyl capping group influences the direction of attack of the acetylide

nucleophile, giving rise to a mixture of products, as compared to the analogous phenyl system.

Table 6.2 Proton and ^{13}C NMR Chemical Shifts for **53a** and **54a**.

	δ, ppm	
^{1}H	53a[a]	54a[b]
O*H*	*c*	*c*
$H_{2,6\text{-eq}}$	1.97	1.89
$H_{3,5\text{-eq}}$	1.72	}1.57 – 1.00
$H_{2,3,5,6\text{-ax}}$	1.39	}1.57 – 1.00
H_{4ax}	0.96	0.89
$C(CH_3)_3$	0.85	0.81
$Si(CH_3)_3$	0.15	0.30
^{13}C		
*C*O	n/a	*c*
C≡C-TMS	109.5	121.0
C≡*C*-TMS	*c*	79.4
C_1	69.8	74.3
C_4	46.8	48.0
$C_{2,6}$	40.3	43.3
$C(CH_3)_3$	32.2	32.5
$C(CH_3)_3$	27.5	28.1
$C_{3,5}$	24.8	24.8
$Si(CH_3)_3$	0.0	0.30

[a] $CDCl_3$ (^{1}H NMR 200MHz, ^{13}C NMR 50 MHz)

[b] C_6D_6, (^{1}H NMR 200 MHz, , ^{13}C NMR 50 MHz)

c signal not observed

6.4.7 Cis- and Trans-[4-*tert*-Butyl-1-(Trimethylsilylethynyl)cyclohexan-1-ol]$Co_2(CO)_6$

Trans-4-*tert*-butyl-1-(trimethylsilylethynyl)cyclohexan-1-ol, **53a**, was treated with $Co_2(CO)_8$, and yielded the corresponding dicobalt cluster **54a**, which was identified with mass spectrometry. The product was characterised by ^1H and ^{13}C NMR spectroscopy; NMR data are collected in Table 6.2.

In a continuation of this work, Deschamps also reported the synthesis of the dicobalt clusters of both the *trans* and *cis* (**54b**) isomers[138] and in addition to full characterisation, was able to determine the solid state structures of both dicobalt clusters. These are shown in Figures 6.7 (a) and (b). The cyclohexyl chair configuration is maintained for both compounds. Deschamps has also reported the syntheses of cis and trans 4-*tert*-butyl-1-(triphenylsilylethynyl)cyclohexan-1-ol and the corresponding dicobalt clusters, and found that increasing the bulk of the attacking acetylide begins to disfavour the formation of the isomer wherein the alkyne group is axial.[138]

6.4.8 Derivatives of Cyclohexanedione: Twist-Boats

Based on the observation that a triphenylethynylsilyl group could occupy either an axial or equatorial position with a bulky substituent already present, Deschamps successfully pursued the synthesis of both the *cis* and *trans* isomers of 1,4-bis(triphenylethynylsilyl)cyclo-hexan-1,4-diol. Deschamps also reported the syntheses of the trimethylsilylethynyl analogues of the diol, as well as the corresponding bis(dicobalt) clusters of these ligands.[138] Dramatic structural effects were observed upon the addition of $Co_2(CO)_8$ to the cis-diol isomers of each ligand. Upon complexation, while the

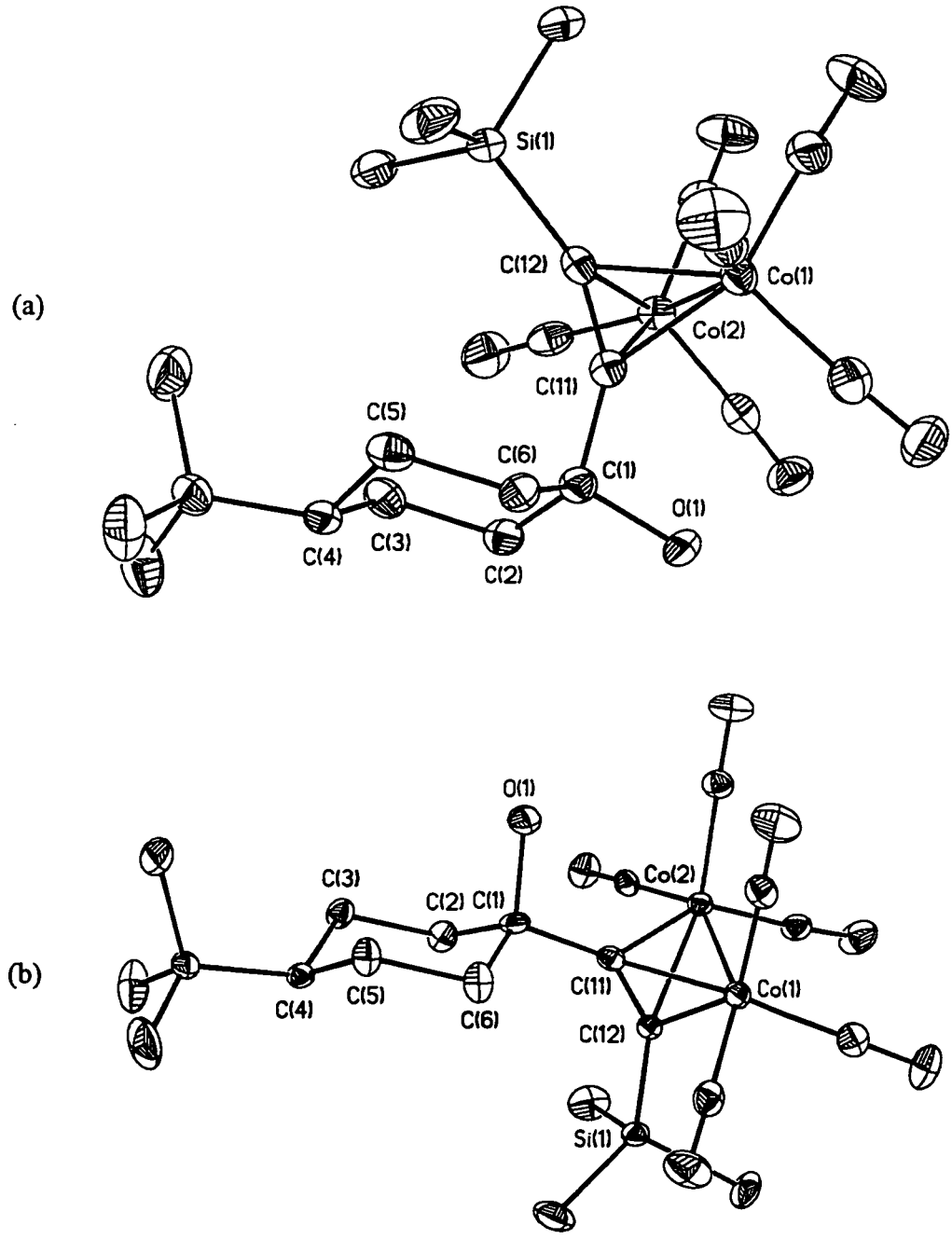

Figure 6.7: Molecular structure of (a) trans--[4-*tert*-Butyl-1-(Trimethylsilylethynyl)cyclohexan-1-ol]$Co_2(CO)_6$, **54a** and (b) cis-[4-*tert*-Butyl-1-(Trimethylsilylethynyl)cyclohexan-1-ol]$Co_2(CO)_6$, **54b** Thermal ellipsoids are shown at the 50% probability level. Hydrogen atoms are removed for clarity.

equatorial alkynyl group maintained its equatorial position, the axial alkynyl substituent was flipped into the equatorial position, thus generating a twist-boat conformation of the cyclohexyl ring! The two twist-boat structures determined by Deschamps are depicted in Figure 6.8.[138] This is an exciting result since crystallographically characterised cyclohexane twist-boats are relatively rare.[153]

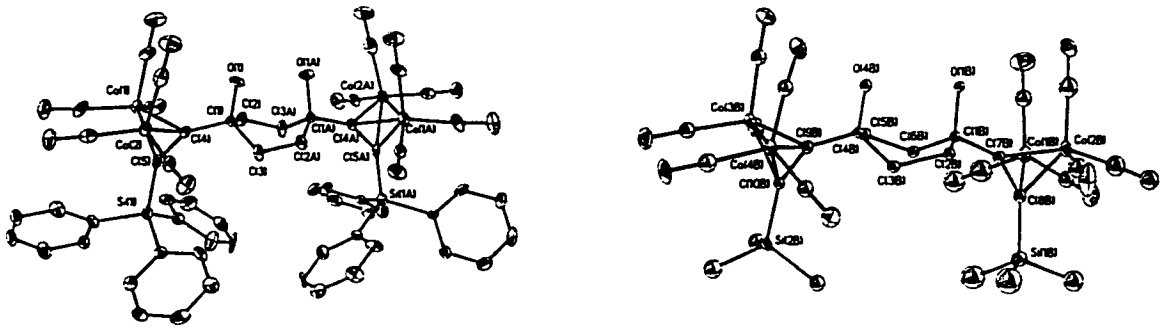

(a) (b)

Figure 6.8: Molecular structures of (a) *cis*-1,4-bis(triphenylsilylethynyl)cyclohexane-1,4-diol$[Co_2(CO)_6]_2$ and (b) *cis*-1,4-bis(trimethylsilylethynyl)cyclohexane-1,4-diol$[Co_2(CO)_6]_2$. Hydrogen atoms removed for clarity.

In principle, the accessibility of a boat conformer of *cis*-cyclohexan-1,4-diol can be turned to synthetic advantage. For example, it has been reported that the reaction of dibutyl-dichlorogermane with *cis*-cyclohexane-1,4-diol yields a mixture of cyclic germanoxane polymers, as depicted in Scheme 6.4(a). However, if the reaction is carried out under conditions of very high dilution, small quantities of the cyclic dimer are obtained.[154] In contrast, use of *cis*-2,5-di-*tert*-butylcyclohexan-1,4-diol (for which infrared data indicate strong intramolecular hydrogen bonding, consistent with a twist-boat conformation[155]) furnishes the monomer, **56**, in 75% yield (Scheme 6.4(b)). Nevertheless, the product still

contains bulky alkyl groups that would be difficult to remove from the cyclohexyl ring, whereas use of cobalt carbonyl clusters to create an impermanent increase of the steric bulk of an appropriately positioned alkynyl substituent can be used for stereochemical control. Removal of the cobalt carbonyl should then be feasible under relatively mild conditions.

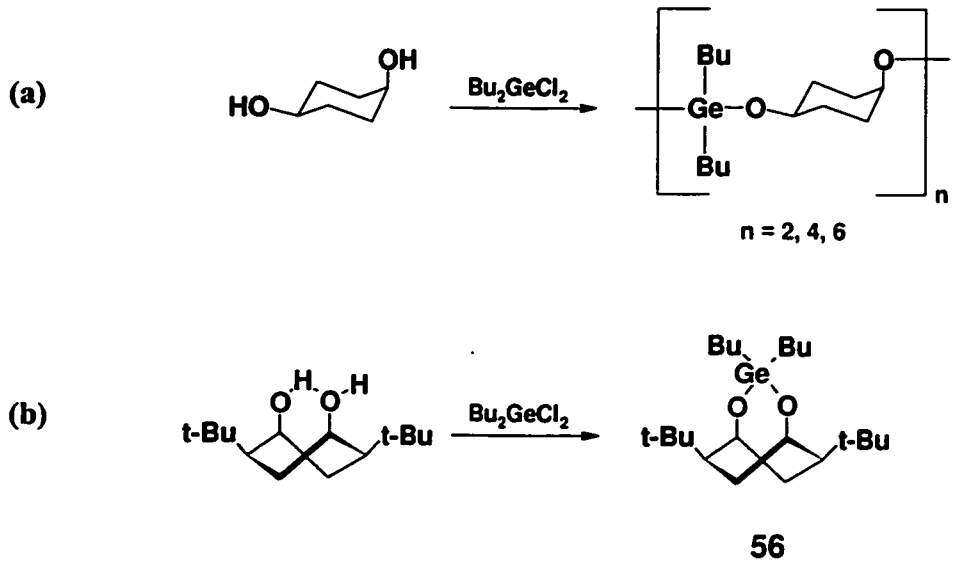

Scheme 6.4: Cyclohexyl twist-boats in germoxanes.

6.4.9 2-*tert*-Butyl-(ethynyl)cyclohexanols and Dicobalt Derivatives

Anchoring the cyclohexyl ring in positions other than the 4-position may also allow an investigation of "twist-boat" ring conformations. The positioning of the cluster and "anchor" groups adjacent to each other may have a further interesting effect on the ring geometry.

To begin an investigation of this idea, 2-*tert*-butyl-phenylethnylcyclohexanol (**55**) was synthesised, analogously to the 4-*tert*-butyl ligand, (**51**). This compound was not sufficiently separated from impurities to allow full characterisation; however, several peaks

were identifiable in the mass spectrum. The ^{1}H NMR spectrum is complicated, although similar in general appearance to that of **51**, and it was possible to assign many ^{13}C signals, particularly those in the phenyl and alkynyl region. There is, however, a multitude of signals in the cyclohexyl region (20 – 40 ppm). It is not surprising that this region of the spectrum should be more complicated than for the other phenylethynylcyclohexanols, as the symmetry is lowered by the presence of the *tert*-butyl group at position 2. It is also possible that both *cis* and *trans* isomers were formed, and are both present. NMR data are collected in Chapter 7.

Complexation of a crude sample of 2-*tert*-Bu-PECH-ol, **55**, with $Co_2(CO)_8$ was carried out, in the hope that it would be easier to separate the corresponding cluster compound from impurities as compared to first purifying the starting ligand. After preliminary efforts, no pure single compound was obtained.

In a similar fashion, the synthesis of the TMS analogue 2-*tert*-butyl-1-(trimethylsilylethynyl)cyclohexan-1-ol and its cobalt complex were attempted, however the products obtained were particularly oily, and not readily conducive to purification.

6.5 Elucidation of a Mechanism

The work of Tanaka and Isobe[156] on the cobalt cluster-mediated epimerisation of the alkynyl sugar **57** into **58** merits some comment. As noted by these authors, complexation of the alkynyl substituent by dicobalt hexacarbonyl and subsequent protonation leads to a propargyl cation, which is stabilised by neighbouring cobalt centres. However, they did not discuss the mechanism of epimerisation, which must be considered in terms of the structure and dynamics of the cationic intermediate. It has been previously noted that generation of

cobalt-stabilised cations proceeds preferentially through an antiperiplanar transition state, such that the elimination of water is anchimerically assisted by the metal.[157] This process maintains the stereochemical integrity of the developing sp^2-carbon centre. However, a symmetry-allowed antarafacial migration (such as the process discussed in Chapter 5) from one cobalt vertex to the other inverts the configuration of the cationic centre.[158]

Scheme 6.5 depicts such a process for the complexed alkynyl sugar **57**, whereby protonation and ring opening affords the cation **59**. Subsequent antarafacial migration (such that the smaller substituent maintains the position proximal to the metal-metal bond) generates the diastereomeric cation **60**. Subsequent attack of –OH and ring closure from the *exo* face yields a chair conformation in which the bulky alkynyl-cobalt cluster moiety occupies the favoured equatorial site, and generates the product of the appropriate sterochemistry. Removal of the Co_2 cluster then yields the epimer of the starting sugar.

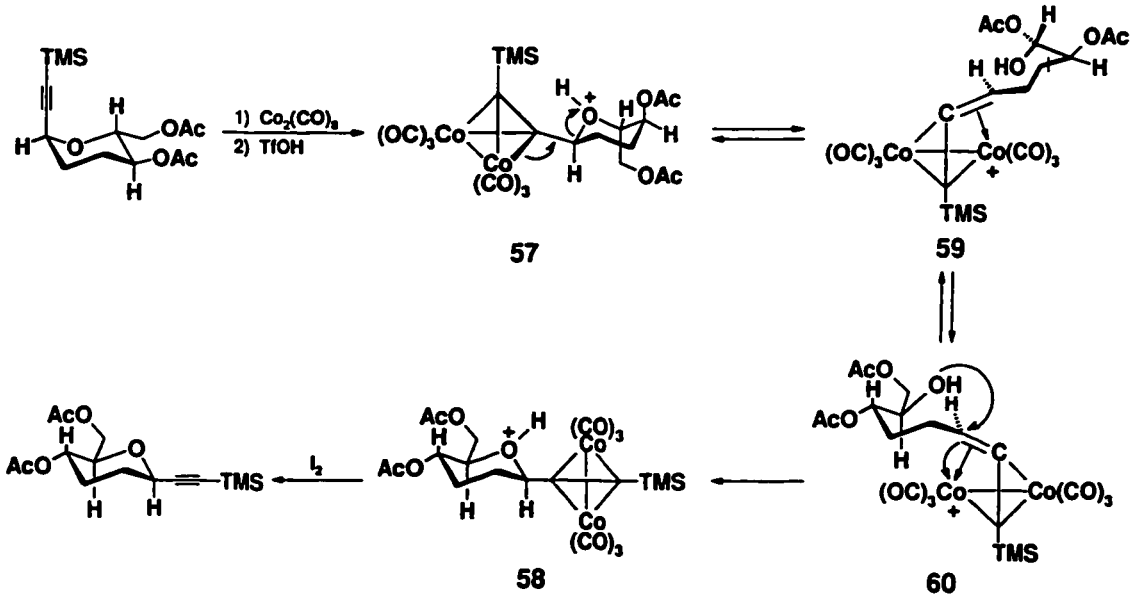

Scheme 6.5: Epimerisation of alkynyl sugar assisted by dicobalt cluster.

6.6 Summary

The synthesis of a series of compounds with various bulky alkyne substituents, and determination of their X-ray crystal structures, have demonstrated that it is possible to affect the geometry of a cyclohexane ring. The original idea that one might be able to use a succession of structures with variations in the cyclohexyl ring conformation to perform a Bürgi-Dunitz analysis of the cyclohexyl chair-to-boat interconversion process has not yet been realised. The structures that have been obtained, however, offer a significantly encouraging start towards the completion of this goal.

Interest in the chair to boat conversion depicted in Scheme 6.6 is stimulated by the idea that if a boat/twist-boat cluster complex were obtained, an intramolecular attack by the hydroxyl group at carbon 1 on a substituent (X) at position 4 might take place. This type of nucleophilic attack could lead to an interesting product from the effective closure of a ring between these two sites.

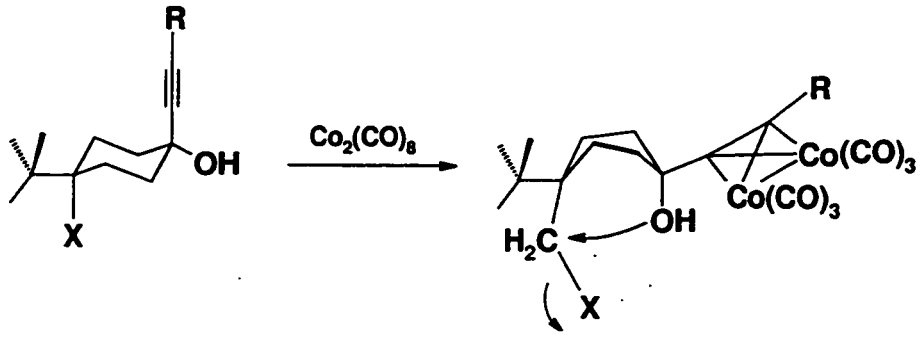

Scheme 6.6: Possible twist-boat synthesis, with subsequent intramolecular attack.

It may be of interest to investigate other ways to potentially induce chair to boat conversion, as discussed in Chapter 7.

Chapter 7

Conclusions and Future Work

7.1 Organometallic-Arene Complexes

7.1.1 Trindane

The initial stages of work involved an investigation of the organometallic chemistry of trindane. Trindane (**5**), with its five-membered rings fused around a central six-membered ring, is viewed in this work as a potential synthetic precursor to the proposed molecule sumanene (**3**). The goal was to synthesise organometallic complexes of trindane, and then derivatise these complexes at the benzylic proton sites in order to begin to build up the framework of the sumanene skeleton. In this study, trindane was found to form complexes of the type (η^6-trindane)ML_n, where ML_n = $Cr(CO)_3$ (**15**), $Mo(CO)_3$ (**17**), $Mn(CO)_3^+$ (**18**), and $(C_5H_5)Fe^+$ (**19a, 19b**). These complexes represent the first reported characterised organometallic complexes of trindane.

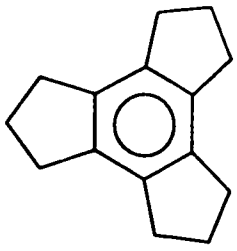

5

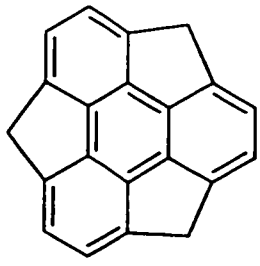

3

Characterisation of these complexes revealed several interesting features. The proton NMR spectrum of trindane shows two signals – a triplet arising from the equivalent benzylic protons, and a quintet arising from the equivalent wingtip protons. Complexation to a metal fragment, however, renders the two faces of the ligand inequivalent, and thus the benzylic and wingtip proton environments are both split into two environments, those of the *exo* (away from the metal) and *endo* (close to the metal) sites. The X-ray crystal structure of **15** shows, in addition, that the cyclopenteno rings of the trindane ligand adopt *endo* conformations in which the central methylene groups are bent towards the metal. Observation of dihedral H-H angles in this structure was useful in assigning proton-proton couplings in the NMR spectra of the trindane complexes.

This work was continued with the synthesis and characterisation of several ruthenium-trindane complexes, including the dimer $[(\eta^6\text{-trindane})RuCl_2]_2$, **25**, and the sandwich compound $[(\eta^6\text{-trindane})_2Ru]^{2+}[BF_4^-]_2$, **23**. The proton NMR spectrum of **23** is by far the most spectacular of those recorded for these complexes. All of the resonances are sufficiently well resolved to clearly show all couplings for the four trindane proton environments. The X-ray crystal structure of **25** reveals that two of the cyclopentene rings adopt *endo* envelope conformations, while the third five-membered ring is folded in an exo fashion to avoid a terminal chlorine atom in the other half of the dimer. The NMR spectra of **25** show the presence of $[\{(\eta^6\text{-trindane})Ru\}_2(\mu\text{-}Cl)_3]Cl$, **27**, in solution. It appears that the steric intrusion of the terminal chlorine atom in **25** is sufficient to promote the ionization of one chlorine atom to give the triply-bridged cation, **27**, and alleviate the strain within the dimer. To model this, **25** was treated with trimethyl phosphite in order to cleave the chloro-bridge in the dimer. The product, (η^6-

trindane)$RuCl_2[P(OMe)_3]$, **28**, again has all three cyclopenteno rings folded such that the wingtip methylene groups are oriented towards the metal, as confirmed by X-ray crystallography.

In order to pursue the goal of derivatising trindane, **15** was treated with DMSO-d_6 in the presence of the base *tert*-BuOK, in an attempt to exchange the benzylic *exo* protons for deuterons. A mixture of partially deuterated products was observed, with up to twelve deuterons being exchanged for protons. In contrast, treatment of **19b** under the same conditions gave complete H/D exchange at all twelve benzylic sites.

7.1.2 Hexaethylbenzene

Hexaethylbenzene (HEB), like trindane, is an hexa-alkylated arene. In contrast to trindane, however, its ethyl arms are unrestricted, and thus HEB (**7**) is conformationally more versatile than trindane, with its fused five-membered rings. The versatility of the HEB ligand allows it to act as a probe of HEB conformation and dynamics in the complexes it forms. The free ligand (7) adopts the lowest energy alternating ethyl group conformation; in a complex this is known as the 3 distal: 3 proximal conformation.

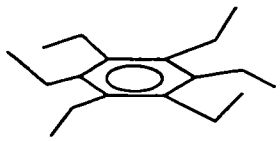

7

A series of HEB-ruthenium complexes were investigated with respect to the HEB conformation (number of distal vs. proximal ethyl groups) and dynamic behaviour of the ligand.

As in the case for trindane, the NMR spectra of the dimer $[(HEB)RuCl_2]_2$, **32**, show the presence of the ionic system $[(HEB)_2Ru_2(\mu\text{-}Cl)_3]Cl$ in solution. It was not possible to determine the X-ray crystal structure of **32** because of poor data quality, and so $[(HEB)_2Ru_2(\mu\text{-}Cl)_3][C_5(CO_2Me)_5]$ was synthesised to model the cation obtained when **32** ionizes in solution. The X-ray crystal structure of **33** shows that the cation has D_{3h} symmetry, and the HEB ligands adopt the 3 distal: 3 proximal ethyl group conformation. The NMR spectral data for **33** parallel those of **32**, indicating that in solution the 3:3 HEB ligand is found in both cases. The use of trimethyl phosphite or trimethylphosphine to cleave the chloro bridge in **32** gives $(HEB)RuCl_2[P(OMe)_3]$, **35**, and $(HEB)RuCl_2P(Me)_3$, **36**, respectively. Complex **35** shows a 5 distal: 1 proximal ethyl group arrangement, with the lone proximal ethyl group opposite the phosphite group. A preliminary structure determination of complex **36** shows that the ligand adopts the "all distal" (6:0) conformation. The ligand conformations are rationalized on the basis of the differing cone angles for $P(OMe)_3$ (107°) and PMe_3 (118°). Crystals of a minor by-product in the synthesis of **36** were isolated, and proved to be of the known compound *trans*-$RuCl_2(PMe_3)_4$, the crystal structure of which is reported here for the first time. An attempt to synthesise the sandwich compound $(HEB)_2Ru^{2+}$, analogue of the trindane system, gave instead $(HEB)Ru(H_2O)_3^{2+}$, **34**, in which the HEB ligand also adopts the 3:3 conformation.

7.1.3 Future Work

It would appear that the "all-endo" conformation of trindane is favoured in an organometallic complex. As discussed in Chapter 2, the only report of a structure for the

free trindane ligand indicates disorder in the region of the wingtip carbon atoms, and thus there is no definitive picture of the conformation of the uncomplexed ligand. It would be of interest to determine the structure of trindane, in order to make further comparisons of how complexation may affect its conformation.

Attempts to derivatise trindane with larger groups should be continued, in order to realise that goal of building up to the sumanene skeleton from trindane. Based on the results of the deuteration experiments carried out on **15** and **19b**, derivatisation appears to occur more cleanly for a cationic complex as opposed to a neutral complex. These attempts should be continued for cationic complexes, and it is possible that the ruthenium dicationic complexes may, in principle, provide a heightened activation towards *exo* substitution. Initially, the goal was to exchange 6 D for the six *exo* benzylic protons. When it was observed that all twelve (*exo* and *endo*) benzylic H could be exchanged, it was then thought that a group larger than D would prove to be more selective, and exchange only at the *exo* benzylic sites, because of increase in size. Efforts to incorporate groups other then D have been continued by other researchers in this group. Attempts to benzylate (trindane)Fe$(C_5H_5)^+$ led, however, to the incorporation of up to ten benzyl groups, indicating again that substitution at the *endo* benzylic sites also occurred. The major challenge continues to lie in selectively derivatising only the *exo* benzylic sites. The sandwich complex **23** may be more useful for this goal than the monometallic complexes. In **23**, with one face of the trindane ligand perhaps more effectively blocked because of the proximity of the other trindane ligand, this may promote selectivity of groups adding to the *exo* face only. For **23** it may even be possible to derivatise two trindane ligands at the same time.

To complete the HEB work, it should prove possible to complete the structure determination of (HEB)$RuCl_2P(Me)_3$, **36**. It seems as though there may be absorption problems with the data set, likely caused by the fact that the crystal shape was a very thin plate. It may prove possible to correct the original data sufficiently to allow a complete structure solution, and work on this structure continues.

7.2 Bimetallic Clusters

7.2.1 Migration Pathway in Bimetallic Cluster Cations

For systems of the type $[Cp_2Mo_2(CO)_4(RC{\equiv}C\text{-}CR'R'')]^+$, wherein the carbocationic centre is known to be stabilised by bending towards a metal vertex, the fluxional behaviour of these cations has been studied previously by variable-temperature NMR techniques. In this project several other methods have been incorporated in order to propose a mechanism describing the migration of the carbocationic centre between molybdenum vertices. In contrast to similar dicobalt systems, there are many reported crystal structures of the dimolybdenum systems. A Bürgi-Dunitz analysis of these X-ray structures, along with NMR data and extended Hückel molecular orbital (EHMO) calculations, have been used to determine a model of the lowest energy pathway by which the migration occurs.

Calculations carried out on the fulvalene complex $[\eta^5{:}\eta^5\text{-}(C_5H_4\text{-}C_5H_4)Mo_2(CO)_4\text{-}(MeC{\equiv}C\text{–}CH_2)]^+$, **42**, allowed the generation of an energy hypersurface describing the migration of a vinylidene moiety over the surface of a Mo_2C triangle. The three parameters under investigation included, firstly, the bend angle of the CH_2 group from 180° down towards the Mo-Mo bond. The other parameters were the dihedral (torsion) angle that

describes the movement of the CH_2 group from bisecting the Mo-Mo bond outwards towards a Mo vertex, and the twist angle of the CH_2 group, which defines the positions of the hydrogen atoms. The energy hypersurface shows that as the bend and dihedral angles evolve to allow the CH_2 group to (i) bend closer to the Mo-Mo vector, and (ii) move out towards a vertex, the energy drops significantly. Effectively, on the hypersurface, the system is dropping into a "potential well" as the optimal (lowest energy) values for the angles are approached. The optimal bend angle is about 140°, and the global minimum occurs for this bend at a dihedral angle of 54°, with a subtly differentiated minimum at 62°. The EHMO calculated barrier for the migration is 9 kcal mol^{-1}.

To complete this study, data from a series of X-ray crystal structures for systems of the type $[Cp_2Mo_2(CO)_4(RC{\equiv}C{-}CR'R'')]^+$ were compiled. The structures used encompassed a variety of substituents, giving rise to a data set with varying bend and torsion angles, and allowing comparison of primary to secondary and tertiary cationic systems. For example, for tertiary cationic centres the Mo--C^+ distances are lengthened relative to those in the CH_2^+ systems, and the torsion angles show that the tertiary systems are also "climbing out of the potential well" as the torsion angle decreases back towards the central mirror plane of the cluster. There was excellent correlation between the EHMO-calculated lowest-energy pathway and the positions of the X-ray determined series of structures along this pathway.

7.2.2 A Dicobalt Cluster as a Conformational Switch

The Bürgi-Dunitz structure correlation method is a powerful tool that has been applied to many problems. For this final project it was thought that the method could be applied to investigate an induced chair-to-boat interconversion in cyclohexylalkynols. The

objective was to synthesise molecules which demonstrated geometries intermediate of these two extremes (chair and boat) and determine their X-ray crystal structures in order to perform a trajectory analysis. The synthetic strategy involved the incorporation of a dicobalt cluster as a switch to induce changes in cyclohexyl ring conformation.

It has been reported that in (1-trimethylsilylethynyl)cyclohexan-1-ol, **47**, the alkynyl group occupies an axial position while the OH group sits in an equatorial site. Addition of $Co_2(CO)_8$ generates the cluster compound [(1-trimethylsilylethynyl)-cyclohexanol]$Co_2(CO)_6$, **48**, and the X-ray crystal structure of 48 shows that the cyclohexyl ring has undergone a flip to place the bulky cluster group in an equatorial position. The analogous synthesis of *trans*-4-*tert*-butyl-1-(phenylethynyl)cyclohexan-1-ol, **51**, again gives a ligand with the alkynyl group in an axial position, as determined by a series of NMR experiments. In this case, however, there is also a bulky (*tert*-butyl) group in place on the cyclohexyl ring, such that addition of $Co_2(CO)_8$ does not induce the same structural flip observed for **48**. In the product, [*trans*-4-*tert*-butyl-1-(phenylethynyl)cyclohexan-1-ol]$Co_2(CO)_6$, **52**, the *tert*-butyl successfully competes with the dicobalt cluster for the favoured equatorial position, and the cluster does not flip also into an equatorial position, although it bends away from ideal chair geometry by a few degrees. In fact, in a continuation of this work it was found that a twist-boat structure was accessible by starting from *cis*-1,4-cyclohexandiols. Complexation of the two alkynyl units with $Co_2(CO)_8$ maintains one group in its equatorial position, and flips the axial group into an equatorial position, to give the twist-boat structure.

7.2.3 Future Work

The Use of Metal Fragments to Induce Structural Change

In order to create a sterically demanding environment about the cyclohexyl ring, one could turn the focus instead to the manipulation of the metallic moieties used in the cluster, rather than ligand design. It would be interesting to see what might happen if one were able to make the phenyl ring of 4-*tert*-Bu-PECH-1-ol, **51**, larger by incorporating an organometallic fragment. A possible reaction would be the addition of $Cr(CO)_6$ to 4-*tert*-Bu-PECH-ol (**51**) in order to coordinate a $Cr(CO)_3$ moiety to the phenyl ring, with subsequent reaction of this new chromium complex (**61**) with $Co_2(CO)_8$ to create the Co_2C_2 cluster at the alkyne (**62**) (Scheme 7.1). Determination of the crystal structure of this compound would indicate if the added steric bulk of the $Cr(CO)_3$ moiety has affected the geometry of the cyclohexyl ring.

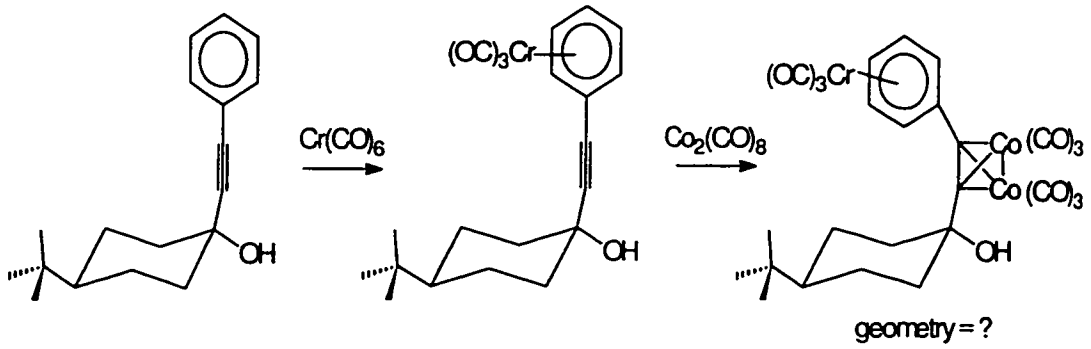

61 **62**

Scheme 7.1: Mixed-metal complexes.

To create a potentially more sterically demanding environment, one might also investigate the addition of $Cr(CO)_3$ followed by reaction with $[CpMo(CO)_3]_2$, instead of

$Co_2(CO)_8$, in order to discern whether changes in the cluster atom ligands have any effect on the structure.

Further Ideas on Ligand Design

In the interest of creating an environment as sterically demanding as possible, it would of interest to attempt the synthesis of a ligand which, in addition to (1) the *t*-butyl group at the 4-position and (2) a bulky capping group on the alkyne at position 1, has (3) substituents at the 3-, and 5-axial positions of the cyclohexyl ring. This would create more significant steric interactions between the cyclohexyl ring and the alkyne capping group, giving a situation where one might expect greater progression of the cluster moiety along the trajectory from axial to equatorial position. Ideas for possible substituents include large atoms such as bromine and iodine, or methyl groups, for example.

Chapter 8

Experiments

8.1 General Procedures

All reactions were carried out in oven-dried glassware under an atmosphere of dry nitrogen with use of conventional bench top and glove bag techniques. Acetone was dried over molecular sieves and all other solvents were dried and distilled by standard procedures.[159] Unless otherwise stated, reagents were purchased from Aldrich Chemicals Co., Inc., and used as received. $AlCl_3$ was sublimed before use. Dicobalt octacarbonyl was purchased from Strem Chemical Inc., and deuterated NMR solvents were obtained from Cambridge Isotope Laboratories, Inc., and used as received. Trindane[48] and [(*p*-Cymene)$RuCl_2$]$_2$[80] were prepared as described in the literature. Silica gel (particle size 20-45 microns) was used for flash column chromatography. Melting points (uncorrected) were determined on a Fisher-Johns melting point apparatus or a Gallenkamp capillary melting point apparatus. Microanalyses were performed by Guelph Chemical Laboratories, Guelph, Ontario, Canada. Infrared spectra were recorded on a Bio-Rad FTS-40 spectrometer, the compounds being contained in solution cells having NaCl windows.

8.2 NMR Spectroscopy

NMR spectra were recorded on Bruker DRX-500, AC-300 or AC-200 spectrometers. Spectra were recorded on spinning samples (except during the acquisition of

two-dimensional spectra), locked to a solvent signal. Peaks were referenced to the residual proton signal of the solvent, or the ^{13}C solvent signal, unless stated otherwise. ^{1}H and ^{13}C chemical shifts are given relative to TMS.

Selected spectra were recorded on a Bruker Avance DRX-500 spectrometer. Proton spectra were acquired at 500.13 MHz with a 5 mm broadband inverse probe with triple axis gradient capability. Spectra were acquired in 8 scans in 32K data points over a 3.931 kHz spectral width (4.168 s acquisition time). A Bruker Eurotherm variable temperature unit was used to maintain sample temperature. The free induction decay (FID) was processed with the use of exponential multiplication (line broadening: 0.15 Hz) and was zero-filled to 64K before Fourier transformation. Coupling constants (J) were reported in Hz. Carbon-13 NMR spectra were recorded at 125.758 MHz with a 5 mm broadband inverse probe with triple axis gradient capability. The spectra were acquired over a 28.986 kHz spectral width in 32K data points (0.557 s acquisition time). The ^{13}C pulse width was 4.4 μs (31° flip angle). A relaxation delay of 1.0 s was used. Exponential multiplication (line broadening: 4.0 Hz) was used to process the FID which was zero-filled to 64K before Fourier transformation.

Proton COSY two-dimensional NMR spectra were recorded in the absolute value mode with the pulse sequence $90° - t_1 - 45° - ACQ$ and included pulsed field gradients for coherence selection. Spectra were acquired in 2 scans for each of the 256 FIDs that contained 2K data points in F2 over a spectral width of 3930.82 Hz. The ^{1}H 90° pulse width was 6.6 μs. A 1.0 s relaxation delay was used between acquisitions. Zero-filling in F1 produced a 1K × 1K data matrix with a digital resolution of 3.84 Hz/point in both

dimensions. During two-dimensional Fourier transformations a sine-bell squared window function was applied to both dimensions. The transformed data were then symmetrised.

Inverse detected $^{1}H - ^{13}C$ two-dimensional chemical shift correlation spectra were acquired in the phase sensitive mode, and used the pulsed field gradient version of the HSQC pulse sequence. The FIDs in the F2 (^{1}H) dimension were recorded over a 3.655 kHz spectral width in 1K data points. The 128 FIDs in the F1 (^{13}C) dimension were obtained over a 21.368 kHz spectral width. Each FID was acquired in 2 scans. The fixed delays during the pulse sequence were a 1.0 s relaxation delay and a 1.786 ms polarization transfer delay. The 90° ^{1}H pulse was 6.6 μs while the ^{13}C 90° pulse was 11.6 μs. The data were processed with a sine-bell squared window function shifted by $\pi/2$ in both dimensions and linear prediction to 256 data points in F1, followed by zero-filling to 1K.

Inverse detected $^{1}H - ^{13}C$ two-dimensional chemical shift correlation spectra through two- and three-bond coupling interactions were acquired in the absolute value mode with the use of the pulsed field gradient version of the HMBC pulse sequence. The FIDs in the F2 (^{1}H) dimension were recorded over a 3.655 kHz spectral width in 1K data points. The 128 FIDs in the F1 (^{13}C) dimension were obtained over a 21.368 kHz spectral width. Each FID was acquired in 2 scans. The fixed delays during the pulse sequence were a 1.0 s relaxation delay, a 3.3 ms delay for the low pass J-filter and 0.08 s delay to allow evolution of the long-range coupling. The 90° ^{1}H pulse was 6.6 μs while the ^{13}C 90° pulse was 11.6 μs. The data were processed with a sine-bell squared window function shifted by $\pi/2$ in both dimensions and linear prediction to 256 data points in F1, followed by zero-filling to 1K.

Proton-proton NOE difference spectra were obtained by subtraction of a control FID from an on-resonance FID. The decoupler in the control FID irradiated a position in the spectrum where there was no proton signal. The on-resonance FID was obtained while the proton of interest was selectively saturated. In both cases the same decoupler power and duration of saturation (5.0 s) were used. This saturation period also served as the relaxation delay for both the control and on-resonance FIDs. The decoupler was gated off during acquisition. Eight scans were acquired for both the control and on-resonance FIDs; this was repeated four times for a total of 32 scans for the final difference spectrum. A 90° ^{1}H pulse width of 6.6 μs was used. The FIDs were processed with exponential multiplication (line broadening: 4.0 Hz) and were zero filled to 64K during Fourier transformation.

Selected Phosphorus-31 spectra were recorded at 121.496 MHz on a Bruker AC-300 NMR spectrometer using a 5 mm QNP probe, and referenced to an external 85% H_3PO_4 sample.

All other NMR spectra were recorded on a Bruker AC-200 spectrometer. Proton spectra were acquired at 200.133 MHz with a 5 mm dual frequency probe. Spectra were obtained in 8 scans in 16K data points over a 2.403 kHz spectral width (3.408 s acquisition time). Spectra were acquired at ambient probe temperature. The free induction decay (FID) was processed with exponential multiplication (line broadening 0.1 Hz) and was zero-filled to 32K before Fourier transformation. Carbon-13 NMR spectra were recorded at 50.323 MHz with the 5 mm QNP probe. The spectra were acquired over a 12.195 kHz spectral width in 16K data points (0.672 s acquisition time). The ^{13}C pulse width was 1.5 μs (42° flip angle). A 0.5 s relaxation delay was used. The

FIDs were processed with exponential multiplication (line broadening: 3.0 Hz) and zero-filled to 32K before Fourier transformation.

8.3 Mass Spectrometry

Electron impact (EI) and chemical ionisation (CI, with ammonia as the reagent gas) mass spectra were recorded on a VG analytical ZAB-E double focusing mass spectrometer. Typical experimental conditions were: mass resolution 1000 (high resolution elemental composition determinations performed at 5000), electron energy 70 eV, source temperature 200 °C, source pressure 2×10^{-6} mbar for EI and 4×10^{-5} mbar for CI. Mass spectra were recorded as percent intensity *versus* mass/charge ratio (*m/z*). Where applicable, *m/z* values listed are for $^{35}Cl/^{102}Ru$ isotopomers; all peak clusters showed correct isotopic abundance patterns.

Electrospray ionization mass spectrometry experiments were performed with a Fisons Platform quadrupole mass spectrometer. Typically, 50:50 CH_3CN: H_2O was the mobile phase, at a flow rate of 15 μL per minute, with the use of a Brownlee Microgradient syringe pump.

8.4 X-Ray Crystallography

8.4.1 X-ray Crystallographic Analyses – Data Collection

X-ray intensity data for **15** and **25** were collected at 292 K and 157 K, respectively, with the use of graphite-monochromated Ag Kα (λ = 0.56086 Å) radiation on a Siemens P3 diffractometer. Data were corrected for Lorentz and polarisation factors. Crystal stability

was monitored by measuring three standard reflections every 97 measurements. For **15**, an empirical absorption correction was based on 360 reflections (transmission factors 0.313 (maximum) and 0.290 (minimum)). Calculations were performed with the use of the SHELXTL PC[160] program library. For **25**, an empirical absorption correction was based on 396 data (transmission factors 1.000 (maximum) and 0.300 (minimum)). Calculations were performed with the use of the SHELXTL PC[161] program library.

X-ray intensity data for **28, 33, 34, 35, 36, 37** and **52** were collected with the use of graphite-monochromated Mo Kα (λ = 0.71073 Å) radiation on a Bruker P4 diffractometer, equipped with a Bruker Smart 1K Charge Coupled Device (CCD) Area Detector (using the program SMART[162]), and a rotating anode. The crystal-to-detector distance was 3.991 cm, and the data collection was carried out in 512 x 512 pixel mode, with 2 x 2 pixel binning. One hemisphere of data was collected, to better than 0.8 Å resolution. Upon completion of the data collection, the first fifty frames were recollected in order to improve the decay corrections analysis (if required). Also, redundant reflections were monitored as a function of time to check for decay. Data were processed with the use of the program SAINT[163], which applied Lorentz and polarisation corrections to three-dimensionally integrated diffraction spots. The program SADABS[164] was used to merge scans to apply decay corrections, if any, and to apply an empirical absorption correction based on redundant measurements. Calculations were performed with the use of the SHELXTL PC[161] program library. Data collection for **28** was carried out at 300 K, and for **33, 34, 35, 36, 37** and **52** at 210 K. Crystal data, data collection and reduction details, and structure details for all structures are listed in Appendix 1. Salient bond lengths and bond angles for **25** and **28** are listed in Figures 3.2 and 3.6 respectively.

8.4.2 X-ray Analysis Details

All crystals were grown from solution by slow evaporation of solvent. For **15**, **25**, **33**, **34**, **35**, **36** and **37** the solvent was CH_2Cl_2/hexane, for **28** the solvent was CH_2Cl_2 and for **52** the solvent was hexane/ether. In each case a suitable crystal was selected and mounted with epoxy cement: for **15** and **28**, on a glass pin; and for **25**, **33**, **34**, **35**, **36**, **37**, and **52** on a glass fibre attached with epoxy cement to a brass pin.

For **28**, **33**, **34**, **35**, **36**, **37**, and **52**, initial unit cell parameters were determined by a least squares fit of the angular settings of 112 strong reflections collected by a 4.5 ° scan in 15 frames over three different parts of reciprocal space. After data collection the respective unit cells were refined on 8,000 reflections. There was one molecule in the asymmetric unit for each sample, with the exception of **37** and **52**, which crystallized with 2 and 4 crystallographically independent molecules in their unit cells, respectively.

$C_{15}H_{18}Cr(CO)_3$ (15). A yellow crystal of **15** measuring approximately 0.31 × 0.25 × 0.20 mm was aligned on the diffractometer. Unit cell parameters were determined by a least squares fit of the angular settings of 38 reflections with $15.45° \leq 2\theta \leq 27.98°$. The structure was successfully solved in space group *Pbca* (No. 61) with a = 14.376(3) Å, b = 14.600(4) Å, c = 14.973(4) Å, V = 3145(1) Å^3, and Z = 8. The positions of the non-hydrogen atoms were determined by direct methods and refined anisotropically with the use of full matrix least-squares methods. All H atoms were included with the use of a riding model; isotropic thermal parameters were set at 0.05 Å^2. The refinement on 2041 unique reflections (R(int) = 2.95 %) from 3.80° to 35.10° in 2θ converged to R = 10.90 %. R_w = 5.5 %, and GOF = 0.745 for 199 parameters.

$C_{30}H_{36}Cl_4Ru_2$ (25). A red crystal of **25** measuring approximately 0.43 × 0.24 × 0.08 mm was aligned on the diffractometer. Unit cell parameters were determined by a least squares fit of the angular settings of 25 reflections with $15.26° \leq 2\theta \leq 44.23°$. The structure was successfully solved in space group $P2_1/n$ (No. 14) with a = 9.412(2) Å, b = 14.991(3) Å, c = 10.367(2) Å, β = 112.41(3), V = 1352.3(5) Å^3, and Z = 2. The positions of the non-hydrogen atoms were determined by direct methods and refined anisotropically with the use of full matrix least-squares methods. All H atoms were included in calculated positions and refined with the use of a riding model; isotropic thermal parameters were set at 50% greater than the equivalent isotropic thermal parameters for the C atoms to which they were attached. The refinement on 1765 unique reflections (R(int) = 3.91 %) from 3.94° to 40.00° in 2θ converged to R = 7.45 %. R_w = 13.27 %, and GOF = 0.904 for 163 parameters.

$C_{18}H_{27}O_3Cl_2PRu$ (28). A red crystal of **28** measuring approximately 0.20 × 0.12 × 0.04 mm was aligned on the diffractometer. The structure was successfully solved in space group $P2_1/c$ (No. 14) with a = 9.141(2) Å, b = 14.931(1) Å, c = 14.996(3) Å, β = 94.58(1), V = 2040.0(6) Å^3, and Z = 4. The positions of the non-hydrogen atoms were determined by direct methods and refined anisotropically with the use of full matrix least-squares methods. All H atoms were included in calculated positions and refined with the use of a riding model. Isotropic thermal parameters for methylene H atoms and methyl H atoms were set respectively at 20% and 50% greater than the equivalent isotropic thermal parameters for the C atoms to which they were attached. Disorder in the methoxy oxygen and carbon atoms was successfully refined in two parts, with 35% and 65% occupancies of the parts,

respectively. The refinement on 5240 unique reflections (R(int) = 7.90 %) from 3.86° to 60.94° in 2θ converged to R = 9.62 %. R_w = 10.47 %, and GOF = 1.049 for 236 parameters.

$C_{51}H_{75}O_{10}Cl_3Ru_2$ (33). A red crystal of **33** measuring approximately 0.40 × 0.28 × 0.09 mm was aligned on the diffractometer. The structure was successfully solved in space group *P-1* (No. 2) with a = 13.41060(10) Å, b = 14.9194(2) Å, c = 14.98330(10) Å, α = 103.2500(10), β = 94.7710(10), γ = 110.8320(10), V = 2682.21(4) Å^3, and Z = 2. The program PLATON[107] was used to subtract the averaged scattering contribution of the disordered $[C_5(COOCH_3)_5]^-$ anion from the intensity data for **33**. For the [(HEB)Ru-μCl_3-Ru(HEB)]$^+$ cation, the positions of the non-hydrogen atoms were determined by direct methods and refined anisotropically with the use of full matrix least-squares methods. All H atoms were included in calculated positions and refined with the use of a riding model. Isotropic thermal parameters for methylene H atoms and methyl H atoms were set respectively at 20% and 50% greater than the equivalent isotropic thermal parameters for the C atoms to which they were attached. The refinement on 10095 unique reflections (R(int) = 3.52 %) from 2.84° to 53.02° in 2θ converged to R = 5.86 %. R_w = 10.45 %, and GOF = 0.997 for 370 parameters.

$C_{18}H_{38}O_4B_2F_4Ru$ (34). A red crystal of **34** measuring approximately 0.40 × 0.30 × 0.20 mm was aligned on the diffractometer. The structure was successfully solved in space group $P2_12_12_1$ (No. 19) with a = 10.07260(10) Å, b = 13.8284(2) Å, c = 18.3629(2) Å, V = 2557.73(5) Å^3, and Z = 4. The positions of the non-hydrogen atoms were determined by direct methods and refined anisotropically with the use of full matrix least-squares methods.

All H atoms were located from the electron density map and refined isotropically. The refinement on 5245 unique reflections (R(int) = 1.75 %) from 3.68° to 53.08° in 2θ converged to R = 1.52 %. R_w = 3.90 %, and GOF = 1.040 for 451 parameters.

$C_{21}H_{39}O_3Cl_2PRu$ (35). A red crystal of **35** measuring approximately 0.30 × 0.18 × 0.08 mm was aligned on the diffractometer. The structure was successfully solved in space group *P-1* (No. 2) with a = 9.8280(10) Å, b = 10.2520(10) Å, c = 13.364(2) Å, α = 71.768(4), β = 85.496(3), γ = 68.6570(10), V = 1190.3(2) Å^3, and Z = 2. The positions of the non-hydrogen atoms were determined by direct methods and refined anisotropically with the use of full matrix least-squares methods. All H atoms were located from the electron density map and refined isotropically. The refinement on 5358 unique reflections (R(int) = 2.29 %) from 4.46° to 56.86° in 2θ converged to R = 2.47 %, R_w = 6.14 %, and GOF = 1.042 for 410 parameters.

$C_{21}H_{39}Cl_2PRu$ (36). A red crystal of **36** measuring approximately 0.23 × 0.13 × 0.03 mm was aligned on the diffractometer. The structure has not yet been satisfactorily refined, and work on this structure is in progress.

$C_{12}H_{36}Cl_2P_4Ru$ (37). A red crystal of **37** measuring approximately 0.40 × 0.28 × 0.09 mm was separated from the crystalline sample of **36**, and aligned on the diffractometer. The structure was successfully solved in space group *P2/n* (No. 13) with a = 15.67730(10) Å, b = 9.44760(10) Å, c = 15.6812(2) Å, β = 111.578(1), V = 2159.81(4) Å^3, and Z = 4. The crystal of **37** exhibited pseudo-merohedral twinning, which was solved by applying the

appropriate twin law, and refining a batch scale factor. This allowed the calculation and subtraction of the scattering contribution of the minor (28.9%) twin component from the intensity data for **37**. The positions of the non-hydrogen atoms were determined by direct methods and refined anisotropically with the use of full matrix least-squares methods. All H atoms were included in calculated positions and refined with the use of a riding model; isotropic thermal parameters for methyl H atoms were set at 50% greater than the equivalent isotropic thermal parameters for the C atoms to which they were attached. The refinement on 4408 unique reflections (R(int) = 4.22 %) from 2.80° to 52.94° in 2θ converged to R = 2.48 %. R_w = 6.14 %, and GOF = 1.051 for 174 parameters.

$C_{24}H_{24}O_7Co_2$, 52. A dark red crystal of **52** measuring approximately 0.20 mm × 0.10 mm × 0.06 mm was aligned on the diffractometer. The structure was successfully solved in space group *P-1* (No. 2), with a = 17.0510(10) Å, b = 17.1450(10) Å, c = 20.281(3) Å, α = 112.590(10)°, β = 99.160(10) °, γ = 110.620(10) °, V = 4816.7 Å^3, and Z = 8. The positions of non-hydrogen atoms were determined by direct methods and refined anisotropically with the use of full-matrix least-squares methods. All H atoms were included in calculated positions and refined with the use of a riding model. Isotropic thermal parameters for methylene and phenyl H atoms, and methyl H atoms and O-H atoms, were set at 20% and 50% greater than the equivalent isotropic thermal parameters for the C atoms to which they were attached, respectively. The refinement on 18151 reflections (R(int) = 6.61 %) from 2.32° to 52.84° in 2θ converged to R = 10.56 %. R_w = 11.67 %, and GOF = 1.064 for 1190 parameters.

8.5 Compound Preparation and Characterisation

Preparation of [(η^6-trindane)Cr(CO)$_3$], 15.

A mixture of trindane (0.891 g, 4.5 mmol) and $Cr(CO)_6$ (0.99 g, 4.5 mmol) in dry di-*n*-butyl ether (30 mL) and dry THF (20 mL) was heated under reflux in the dark for 72 h. The resulting yellow solution was then cooled and filtered, the solvent removed under reduced pressure, and the residue chromatographed on a silica gel column (eluent CH_2Cl_2 / hexane 20/80). A yellow band was collected, the solvents were removed under reduced pressure, and the residue was crystallised from CH_2Cl_2 / hexane solution to give **15** (1.07 g, 3.20 mmol; 71%), mp 202 °C. ^{1}H NMR (500 MHz, CD_2Cl_2): δ 2.71 (m, 12H), 2.10 (m, 3H), 1.99 (m, 3H). ^{13}C NMR (50.288 MHz, $CDCl_3$): δ 227.4 (Cr-*C*O), 110.6 (aromatic *C*), 30.2 (benzylic *C*H$_2$), 24.0 (wingtip *C*H$_2$). IR ($CDCl_3$): υ_{CO} 1869 (s), 1947 (s) cm^{-1}. Mass spectrum *m/z* (%) (EI): 585 (100) $[(C_{15}H_{18})_2Cr_2(CO)_3H]^+$, 557 (30) $[(C_{15}H_{18})_2Cr_2(CO)_2H]^+$, 448 (15) $[(C_{15}H_{18})_2Cr]^+$, 334 (79) $[M^+, (C_{15}H_{18})Cr(CO)_3{}^+]$, 278 (13) $[M\text{-}2CO]^+$, 250 (58) $[M\text{-}3CO]^+$, 197 (17) $[C_{15}H_{17}]^+$. (CI): 584 (16) $[(C_{15}H_{18})_2Cr_2(CO)_3]^+$, 335 (100) $[M+H]^+$, 197 (5) $[C_{15}H_{17}]^+$. Anal. Calcd for $C_{18}H_{18}O_3Cr$: C, 64.67; H, 5.39. Found: C, 64.49; H, 5.35.

Deuteration of [(η^6-trindane)Cr(CO)$_3$], 15.

In a typical experiment, [(η^6-trindane)Cr(CO)$_3$] (33.0 mg, 0.10 mmol) was dissolved in 2 mL DMSO-d_6 containing 0.112 g KO^{t}Bu and left under N_2 at room temperature for 1.5 h. Distilled water (5 mL) was added, and the mixture was filtered. The residue was extracted with diethyl ether, the ether layer dried over anhydrous $MgSO_4$, and the solvent removed under reduced pressure, leaving 22 mg (0.065 mmol) of product. ^{1}H NMR (200 MHz,

$CDCl_3$): δ 2.68 (m, br, 5H, benzylic CH_2), 2.02 (m, br, 6H, wingtip CH_2). ^{13}C NMR (50.288 MHz, $CDCl_3$): δ 227.5 (Cr-*C*O), 110.7 (aromatic *C*), 30.2 (benzylic *C*H_2), 24.1 (wingtip *C*H_2). Mass spectrum *m/z* (%): (CI): 363 (8) $[C_{15}H_6D_{12}Cr(CO)_3NH_3]^+$, 361 (58) $[C_{15}H_8D_{10}Cr(CO)_3NH_3]^+$, 359 (100) $[C_{15}H_{10}D_8Cr(CO)_3NH_3]^+$, 358 (94) $[C_{15}H_{11}D_7Cr(CO)_3NH_3]^+$, 357 (60) $[C_{15}H_{12}D_6Cr(CO)_3NH_3]^+$, 356 (62) $[C_{15}H_{13}D_5Cr(CO)_3NH_3]^+$, 355 (53) $[C_{15}H_{14}D_4Cr(CO)_3NH_3]^+$, 354 (60) $[C_{15}H_{15}D_3Cr(CO)_3NH_3]^+$, 353 (52) $[C_{15}H_{16}D_2Cr(CO)_3NH_3]^+$, 352 (12) $[C_{15}H_{17}D_1Cr(CO)_3NH_3]^+$, 351 (7) $[C_{15}H_{18}Cr(CO)_3NH_3]^+$, 346 (4) $[C_{15}H_6D_{12}Cr(CO)_3]^+$, 345 (10) $[C_{15}H_7D_{11}Cr(CO)_3]^+$, 344 (22) $[C_{15}H_8D_{10}Cr(CO)_3]^+$, 343 (19) $[C_{15}H_9D_9Cr(CO)_3]^+$, 342 (19) $[C_{15}H_{10}D_8Cr(CO)_3]^+$, 341 (21) $[C_{15}H_{11}D_7Cr(CO)_3]^+$, 340 (13) $[C_{15}H_{12}D_6Cr(CO)_3]^+$, 339 (5) $[C_{15}H_{13}D_5Cr(CO)_3]^+$, 338 (3) $[C_{15}H_{14}D_4Cr(CO)_3]^+$. (EI): 210 (5) $[C_{15}H_6D_{12}]^+$, 209 (16) $[C_{15}H_7D_{11}]^+$, 208 (13) $[C_{15}H_8D_{10}]^+$, 207 (20) $[C_{15}H_9D_9]^+$, 206 (70) $[C_{15}H_{10}D_8]^+$, 205 (65) $[C_{15}H_{11}D_7]^+$, 204 (50) $[C_{15}H_{12}D_6]^+$, 203 (39) $[C_{15}H_{13}D_5]^+$, 202 (45) $[C_{15}H_{14}D_4]^+$, 201 (37) $[C_{15}H_{15}D_3]^+$, 200 (47) $[C_{15}H_{16}D_2]^+$, 199 (15) $[C_{15}H_{17}D]^+$, 198 (9) $[C_{15}H_{18}]^+$.

Preparation of [(η^6-trindane)Mo(CO)$_3$], 17.

A mixture of trindane (1.98 g, 10 mmol) and $Mo(CO)_6$ (2.64 g, 10 mmol) in dry THF (50 mL) was heated under reflux for 66 h under nitrogen. The reaction mixture was cooled, concentrated to a volume of 20 mL under reduced pressure, and treated with excess hexane (approx. 50 mL). The resulting yellow powdery precipitate was filtered, dried, and recrystallised from chloroform / hexane (60/40) to give **17** as a yellow microcrystalline solid (2.34 g, 6.19 mmol; 62%), mp 145 °C (dec.). ^1H NMR (500 MHz, CD_2Cl_2): δ 2.77 (m, 12 H), 2.17 (d (12.4 Hz) of t (4.4 Hz), 3H), 2.06 (d (12.4 Hz) of t (12.2 Hz) of t (9.6 Hz),

3H); ^{2}J(*exo*-wingtip / *endo*-wingtip) 12.4 Hz; ^{3}J(*endo*-wingtip / *exo*-benzylic) 12.2 Hz; ^{3}J(*endo*-wingtip / *endo*-benzylic) 9.6 Hz; ^{3}J(*exo*-wingtip / *exo*-benzylic) 4.4 Hz. ^{13}C NMR (50.288 MHz, $CDCl_3$): δ 224.6 (Mo-CO), 115.3 (aromatic *C*), 30.8 (benzylic *C*H_2), 24.6 (wingtip *C*H_2). IR ($CDCl_3$): υ_{CO} 1866 (s), 1947 (s) cm^{-1}. Mass spectrum *m/z* (%) (EI): 676 (10) $[(C_{15}H_{18})_2Mo_2(CO)_3]^+$, 492 (5) $[(C_{15}H_{18})_2Mo]^+$, 380 (100) $[M^+, (C_{15}H_{18})Mo(CO)_3^+]$, 352 (15) $[M\text{-}CO]^+$, 324 (15) $[M\text{-}2CO]^+$, 296 (5) $[M\text{-}3CO]^+$, 198 (30) $[C_{15}H_{18}]^+$. (CI): 381 (100) $[M+H]^+$, 198 (22) $[C_{15}H_{18}]^+$. Mass spectral data quoted for ^{98}Mo; appropriate isotopic abundance patterns for Mo were observed. Anal. Calcd for $C_{18}H_{18}O_3Mo$: C, 57.14; H, 4.76. Found: C, 57.09; H, 4.66.

Preparation of [(η^6-trindane)Mn(CO)$_3$][BF_4], 18.

A mixture of $Mn(CO)_5Br$ (2.75 g, 10 mmol) and $AgBF_4$ (1.95 g, 10 mmol) in dry CH_2Cl_2 (50 mL) was heated under reflux for 3 h under nitrogen and then cooled to room temperature. To this reaction mixture a solution of trindane (1.98 g, 10 mmol) in dry CH_2Cl_2 (10 mL) was added and the reaction mixture was heated at reflux overnight. After cooling and filtration, the filtrate was passed through celite, concentrated to about one third of its volume under reduced pressure, and excess hexane (50 mL) was added. The resulting orange-yellow solid precipitate was filtered and dried *in vacuo* to give **18** (2.37 g, 5.59 mmol; 56%), mp 227 °C. ^{1}H NMR (200 MHz, CD_2Cl_2): δ 3.03 (m, 6H), 2.75 (m, 6H), 2.33 (m, 3H), 1.85 (m, 3H). ^{13}C NMR (50.288 MHz, $CDCl_3$): δ 215.7 (Mn-*C*O), 117.2 (aromatic *C*), 29.4 (benzylic *C*H_2), 23.3 (wingtip *C*H_2). IR ($CDCl_3$): υ_{CO} 1996 (s), 2050 (s) cm^{-1}. Mass spectrum *m/z* (%): (Positive ion electrospray) 337 (100) ($[M]^+$), 281 (15) ($[M\text{-}2CO]^+$),

253 35) ([M-3CO]$^+$). Anal. Calcd for $C_{18}H_{18}O_3BF_4Mn$: C, 50.94; H, 4.25. Found: C, 51.15; H, 4.05.

Preparation of [(η^6-trindane)Fe(η^5-C_5H_5)][BF_4], 19a.

A mixture of (η^5-C_5H_5)Fe(CO)$_2$I (3.04 g, 10 mmol), $AlCl_3$ (1.34 g, 10 mmol) and trindane (1.98 g, 10 mmol) in dry $CHCl_3$ (50 mL) was heated at reflux under nitrogen for 17 h. The reaction mixture was cooled, 50 mL of water added, and the resulting aqueous solution was filtered and washed several times with ether. Upon slow addition of an aqueous solution of $AgBF_4$ (1.76 g, 10 mmol) in water (10 mL), **19a** precipitated out as a beige solid. The precipitate was filtered, washed with water and then with ether, and dried *in vacuo*. Yield 2.80 g, (6.90 mmol; 69%), mp 145 °C (dec.). ^{1}H NMR (200 MHz, CD_3OD): δ 4.64 (s, 5H, C_5H_5), 3.05 (m, 6H), 2.79 (m, 6H), 2.30 (m, 6H). ^{13}C NMR (50.288 MHz, CD_3OD): δ 103.8 (aromatic *C*), 78.8 (Cp ring), 30.8 (benzylic C's), 24.1 (wingtip methylene C's). Mass spectrum *m/z* (%): (Positive ion electrospray) 319 (100) [M$^+$].

Preparation of [(η^6-trindane)Fe(η^5-C_5H_5)][PF_6], 19b.

A mixture of ferrocene (1.81 g, 10 mmol), trindane (1.98 g, 10 mmol), $AlCl_3$ (2.68 g, 20 mmol) and Al powder (0.27 g, 10 mmol) was heated at 150-200 °C to melt together under nitrogen for 20 h. The melt was cooled and extracted with water (150 mL). The aqueous solution was filtered and washed several times with excess light petroleum ether, until all unreacted ferrocene was washed away. Adding an aqueous solution of NH4PF6 (1.63 g, 10 mmol) in water (10 mL) precipitated the salt 19b. The precipitate was filtered, washed with water and ether, and dried *in vacuo* to give **19b** (3.99 g, 8.60 mmol; 86%), mp

230 °C (dec.). ^{1}H NMR (200 MHz, acetone-d_6): δ 4.86 (m, 5H) (Cp ring); 3.27 (m, 6H), 2.95 (m, 6H), 2.74 (m, 3H), 2.49 (m, 3H). ^{13}C NMR (50.288 MHz, acetone-d_6): δ 102.70 (aromatic *C*), 79.14 (Cp ring), 31.31 (benzylic *C*H$_2$), 23.94 (wingtip *C*H$_2$). Mass spectrum *m/z* (%): (Positive ion electrospray) 319 (100) [M$^+$].

Deuteration of [(η^6-trindane)Fe(η^5-C$_5$H$_5$)][PF$_6$], 19b.

[(η^6-trindane)Fe(η^5-C$_5$H$_5$)][PF$_6$] (46.4 mg, 0.10 mmol) was dissolved in 2 mL DMSO-d_6 containing 0.112 g KO^{t}Bu and left at room temperature overnight. Distilled water (5 mL) was added, and the mixture was filtered. The residue was extracted from 10 mL ethanol, and solvent was removed under pressure, leaving 30 mg (0.063 mmol) of product. ^{1}H NMR (200 MHz, acetone-d_6): δ 2.98 (s, br, integration not resolvable, benzylic C*H*$_2$), 2.50 (s, br, 3H, wingtip C*H*$_2$), 2.40 (s, br, 3H, wingtip C*H*$_2$). ^{13}C NMR (50.288 MHz, acetone-d_6): δ 78.4 (Cp ring), 30.1 (1:2:3:2:1 quintet, $^1J(^2D\text{-}^{13}C)$ = 19.3 Hz, benzylic *C*D$_2$), 24.0 (wingtip *C*H$_2$). Mass spectrum *m/z* (%): (Positive ion electrospray) 331 (100) [M$^+$-d_{12}, $C_{20}H_{11}D_{12}Fe^+$]; 319 (10) [M$^+$, $C_{20}H_{23}Fe^+$]. (DEI): 210 (48) $[C_{15}H_6D_{12}]^+$, 198 (50) $[C_{15}H_{18}]^+$, 66 (100) $[C_5H_6]^+$.

Preparation of [(η^6-trindane)$_2$Ru][BF$_4$]$_2$, 23.

To 0.065 g (0.087 mmol) of [(η^6-trindane)RuCl$_2$]$_2$, **25**, in 5 mL of dry acetone was added 0.068 g (0.35 mmol) AgBF$_4$, and the reaction mixture stirred for 15 min. at room temperature. The reaction mixture was then transferred to a clean Schlenk flask through a cannula, one end of which was covered with filter paper. The solution was taken to dryness under reduced pressure. Trifluoroacetic acid (3 mL) was introduced in the flask along with

trindane (0.07 g, 0.36 mmol) and the reaction mixture was heated at reflux for 15 min. and cooled to room temperature. The removal of solvent under reduced pressure gave a light yellow compound, which was washed with 10 mL of hexane, and then with 10 mL of ether and then dried *in vacuo* to give **23** as a white solid (135 mg, 0.043 mmol, 49.5 %; mp 210° C (dec.)). ^{1}H NMR data are collected in Table 3.1. ^{13}C NMR (125 MHz, CD_3NO_2): δ 111.9 (aromatic *C*); 29.8 (benzylic *C*H_2); 24.9 (wingtip *C*H_2). Mass spectrum *m/z* (%): (Positive ion electrospray) 585 (35) $[(trindane)_2RuBF_4]^+$, 517 (10) $[(trindane)_2RuF]^+$, 249 (100) $[(trindane)_2Ru]^{2+}$. Anal. Calcd for $C_{30}H_{36}B_2F_8Ru$: C, 53.68; H, 5.41. Found: C, 53.83; H, 5.26.

Preparation of [(η^6-trindane)Ru(η^6-cymene)][BF_4]$_2$, 24.

To a solution of [(*p*-cymene)$RuCl_2$]$_2$ (0.200 g, 0.327 mmol) in 7 mL of dry acetone was added 0.26 g (1.33 mmol) of $AgBF_4$, and the reaction mixture was stirred for 15 min. at room temperature. The reaction mixture was then transferred to a clean Schlenk flask through a cannula, one end of which was covered with filter paper, and taken to dryness under reduced pressure. Dichloromethane (10 mL) was introduced into the flask along with 0.177 g (0.89 mmol) of trindane, and the reaction mixture was heated at reflux for 48 h. The reaction mixture was cooled, and CH_2Cl_2 was decanted from the flask, leaving behind a light yellow viscous oil which was washed with 5 mL of CH_2Cl_2 and then with 10 mL of ether. On drying under vacuum, the oil changed to an off-white fluffy compound, **24**, (0.132 g, 0.217 mmol, 33 %; mp 60 °C (dec.)). ^{1}H NMR data are collected in Table 3.1. ^{13}C NMR (125 MHz, CD_3NO_2): δ Trindane: 114.8 aromatic *C*; 30.6 benzylic *C*H_2; 24.3 wingtip *C*H_2; Cymene: 112.2 ^{i}Pr-*C* (aromatic); 112.9 Me-*C* (aromatic); 94.8 *C*-H (aromatic); 92.2 *C*-

H (aromatic); 32.5 $(Me)_2$-*C*H-; 22.9 C-$(CH_3)_2$; 18.3 -CH_3. Mass spectrum *m/z* (%): (Positive ion electrospray) 453 (22) [(trindane)Ru(cymene)F]$^+$, 217 (100) [$(C_{25}H_{32}Ru)^{2+}$, M^{2+}]. Anal. Calcd for $C_{25}H_{32}B_2F_8Ru$: C, 49.45; H, 5.31. Found: C, 49.25; H, 5.60.

Preparation of [(η^6-trindane)$RuCl_2$]$_2$, 25, and [{(η^6-trindane)Ru}$_2Cl_3$]$^+$Cl$^-$, 27.

Data for **25**: A mixture of [(*p*-cymene)$RuCl_2$]$_2$ (0.205 g, 0.324 mmol) and trindane (2.0 g, 10.1 mmol) was sealed under vacuum and heated at 175 °C for 96 h, and then cooled to room temperature. To remove the large excess of unreacted trindane, the resulting red orange solid was washed with excess hexane (250 mL) and then washed with 20 mL of ether and dried *in vacuo*, to give **25** as an orange red solid (204 mg, 0.275 mmol, 85 %; mp 205 °C (dec.)). ^{1}H NMR data are collected in Table 3.1. ^{13}C NMR (125 MHz, CD_2Cl_2): δ 92.5 *C* (aromatic), 27.8 CH_2 (benzylic), 22.5 CH_2 (wingtip). Mass spectra *m/z* (%): (DEI) 740 (5) [$(C_{30}H_{36}Ru_2Cl_4)^+$, M^+], 705 (15) [M-Cl]$^+$, 370 (65) [(trindane)$RuCl_2$]$^+$, 298 (100) [Ru($C_{15}H_{16}$)]$^+$, 198 (75) [trindane]$^+$. (CI) 741 (5) [M+H]$^+$, 705 (55) [M-Cl]$^+$. (Positive ion electrospray) 705 (100) [Ru_2(trindane)$_2$Cl]$_3^+$. Data for **27**: Upon dissolution of **25** in CD_2Cl_2 there were observed two species in the ^{1}H and ^{13}C solution NMR spectra: these species were the neutral complex **25**, and the ionised species **27**. Recording of the NMR spectra of **25** in toluene-d_8 and CD_3NO_2 supplied further evidence for the formation of the ionised species **27** in solution, in particular, from a comparison of peak intensity ratios, formation of the ionised species **27** is greatly favoured in the most polar solvent, CD_3NO_2. ^{1}H NMR data are collected in Table 3.1. ^{13}C NMR (125 MHz, CD_2Cl_2): δ 93.6 *C* (aromatic), 28.4 CH_2 (benzylic), 22.8 CH_2 (wingtip). Anal. Calcd for $C_{30}H_{36}Cl_4Ru_2$: C, 48.66; H, 4.90. Found: C, 48.39; H, 5.08.

Preparation of (η^6-trindane)$RuCl_2[P(OMe)_3]$, 28.

[(Trindane)$RuCl_2]_2$, **25**, (74 mg, 0.1 mmol) and trimethyl phosphite (25 mg, 0.2 mmol) were taken into 10 mL of dry CH_2Cl_2 and the reaction mixture was stirred at room temperature for 3 h. The solvent was removed under reduced pressure and the residue was washed with 3 × 5 mL of hexane and dried *in vacuo*. The red residue was recrystallised from CH_2Cl_2 to give red X-ray quality crystals of **28** (69.6 mg, 0.201 mmol, 70 %; mp 165 °C). ^{1}H NMR data are collected in Table 3.1. ^{13}C NMR (125 MHz, CD_2Cl_2): δ 102.9 (d, $^3J(^{13}C\text{-}^{31}P) = 4.1$ Hz) aromatic *C*; 28.6, benzylic *C*H_2; 22.6 wingtip *C*H_2; 54.8 (d, $^2J(^{13}C\text{-}^{31}P) = 7.9$ Hz), O-*C*H_3. Mass spectrum *m/z* (%): (EI) 494 (10) [(trindane)$RuCl_2P(OMe)_3]^+$, 370 (10) $[M\text{-}P(OMe)_3]^+$, 298 (10) $[Ru(C_{15}H_{16})]^+$, 198 (15) [trindane]$^+$; (high resolution, EI): calculated mass for $^{12}C_{18}{}^1H_{27}{}^{16}O_3{}^{31}P{}^{35}Cl_2{}^{102}Ru$ $[M]^+$, 494.0118 amu, observed mass 494.0142 amu. Anal. Calcd for $C_{18}H_{27}O_3PCl_2Ru$: C, 43.73; H, 5.50. Found: C, 44.00; H, 5.60.

Preparation of [(η^6-hexaethylbenzene)$RuCl_2]_2$, 32.

A mixture of [(*p*-cymene)$RuCl_2]_2$ (1.0 g, 1.63 mmol) and hexaethylbenzene (8.04 g, 32.7 mmol) was sealed under vacuum, heated at 170 °C for 72 h, and then cooled to room temperature. The residue was washed with a large excess (250 mL) of hexane to remove the unreacted HEB, then dissolved in 10 mL of dry CH_2Cl_2. Hexane (25 mL) was added to cause the precipitation of the product. A dark purple-red compound was filtered and dried *in vacuo*, then recrystallised from CH_2Cl_2/hexane to give **32** (0.680 g, 0.81 mmol, 50%), mp (dec.) 240 °C. ^{1}H NMR (500 MHz, CD_2Cl_2, 30 °C): δ 2.53 (broad quartet, 7.45 Hz, 12H, *C*H_2), 1.42 (t, 7.45 Hz, 18H, *C*H_3). At -90.6 °C these signals

resolve into singlets at 2.57 and 2.27, and 1.40 and 1.27 ppm. ^{13}C NMR (125 MHz, CD_2Cl_2): δ 94.2 (arene *C*), 20.5 (*C*H_2), 14.2 (*C*H_3). At -90.6 °C these signals resolve into singlets at δ 99.1, 85.1; 20.3, 17.6; 15.0, 11.2. MS *m/z* (EI): 418 (50) $[(HEB)RuCl_2]^+$, 348 (12) $[(HEB)Ru]^+$, 246 (52) $[HEB]^+$. MS *m/z* (CI): 436 (18) $[(HEB)RuCl_2+NH_4]^+$, 247 (100) $[HEB+H]^+$. MS *m/z* (Positive ion electrospray): 801 (85) $[M-Cl]^+$, 383 (100) $[M-2Cl]^{2+}$.

Preparation of $[(\eta^6$-hexaethylbenzene$)_2Ru_2Cl_3][C_5(COOCH_3)_5]$, 33.

To a solution of $[(HEB)RuCl_2]_2$, **32**, (0.418 g, 0.5 mmol) in CH_2Cl_2 (25 mL) a solution of $K[C_5(COOCH_3)_5]$ (0.792 g, 2 mmol) in methanol (50 mL) was added under N_2, and the reaction mixture was heated at 70 °C for 3 h. After the color of the solution turned to greenish-yellow, solvents were removed under reduced pressure, and the residue was taken into 25 mL of CH_2Cl_2 and filtered. Hexane (20 mL) was added to the filtrate, and the solution was left to crystallize by slow evaporation. After 2-3 d, a yellow-orange microcrystalline solid was separated and dried *in vacuo* to give **33** (305 mg, 0.26 mmol, 53%), mp 216 °C. ^1H NMR (500 MHz, CD_2Cl_2,): δ 3.69 (s, 15H, O-C*H*$_3$), 2.39 (quartet, 7.5 Hz, 12H, C*H*$_2$), 1.29 (t, 7.5 Hz, 18H, C*H*$_3$). ^{13}C NMR (125 MHz, CD_2Cl_2): δ 167.9 (CO), 95.3 (arene *C*), 51.4 (O-*C*H_3), 21.5 (*C*H_2), 15.0 (*C*H_3). MS *m/z* (Positive ion electrospray): 801 (30) $[M]^+$, 383 (100) $[M-Cl]^{2+}$.

Preparation of $[(\eta^6$-hexaethylbenzene$)Ru(H_2O)_3](BF_4)_2 \cdot H_2O$, 34.

To a purple-red solution of $[(HEB)RuCl_2]_2$, **32**, (0.105 g, 0.125 mmol) in CH_2Cl_2 (10 mL) was added $AgBF_4$ (0.100 g, 0.5 mmol) under N_2; the mixture was stirred for 1 h

at room temperature. After the colour of the solution changed to orange-yellow, the resulting mixture was filtered and the filtrate was concentrated to approx. 5 mL. Hexane (5 mL) was added and under refrigeration **34** crystallized as a yellow-orange crystalline solid (100 mg, 0.17 mmol, 69%), mp 155 °C. ^{1}H NMR (500 MHz, CD_2Cl_2, 30 °C): δ 4.14 (s, broad, H_2O), 2.66 (s, broad, 12H, CH_2), 1.39 (t, 7.39 Hz, 18H, CH_3). At -73.6 °C these signals resolve into singlets at 2.55, 2.25; 1.36, 1.21 ppm. ^{13}C NMR (125 MHz, CD_2Cl_2): δ 95.3 (arene *C*), 21.6 (CH_2), 14.2 (CH_3). MS *m/z* (Positive ion electrospray, in CH_3CN/H_2O): 408 (100) $[M+H+CH_3CN-2H_2O]^+$, 192 (32) $[M-2H_2O]^{2+}$.

Attempted preparation of [(η^6-hexaethylbenzene)$_2$Ru](BF$_4$)$_2$.

Excess HEB was added to the yellow-orange filtrate obtained from the reaction for **34**, and the mixture heated at reflux overnight. The solvent was removed under reduced pressure and the residue was washed with hexane. A yellow-orange powder was separated, dried and identified by ^{1}H and ^{13}C NMR spectroscopy and X-ray crystallography as **34**.

Preparation of [(η^6-hexaethylbenzene)RuCl$_2$P(OMe)$_3$], 35.

To a solution of $[(HEB)RuCl_2]_2$, **32**, (0.167 g, 0.2 mmol) in CH_2Cl_2 (10 mL) under N_2, $P(OMe)_3$ (1.0 mL, 0.8 mmol) was added *via* syringe and the mixture was stirred at room temperature for 3 h. The resulting orange-red solution was concentrated to about 3 mL under reduced pressure and 5 mL of hexane were added. Recrystallisation overnight produced **35** as a red crystalline solid (174 mg, 0.32 mmol, 80%), mp 150° C. ^{1}H NMR (200 MHz, CD_2Cl_2,): δ 3.71 (d, 9H, O-CH_3, $^3J(^1H-^{31}P)$ = 10.2 Hz), 2.57 (quartet, 7.6 Hz,

12H, C*H*$_2$), 1.31 (t, 7.6 Hz, 18H, C*H*$_3$). ^{13}C NMR (50 MHz, CD_2Cl_2): δ 103.7 (arene *C*), 54.6 (O-*C*H$_3$), 22.5 (*C*H$_2$), 14.9 (*C*H$_3$). MS *m/z* (EI): 542 (37) [M, $C_{21}H_{39}O_3PCl_2Ru$]$^+$, 507 (14) [M-Cl] $^+$, 418 (100) [M- P(OCH$_3$)$_3$]$^+$, 383 (44) [(HEB)RuCl]$^+$, 348 (37) [(HEB) Ru]$^+$. MS *m/z* (CI): 436 (15) [M-P(OCH$_3$)$_3$+NH$_4$]$^+$, 247 (35) [HEB+H]$^+$, 125 (100, [P(OCH$_3$)$_3$H]$^+$.

Preparation of [(η^6-hexaethylbenzene)RuCl$_2$PMe$_3$], 36.

To a solution of [(HEB)RuCl$_2$]$_2$, **32**, (0.418 g, 0.5 mmol) in CH_2Cl_2 (50 mL) under N_2, PMe_3 (0.3 mL, 0.24 mmol) was added *via* syringe and the mixture was stirred at room temperature for 24 h. The resulting orange-red solution was concentrated to about 3 mL under reduced pressure and 10 mL of hexane were added. Recrystallisation overnight produced **36** as a red crystalline solid (400 mg, 0.81 mmol, 81%), mp 192 °C. ^{1}H NMR (200 MHz, CD_2Cl_2, 30 °C): 2.55 (quartet, 7.6 Hz, 12H, C*H*$_2$), 1.40 (d, ^{2}J(^{1}H-^{31}P) = 10.5 Hz, 9H, P-C*H*$_3$), 1.32 (t, 7.6 Hz, 18H, C*H*$_3$). ^{13}C NMR (50 MHz, CD_2Cl_2): δ 100.9 (arene *C*), 23.0 (*C*H$_2$), 15.9 (P-(*C*H$_3$)$_3$), 15.2 (*C*H$_3$). ^{31}P NMR (121.5 MHz, CD_2Cl_2): δ -3.08 (decet, ^{2}J(^{1}H-^{31}P) = 10.5 Hz, *P*-(CH$_3$)$_3$). MS *m/z* (EI): 494 (40) [M]$^+$, 459 (16) [M-Cl]$^+$, 418 (100) [M-P(CH$_3$)$_3$]$^+$, 383 (67) [M-P(CH$_3$)$_3$-Cl]$^+$, 246 (38) [HEB]$^+$, 76 (98) [P(CH$_3$)$_3$]$^+$. MS *m/z* (CI): 495 (28) [M+H]$^+$, 460 (50) [M+H-Cl]$^+$, 77 (100) [P(CH$_3$)$_3$+H]$^+$.

From the crystalline sample of **36** red crystals of a second minor product of the reaction were separated, and shown by X-ray crystallography to be of the known compound *trans*-RuCl$_2$[P(CH$_3$)$_3$]$_4$, **37**.

Preparation of 1-phenylethynylcyclohexanol, 45.

Cyclohexanone (2.6 mL, 25 mmol) was added to a solution of phenylacetylene (2.75 mL, 25 mmol) and *n*BuLi (18.7 mL, 30 mmol) in diethyl ether at a temperature of –78 °C. The reaction mixture was quenched with HCl, extracted with diethyl ether/water, and ether removed from the organic phase to give **45** as a white solid (3.356 g, 16.8 mmol, 67%). ^{1}H NMR (DMSO-d_6, 500 MHz): δ 7.36 (5H, m, C_6H_5), 5.38 (1H, s, O*H*), 1.83 (2H, m, $H_{2,6\text{-eq}}$), 1.64 (2H, m, $H_{3,5\text{-eq}}$), 1.50 (5H, m, $H_{2,3,5,6\text{-ax}}$, $H_{4\text{eq}}$), 1.23 (1H, m, $H_{4\text{ax}}$). ^{13}C NMR (DMSO-d_6, 125 MHz): δ 131.5, 128.9 (ortho, meta-*C*), 128.5 (para-*C*), 123.1 (ipso-*C*), 95.3 (*C*C-C_6H_5), 83.0 (C*C*-C_6H_5), 67.3 (C_1), 42.2 ($C_{2,6}$), 25.2 (C_4), 24.3 ($C_{3,5}$). Mass spectrum (EI, *m/z* (%)): 200 (45) ($[M]^+$), 183 (100) ($[M+H-H_2O]^+$). (CI, NH_3, m/z (%)): 200 (20) ($[M]^+$), 183 (100) ($[M+H-H_2O]^+$).

Preparation of 1-phenylethynylcyclohexanol•$Co_2(CO)_6$, 46.

Dicobalt octacarbonyl (1.706 g, 4.99 mmol) was dissolved in 30 mL THF. 1-Phenylethynylcyclohexanol (0.999 g, 4.99 mmol) dissolved in 20 mL THF was added dropwise while stirring. After 1 hour, removal of THF gave a purple-red solid (2.375 g, 4.89 mmol, 98 %). Mass spectrum EI, *m/z* (%) : 458 (15) [M^+-CO], 430 (21) [M^+-2 CO], 374 (20) [M^+-4 CO], 346 (27) [M^+-5 CO], 318 (25) [M^+-6 CO].

Preparation of *Trans*-4-*t*-Bu-1-phenylethynylcyclohexanol, 51.

Bromoethane (4.3 mL, 0.058 mol) was added slowly to a solution of magnesium (1.413 g, 0.058 mol) in THF. After stirring for 20 minutes, phenylacetylene (6.35 mL, 0.058 mol) was added dropwise to the THF solution, and the mixture allowed to stir for 15

minutes. To this solution, 4-*t*-butyl-cyclohexanone (8.960 g, 0.058 mol) dissolved in THF was added slowly, and the solution was stirred for 2 hours. The reaction mixture was quenched with 30 mL of 20% HCl, and extracted with diethyl ether/water. Removal of ether from the organic phase gave a cream coloured solid, crude yield 10.759 g (0.042 mol, 72 %). Recrystallisation from petroleum ether (50-100 °C) gave a white solid (4.840 g, 0.019 mol, 32% recovered, mp 125-126 °C). ^{1}H NMR (DMSO-d_6, 500 MHz): δ 7.36 (5H, m, C_6H_5), 5.47 (1H, s, O*H*), 1.96 (2H, m, $H_{2,6\text{-eq}}$), 1.68 (2H, m, $H_{3,5\text{-eq}}$), 1.38 (4H, m, $H_{2,3,5,6\text{-ax}}$), 1.01 (1H, t ($^3J_{H\text{-}H}$ = 11.6 Hz) of t ($^3J_{H\text{-}H}$ = 3.3 Hz), H_4), 0.84 (9H, s, C(CH_3)$_3$). ^{13}C NMR (DMSO-d_6, 125 MHz): δ 130.9, 128.6 (ortho-, meta-*C*), 128.1 (para-*C*), 122.7 (ipso-*C*), 94.1 (*C*C-C_6H_5), 83.7 (C*C*-C_6H_5), 67.9 (C_1), 46.4 (C_4), 40.2 ($C_{2,6}$), 31.9 (*C*(CH$_3$)$_3$), 27.4 (C(*C*H$_3$)$_3$), 24.3 ($C_{3,5}$). Mass spectrum (EI, *m/z* (%)): 256 (25) ([M]$^+$), 199 (18) ([M-C(CH$_3$)$_3$]$^+$), 57 (100) ([C(CH$_3$)$_3$]$^+$). (CI, NH$_3$, m/z (%)): 256 (20) ([M]$^+$), 239 (100) ([M+H-H$_2$O]$^+$).

Preparation of *Trans*-4-*t*-Bu-1-phenylethynylcyclohexanol•Co$_2$(CO)$_6$, 52.

Trans-4-*t*-butyl-phenylethynylcyclohexanol, **51**, (0.641 g, 2.5 mmol) was dissolved in 10 mL warm THF and added dropwise to a solution of dicobalt octacarbonyl (0.856 g, 2.5 mmol) dissolved in 30 mL THF. After stirring for 1 hour, removal of solvent gave a dark red solid (1.240g, 2.29 mmol, 91%, mp (dec.) > 156 °C). Flash column chromatography with 80:20 hexanes/diethyl ether gave dark red crystals of **52** suitable for X-ray diffraction. ^{1}H NMR (C$_6$D$_6$, 300 MHz): δ 7.43 (2H, m, C_6H_5), 6.97 (3H, m, C_6H_5), 4.30 (1H, s, O*H*), 2.03 (2H, m, $H_{2,6\text{-eq}}$), 1.63-1.07 (m, 6H, $H_{3,5\text{-eq}}$, $H_{2,3,5,6\text{-ax}}$), 0.85 (1H, m, H_4), 0.54 (9H, s, C(CH_3)$_3$). ^{13}C NMR (CD$_2$Cl$_2$, 75 MHz): δ 170.0 (Co-*C*O). ^{13}C NMR (C$_6$D$_6$, 75 MHz) δ

130.3 (ortho-, meta-*C*), 127.7 (ipso-*C*), 74.1 (C_1), 69.1 (*C*C-C_6H_5), 48.0 (C_4), 43.2 ($C_{2,6}$), 32.2 ($C(CH_3)_3$), 27.5 ($C(CH_3)_3$), 24.3 ($C_{3,5}$). Mass spectrum (EI, *m/z* (%)): 514 (4) ([M-CO]$^+$), 486 (6) ([M-2CO]$^+$), 458 (5) ([M-3CO]$^+$), 430 (5) ([M-4CO]$^+$), 402 (16) ([M-5CO]$^+$), 374 (16) ([M-6CO]$^+$), 57 (100) ([*t*Bu]$^+$). (CI, NH_3, m/z (%)): 525 (20) ([M+H-H_2O]$^+$), 256 (38) ([M-$Co_2(CO)_6$]$^+$), 239 (100) ([M+H-$Co_2(CO)_6$-H_2O]$^+$). IR (THF) ν_{CO} at 2088, 2049 and 2066 cm^{-1}.

Preparation of *Trans*-4-*t*-Bu-1-trimethylsilylethynylcyclohexanol, 53a.

Bromoethane (3.8 mL, 50 mmol) was added dropwise to magnesium (1.216 g, 50 mmol) in Et_2O. After stirring for 20 minutes, trimethylsilylacetylene (7.1 mL, 50 mmol) was added dropwise. After stirring for 15 minutes, 4-*t*-butyl-cyclohexanone (7.713 g, 50 mmol) dissolved in Et_2O was added dropwise. The reaction mixture was quenched with 5 mL of 15% HCl. The mixture was extracted with diethyl ether and water. Yield (crude, pale yellow oil) 7.352 g (29.1 mmol, 58 %). ^{1}H NMR ($CDCl_3$, 200 MHz): δ 1.97 (2H, m, $H_{2,6\text{-eq}}$), 1.72 (2H, m, $H_{3,5\text{-eq}}$), 1.39 (4H, m, $H_{2,3,5,6\text{-ax}}$), 0.96 (1H, m, H_4), 0.85 (9H, s, $C(CH_3)_3$), 0.14 (s, $Si(CH_3)_3$). ^{13}C NMR ($CDCl_3$, 50 MHz): δ 109.5 (*C*≡CSi), 69.8 (C_1), 46.8 (C_4), 40.3 ($C_{2,6}$), 32.2 ($C(CH_3)_3$), 2754 ($C(CH_3)_3$), 24.8 ($C_{3,5}$), 0.0 ($Si(CH_3)_3$). Mass spectrum (EI, *m/z* (%)): 73 (10) ([$Si(CH_3)_3$]$^+$), 57 (100) ([$C(CH_3)_3$]$^+$). (CI, NH_3, m/z (%)): 252 (16) [M$^+$], 235 (9) ([M+H-H_2O]$^+$).

Preparation of 4-*t*-Bu-1-trimethylsilylethynylcyclohexanol•$Co_2(CO)_6$, 54a.

4-*t*-butyl-trimethylsilylethynylcyclohexanol, **53a**, (crude oil, 0.631 g, 2.5 mmol) was dissolved in 10 mL THF and added dropwise to a solution of dicobalt octacarbonyl (0.854 g,

2.5 mmol) dissolved in 30 mL THF. After stirring for 1.5 hour, removal of solvent gave a dark red partially oily product (0.681 g, 1.26 mmol, 51%). Purification by flash column chromatography (80 hexanes: 20 diethyl ether) was attempted. ^{1}H NMR ($CDCl_3$, 200 MHz): δ 1.83, 1.54, 1.23 (m, (CH_2)$_{2,3,5,6}$, H_4), 0.89 (s, C(CH_3)$_3$), 0.35 (s, Si(CH_3)$_3$). ^{13}C NMR (C_6D_6, 50 MHz): δ 121.0 (C≡CSi), 79.4 (C≡CSi), 74.3 (C_1), 48.0 (C_4), 43.3 ($C_{2,6}$), 32.5 (C(CH_3)$_3$), 28.1 (C(CH_3)$_3$), 24.8 ($C_{3,5}$), 1.6 (Si(CH_3)$_3$). Mass spectrum (EI, *m/z* (%)): 426 (2) ([M-4CO]$^+$), 370 (1) ([M-6CO]$^+$), 179 (9) ([M-$Co_2(CO)_6$-Si(CH_3)$_3$]$^+$), 73 (40) ([Si(CH_3)$_3$]$^+$, 57 (100) ([C(CH_3)$_3$]$^+$). (CI, NH_3, m/z (%)):426 (5) ([M-4CO]$^+$), 252 (17) ([M-$Co_2(CO)_6$]$^+$), 235 (100) ([M+H-$Co_2(CO)_6$-H_2O]$^+$) 73 (8) ([Si(CH_3)$_3$]$^+$).

Preparation of 2-*t*-butyl-phenylethynylcyclohexanol, 55.

Bromoethane (4.3 mL, 0.058 mol) was added dropwise to magnesium (1.412 g, 0.058 mol) in THF. After stirring for 20 minutes, phenylacetylene (6.4 mL, 0.058 mol) was added dropwise. After stirring for 15 minutes, 2-*t*-butyl-cyclohexanone (10 mL, 0.058 mol) in THF was added dropwise. The reaction mixture was quenched with 20 mL of 20% HCl. The mixture was extracted with diethyl ether and water. Removal of solvent gave a pale yellow oil. ^{1}H NMR ($CDCl_3$, 200 MHz): δ 7.45 (5H, m, C_6H_5), 5.29 (s, OH), 2.35-1.15 (m, $H_{3,4,5,6eq}$, $H_{3,4,5,6ax}$, $H2$), 0.99 (9H, s, C(CH_3)$_3$). ^{13}C NMR ($CDCl_3$, 50 MHz): δ 131.7, 128.2 (ortho-, meta-C), 122.9 (ipso-C), 92.8 (C≡C-C_6H_5), 85.6 (C≡C-C_6H_5), 69.1 (C_1), 40-20 ppm (numerous peaks, including $C_{2,3,4,5,6}$, C(CH_3)$_3$, C(CH_3)$_3$). Mass spectrum (EI, *m/z* (%)): 199 (49) ([M- C(CH_3)$_3$]$^+$), 57 (16) ([C(CH_3)$_3$]$^+$). (CI, NH_3, m/z (%)): 183 (100) [M+H-C(CH_3)$_3$-H_2O]$^+$), 57 (5) ([C(CH_3)$_3$]$^+$).

References

1. Abd-El-Aziz, A. S.; de Denus, C. R.; Zaworotko, M. J.; MacGillivray, L. R. *J. Chem. Soc., Dalton Trans.* **1995**, 3375.

2. See, for example: Silverthorn, W. E. *Adv. Organomet. Chem.* **1975**, *13*, 47.

3. Le Bozec, H.; Touchard, D.; Dixneuf, P. *Adv. Organomet. Chem.* **1989**, *29*, 163, (and references therein).

4. Kroto, H. W.; Heath, J. R.; O'Brien, S. C.; Curl, R. F.; Smalley, R. E. *Nature* **1985**, *318*, 162.

5. Kroto, H. W.; Allaf, A. W.; Balm, S. P. *Chem. Rev.* **1991**, *91*, 1213.

6. Curl, R. F.; Smalley, R. E. *Scientific American* **1991**, *265*, 54.

7. Sastry, G. N.; Jemmis, E. D.; Mehta, G.; Shah, S. R. *J. Chem. Soc., Perkin Trans.* **1993**, *2*, 1867.

8. Mehta, G.; Rao, H. S. P. *Tetrahedron* **1998**, *54*, 13325.

9. Barth, W. E.; Lawton, R. G. *J. Am. Chem. Soc.* **1966**, *88*, 380.

10. Scott, L. T.; Hashemi, M. M.; Bratcher, M. S. *J. Am. Chem. Soc.* **1992**, *114*, 1920.

11. Jaouen, G.; Top, S.; Laconi, A.; Coutourier, D.; Brocard, J. *J. Am. Chem. Soc.* **1984**, 2207.

12. Hamon, J.-R.; Saillard, J.-Y.; Le Beuze, A.; McGlinchey, M. J.; Astruc, D. *J. Am. Chem. Soc.* **1982**, *104*, 7549.

13. Cotton, F. A.; Wilkinson, G. *Advanced Inorganic Chemistry*, 5th ed., Wiley-Interscience, New York, **1988**, p.1053.

14. Hoffmann, R. *Angew. Chem., Int. Ed. Engl.* **1982**, *21*, 711.

15. Greenfield, H.; Sternberg, H. W.; Friedel, R. A.; Wotiz, J. H.; Markby, R.; Wender, I. *J. Am. Chem. Soc.* **1956**, *78*, 120.

16. Markby, R.; Wender, I.; Friedel, R. A.; Cotton, F. A.; Sternberg, H. W. *J. Am. Chem. Soc.* **1958**, *80*, 6529.

17. D'Agostino, M. F.; Frampton, C. S.; McGlinchey, M. J. *J. Organomet. Chem.* **1990**, *394*, 145.

18. Seyferth, D. *Adv.Organomet. Chem.* **1976**, *14*, 97.

19. Schilling, B. E. R; Hoffmann, R. *J. Am. Chem. Soc.* **1979**, *101*, 3456.

20. McGlinchey, M. J.; Girard, L.; Ruffolo, R. *Coord. Chem. Rev.* **1995**, *143*, 331, and references therein.

21. El Amouri, H.; Gruselle, M. *Chem. Rev.* **1996**, *96*, 1077.

22. Gruselle, M.; El Hafa, H.; Nikolski, M.; Jaouen, G.; Vaissermann, J.; Li, L.; McGlinchey, M. J. *Organometallics* **1993**, *12*, 4917.

23. Nicholas, K. M.; Pettit, R. *J. Organomet. Chem.* **1972**, *44*, C21.

24. Osella, D.; Dutto, G.; Vessières, A.; Raithby, P. R.; De Benedetto, L.; McGlinchey, M. J. *Organometallics* **1993**, *12*, 4545.

25. Ruffolo, R.; Brook, M. A.; McGlinchey, M. J. *Organometallics* **1998**, *17*, 4992.

26. Dunn, J. A.; Hunks, W. J.; Ruffolo, R.; Rigby, S. S.; Brook, M. A.; McGlinchey, M. J. *Organometallics* **1999**, *18*, 3372.

27. Melikyan, G. G.; Bright, S.; Monroe, T.; Hardcastle, K. I.; Ciurash, J. *Angew. Chem., Int. Ed. Engl.* **1998**, *37*, 161.

28. Nicholas, K. M., Pettit, D. *Tetrahedron Lett.* **1971**, *37*, 3475.

29. Iwasawa, N.; Matsuo, T.; Iwamoto, M.; Ikeno, T. *J. Am. Chem. Soc.* **1998**, *120*, 3903.

30. Tanaka, S.; Isobe, M. *Tetrahedron* **1994**, *50*, 5633.

31. Malisza, K. L.; Girard, L.; Hughes, D. W.; Britten, J. F.; McGlinchey, M. J. *Organometallics* **1995**, *14*, 4676.

32. Gupta, H. K.; Lock, P. E.; McGlinchey, M. J. *Organometallics,* **1997**, *16*, 3628.

33. Gupta, H. K.; Lock, P. E.; Hughes, D.W.; McGlinchey, M. J. *Organometallics* **1997**, *16*, 4355.

34. See, for example Reference 3, and (a) *Acc. Chem. Res.* **1992**, *25* (Special issue on Buckminsterfullerenes). (b) Billups, W. E., Ciufolini, M. A., Eds. *Buckminsterfullerenes*; VCH Publishers: New York, **1993**. (c) Kroto, H. W., Fischer, J. E., Cox, D. E., Eds. *The Fullerenes*; Pergamon: Oxford, **1993**. (d) Hirsch, A. *The Chemistry of the Fullerenes*; Thieme: New York, **1994**.

35. Reference 9, and Barth, W. E.; Lawton, R. G. *J. Am. Chem. Soc.* **1971**, *93*, 1730.

36. (a) Scott, L. T.; Hashemi, M. M.; Meyer, D. T.; Warren, H. B. *J. Am. Chem. Soc.* **1991**, *113*, 7082. (b) Scott, L. T.; Bratcher, M. S.; Hagen, S. *J. Am. Chem. Soc.* **1996**, *118*, 8743.

37. Borchardt, A.; Fuchicello, A.; Kilway, K. V.; Baldridge, K. K.; Siegel , J. S. *J. Am. Chem. Soc.* **1992**, *114*, 1921.

38. Zimmermann, G.; Nuechter, U.; Hagen, S.; Nuechter, M. *Tetrahedron Lett.* **1994**, *35*, 4747.

39. Siegel, J. S.; Seiders, T. J. *Chem. Br.* **1995**, 313.

40. Rabideau, P. W.; Sygula, A. *Acc. Chem. Res.* **1996**, *29*, 235.

41. Rabideau, P. W.; Abdourazak, A. H.; Folsom, H. E.; Marcinow, Z.; Sygula, A.; Sygula, R. *J. Am. Chem. Soc.* **1994**, *116*, 7891.

42. Abdourazak, A. H.; Marcinow, Z.; Sygula, A.; Sygula, R.; Rabideau, P. W. *J. Am. Chem. Soc.* **1995**, *117*, 6410.

43. Sygula, A.; Rabideau, P. W. *J. Am. Chem. Soc.* **1998**, *120*, 12666.

44. Sygula, A.; Rabideau, P. W. *J. Am. Chem. Soc.* **1999**, *121*, 7800.

45. Seiders, T. J.; Elliott, E. L.; Grube, G. H.; Siegel, J. S. *J. Am. Chem. Soc.* **1999**, *121*, 7804.

46. Sumanene is derived from the Sanskrit word *suman* which translates as "flower". The ring edges are considered to resemble petals, hence the trivial name `sumanene' has been proposed for this molecule (see reference 18).

47. Mehta, G.; Shah, S. R.; Ravikumar, K. *J. Chem. Soc., Chem. Commun.* **1993**, 1006.

48. (a) Mayer, R. *Chem. Ber.* **1956**, *89*, 1443. (b) Petru, F.; Galik, V. *Chem. Listy* **1957**, *51*, 2371. (c) Wallach, O. *Chem. Ber.* **1897**, *30*, 1094.

49. Katz, T. J.; Slusarek, W. *J. Am. Chem. Soc.* **1980**, *102*, 1058.

50. (a) Helvenston, M. C.; Lynch, T. J. *J. Organomet. Chem.* **1989**, *359*, C50. (b) Lynch, T. J.; Helvenston, M. C.; Rheingold, A. L.; Staley, D. L. *Organometallics* **1989**, *8*, 1959. (c) Bang, H.; Lynch, T. J.; Basolo, F. *Organometallics* **1992**, *11*, 40. (d) Winter, R.; Pierce, D. T.; Geiger, W. E.; Lynch, T. J. *J. Chem. Soc., Chem. Comm.* **1994**, 1949.

51. (a) Seka, R.; Kellerman, W. *Chem. Ber.* **1942**, *75*, 1730. (b) Bergman, J.; Egestad, B. *Chemica Scripta* **1986**, *26*, 287. (c) Drake, J. A. G.; Jones, D. W. *Org. Magn. Res.* **1980**, *14*, 276.

52. Tisch, T. L.; Lynch, T. J.; Dominguez, R. *J. Organomet. Chem.* **1989**, *377*, 265.

53. Ranganathan, S.; Muraleedharan, K. M.; Bharadwaj, P.; Madhusudanan, K. P. *J. Chem. Soc., Chem. Commun.* **1998**, 2239.

54. Holý, P.; Havránek, M.; Pánková, M.; Ridvan, L.; Závada, J. *Tetrahedron*, **1997**, *53*, 8195.

55. Podlaha, J.; Císa⋆ová, I.; Holý, P.; Závada, J. *Z. Kristallogr. NCS* **1999**,*214*, 185.

56. Bürgi, H.-B.; Baldridge, K. K.; Hardcastle, K.; Frank, N. L.; Gantzel, P.; Siegel, J. S.; Ziller, J. *Angew. Chem., Int. Ed. Engl.* **1995**, *34*, 1454.

57. Wester, D. W.; Coveney, J. R.; Nosco, D. L.; Robbins, M. S.; Dean, R. T. *J. Med. Chem.* **1991**, *34*, 3284.

58. For a comprehensive summary of recent thinking on the Mills-Nixon effect, see: (a) Frank, N. L.; Baldridge, K. K.; Gantzel, P.; Siegel, J. S. *Tetrahedron Lett.* **1995**, *36*, 4389. (b) Bürgi, H.-B.; Baldridge, K. K.; Hardcastle, K.; Frank, N. L.; Gantzel, P.; Siegel, J. S.; Ziller, J. *Angew. Chem., Int. Ed. Engl.* **1995**, *34*, 1454.

59. Boyko, E. R.; Vaughan, P. A. *Acta Cryst.* **1964**, *17*, 152.

60. Grepioni, F.; Braga, D.; Dyson, P. J.; Johnson, B. F. G.; Sanderson, F. M.; Calhorda, M. J.; Veiros, L. F. *Organometallics* **1995**, *14*, 121.

61. Gommans, L. H. P.; Main, L.; Nicholson, B. K. *J. Organomet. Chem.* **1988**, *346*, 385.

62. (a) McGlinchey, M. J.; Burns, R. C.; Hofer, R.; Top, S.; Jaouen, G. *Organometallics* **1986**, *5*, 104. (b) Top, S.; Jaouen, G.; Vessières, A.; Abjean, J.; Davoust, D.; Rodger, C. A.; Sayer, B. G.; McGlinchey, M. J. *Organometallics* **1985**, *4*, 2143. (c) Mailvaganam, B.; Perrier, R. E.; Sayer, B. G.; McCarry, B. E.; Bell, R. A.; McGlinchey, M. J. *J. Organomet. Chem.* **1988**, *354*, 325. (d) Moriarty, R. M.; Ku, Y-Y.; Gill, U. S.; Gilardi, R.; Perrier, R. E.; McGlinchey, M. J. *Organometallics* **1989**, *8*, 960.

63. (a) Karplus, M. *J. Am. Chem. Soc.* **1963**, *85*, 2870. (b) Bothner-By, A. A. *Adv. Magn. Reson.* **1965**, *1*, 195.

64. Hoyano, J. K.; Graham, W. A. G. *J. Chem. Soc., Chem. Commun.* **1982**, 27.

65. Kudinov, A. R.; Rybinskaya, M. I.; Struchkov, Yu. T.; Yanovskii, A. I.; Petrovskii, P. V. *J. Organomet. Chem.* **1987**, *336*, 187.

66. Lamanna, W. M.; Gleason, W. B.; Britton, D. *Organometallics* **1987**, *6*, 1583.

67. (a) Schumacher, E.; Taubenest, R. *Helv. Chim. Acta* **1964**, *47*, 1525. (b) Werner, H.; Salzer, A. *Synth. Inorg. Metal-org. Chem.* **1972**, *2*, 239.

68. Trahanovsky, W. S.; Card, R. J. *J. Am. Chem. Soc.* **1972**, *94*, 2897.

69. (a) Jaouen, G.; Top, S.; Laconi, A.; Couturier, D.; Brocard, J. *J. Am. Chem. Soc.* **1984**, *106*, 2207. (b) CH_2O has also been used to trap a chromium-stabilised benzylic anion: Brocard, J.; Goetgheluck, S.; Pelinski, L. *J. Organomet. Chem.* **1994**, *476*, C12.

70. Rabaâ, H.; Lacoste, M.; Delville-Desbois, M-H.; Ruiz, J.; Gloaguen, B.; Ardoin, N.; Astruc, D.; Le Beuze, A.; Saillard, J-Y.; Linares, J.; Varret, F.; Dance, J-M.; Marquestaut, E. *Organometallics* **1995**, *14*, 5078, and references cited therein.

71. Moriarty, R. M.; Gill, U. S.; Ku, Y-Y. *J. Organomet. Chem.* **1988**, *350*, 157.

72. For structural data on **6** see: Hamon, J-R.; Astruc, D; Roman, E. *J. Am. Chem. Soc.* **1981**, *103*, 2431.

73. For kinetic data on related systems, see: Terrier, F.; Vichard, D.; Chatrousse, A-P.; Top, S.; McGlinchey, M. J. *Organometallics* **1994**, *13*, 690.

74. Clark, D. T.; Mlekuz, M.; Sayer, B. G.; McCarry, B. E.; McGlinchey, M. J. *Organometallics* **1987**, *6*, 2201.

75. Treichel, P. M.; Johnson, J. W. *J. Organomet. Chem.* **1975**, *88*, 207.

76. Reference 12, and Valério, C.; Gloaguen, B.; Fillaut, J.-L.; Astruc, D. *Bull. Soc. Chim. Fr.* **1996**, *133*, 101.

77. Winkhans, G.; Singer, H. *J. Organomet. Chem.*, *7*, 487, **1967**.

78. Bennet, M. A.; Smith, A. K. *J. Chem. Soc., Dalton Trans.*, 233, **1974**.

79. (a) Porter, L. C.; Polam, J. R. *Organometallics* **1994**, *13*, 2092. (b) Suravajjala, S.; Porter, L. C.; Polam, J. R. *Organometallics* **1994**, *13*, 37.

80. (a) Zelonka, R. A.; Baird, M. C. *Can. J. Chem.* **1972**, *50*, 3063. (b) Bennett, M. A.; Matheson, T. W.; Robertson, G. B.; Smith, A. K.; Tucker, P. A. *Inorg. Chem.*

1980, *19*, 1014. (c) Bennett, M. A.; Huang, T.-N.; Matheson, T. W.; Smith, A. K. *Inorganic Syntheses* **1982**, *21*, 75.

81. (a) Karplus, M. *J. Chem. Phys.* **1959**, *30*, 11. (b) Bothner-By, A. A. *Adv. Magn. Reson.* **1965**, *1*, 195. (c) Booth, H. *Progr. NMR Spectrosc.* **1969**, *5*, 149. (d) Colucci, W. J.; Jungk, S. J.; Gandour, R. D. *Magn. Reson. Chem.* **1985**, *23*, 335. (e) Breitmaier, E. *Structure Determination by NMR in Organic Chemistry* **1993**, John Wiley & Sons: Chichester, U.K., pp 42-43.

82. It is known that complexes such as $[(C_6Me_6)RuCl_2]_2$ can be obtained by this arene exchange method: see reference 3.

83. Watkins, S. F.; Fronczek, F. R. *Acta Cryst.* **1982**, *B38*, 270.

84. (a) McGlinchey, M. J. *Adv. Organomet. Chem.* **1992**, *34*, 285. (b) Nambu, M.; Siegel, J. S. *J. Am. Chem. Soc.* **1988**, *110*, 3675. (c) Downton, P. A.; Sayer, B. G.; McGlinchey, M. J. *Organometallics* **1992**, *11*, 3281. (d) Downton, P. A.; Mailvaganam, B.; Frampton, C. S.; Sayer, B. G.; McGlinchey, M. J. *J. Am. Chem. Soc.* **1990**, *112*, 27. (e) Kilway, K. V.; Siegel, J. S. *J. Am. Chem. Soc.* **1991**, *113*, 2332. (f) Kilway, K. V.; Siegel, J. S. *J. Am. Chem. Soc.* **1992**, *114*, 255. (g) Chudek, J. A.; Hunter, G.; MacKay, R. L.; Fäber, G.; Weissensteiner, W. *J. Organomet. Chem.* **1989**, *377*, C69. (h) Kremminger, P.; Weissensteiner, W.; Kratky, C.; Hunter, G.; MacKay, R. L. *Monatsh. Chem.* **1989**, *120*, 1175. (i) Mailvaganam, B.; Frampton, C. S.; Sayer, B. G.; Top, S.; McGlinchey, M. J. *J. Am. Chem. Soc.* **1991**, *113*, 1177. (j) Howell, J. A. S.; Beddows, C. J.; O'Leary, P. J.; Yates, P. C.; McArdle, P.; Cunningham, D.; Gottlieb, H. E. *J. Organomet. Chem.* **1997**, *527*, 21.

85. Pomeroy, R. K.; Harrison, D. *J. Chem. Soc., Chem. Commun.* **1980**, 661.

86. Grepioni, F.; Braga, D.; Dyson, P. J.; Johnson, B. F. G.; Sanderson, F. M.; Calhorda, M. J.; Veiros, L. F. *Organometallics* **1995**, *14*, 121.

87. Bennett, M. A.; Robertson, G. B.; Smith, A. K. *J. Organomet. Chem.* **1972**, *43*, C41.

88. Gupta, H. K.; Lock, P.E.; Hughes, D. W.; Britten, J. F.; McGlinchey, M. J. "A Synthetic, NMR and X-Ray Crystallographic Study of $[(C_6Et_6)Ru(H_2O)_3][BF_4]_2 \bullet H_2O$, $[(C_6Et_6)_2Ru_2\mu\text{-}Cl_3][C_5(CO_2Me)_5]$, $(C_6Et_6)RuCl_2[P(OMe)_3]$, $(C_6Et_6)RuCl_2(PMe)_3$ and *trans*-$(PMe_3)_4RuCl_2$: Hexaethylbenzene as a Probe for Molecular Symmetry", in preparation, for submission to *Organometallics*, **2001**.

89. Hunter, G.; Iverson, D. J.; Mislow, K.; Blount, J. F. *J. Am. Chem. Soc.* **1980**, *102*, 5942.

90. (a) Reference 12; (b) Dubois, R. H.; Zaworotko, M. J.; White, P. S. *J. Organomet. Chem.* **1989**, *362*, 155.

91. Herrmann, W. A.; Thiel, W. R.; Herdtweck, E. *Polyhedron* **1988**, *7*, 2027.

92. McGlinchey, M. J. *Adv. Organomet. Chem.* **1992**, *34*, 285.

93. Pal, H. K.; Guha, A. C. *Z. Kristallogr. Kristallgeom. Kristallphys. Kristallchem.* **1935**, *92*, 392.

94. Iverson, D. J.; Hunter, G.; Damewood, J. R. Jr.; Blount, J. F.; Mislow, K. *J. Am. Chem. Soc.* **1981**, *103*, 6073.

95. Reference 84(i).

96. McGlinchey, M. J.; Bougeard, P.; Sayer, B. G.; Hofer, R.; Lock, C. J. L. *J. Chem. Soc., Chem. Commun.* **1984**, 789.

97. Downton, P. A.; Mailvaganam, B.; Frampton, C. S.; Sayer, B. G.; McGlinchey, M. J. *J. Am. Chem. Soc.* **1990**, *112*, 27.

98. References 84 (e) and (f).

99. Blount, J. F.; Hunter, G.; Mislow, K. *J. Chem. Soc., Chem. Commun.* **1984**, 170.

100. Hunter, G.; Blount, J. F.; Damewood, J. R. Jr.; Iverson, D. J.; Mislow, K. *Organometallics* **1981**, *1*, 448.

101. Flood, T. C.; Rosenberg, E.; Sarhangi, A. *J. Am. Chem. Soc.* **1977**, *99*, 4335.

102. Olah, G. A.; Yu, H. *J. Org. Chem.* **1976**, *41*, 717.

103. Mailvaganam, B.; Sayer, B. G.; McGlinchey, M. J. *Organometallics* **1990**, *9*, 1089.

104. Bruce, M. I. *Aust. J. Chem.* **1990**, *43*, 949.

105. (a) Reference 86. (b) McCormick, F. B.; Gleason, W. B. *Acta Cryst.* **1993**, *C49*, 1493. (c) Tocher, D. A.; Walkinshaw, M. D. *Acta Crystallogr., Sect. B* **1982**, *B38*, 3083.

106. Bruce, M. I.; White, A. H. *Aust. J. Chem.* **1990**, *43*, 949, and references therein.

107. Spek, A. L. *PLATON*, Program for the Automated Analysis of Molecular Geometry, Version 200296, University of Utrecht, Netherlands, 1996.

108. Bennett, M. A.; Matheson, T. W.; Robertson, G. B.; Steffen, W. L.; Turney, T. W. *J. Chem. Soc., Chem. Commun.* **1979**, 32.

109. Bürgi, H.-B. *Inorg. Chem.*, **1988**, *27*, 1358.

110. (a) Tolman C. A. *Chem. Rev.* **1977**, *77*, 313. (b) Collman, J. P.; Hegedus, L. S. *Principles and Applications of Organotransition Metal Chemistry*; University Science Books: Mill Valley, CA, 1980; pp. 57-58.

111. The X-ray crystal structures of (arene)$RuCl_2(PMePh_2)$, where arene = benzene or cymene, have been reported previously: Bennett, M. A.; Robertson, G. B.; Smith, A. K. *J. Organomet. Chem.* **1972**, *43*, C41.

112. Serron, S. A.; Nolan, S. P. *Organometallics* **1995**, *14*, 4611, and references therein.

113. Jones, R. A.; Real, F. M.; Wilkinson G. J.; Galas, A. M. R.; Hursthouse, M. B.; Malik, K. M. A. *J. Chem. Soc., Dalton Trans.* **1980**, 511.

114. See, for example, (a) Statler, J. A.; Wilkinson, G.; Thornton-Pett, M.; Hursthouse, M. B. *J. Chem. Soc., Dalton Trans.* **1984**, 1731. (b) Wong, W.-K.; Chiu, K. W.; Statler, J. A.; Wilkinson, G. *Polyhedron*, **1984**, *3* 1255. (c) Hartwig, J. F.; Andersen, R. A.; Bergman, R. G. *J. Am. Chem. Soc.* **1990**, *112*, 5670. (d) Osakada, K.; Ohshiro, K.; Yamamoto, A. *Organometallics*, **1991**, *10*, 404. (e) Hartwig, J. F.; Bergman, R.G.; Andersen, R. A. *J. Am. Chem. Soc.* **1991**, *113*, 3404. (f) Hartwig, J. F.; Andersen, R. A.; Bergman, R. G. *Organometallics*, **1991**, *10*, 1875. (g) Hartwig, J. F.; Bergman, R.G.; Andersen, R. A. *Organometallics*, **1991**, *10*, 3326. (h) ibid, p. 3344. (I) Dahlenburg, L.; Frosin, K.-M. *Polyhedron*, **1993**, *12*, 427.

115. Guggenberger, L. J. *Inorg. Chem.* **1973**, *12*, 1317.

116. Bennett, M. A. *Coord. Chem. Rev.* **1997**, *166*, 225.

117. Girard, L.; Lock, P. E.; El Amouri, H.; McGlinchey, M. J. *J. Organomet. Chem.*, **1994**, *478*, 189-196.

118. Bürgi, H. B.; Dunitz, J. D. *Acc. Chem. Res.*, **1983**, *16*, 153.

119. Bürgi, H. B.; J. D. Dunitz, J. D.; Shefter, E. *J. Am. Chem. Soc.*, **1973**, *95*, 5065.

120. Baldwin, J. E.*J. Chem. Soc., Chem. Commun.*, **1976**, 734.

121. Bye, E.; Schweizer, W. B.; Dunitz, J. D. *J. Am. Chem. Soc.*, **1982**, *104*, 5893.

122. (a) Gust, D.; Mislow, K. *J. Am. Chem. Soc.*, **1973**, *95*, 1535. (b) Blount, J. F.; Finocchiaro, P.; Gust, D.; Mislow, K. *J. Am. Chem. Soc.*, **1973**, *95*, 7019. (c) Andose, J. D.; Mislow, K. *J. Am. Chem. Soc.*, **1974**, *96*, 2168. (d) Mislow, K. *Acc. Chem. Res.*, **1976**, *9*, 26.

123. Crabtree, R. H.; Lavin, M. *Inorg. Chem.*, **1986**, *25*, 805-812.

124. Seyferth, D. *Adv. Organomet. Chem.*, **1976**, *14*, 97.

125. D'Agostino, M. F.; Mlekuz, M.; Kolis, J. W.; Sayer, B. G.; Rodger, C. A.; Halet, J.-F.; Saillard, J.-Y.; McGlinchey, M. J. *Organometallics*, **1985**, *5*, 2345-2350.

126. Nicholas, K. M. *Acc. Chem. Res.*, **1986**, *20*, 207.

127. Schreiber, S. L.; Klimas, M. T.; Sammakia, S. *J. Am. Chem. Soc.*, **1987**, *109*, 5749.

128. Edidin, R. T.; Norton, J. R.; Mislow, K. *Organometallics*, **1982**, *1*, 561-562.

129. Meyer, A.; McCabe, D.J.; Curtis, M. D. *Organometallics*, **1987**, *6*, 1491-1498.

130. (a) Solokov, V. I.; Barinov, I. V.; Reutov, O. A. *Isv. Akad. Nauk SSR, Ser. Khim.*, **1982**, 1922. (b) Padmanabhan, S.; Nicholas, K. M. *J. Organomet. Chem.*, **1983**, *268*, C23. (c) Froom, S. F. T.; Green, M.; Nagle, K. R.; Williams, D. J. *J. Chem. Soc., Chem. Commun.*, **1987**, 1305. (d) Galakhov, M. V.; Bakhmutov, V. I.; Barinov, I. V.; Reutov, O. A. *J. Organomet. Chem.*, **1991**, *421*, 65. (e) Cordier, C.; Gruselle, M.; Jaouen, G.; Bakhmutov, V. I.; Galakhov, M. V.; Troitskaya, L. L.; Solokov, V. I. *Organometallics*, **1991**, *10*, 2303-2309.

131. (a) Barinov, I. V.; Reutov, O. A.; Polyakov, A. V.; Yanovsky, A. L.; Struchkov Yu.T.; Sokolov, V. I. *J. Organomet. Chem.*, **1991**, *418*, C24. (b) Cordier, C.Ph.D. Thesis, Université Pierre et Marie Curie, Paris, France, **1991**. (c) El Amouri, H.; Vaissermann, J.; Besace, Y.; Vollhardt, K. P. C.; Ball, G. E. *Organometallics*, **1993**, *12*, 605. (d) Leberre-Cosquer, N.; Kergoat R.; L'Haridon, P. *Organometallics*, **1992**, *11*, 721-728. (e) El Amouri, H.; Besace Y.; Vaissermann, J.; Jaouen, G.; McGlinchey, M. J. *Organometallics*, **1994**, *13*, 4426-4430. (f) Cordier, C.; Gruselle, M.; Vaissermann, J.; Troitskaya, L. L.; Bakhmutov, V. I.; Sokolov V. I.; Jaouen, G. *Organometallics*, **1992**, *11*, 3825-3832. (g) Gruselle, M.; Cordier, C.; Salmain, M.; El Amouri, H.; Guérin, C.; Vaissermann, J.; Jaouen, G. *Organometallics*, **1990**, *9*, 2993-2997. (h) Gruselle, M.; El Hafa, H.; Nikolski, M.; Jaouen, G.; Vaissermann, J.; Li L.; McGlinchey, M. J. *Organometallics*, **1993**, *12*, 4917-4925.

132. (a) Bailey, W. I. Jr.; Chisholm, M. H.; Cotton F. A.; Rankel, L. A. *J. Am. Chem. Soc.*, **1978**, *100*, 5764. (b) Bougeard, P.; Peng, S.; Mlekuz, M.; McGlinchey, M. J. *J. Organomet. Chem.*, **1985**, *296*, 386, and references therein. (c) Carriedo, G. A; Howard, J. A. K.; Lewis, D. B.; Lewis G. E.; Stone, F. G. A. *J. Chem. Soc., Dalton Trans.*, **1985**, 905.

133. Tondu, S. ;Jaouen, G.; D'Agostino, M. F.; Malisza K. L.; McGlinchey, M. J. *Can. J. Chem.*, **1992**, *70*, 1743.

134. (a) Hoffmann, R. *J. Chem. Phys.*, **1963**, *39*, 1397. (b) Hoffmann, R.; Lipscomb, W. N. *J. Chem. Phys.*, **1962**, *36*, 2179, 3489. (c) Ammeter, J. H.; Bürgi, H. B.; Thibeault, J. C.; Hoffmann, R. *J. Am. Chem. Soc.*, **1978**, *100*, 3686.

135. Mealli, C.; Proserpio, D. M. *J. Chem. Ed.*, **1990**, *67*, 3399.

136. Wingrove, A. S.; Caret, R. L. *Organic Chemistry*, Harper & Row, New York, **1981**, p.105.

137. Deschamps, N. M., Kaldis, J. H., Lock, P. E., Britten, J. F., McGlinchey, M. J. Submitted to *J. Am. Chem. Soc.*, 2001.

138. Deschamps, N. M., B.Sc. Thesis (Chemistry), McMaster University, 2000.

139. (a) Battioni, J-P.; Chodkiewicz, W.; Cadiot, P. *C. R. Seances Acad. Sci. Ser. C* **1967**, *264*, 991. (b) Battioni, J-P.; Capmau, M-L.; Chodkiewicz, W. *Bull. Soc. Chim. Fr.* **1969**, 976. (c) Battioni, J-P.; Chodkiewicz, W. *Bull. Soc. Chim. Fr.* **1969**, 981. (c) Cram, D. J.; Abd Elhafez, F. A. *J. Am. Chem. Soc.* **1952**, *74*, 5828.

140. (a) Cherest, M.; Felkin, H.; Prudent, N. *Tetrahedron Lett.* **1968**, 2201. (b) Cherest, M.; Felkin, H. *Tetrahedron Lett.* **1968**, 2205.

141. (a) Nguyên Trong Anh; Eisenstein, O. *Nouv. J. Chim.* **1977**, *1*, 61. (b) Nguyên Trong Anh *Top. Curr. Chem.* **1980**, *88*, 145.

142. For more recent analyses of this concept, see: (a) Wu, Y-D.; Tucker, J. A.; Houk, K. N. *J. Am. Chem. Soc.* **1991**, *113*, 5018. (b) Frenking, G.; Köhler, K. F.; Reetz, M. T. *Angew. Chem., Int. Ed. Engl.* **1991**, *30*, 1146. (c) Wu, Y-D.; Houk, K, N. *Angew. Chem., Int. Ed. Engl.* **1992**, *31*, 1019.

143. Reference 31 and references therein.

144. See, for example, (a) Reference 126. (b) Caffyn, A. J. M.; Nicholas, K. M. In *Comprehensive Organometallic Chemistry II*; Wilkinson, G., Stone, F. G. A.; Abel, E. W. Eds., Pergamon Press: Oxford, U.K., 1995; Vol 12., Chapter 7.1, pp 685-702. (c) Reference 20. (d) Reference 21. (e) Melikyan, G. G.; Bright, S.; Monroe, T.; Hardcastle, K. I.; Ciurash, J. *Angew. Chem., Int. Ed. Engl.* **1998**, *37*, 161. (f) Ruffolo, R.; Brook, M. A.; McGlinchey, M. J. *Organometallics* **1998**, *17*, 4992. (g) Guo, R.; Green, J. *J. Chem. Soc., Chem. Commun.* **1999**, 2503, and references therein.

145. Melikyan, G. G.; Vostrowsky, O.; Bauer, W.; Bestmann, H. J.; Khan, M.; Nicholas, K. M. *J. Org. Chem.* **1994**, *59*, 222.

146. (a) Grove, D. D.; Miskevich, F.; Smith, C. C.; Corte, J. R. *Tetrahedron Lett.* **1990**, 6277. (b) Grove, D. D.; Corte, J. R.; Spencer, R. P.; Pauly, M. E.; Rath, N. P. *J. Chem. Soc., Chem. Commun.* **1994**, 49.

147. Malisza, K. L.; Girard, L.; Hughes, D. W.; Britten, J. F.; McGlinchey, M. J. *Organometallics* **1995**, *14*, 4676.

148. Reference 136, p.110-111.

149. The synthesis of 1-(phenylethynyl)cyclohexan-1-ol has been reported previously, but no NMR data are available: (a) Hurd, C. D.; Cohen, F. L.; *J. Am. Chem. Soc.*, *53*, 1068-1077, **1931**. (b) Pinkney, P. S.; Nesty, G. A.; Pearson, D. E.; Marvel, C. S. *J. Am. Chem. Soc.*, *59*, 2666-2668, **1931**.

150. The synthesis of 1-(trimethylsilylethynyl)cyclohexan-1-ol has been reported previously, but no NMR data are available: Iritani, K.; Yanagihara, N.; Utimoto, K. *J. Org. Chem.* **1986**, *51*, 5499.

151. Braga, D.; Grepioni, F.; Walther, D.; Heubach, K.; Schmidt, A.; Imhof, W.; Görls, H.; Klettke, T. *Organometallics* **1997**, *16*, 4910.

152. Levy, G. C.; Nelson, G. L. *Carbon-13 Nuclear Magnetic Resonance for Organic Chemists*, Wiley-Interscience, New York, **1972**.

153. (a) Bellucci, G.; Berti, G.; Colapietro, M.; Spagna, R.; Zambonelli, L. *J. Chem. Soc., Perkin Trans.2* **1976**, 1213. (b) Columbus, I.; Hoffman, R. E.; Biali, S. E. *J. Chem. Soc.* **1996**, *118*, 6890. (c) Golan, O.; Cohen, S.; Biali, S. E. *J. Org. Chem.* **1999**, *64*, 6505. (d) Dieks, H.; Senge, M. O.; Kirste, B.; Kurreck, H. *J. Org. Chem.* **1997**, *62*, 8666.

154. Sara, A. N. *J. Organomet. Chem.* **1973**, *47*, 331.

155. Stolow, R. D. *J. Am. Chem. Soc.* **1961**, *83*, 2592.

156. (a) Tanaka, S.; Tsukiyama, T.; Isobe, M. *Tetrahedron Lett.* **1993**, *34*, 5757. (b) Reference 30.

157. El Hafa, H.; Cordier, C.; Gruselle, M.; Besace, Y.; Jaouen, G.; McGlinchey, M. J. *Organometallics* **1994**, *13*, 5149.

158. (a) Padmanabhan, S.; Nicholas, K. M. *J. Organomet. Chem.* **1984**, *212*, C23. (b) Schreiber, S. L.; Sammakia, T; Crowe, W. E. *J. Am. Chem. Soc.* **1986**, *108*, 3128. (c) Edidin, R. T.; Norton, J. R.; Mislow, K. *Organometallics* **1982**, *1*, 561. (d) Schilling, B. E. R.; Hoffmann, R. *J. Am. Chem. Soc.* **1979**, *101*, 3456. (e) Reference 17.

159. Perrin, D. D., Armarego, W. L. F., Perrin, D. R., Eds. *Purification of Laboratory Chemicals*, 2nd ed.; Pergamon: Oxford, **1980**.

160. Sheldrick, G. M. SHELXTL PC (1990), Release 4.1, Siemens Crystallographic Research Systems, Madison, WI, 53719.

161. Sheldrick, G. M. SHELXTL (1994), Release 5.03, Siemens Crystallographic Research Systems, Madison, WI, 53719.

162. SMART, version 4.05, Siemens Energy and Automotive Analytical Instrumentation, **1996**, Madison, WI, 53719.

163. SAINT, version 4.05, Siemens Energy and Automotive Analytical Instrumentation, **1996**, Madison, WI, 53719.

164. Sheldrick, G. M. SADABS (Siemens Area Detector Absorption Corrections), **1996**.

Appendix 1: X-Ray Crystallographic Data

Compound	Appendix Tables
[(η^6-trindane)$Cr(CO)_3$], **15**.	A1 – A5
[(η^6-trindane)$RuCl_2]_2$, **25**.	B1 – B5
(η^6-trindane)$RuCl_2[P(OMe)_3]$, **28**.	C1 – C5
[(η^6-hexaethylbenzene)$_2Ru_2Cl_3][C_5(COOCH_3)_5]$, **33**.	D1 – D5
[(η^6-hexaethylbenzene)$Ru(H_2O)_3](BF_4)_2 \cdot H_2O$, **34**.	E1 – E5
[(η^6-hexaethylbenzene)$RuCl_2P(OMe)_3$], **35**.	F1 – F5
trans-$RuCl_2[P(CH_3)_3]_4$, **37**.	G1 – G5
Trans-4-*t*-Bu-1-phenylethynylcyclohexanol$\cdot Co_2(CO)_6$, **52**.	H1 – H5

Table A1. Crystal data and structure refinement for **15**.

Empirical formula	$C_{18}H_{18}CrO_3$	
Formula weight	334.32	
Crystal colour, habit	yellow, multifaceted block	
Temperature	292(2) K	
Wavelength	0.56086 Å	
Crystal system	orthorhombic	
Space group	Pbca	
Unit cell dimensions	a = 14.376(3)	$\alpha = 90°$
	b = 14.600(4)	$\beta = 90°$
	c = 14.973(4)	$\gamma = 90°$
Volume	3145(1) $Å^3$	
Z	8	
Density (calc)	1.413 Mg/m^3	
Absorption coefficient	0.389 mm^{-1}	
F(000)	1392	
Crystal size	0.31 × 0.25 × 0.20 mm	
θ range for data collection	1.90 to 17.55°	
Limiting indices	$-1 \le h \le 15, -1 \le k \le 15, -1 \le l \le 16$	
Reflections collected	2645	
Independent reflections	2041 [R(int) = 0.0295]	
Absorption correction	ψ scan	
Refinement method	Full-matrix least-squares on F^2	
Data/restraints/parameters	2041 / 0 / 199	
Goodness-of-fit on F^2	0.745	
R indices (all data, used) [a]	R_1=0.1090, wR_2=0.0550	
Largest diff. peak and hole	0.220 and -0.162 $eÅ^3$	

[a] $R1 = \Sigma(\|Fo\| - \|Fc\|)/\Sigma|Fo|$; $wR2 = [\Sigma[w(Fo^2 - Fc^2)^2]/\Sigma[w(Fo^2)^2]]^{0.5}$

Table A2. Atomic coordinates ($\text{Å} \times 10^4$) and equivalent isotropic displacement parameters (2×10^3) for **15**. U(eq) is defined as one third of the trace of the orthogonalized Uij tensor.

	x	y	z	U(eq)
Cr(1)	2058 (1)	3993 (1)	3698 (1)	47 (1)
C(1)	736 (3)	5500 (3)	2573 (3)	71 (2)
C(2)	649 (3)	4830 (4)	1809 (3)	91 (2)
C(3)	317 (3)	3939 (4)	2200 (3)	70 (2)
C(3A)	628 (3)	3985 (4)	3148 (3)	46 (1)
C(3B)	685 (3)	3305 (3)	3807 (4)	48 (1)
C(4)	436 (3)	2309 (3)	3742 (4)	76 (2)
C(5)	887 (4)	1910 (3)	4567 (4)	98 (2)
C(6)	985 (3)	2685 (4)	5217 (3)	76 (2)
C(6A)	997 3)	3531 (4)	4655 (4)	49 (1)
C(6B)	1230 (3)	4420 (4)	4866 (3)	47 (1)
C(7)	1557 (3)	4824 (4)	5732 (3)	75 (2)
C(8)	1948 (4)	5740 (4)	5472 (3)	96 (2)
C(9)	1451 (3)	5996 (3)	4605 (3)	74 (2)
C(9A)	1166 (3)	5093 (4)	4224 (4)	47 (1)
C(9B)	869 (3)	4881 (4)	3364 (3)	43 (1)
C(10)	2436 (3)	3154 (3)	2885 (3)	58 (2)
O(1)	2681 (2)	2615 (2)	2363 (2)	99 (1)
C(11)	2977 (3)	3640 (3)	4433 (3)	64 (2)
O(2)	3580 (2)	3434 (3)	4913 (2)	106 (2)
C(12)	2821 (3)	4828 (3)	3218 (3)	51 (1)
O(3)	3304 (2)	5398 (2)	2922 (2)	80 (1)

Table A3. Bond lengths [Å] and angles [°] for **15**.

Cr(1)-C(3A)	2.214	(4)	Cr(1)-C(3B)	2.221	(5)
Cr(1)-C(6A)	2.199	(5)	Cr(1)-C(6B)	2.205	(5)
Cr(1)-C(9A)	2.200	(5)	Cr(1)-C(9B)	2.203	(5)
C(1)-C(2)	1.511	(6)	C(2)-C(3)	1.504	(6)
C(4)-C(5)	1.511	(6)	C(5)-C(6)	1.500	(5)
C(7)-C(8)	1.502	(6)	C(8)-C(9)	1.528	(5)
C(1)-C(9B)	1.501	(5)	C(3)-C(3A)	1.491	(5)
C(3B)-C(4)	1.501	(5)	C(6)-C(6A)	1.494	(6)
C(6B)-C(7)	1.501	(6)	C(9)-C(9A)	1.494	(6)
C(3A)-C(3B)	1.401	(6)	C(3B)-C(6A)	1.388	(6)
C(6A)-C(6B)	1.376	(6)	C(6B)-C(9A)	1.378	(6)
C(9A)-C(9B)	1.391	(5)	C(3A)-C(9B)	1.392	(6)
Cr(1)-C(11)	1.795	(5)	Cr(1)-C(10)	1.810	(5)
Cr(1)-C(12)	1.790	(5)	C(10)-O(1)	1.164	(5)
C(11)-O(2)	1.165	(5)	C(12)-O(3)	1.171	(4)
C(12)-Cr(1)-C(11)	89.5	(2)	C(12)-Cr(1)-C(10)	90.4	(2)
C(11)-Cr(1)-C(10)	89.8	(2)	C(12)-Cr(1)-C(6A)	153.6	(2)
C(11)-Cr(1)-C(6A)	91.3	(2)	C(10)-Cr(1)-C(6A)	116.0	(2)
C(12)-Cr(1)-C(9A)	90.3	(2)	C(11)-Cr(1)-C(9A)	114.8	(2)
C(10)-Cr(1)-C(9A)	155.4	(2)	C(6A)-Cr(1)-C(9A)	65.6	(2)
C(12)-Cr(1)-C(9B)	89.1	(2)	C(11)-Cr(1)-C(9B)	151.6	(2)
C(10)-Cr(1)-C(9B)	118.6	(2)	C(6A)-Cr(1)-C(9B)	77.9	(2)
C(9A)-Cr(1)-C(9B)	36.84	(14)	C(12)-Cr(1)-C(6B)	117.2	(2)
C(11)-Cr(1)-C(6B)	89.6	(2)	C(10)-Cr(1)-C(6B)	152.4	(2)
C(6A)-Cr(1)-C(6B)	36.4	(2)	C(9A)-Cr(1)-C(6B)	36.5	(2)
C(9B)-Cr(1)-C(6B)	66.1	(2)	C(12)-Cr(1)-C(3A)	115.0	(2)
C(11)-Cr(1)-C(3A)	155.4	(2)	C(10)-Cr(1)-C(3A)	91.4	(2)
C(6A)-Cr(1)-C(3A)	66.2	(2)	C(9A)-Cr(1)-C(3A)	66.2	(2)
C(9B)-Cr(1)-C(3A)	36.7	(2)	C(6B)-Cr(1)-C(3A)	78.2	(2)
C(12)-Cr(1)-C(3B)	151.9	(2)	C(11)-Cr(1)-C(3B)	118.6	(2)
C(10)-Cr(1)-C(3B)	90.6	(2)	C(6A)-Cr(1)-C(3B)	36.6	(2)
C(9A)-Cr(1)-C(3B)	77.6	(2)	C(9B)-Cr(1)-C(3B)	66.0	(2)
C(6B)-Cr(1)-C(3B)	65.8	(2)	C(3A)-Cr(1)-C(3B)	36.8	(2)
C(9B)-C(1)-C(2)	102.6	(4)	C(3)-C(2)-C(1)	106.9	(4)

C(3A)-C(3)-C(2)	103.7	(4)	C(9B)-C(3A)-C(3B)	119.2	(4)
C(9B)-C(3A)-C(3)	109.7	(5)	C(3B)-C(3A)-C(3)	131.0	(5)
C(9B)-C(3A)-Cr(1)	71.2	(3)	C(3B)-C(3A)-Cr(1)	71.8	(3)
C(3)-C(3A)-Cr(1)	129.3	(3)	C(6A)-C(3B)-C(3A)	119.6	(5)
C(6A)-C(3B)-C(4)	111.5	(5)	C(3A)-C(3B)-C(4)	128.8	(6)
C(6A)-C(3B)-Cr(1)	70.9	(3)	C(3A)-C(3B)-Cr(1)	71.3	(3)
C(4)-C(3B)-Cr(1)	130.2	(3)	C(3B)-C(4)-C(5)	102.7	(4)
C(6)-C(5)-C(4)	106.2	(4)	C(6A)-C(6)-C(5)	105.1	(4)
C(6B)-C(6A)-C(3B)	120.8	(5)	C(6B)-C(6A)-C(6)	130.8	(5)
C(3B)-C(6A)-C(6)	108.3	(5)	C(6B)-C(6A)-Cr(1)	72.0	(3)
C(3B)-C(6A)-Cr(1)	72.6	(3)	C(6)-C(6A)-Cr(1)	128.9	(3)
C(6A)-C(6B)-C(9A)	119.8	(5)	C(6A)-C(6B)-C(7)	130.2	(5)
C(9A)-C(6B)-C(7)	110.1	(5)	C(6A)-C(6B)-Cr(1)	71.6	(3)
C(9A)-C(6B)-Cr(1)	71.6	(3)	C(7)-C(6B)-Cr(1)	128.9	(3)
C(6B)-C(7)-C(8)	104.1	(4)	C(7)-C(8)-C(9)	105.3	(4)
C(9A)-C(9)-C(8)	103.7	(5)	C(6B)-C(9A)-C(9B)	120.5	(5)
C(6B)-C(9A)-C(9)	110.2	(5)	C(9B)-C(9A)-C(9)	129.3	(5)
C(6B)-C(9A)-Cr(1)	71.9	(3)	C(9B)-C(9A)-Cr(1)	71.7	(3)
C(9)-C(9A)-Cr(1)	128.4	(3)	C(9A)-C(9B)-C(3A)	120.0	(5)
C(9A)-C(9B)-C(1)	129.5	(5)	C(3A)-C(9B)-C(1)	110.5	(4)
C(9A)-C(9B)-Cr(1)	71.5	(3)	C(3A)-C(9B)-Cr(1)	72.1	(3)
C(1)-C(9B)-Cr(1)	129.2	(3)	O(1)-C(10)-Cr(1)	179.9	(3)
O(2)-C(11)-Cr(1)	178.2	(5)	O(3)-C(12)-Cr(1)	177.4	(4)

Table A4. Anisotropic displacement parameters ($Å^2x10^3$) for **15**. The anisotropic displacement factor exponent takes the form: $-2\pi^2 [h^2 a^{*2} U11 + ... + 2 h k a^* b^* U12]$

	U11	U22	U33	U23	U13	U12
Cr(1)	37 (1)	54 (1)	49 (1)	3 (1)	1 (1)	4 (1)
C(1)	51 (3)	81 (4)	81 (4)	13 (4)	0 (4)	2 (3)
C(2)	61 (4)	145 (6)	67 (4)	36 (5)	-4 (3)	12 (4)
C(3)	59 (3)	92 (5)	61 (4)	-20 (4)	-12 (3)	17 (4)
C(3A)	33 (3)	54 (3)	50 (3)	-4 (4)	-8 (3)	5 (3)
C(3B)	36 (3)	43 (3)	64 (4)	1 (4)	1 (3)	3 (3)
C(4)	47 (3)	67 (4)	113 (5)	0 (5)	7 (4)	-5 (3)
C(5)	59 (4)	58 (4)	177 (7)	44 (5)	-7 (5)	-12 (4)
C(6)	46 (3)	84 (4)	97 (5)	25 (4)	12 (4)	2 (4)
C(6A)	35 (3)	58 (4)	53 (4)	18 (4)	6 (3)	9 (3)
C(6B)	35 (3)	63 (4)	45 (4)	-3 (4)	-6 (3)	-1 (3)
C(7)	50 (3)	114 (5)	62 (4)	-2 (4)	2 (3)	-11 (4)
C(8)	78 (4)	123 (6)	87 (4)	-49 (4)	-1 (4)	-8 (5)
C(9)	49 (3)	67 (4)	107 (5)	-23 (5)	8 (3)	10 (4)
C(9A)	32 (3)	47 (4)	63 (4)	-8 (3)	1 (3)	-3 (3)
C(9B)	32 (3)	49 (4)	49 (3)	8 (3)	-2 (3)	4 (3)
C(10)	56 (3)	59 (4)	59 (4)	2 (3)	8 (3)	2 (3)
O(1)	114 (3)	86 (3)	96 (3)	-21 (2)	24 (3)	21 (3)
C(11)	43 (3)	83 (4)	66 (3)	-1 (3)	1 (3)	2 (4)
O(2)	73 (2)	140 (4)	106 (3)	17 (3)	-36 (2)	23 (3)
C(12)	31 (3)	63 (4)	59 (3)	-3 (3)	4 (3)	5 (3)
O(3)	68 (2)	83 (3)	90 (3)	2 (3)	19 (2)	-20 (2)

Table A5. Hydrogen coordinates ($x10^3$) and isotropic displacement parameters ($Å^2x10^3$) for **15**.

	x	y	z	U(eq)
H(1A)	20	579	268	50
H(1B)	125	592	252	50
H(2A)	28	502	136	50
H(2B)	124	484	157	50
H(3A)	-41	392	220	50
H(3B)	53	343	190	50
H(4A)	-23	228	372	50
H(4B)	5	208	320	50
H(5A)	56	145	472	50
H(5B)	147	171	450	50
H(6A)	53	275	565	50
H(6B)	159	262	556	50
H(7A)	103	478	610	50
H(7B)	196	443	600	50
H(8A)	186	617	589	50
H(8B)	259	564	534	50
H(9A)	98	633	471	50
H(9B)	185	638	428	50

Table B1. Crystal data and structure refinement for **25**.

Empirical formula	$C_{30}H_{36}Cl_4Ru_2$
Formula weight	740.53
Crystal colour, habit	red, plate
Temperature	157(2) K
Wavelength	0.56086 Å
Crystal system	monoclinic
Space group	$P2_1/n$
Unit cell dimensions	a = 9.412(2) Å $\alpha = 90°$
	b = 14.991(3) Å $\beta = 112.41(3)°$
	c = 10.367(2) Å $\gamma = 90°$
Volume	1352.3(5) $Å^3$
Z	2
Density (calc)	1.819 Mg/m^3
Absorption coefficient	0.806 mm^{-1}
F(000)	744
Crystal size	0.43 × 0.24 × 0.08 mm^3
θ range for data collection	1.97 to 20.00°
Index ranges	$-12 \le h \le 11, -8 \le k \le 20, -2 \le l \le 14$
Reflections collected	2144
Independent reflections	766 [R(int) = 0.0391]
Refinement method	Full-matrix least-squares on F^2
Data/restraints/parameters	1765 / 0 / 163
Goodness-of-fit on F^2	0.904
Final R indices [$I>2\sigma(I)$] [a]	R_1=0.0536, wR_2=0.1252
R indices (all data, used) [a]	R_1=0.0745, wR_2=0.1327
Largest diff. peak and hole	1.140 and -0.376 $eÅ^3$

[a] $R1 = \Sigma(\|Fo\| - \|Fc\|)/\Sigma|Fo|$; $wR2 = [\Sigma[w(Fo^2 - Fc^2)^2]/\Sigma[w(Fo^2)^2]]^{0.5}$

Table B2. Atomic coordinates [Å x 10^4] and equivalent isotropic displacement parameters [$Å^2$ x 10^3] for **25**. U(eq) is defined as one third of the trace of the orthogonalized Uij tensor.

	x	y	z	U(eq)
Ru(1)	4298 (1)	44 (1)	8066 (1)	36 (1)
Cl(2)	4434 (2)	1003 (1)	10024 (2)	40 (1)
Cl(1)	1884 (2)	-482 (1)	8025 (2)	44 (1)
C(1)	8000 (9)	-60 (6)	8423 (9)	50 (2)
C(2)	8553 (10)	911 (7)	8808 (9)	54 (2)
C(3)	7120 (9)	1489 (6)	8474 (8)	46 (2)
C(3A)	5829 (9)	940 (5)	7535 (8)	37 (2)
C(3B)	4272 (9)	1168 (5)	6785 (7)	37 (2)
C(4)	3488 (9)	2042 (5)	6782 (8)	43 (2)
C(5)	1781 (9)	1770 (6)	6219 (9)	46 (2)
C(6)	1640 (9)	944 (6)	5314 (8)	44 (2)
C(6A)	3215 (9)	537 (6)	5950 (7)	36 (2)
C(6B)	3687 (10)	-356 (5)	5934 (8)	39 (2)
C(7)	2764 (10)	-1168 (5)	5244 (8)	47 (2)
C(8)	3771 (11)	-1940 (6)	6057 (10)	55 (2)
C(9)	5418 (11)	-1597 (5)	6607 (9)	49 (2)
C(9A)	5217 (10)	-601 (6)	6709 (7)	39 (2)
C(9B)	6314 (9)	47 (6)	7473 (8)	41 (2)

Table B3. Bond lengths [Å] and angles [°] for **25**.

Ru(1)-C(3A)	2.188	(8)	Ru(1)-C(3B)	2.140	(7)
Ru(1)-C(6A)	2.166	(7)	Ru(1)-C(6B)	2.146	(7)
Ru(1)-C(9A)	2.142	(7)	Ru(1)-C(9B)	2.207	(7)
Ru(1)-Cl(1)	2.389	(2)	Ru(1)-Cl(2)	2.451	(2)
Ru(1)-Cl(2)A	2.451	(2)	Cl(2)-Ru(1)A	2.451	(2)
C(1)-C(9B)	1.524	(10)	C(1)-C(2)	1.546	(13)
C(2)-C(3)	1.528	(11)	C(3)-C(3A)	1.484	(11)
C(3B)-C(4)	1.502	(11)	C(4)-C(5)	1.541	(10)
C(5)-C(6)	1.529	(11)	C(6)-C(6A)	1.503	(10)
C(6B)-C(7)	1.508	(11)	C(7)-C(8)	1.530	(12)
C(8)-C(9)	1.523	(12)	C(9)-C(9A)	1.514	(11)
C(3A)-C(3B)	1.414	(11)	C(3B)-C(6A)	1.406	(11)
C(6A)-C(6B)	1.412	(12)	C(6B)-C(9A)	1.404	(11)
C(9A)-C(9B)	1.418	(12)	C(3A)-C(9B)	1.424	(11)
C(3B)-Ru(1)-C(9A)	82.0	(3)	C(3B)-Ru(1)-C(6B)	69.2	(3)
C(9A)-Ru(1)-C(6B)	38.2	(3)	C(3B)-Ru(1)-C(6A)	38.1	(3)
C(9A)-Ru(1)-C(6A)	69.0	(3)	C(6B)-Ru(1)-C(6A)	38.2	(3)
C(3B)-Ru(1)-C(3A)	38.1	(3)	C(9A)-Ru(1)-C(3A)	69.0	(3)
C(6B)-Ru(1)-C(3A)	81.7	(3)	C(6A)-Ru(1)-C(3A)	68.7	(3)
C(3B)-Ru(1)-C(9B)	68.5	(3)	C(9A)-Ru(1)-C(9B)	38.0	(3)
C(6B)-Ru(1)-C(9B)	68.6	(3)	C(6A)-Ru(1)-C(9B)	80.8	(3)
C(3A)-Ru(1)-C(9B)	37.8	(3)	C(3B)-Ru(1)-Cl(1)	117.6	(2)
C(9A)-Ru(1)-Cl(1)	117.3	(2)	C(6B)-Ru(1)-Cl(1)	90.6	(2)
C(6A)-Ru(1)-Cl(1)	91.0	(2)	C(3A)-Ru(1)-Cl(1)	155.6	(2)
C(9B)-Ru(1)-Cl(1)	155.3	(2)	C(3B)-Ru(1)-Cl(2)A	153.2	(2)
C(9A)-Ru(1)-Cl(2)A	92.7	(2)	C(6B)-Ru(1)-Cl(2)A	120.7	(2)
C(6A)-Ru(1)-Cl(2)A	158.9	(2)	C(3A)-Ru(1)-Cl(2)A	115.6	(2)
C(9B)-Ru(1)-Cl(2)A	91.2	(2)	Cl(1)-Ru(1)-Cl(2)A	88.30	(7)
C(3B)-Ru(1)-Cl(2)	92.1	(2)	C(9A)-Ru(1)-Cl(2)	154.4	(2)
C(6B)-Ru(1)-Cl(2)	157.8	(2)	C(6A)-Ru(1)-Cl(2)	119.6	(2)
C(3A)-Ru(1)-Cl(2)	91.0	(2)	C(9B)-Ru(1)-Cl(2)	16.8	(2)
Cl(1)-Ru(1)-Cl(2)	87.56	(7)	Cl(2)A-Ru(1)-Cl(2)	81.44	(7)
Ru(1)A-Cl(2)-Ru(1)	98.56	(7)	C(9B)-C(1)-C(2)	103.5	(7)
C(3)-C(2)-C(1)	107.1	(7)	C(3A)-C(3)-C(2)	105.4	(7)

C(3B)-C(3A)-C(9B)	119.1	(7)	C(3B)-C(3A)-C(3)	130.1	(7)
C(9B)-C(3A)-C(3)	110.8	(7)	C(3B)-C(3A)-Ru(1)	69.1	(4)
C(9B)-C(3A)-Ru(1)	71.8	(4)	C(3)-C(3A)-Ru(1)	129.0	(5)
C(6A)-C(3B)-C(3A)	121.1	(7)	C(6A)-C(3B)-C(4)	110.7	(7)
C(3A)-C(3B)-C(4)	128.1	(7)	C(6A)-C(3B)-Ru(1)	71.9	(4)
C(3A)-C(3B)-Ru(1)	72.8	(4)	C(4)-C(3B)-Ru(1)	125.3	(5)
C(3B)-C(4)-C(5)	102.2	(6)	C(6)-C(5)-C(4)	106.3	(6)
C(6A)-C(6)-C(5)	102.7	(6)	C(3B)-C(6A)-C(6B)	119.5	(7)
C(3B)-C(6A)-C(6)	110.2	(7)	C(6B)-C(6A)-C(6)	129.9	(7)
C(3B)-C(6A)-Ru(1)	70.0	(4)	C(6B)-C(6A)-Ru(1)	70.1	(4)
C(6)-C(6A)-Ru(1)	126.0	(5)	C(9A)-C(6B)-C(6A)	120.0	(7)
C(9A)-C(6B)-C(7)	109.9	(7)	C(6A)-C(6B)-C(7)	130.0	(8)
C(9A)-C(6B)-Ru(1)	70.7	(4)	C(6A)-C(6B)-Ru(1)	71.7	(4)
C(7)-C(6B)-Ru(1)	126.4	(5)	C(6B)-C(7)-C(8)	103.0	(7)
C(9)-C(8)-C(7)	106.2	(7)	C(9A)-C(9)-C(8)	102.9	(7)
C(6B)-C(9A)-C(9B)	120.6	(8)	C(6B)-C(9A)-C(9)	110.3	(7)
C(9B)-C(9A)-C(9)	129.1	(8)	C(6B)-C(9A)-Ru(1)	71.0	(4)
C(9B)-C(9A)-Ru(1)	73.5	(4)	C(9)-C(9A)-Ru(1)	125.7	(5)
C(9A)-C(9B)-C(3A)	119.4	(8)	C(9A)-C(9B)-C(1)	130.2	(8)
C(3A)-C(9B)-C(1)	110.0	(7)	C(9A)-C(9B)-Ru(1)	68.5	(5)
C(3A)-C(9B)-Ru(1)	70.4	(4)	C(1)-C(9B)-Ru(1)	127.9	(5)

Symmetry transformations used to generate equivalent atoms: -x+1,-y,-z+2

Table B4. Anisotropic displacement parameters ($Å^2 \times 10^3$) for **25**. The anisotropic displacement factor exponent takes the form: $-2\pi^2[h^2 a^{*2} U_{11} + ... + 2 h k a^* b^* U_{12}]$

	U11	U22	U33	U23	U13	U12
Ru(1)	36 (1)	34 (1)	39 (1)	1 (1)	15 (1)	1 (1)
Cl(2)	44 (1)	35 (1)	41 (1)	0 (1)	17 (1)	1 (1)
Cl(1)	40 (1)	47 (1)	47 (1)	0 (1)	18 (1)	-3 (1)
C(1)	39 (4)	56 (5)	56 (5)	9 (4)	20 (4)	4 (4)
C(2)	43 (4)	75 (7)	43 (4)	-1 (4)	15 (4)	-1 (4)
C(3)	43 (4)	50 (5)	44 (4)	0 (4)	14 (4)	-4 (4)
C(3A)	44 (4)	30 (4)	36 (4)	5 (3)	12 (4)	0 (3)
C(3B)	42 (4)	38 (4)	32 (4)	4 (3)	15 (4)	-3 (3)
C(4)	43 (4)	40 (4)	45 (5)	5 (3)	16 (4)	5 (3)
C(5)	43 (4)	43 (5)	50 (5)	3 (4)	15 (4)	9 (4)
C(6)	37 (3)	49 (5)	45 (5)	4 (4)	15 (4)	-1 (4)
C(6A)	38 (3)	41 (4)	29 (4)	1 (3)	10 (3)	0 (4)
C(6B)	47 (4)	35 (4)	34 (4)	-3 (3)	17 (4)	-10 (4)
C(7)	52 (4)	41 (5)	50 (5)	-6 (4)	23 (4)	-9 (4)
C(8)	65 (5)	32 (5)	70 (6)	-1 (4)	31 (6)	-2 (4)
C(9)	66 (5)	38 (5)	50 (5)	7 (4)	32 (5)	13 (4)
C(9A)	47 (4)	44 (4)	32 (4)	-1 (3)	21 (4)	5 (4)
C(9B)	36 (3)	51 (5)	42 (4)	-1 (4)	22 (4)	-2 (4)

Table B5. Hydrogen coordinates (x 10^3) and isotropic displacement parameters ($Å^2$ x 10^3) for **25**.

	x	y	z	U(eq)
H(1B)	857	-35	794	74
H(1A)	811	-40	925	74
H(2A)	920	95	979	81
H(2B)	914	111	827	81
H(3A)	696	164	932	69
H(3B)	721	204	801	69
H(4A)	369	247	618	64
H(4B)	381	229	772	64
H(5B)	146	163	698	69
H(5A)	114	225	567	69
H(6B)	86	54	537	66
H(6A)	139	111	435	66
H(7A)	261	-120	426	70
H(7B)	177	-117	533	70
H(8B)	348	-212	682	82
H(8A)	366	-245	545	82
H(9B)	602	-185	751	73
H(9A)	592	-173	597	73

Table C1. Crystal data and structure refinement for **28**.

Empirical formula	$C_{18}H_{27}Cl_2O_3PRu$	
Formula weight	494.34	
Crystal colour, habit	red, plate	
Temperature	300(2) K	
Wavelength	0.71073 Å	
Crystal system	monoclinic	
Space group	$P2_1/c$	
Unit cell dimensions	a = 9.141(2) Å	α = 90°
	b = 14.931(1) Å	β = 94.58(1)°
	c = 14.996(3) Å	γ = 90°
Volume	2040.0(6) $Å^3$	
Z	4	
Density (calc)	1.610 Mg/m^3	
Absorption coefficient	1.123 mm^{-1}	
F(000)	1008	
Crystal size	0.20 × 0.12 × 0.04 mm	
θ range for data collection	1.93 to 30.47°	
Limiting indices	$-9 \le h \le 13$, $-21 \le k \le 21$, $-21 \le l \le 21$	
Reflections collected	21311	
Independent reflections	5240 [R(int) = 0.0790]	
Refinement method	Full-matrix least squares on F^2	
Data/restraints/parameters	5240 / 0 / 236	
Goodness-of-fit on F^2	1.049	
Final R indices [$I>2\sigma(I)$] [a]	R_1=0.0499, wR_2=0.0869	
R indices (all data, used) [a]	R_1=0.0962, wR_2=0.1047	
Largest diff. peak and hole	0.455 and -0.752 $eÅ^3$	

[a] $R1 = \Sigma(\|Fo\|-\|Fc\|)/\Sigma|Fo|$; $wR2 = [\Sigma[w(Fo^2-Fc^2)^2]/\Sigma[w(Fo^2)^2]]^{0.5}$

Table C2. Atomic coordinates [x 10^4] and equivalent isotropic displacement parameters [$Å^2$ x 10^3] for **28**. U(eq) is defined as one third of the trace of the orthogonalized U_{ij} tensor.

	x	y	z	U (eq)
Ru(1)	3096 (1)	214 (1)	2105 (1)	31 (1)
P(1)	2321 (2)	-506 (1)	3322 (1)	48 (1)
Cl(1)	591 (1)	688 (1)	1824 (1)	62 (1)
Cl(2)	3589 (2)	1490 (1)	3072 (1)	59 (1)
C(1)	6094 (5)	-1107 (3)	2605 (3)	49 (1)
C(2)	6913 (6)	-314 (4)	3049 (4)	70 (2)
C(3)	6761 (5)	483 (4)	2415 (4)	56 (1)
C(3A)	5422 (5)	239 (3)	1806 (3)	41 (1)
C(3B)	4626 (5)	777 (3)	1144 (3)	43 (1)
C(4)	4844 (6)	1751 (3)	915 (4)	63 (2)
C(5)	3381 (7)	2007 (4)	419 (4)	77 (2)
C(6)	2703 (6)	1135 (4)	43 (3)	63 (2)
C(6A)	3416 (5)	431 (3)	644 (3)	44 (1)
C(6B)	2954 (5)	-465 (3)	793 (3)	43 (1)
C(7)	1692 (6)	-979 (4)	340 (4)	60 (2)
C(8)	1628 (6)	-1840 (4)	885 (4)	69 (2)
C(9)	3149 (5)	-1953 (3)	1410 (4)	53 (1)
C(9A)	3765 (5)	-1022 (3)	1421 (3)	39 (1)
C(9B)	5014 (5)	-663 (3)	1930 (3)	37 (1)
C(10A)	3747 (9)	-1032 (5)	4844 (5)	99 (2)
O(1A)	3236 (12)	-1171 (8)	3847 (7)	56 (1)
C(11A)	734 (7)	751 (4)	4116 (4)	75 (2)
O(2A)	1158 (76)	-188 (38)	3800 (28)	67 (3)
C(12A)	461 (9)	-1907 (5)	3314 (6)	114 (3)
O(3A)	995 (14)	-1257 (7)	2866 (9)	66 (2)
C(10B)	3747 (9)	-1032 (5)	4844 (5)	99 (2)
O(1B)	3779 (6)	-569 (4)	4084 (4)	56 (1)
C(11B)	734 (7)	751 (4)	4116 (4)	75 (2)
O(2B)	1175 (37)	-98 (19)	4004 (13)	67 (3)
C(12B)	461 (9)	-1907 (5)	3314 (6)	114 (3)
O(3B)	1948 (7)	-1511 (4)	3238 (4)	66 (2)

Table C3. Bond lengths [Å] and angles [°] for **28**.

Ru(1)-C(3A)	2.208	(4)	Ru(1)-C(3B)	2.250	(4)
Ru(1)-C(6A)	2.256	(4)	Ru(1)-C(6B)	2.209	(4)
Ru(1)-C(9A)	2.221	(4)	Ru(1)-C(9B)	2.220	(4)
Ru(1)-Cl(1)	2.402	(1)	Ru(1)-Cl(2)	2.415	(1)
Ru(1)-P(1)	2.278	(1)	P(1)-O(1A)	1.484	(10)
P(1)-O(2A)	1.41	(5)	P(1)-O(3A)	1.751	(12)
P(1)-O(1B)	1.687	(6)	P(1)-O(2B)	1.64	(2)
P(1)-O(3B)	1.542	(5)	C(1)-C(9B)	1.510	(6)
C(1)-C(2)	1.525	(7)	C(2)-C(3)	1.522	(8)
C(3)-C(3A)	1.512	(6)	C(3B)-C(4)	1.510	(6)
C(4)-C(5)	1.526	(8)	C(5)-C(6)	1.530	(8)
C(6)-C(6A)	1.500	(6)	C(6B)-C(7)	1.502	(6)
C(7)-C(8)	1.526	(8)	C(8)-C(9)	1.551	(7)
C(9)-C(9A)	1.500	(6)	C(3A)-C(3B)	1.430	(6)
C(3B)-C(6A)	1.385	(7)	C(6A)-C(6B)	1.425	(6)
C(6B)-C(9A)	1.420	(6)	C(9A)-C(9B)	1.426	(6)
C(3A)-C(9B)	1.413	(6)	C(10A)-O(1A)	1.543	(12)
C(11A)-O(2A)	1.54	(5)	C(12A)-O(3A)	1.297	(13)
C(10B)-O(1B)	1.335	(8)	C(11B)-O(2B)	1.35	(3)
C(12B)-O(3B)	1.495	(9)			

C(3A)-Ru(1)-C(6B)	79.4	(2)	C(3A)-Ru(1)-C(9A)	67.3	(2)
C(6B)-Ru(1)-C(9A)	37.4	(2)	C(3A)-Ru(1)-C(9B)	37.2	(2)
C(6B)-Ru(1)-C(9B)	67.3	(2)	C(9A)-Ru(1)-C(9B)	37.5	(2)
C(3A)-Ru(1)-C(3B)	37.4	(2)	C(6B)-Ru(1)-C(3B)	66.2	(2)
C(9A)-Ru(1)-C(3B)	78.8	(2)	C(9B)-Ru(1)-C(3B)	66.9	(2)
C(3A)-Ru(1)-C(6A)	66.3	(2)	C(6B)-Ru(1)-C(6A)	37.2	(2)
C(9A)-Ru(1)-C(6A)	67.0	(2)	C(9B)-Ru(1)-C(6A)	78.8	(2)
C(3B)-Ru(1)-C(6A)	35.8	(2)	C(3A)-Ru(1)-P(1)	122.44	(13)
C(6B)-Ru(1)-P(1)	119.79	(13)	C(9A)-Ru(1)-P(1)	95.30	(12)
C(9B)-Ru(1)-P(1)	96.61	(12)	C(3B)-Ru(1)-P(1)	159.73	(13)
C(6A)-Ru(1)-P(1)	156.57	(13)	C(3A)-Ru(1)-Cl(1)	151.60	(13)
C(6B)-Ru(1)-Cl(1)	89.53	(12)	C(9A)-Ru(1)-Cl(1)	117.24	(12)
C(9B)-Ru(1)-Cl(1)	154.66	(12)	C(3B)-Ru(1)-Cl(1)	114.23	(12)
C(6A)-Ru(1)-Cl(1)	89.04	(12)	P(1)-Ru(1)-Cl(1)	85.78	(5)

C(3A)-Ru(1)-Cl(2)	88.43	(12)	C(6B)-Ru(1)-Cl(2)	153.16	(13)
C(9A)-Ru(1)-Cl(2)	152.61	(12)	C(9B)-Ru(1)-Cl(2)	115.15	(12)
C(3B)-Ru(1)-Cl(2)	89.68	(13)	C(6A)-Ru(1)-Cl(2)	115.95	(13)
P(1)-Ru(1)-Cl(2)	86.93	(5)	Cl(1)-Ru(1)-Cl(2)	90.14	(5)
O(2A)-P(1)-O(1A)	112	(2)	O(3B)-P(1)-O(2B)	105.3	(11)
O(3B)-P(1)-O(1B)	99.1	(3)	O(2B)-P(1)-O(1B)	96.1	(11)
O(2A)-P(1)-O(3A)	84	(3)	O(1A)-P(1)-O(3A)	97.0	(6)
O(2A)-P(1)-Ru(1)	123	(2)	O(1A)-P(1)-Ru(1)	122.9	(4)
O(3B)-P(1)-Ru(1)	118.4	(2)	O(2B)-P(1)-Ru(1)	125.5	(10)
O(1B)-P(1)-Ru(1)	106.8	(2)	O(3A)-P(1)-Ru(1)	103.9	(4)
C(9B)-C(1)-C(2)	102.9	(4)	C(3)-C(2)-C(1)	108.5	(4)
C(3A)-C(3)-C(2)	102.6	(4)	C(9B)-C(3A)-C(3B)	120.1	(4)
C(9B)-C(3A)-C(3)	111.1	(4)	C(3B)-C(3A)-C(3)	128.8	(4)
C(9B)-C(3A)-Ru(1)	71.9	(2)	C(3B)-C(3A)-Ru(1)	72.9	(2)
C(3)-C(3A)-Ru(1)	128.8	(3)	C(6A)-C(3B)-C(3A)	120.3	(4)
C(6A)-C(3B)-C(4)	110.5	(4)	C(3A)-C(3B)-C(4)	129.0	(5)
C(6A)-C(3B)-Ru(1)	72.3	(3)	C(3A)-C(3B)-Ru(1)	69.7	(2)
C(4)-C(3B)-Ru(1)	127.2	(3)	C(3B)-C(4)-C(5)	103.1	(4)
C(4)-C(5)-C(6)	106.2	(4)	C(6A)-C(6)-C(5)	103.4	(4)
C(3B)-C(6A)-C(6B)	120.0	(4)	C(3B)-C(6A)-C(6)	110.7	(4)
C(6B)-C(6A)-C(6)	129.2	(5)	C(3B)-C(6A)-Ru(1)	71.9	(3)
C(6B)-C(6A)-Ru(1)	69.6	(3)	C(6)-C(6A)-Ru(1)	126.9	(3)
C(9A)-C(6B)-C(6A)	120.5	(4)	C(9A)-C(6B)-C(7)	110.0	(4)
C(6A)-C(6B)-C(7)	129.4	(4)	C(9A)-C(6B)-Ru(1)	71.8	(3)
C(6A)-C(6B)-Ru(1)	73.2	(3)	C(7)-C(6B)-Ru(1)	128.7	(4)
C(6B)-C(7)-C(8)	104.4	(4)	C(7)-C(8)-C(9)	107.0	(4)
C(9A)-C(9)-C(8)	103.0	(4)	C(6B)-C(9A)-C(9B)	119.2	(4)
C(6B)-C(9A)-C(9)	111.1	(4)	C(9B)-C(9A)-C(9)	129.7	(4)
C(6B)-C(9A)-Ru(1)	70.8	(3)	C(9B)-C(9A)-Ru(1)	71.2	(2)
C(9)-C(9A)-Ru(1)	131.2	(3)	C(3A)-C(9B)-C(9A)	119.7	(4)
C(3A)-C(9B)-C(1)	110.0	(4)	C(9A)-C(9B)-C(1)	130.2	(4)
C(3A)-C(9B)-Ru(1)	70.9	(2)	C(9A)-C(9B)-Ru(1)	71.3	(2)
C(1)-C(9B)-Ru(1)	131.3	(3)	P(1)-O(1A)-C(10A)	122.6	(8)
P(1)-O(2A)-C(11A)	133	(5)	C(12A)-O(3A)-P(1)	123.7	(10)
C(10B)-O(1B)-P(1)	122.5	(5)	C(11B)-O(2B)-P(1)	130	(2)
C(12B)-O(3B)-P(1)	125.1	(5)			

Table C4. Anisotropic displacement parameters [$Å^2 \times 10^3$] for **28**. The anisotropic displacement factor exponent takes the form: $-2\pi^2[h^2a^{*2}U_{11} + ... + 2hka^*b^*U_{12}]$

	U11	U22	U33	U23	U13	U12
Ru(1)	29 (1)	29 (1)	35 (1)	0 (1)	4 (1)	1 (1)
P(1)	64 (1)	35 (1)	48 (1)	5 (1)	22 (1)	5 (1)
Cl(1)	37 (1)	88 (1)	61 (1)	5 (1)	5 (1)	21 (1)
Cl(2)	67 (1)	44 (1)	69 (1)	-20 (1)	21 (1)	-14 (1)
C(1)	45 (3)	46 (3)	53 (3)	-1 (2)	-3 (2)	13 (2)
C(2)	55 (3)	73 (4)	79 (4)	-3 (3)	-21 (3)	-2 (3)
C(3)	37 (3)	55 (3)	75 (4)	-6 (3)	-1 (3)	-2 (2)
C(3A)	32 (2)	43 (2)	50 (3)	-5 (2)	13 (2)	3 (2)
C(3B)	39 (3)	45 (3)	49 (3)	7 (2)	18 (2)	4 (2)
C(4)	67 (4)	49 (3)	78 (4)	16 (3)	31 (3)	0 (3)
C(5)	75 (4)	60 (4)	96 (5)	37 (4)	19 (4)	16 (3)
C(6)	70 (4)	78 (4)	42 (3)	22 (3)	12 (3)	24 (3)
C(6A)	46 (3)	52 (3)	35 (2)	6 (2)	11 (2)	15 (2)
C(6B)	40 (3)	51 (3)	38 (3)	-5 (2)	-1 (2)	7 (2)
C(7)	53 (3)	66 (4)	58 (3)	-19 (3)	-13 (3)	6 (3)
C(8)	60 (4)	63 (4)	79 (4)	-15 (3)	-17 (3)	-11 (3)
C(9)	60 (3)	35 (2)	64 (3)	-13 (2)	-2 (3)	5 (2)
C(9A)	40 (3)	38 (2)	40 (3)	-7 (2)	7 (2)	2 (2)
C(9B)	36 (2)	36 (2)	38 (2)	-4 (2)	4 (2)	5 (2)
C(10A)	135 (7)	89 (5)	70 (5)	-1 (4)	-20 (5)	14 (5)
O(1A)	61 (3)	64 (4)	43 (3)	12 (3)	1 (2)	-2 (3)
C(11A)	95 (5)	59 (4)	79 (4)	-13 (3)	47 (4)	5 (3)
O(2A)	99 (3)	55 (6)	55 (10)	8 (6)	54 (8)	21 (4)
C(12A)	98 (6)	85 (5)	162 (9)	-4 (5)	17 (5)	-31 (5)
O(3A)	75 (5)	39 (3)	88 (5)	5 (3)	27 (3)	-11 (3)
C(10B)	135 (7)	89 (5)	70 (5)	-1 (4)	-20 (5)	14 (5)
O(1B)	61 (3)	64 (4)	43 (3)	12 (3)	1 (2)	-2 (3)
C(11B)	95 (5)	59 (4)	79 (4)	-13 (3)	47 (4)	5 (3)
O(2B)	99 (3)	55 (6)	55 (10)	8 (6)	54 (8)	21 (4)
C(12B)	98 (6)	85 (5)	162 (9)	-4 (5)	17 (5)	-31 (5)
O(3B)	75 (5)	39 (3)	88 (5)	5(3)	27 (3)	-11 (3)

Table C5. Hydrogen coordinates ($x10^3$) and isotropic displacement parameters ($Å^2 \times 10^3$) for **28**.

	x	y	z	U(eq)
H(1A)	676	-150	231	58
H(1B)	559	-145	304	58
H(2A)	650	-17	361	84
H(2B)	794	-46	318	84
H(3A)	761	44	197	67
H(3B)	672	123	276	67
H(4A)	565	182	54	76
H(4B)	504	211	145	76
H(5A)	353	242	-6	92
H(5B)	274	229	83	92
H(6A)	165	114	7	76
H(6B)	293	105	-57	76
H(7A)	187	-111	-28	72
H(7B)	79	-64	35	72
H(8A)	142	-235	49	82
H(8B)	86	-180	130	82
H(9A)	305	-217	201	64
H(9B)	377	-236	111	64
H(10A)	432	-154	506	149
H(10B)	291	-97	518	149
H(10C)	433	-50	491	149
H(11A)	-14	71	443	113
H(11B)	57	114	361	113
H(11C)	152	99	451	113
H(12A)	-25	-223	293	172
H(12B)	-0.3	-167	381	172
H(12C)	124	-230	353	172
H(10D)	468	-98	518	149
H(10E)	354	-165	471	149
H(10F)	299	-80	519	149
H(11D)	5	77	457	113
H(11E)	27	97	356	113
H(11F)	157	112	429	113
H(12D)	51	-254	324	172
H(12E)	-22	-17	29	172
H(12F)	14	-178	389	172

Table D1. Crystal data and structure refinement for 33.

Empirical formula	$C_{51}H_{75}Cl_3O_{10}Ru_2$	
Formula weight	1156.60	
Temperature	210(2) K	
Wavelength	0.71073 Å	
Crystal system	Triclinic	
Space group	P-1	
Unit cell dimensions	a = 13.41060(10) Å	α= 103.2500(10)°
	b = 14.9194(2) Å	β= 94.7710(10)°
	c = 14.98330(10) Å	γ = 110.8320(10)°
Volume	2682.21(4) $Å^3$	
Z	2	
Density (calculated)	1.432 Mg/m^3	
Absorption coefficient	0.766 mm^{-1}	
F(000)	1200	
Crystal size	0.30 × 0.20 × 0.08 mm^3	
θ range for data collection	1.42 to 26.51°	
Index ranges	$-16 \le h \le 16, -15 \le k \le 18, -18 \le l \le 18$	
Reflections collected	22408	
Independent reflections	10095 [R(int) = 0.0352]	
Absorption correction	SADABS	
Max. and min. transmission	0.946870 and 0.758383	
Refinement method	Full-matrix least-squares on F^2	
Data / restraints / parameters	10095 / 0 / 370	
Goodness-of-fit on F^2	0.997	
Final R indices [I>2σ (I)] [a]	R1 = 0.0373, wR2 = 0.0962	
R indices (all data) [a]	R1 = 0.0586, wR2 = 0.1045	
Largest diff. peak and hole	0.677 and -0.690 e.$Å^{-3}$	

[a] $R1 = \Sigma(||Fo|-|Fc||)/\Sigma|Fo|$; $wR2 = [\Sigma[w(Fo^2 - Fc^2)^2]/\Sigma[w(Fo^2)^2]]^{0.5}$

Table D2. Atomic coordinates ($\times 10^4$) and equivalent isotropic displacement parameters ($Å^2 \times 10^3$) for 33. U(eq) is defined as one third of the trace of the orthogonalized U_{ij} tensor.

	x	y	z	U(eq)
Ru(1)	5029(1)	1808(1)	3207(1)	31(1)
Ru(2)	4947(1)	3227(1)	1835(1)	33(1)
Cl(1)	6444(1)	2995(1)	2662(1)	38(1)
Cl(2)	4158(1)	1425(1)	1593(1)	39(1)
Cl(3)	4362(1)	3153(1)	3328(1)	40(1)
C(3)	5538(3)	578(2)	3229(2)	35(1)
C(4)	3946(3)	1748(3)	6049(2)	50(1)
C(5)	6296(3)	2122(3)	158(3)	53(1)
C(6)	6248(3)	412(3)	1678(3)	52(1)
C(7)	6774(3)	3864(2)	5204(2)	49(1)
C(8)	4393(3)	4416(2)	1750(2)	41(1)
C(10)	3746(3)	3539(2)	1017(2)	36(1)
C(11)	6548(3)	5582(3)	3608(2)	53(1)
C(12)	7926(3)	1340(3)	4656(3)	57(1)
C(13)	3895(3)	729(2)	3800(2)	34(1)
C(14)	6061(3)	4303(2)	1252(2)	37(1)
C(16)	4587(3)	1595(2)	4529(2)	32(1)
C(17)	5436(3)	3432(2)	517(2)	36(1)
C(18)	3365(3)	2303(3)	-1271(2)	50(1)
C(19)	3369(3)	-1632(2)	2577(3)	55(1)
C(21)	4377(3)	226(2)	3147(2)	36(1)
C(22)	5747(3)	1953(2)	4627(2)	33(1)
C(25)	6032(3)	29(2)	2536(2)	42(1)
C(27)	6237(4)	5748(2)	2654(2)	52(1)
C(28)	6215(3)	1430(2)	3967(2)	34(1)
C(29)	3632(3)	2098(2)	-330(2)	43(1)
C(30)	3655(3)	-627(2)	2338(2)	43(1)
C(31)	7434(3)	1839(2)	4042(3)	42(1)
C(34)	6476(3)	2859(2)	5410(2)	39(1)
C(36)	4274(3)	3044(2)	405(2)	37(1)
C(38)	4086(3)	2159(2)	5196(2)	40(1)
C(40)	5983(3)	2913(2)	-136(2)	42(1)
C(41)	5559(3)	4813(2)	1871(2)	40(1)

C(2A)	7281(3)	4691(2)	1406(2)	45(1)
C(3A)	2677(3)	359(3)	3719(2)	41(1)
C(4A)	3851(3)	4923(3)	2421(2)	48(1)
C(5A)	2532(3)	3148(3)	885(2)	45(1)
C(6A)	2118(3)	818(3)	3125(3)	58(1)
C(7A)	1997(3)	2412(3)	1420(3)	59(1)
C(8A)	3614(4)	5725(3)	2076(3)	63(1)
C(9A)	7702(3)	5451(3)	843(3)	54(1)

Table D3. Bond lengths [Å] and angles [°] for 33.

Ru(1)-C(16)	2.173(3)	C(8)-C(4A)	1.508(4)
Ru(1)-C(3)	2.179(3)	C(10)-C(36)	1.435(4)
Ru(1)-C(21)	2.183(3)	C(10)-C(5A)	1.499(5)
Ru(1)-C(28)	2.184(3)	C(11)-C(27)	1.555(5)
Ru(1)-C(22)	2.190(3)	C(12)-C(31)	1.548(5)
Ru(1)-C(13)	2.199(3)	C(13)-C(21)	1.433(4)
Ru(1)-Cl(1)	2.4362(9)	C(13)-C(16)	1.434(4)
Ru(1)-Cl(2)	2.4419(8)	C(13)-C(3A)	1.511(5)
Ru(1)-Cl(3)	2.4492(8)	C(14)-C(17)	1.421(4)
Ru(2)-C(36)	2.171(3)	C(14)-C(41)	1.427(5)
Ru(2)-C(14)	2.175(3)	C(14)-C(2A)	1.506(5)
Ru(2)-C(8)	2.176(3)	C(16)-C(22)	1.436(4)
Ru(2)-C(17)	2.186(3)	C(16)-C(38)	1.512(4)
Ru(2)-C(10)	2.186(3)	C(17)-C(36)	1.435(5)
Ru(2)-C(41)	2.197(3)	C(17)-C(40)	1.507(4)
Ru(2)-Cl(2)	2.4389(8)	C(18)-C(29)	1.549(4)
Ru(2)-Cl(1)	2.4424(9)	C(19)-C(30)	1.544(4)
Ru(2)-Cl(3)	2.4431(8)	C(21)-C(30)	1.500(4)
C(3)-C(28)	1.425(4)	C(22)-C(28)	1.441(4)
C(3)-C(21)	1.438(5)	C(22)-C(34)	1.518(4)
C(3)-C(25)	1.517(4)	C(27)-C(41)	1.522(5)
C(4)-C(38)	1.538(4)	C(28)-C(31)	1.512(5)
C(5)-C(40)	1.524(5)	C(29)-C(36)	1.487(4)
C(6)-C(25)	1.531(4)	C(2A)-C(9A)	1.541(5)
C(7)-C(34)	1.520(4)	C(3A)-C(6A)	1.534(4)
C(8)-C(10)	1.431(5)	C(4A)-C(8A)	1.525(5)
C(8)-C(41)	1.441(5)	C(5A)-C(7A)	1.518(5)
C(16)-Ru(1)-C(3)	82.01(12)	C(3)-Ru(1)-C(22)	69.45(12)
C(16)-Ru(1)-C(21)	69.04(12)	C(21)-Ru(1)-C(22)	82.20(12)
C(3)-Ru(1)-C(21)	38.51(12)	C(28)-Ru(1)-C(22)	38.47(11)
C(16)-Ru(1)-C(28)	69.23(12)	C(16)-Ru(1)-C(13)	38.29(11)
C(3)-Ru(1)-C(28)	38.11(11)	C(3)-Ru(1)-C(13)	69.41(12)
C(21)-Ru(1)-C(28)	69.15(12)	C(21)-Ru(1)-C(13)	38.17(12)
C(16)-Ru(1)-C(22)	38.43(12)	C(28)-Ru(1)-C(13)	82.01(12)

C(22)-Ru(1)-C(13)	69.54(12)	C(36)-Ru(2)-Cl(2)	90.61(8)
C(16)-Ru(1)-Cl(1)	138.00(9)	C(14)-Ru(2)-Cl(2)	138.71(9)
C(3)-Ru(1)-Cl(1)	106.30(9)	C(8)-Ru(2)-Cl(2)	137.99(10)
C(21)-Ru(1)-Cl(1)	139.96(9)	C(17)-Ru(2)-Cl(2)	105.28(8)
C(28)-Ru(1)-Cl(1)	91.86(9)	C(10)-Ru(2)-Cl(2)	104.57(9)
C(22)-Ru(1)-Cl(1)	104.92(9)	C(41)-Ru(2)-Cl(2)	172.78(9)
C(13)-Ru(1)-Cl(1)	173.77(9)	C(36)-Ru(2)-Cl(1)	137.77(10)
C(16)-Ru(1)-Cl(2)	139.08(9)	C(14)-Ru(2)-Cl(1)	91.45(9)
C(3)-Ru(1)-Cl(2)	104.41(9)	C(8)-Ru(2)-Cl(1)	139.44(10)
C(21)-Ru(1)-Cl(2)	90.80(9)	C(17)-Ru(2)-Cl(1)	104.70(10)
C(28)-Ru(1)-Cl(2)	137.49(9)	C(10)-Ru(2)-Cl(1)	173.34(9)
C(22)-Ru(1)-Cl(2)	172.94(8)	C(41)-Ru(2)-Cl(1)	105.71(10)
C(13)-Ru(1)-Cl(2)	105.37(9)	Cl(2)-Ru(2)-Cl(1)	79.82(3)
Cl(1)-Ru(1)-Cl(2)	79.88(3)	C(36)-Ru(2)-Cl(3)	139.81(10)
C(16)-Ru(1)-Cl(3)	91.82(8)	C(14)-Ru(2)-Cl(3)	138.46(9)
C(3)-Ru(1)-Cl(3)	173.72(9)	C(8)-Ru(2)-Cl(3)	92.31(9)
C(21)-Ru(1)-Cl(3)	137.68(9)	C(17)-Ru(2)-Cl(3)	174.12(8)
C(28)-Ru(1)-Cl(3)	140.07(8)	C(10)-Ru(2)-Cl(3)	106.48(9)
C(22)-Ru(1)-Cl(3)	106.30(8)	C(41)-Ru(2)-Cl(3)	105.71(9)
C(13)-Ru(1)-Cl(3)	104.96(9)	Cl(2)-Ru(2)-Cl(3)	79.69(3)
Cl(1)-Ru(1)-Cl(3)	79.07(3)	Cl(1)-Ru(2)-Cl(3)	79.07(3)
Cl(2)-Ru(1)-Cl(3)	79.52(3)	Ru(1)-Cl(1)-Ru(2)	84.92(3)
C(36)-Ru(2)-C(14)	69.13(13)	Ru(2)-Cl(2)-Ru(1)	84.87(3)
C(36)-Ru(2)-C(8)	69.25(12)	Ru(2)-Cl(3)-Ru(1)	84.62(3)
C(14)-Ru(2)-C(8)	69.03(13)	C(28)-C(3)-C(21)	119.9(3)
C(36)-Ru(2)-C(17)	38.46(13)	C(28)-C(3)-C(25)	120.5(3)
C(14)-Ru(2)-C(17)	38.04(11)	C(21)-C(3)-C(25)	119.6(3)
C(8)-Ru(2)-C(17)	81.89(12)	C(28)-C(3)-Ru(1)	71.1(2)
C(36)-Ru(2)-C(10)	38.45(12)	C(21)-C(3)-Ru(1)	70.9(2)
C(14)-Ru(2)-C(10)	81.95(13)	C(25)-C(3)-Ru(1)	131.2(2)
C(8)-Ru(2)-C(10)	38.28(12)	C(10)-C(8)-C(41)	121.0(3)
C(17)-Ru(2)-C(10)	69.47(12)	C(10)-C(8)-C(4A)	119.8(3)
C(36)-Ru(2)-C(41)	82.17(12)	C(41)-C(8)-C(4A)	119.3(3)
C(14)-Ru(2)-C(41)	38.10(12)	C(10)-C(8)-Ru(2)	71.2(2)
C(8)-Ru(2)-C(41)	38.47(13)	C(41)-C(8)-Ru(2)	71.5(2)
C(17)-Ru(2)-C(41)	69.07(11)	C(4A)-C(8)-Ru(2)	129.4(2)
C(10)-Ru(2)-C(41)	69.52(13)	C(8)-C(10)-C(36)	119.1(3)

C(8)-C(10)-C(5A)	120.4(3)	C(16)-C(22)-C(34)	121.2(3)
C(36)-C(10)-C(5A)	120.5(3)	C(28)-C(22)-C(34)	120.1(3)
C(8)-C(10)-Ru(2)	70.5(2)	C(16)-C(22)-Ru(1)	70.2(2)
C(36)-C(10)-Ru(2)	70.2(2)	C(28)-C(22)-Ru(1)	70.6(2)
C(5A)-C(10)-Ru(2)	132.0(2)	C(34)-C(22)-Ru(1)	131.6(2)
C(21)-C(13)-C(16)	118.9(3)	C(3)-C(25)-C(6)	115.5(3)
C(21)-C(13)-C(3A)	120.7(3)	C(41)-C(27)-C(11)	116.2(3)
C(16)-C(13)-C(3A)	120.4(3)	C(3)-C(28)-C(22)	120.6(3)
C(21)-C(13)-Ru(1)	70.3(2)	C(3)-C(28)-C(31)	120.8(3)
C(16)-C(13)-Ru(1)	69.9(2)	C(22)-C(28)-C(31)	118.6(3)
C(3A)-C(13)-Ru(1)	131.5(2)	C(3)-C(28)-Ru(1)	70.7(2)
C(17)-C(14)-C(41)	121.5(3)	C(22)-C(28)-Ru(1)	71.0(2)
C(17)-C(14)-C(2A)	120.0(3)	C(31)-C(28)-Ru(1)	128.4(2)
C(41)-C(14)-C(2A)	118.5(3)	C(36)-C(29)-C(18)	111.2(3)
C(17)-C(14)-Ru(2)	71.4(2)	C(21)-C(30)-C(19)	111.1(3)
C(41)-C(14)-Ru(2)	71.8(2)	C(28)-C(31)-C(12)	109.3(3)
C(2A)-C(14)-Ru(2)	128.8(2)	C(22)-C(34)-C(7)	116.2(3)
C(13)-C(16)-C(22)	121.4(3)	C(10)-C(36)-C(17)	120.5(3)
C(13)-C(16)-C(38)	119.4(3)	C(10)-C(36)-C(29)	120.6(3)
C(22)-C(16)-C(38)	119.2(3)	C(17)-C(36)-C(29)	118.8(3)
C(13)-C(16)-Ru(1)	71.8(2)	C(10)-C(36)-Ru(2)	71.4(2)
C(22)-C(16)-Ru(1)	71.4(2)	C(17)-C(36)-Ru(2)	71.3(2)
C(38)-C(16)-Ru(1)	128.9(2)	C(29)-C(36)-Ru(2)	128.1(2)
C(14)-C(17)-C(36)	119.4(3)	C(16)-C(38)-C(4)	109.6(3)
C(14)-C(17)-C(40)	120.5(3)	C(17)-C(40)-C(5)	116.8(3)
C(36)-C(17)-C(40)	120.1(3)	C(14)-C(41)-C(8)	118.6(3)
C(14)-C(17)-Ru(2)	70.6(2)	C(14)-C(41)-C(27)	121.0(3)
C(36)-C(17)-Ru(2)	70.2(2)	C(8)-C(41)-C(27)	120.4(3)
C(40)-C(17)-Ru(2)	131.2(2)	C(14)-C(41)-Ru(2)	70.1(2)
C(13)-C(21)-C(3)	120.5(3)	C(8)-C(41)-Ru(2)	70.0(2)
C(13)-C(21)-C(30)	119.0(3)	C(27)-C(41)-Ru(2)	131.1(2)
C(3)-C(21)-C(30)	120.4(3)	C(14)-C(2A)-C(9A)	109.2(3)
C(13)-C(21)-Ru(1)	71.5(2)	C(13)-C(3A)-C(6A)	115.1(3)
C(3)-C(21)-Ru(1)	70.6(2)	C(8)-C(4A)-C(8A)	110.9(3)
C(30)-C(21)-Ru(1)	127.1(2)	C(10)-C(5A)-C(7A)	116.7(3)
C(16)-C(22)-C(28)	118.7(3)		

Table D4. Anisotropic displacement parameters ($Å^2 \times 10^3$)for 33. The anisotropic displacement factor exponent takes the form: $-2\pi^2[h^2a^{*2}U_{11} + ... + 2\ h\ k\ a^*\ b^*\ U_{12}]$

	U_{11}	U_{22}	U_{33}	U_{23}	U_{13}	U_{12}
Ru(1)	46(1)	26(1)	25(1)	10(1)	7(1)	17(1)
Ru(2)	54(1)	25(1)	24(1)	8(1)	7(1)	19(1)
Cl(1)	53(1)	32(1)	33(1)	12(1)	10(1)	19(1)
Cl(2)	61(1)	28(1)	28(1)	9(1)	4(1)	18(1)
Cl(3)	62(1)	38(1)	29(1)	12(1)	12(1)	29(1)
C(3)	47(2)	26(2)	36(2)	12(1)	5(2)	18(2)
C(4)	62(3)	55(2)	33(2)	16(2)	14(2)	19(2)
C(5)	78(3)	49(2)	44(2)	10(2)	16(2)	38(2)
C(6)	76(3)	39(2)	46(2)	8(2)	24(2)	28(2)
C(7)	62(3)	40(2)	40(2)	4(2)	9(2)	17(2)
C(8)	68(3)	33(2)	30(2)	15(2)	11(2)	27(2)
C(10)	58(2)	32(2)	30(2)	14(1)	11(2)	27(2)
C(11)	72(3)	44(2)	35(2)	4(2)	-3(2)	20(2)
C(12)	56(3)	50(2)	68(3)	18(2)	-3(2)	26(2)
C(13)	47(2)	31(2)	31(2)	18(1)	5(2)	17(2)
C(14)	54(2)	26(2)	30(2)	9(1)	7(2)	15(2)
C(16)	40(2)	33(2)	29(2)	16(1)	8(1)	15(2)
C(17)	60(2)	24(2)	28(2)	8(1)	8(2)	18(2)
C(18)	66(3)	59(2)	30(2)	13(2)	3(2)	30(2)
C(19)	57(3)	34(2)	63(3)	13(2)	-2(2)	10(2)
C(21)	47(2)	30(2)	36(2)	16(1)	5(2)	18(2)
C(22)	48(2)	33(2)	27(2)	13(1)	8(2)	21(2)
C(25)	56(2)	32(2)	43(2)	10(2)	11(2)	24(2)
C(27)	89(3)	30(2)	35(2)	4(2)	6(2)	23(2)
C(28)	53(2)	29(2)	29(2)	13(1)	6(2)	22(2)
C(29)	64(2)	31(2)	32(2)	7(1)	3(2)	20(2)
C(30)	52(2)	31(2)	41(2)	9(2)	-2(2)	14(2)
C(31)	44(2)	34(2)	50(2)	13(2)	11(2)	16(2)
C(34)	44(2)	40(2)	31(2)	10(2)	4(2)	15(2)
C(36)	64(3)	30(2)	23(2)	10(1)	7(2)	23(2)
C(38)	48(2)	41(2)	35(2)	10(2)	12(2)	20(2)
C(40)	59(2)	40(2)	28(2)	10(2)	9(2)	20(2)
C(41)	70(3)	25(2)	28(2)	11(1)	7(2)	19(2)

C(2A)	60(3)	35(2)	35(2)	4(2)	-2(2)	17(2)
C(3A)	43(2)	41(2)	38(2)	14(2)	8(2)	14(2)
C(4A)	81(3)	51(2)	27(2)	7(2)	12(2)	44(2)
C(5A)	66(3)	45(2)	37(2)	14(2)	9(2)	34(2)
C(6A)	48(2)	76(3)	66(3)	35(2)	8(2)	32(2)
C(7A)	69(3)	60(3)	54(2)	23(2)	15(2)	27(2)
C(8A)	108(4)	58(2)	43(2)	10(2)	6(2)	58(3)
C(9A)	67(3)	42(2)	50(2)	14(2)	11(2)	15(2)

Table D5. Hydrogen coordinates ($\times 10^4$) and isotropic displacement parameters ($Å^2 \times 10^3$) for **33**.

	x	y	z	U(eq)
H(4A)	3624(3)	2110(3)	6476(2)	75
H(4B)	4649(3)	1829(3)	6361(2)	75
H(4C)	3476(3)	1045(3)	5848(2)	75
H(5A)	6640(3)	1841(3)	-312(3)	80
H(5B)	5650(3)	1597(3)	225(3)	80
H(5C)	6797(3)	2424(3)	749(3)	80
H(6A)	6562(3)	16(3)	1278(3)	78
H(6B)	6748(3)	1105(3)	1875(3)	78
H(6C)	5571(3)	356(3)	1338(3)	78
H(7A)	7239(3)	4389(2)	5747(2)	74
H(7B)	6119(3)	3977(2)	5051(2)	74
H(7C)	7154(3)	3868(2)	4681(2)	74
H(11A)	6976(3)	6221(3)	4055(2)	80
H(11B)	6967(3)	5166(3)	3534(2)	80
H(11C)	5893(3)	5255(3)	3833(2)	80
H(12A)	8708(3)	1601(3)	4705(3)	86
H(12B)	7631(3)	624(3)	4374(3)	86
H(12C)	7746(3)	1482(3)	5272(3)	86
H(18A)	2947(3)	1675(3)	-1737(2)	75
H(18B)	4035(3)	2641(3)	-1470(2)	75
H(18C)	2948(3)	2720(3)	-1195(2)	75
H(19A)	2902(3)	-2171(2)	2044(3)	82
H(19B)	2995(3)	-1622(2)	3104(3)	82
H(19C)	4029(3)	-1735(2)	2734(3)	82
H(25A)	5545(3)	-678(2)	2324(2)	50
H(25B)	6719(3)	70(2)	2860(2)	50
H(27A)	5837(4)	6188(2)	2748(2)	63
H(27B)	6908(4)	6099(2)	2450(2)	63
H(29A)	2955(3)	1746(2)	-135(2)	51
H(29B)	4044(3)	1667(2)	-410(2)	51
H(30A)	4022(3)	-642(2)	1799(2)	51
H(30B)	2987(3)	-529(2)	2169(2)	51

H(31A)	7734(3)	2564(2)	4320(3)	50
H(31B)	7620(3)	1704(2)	3419(3)	50
H(34A)	7148(3)	2770(2)	5584(2)	47
H(34B)	6116(3)	2878(2)	5953(2)	47
H(38A)	3378(3)	2085(2)	4882(2)	48
H(38B)	4554(3)	2871(2)	5396(2)	48
H(40A)	6642(3)	3422(2)	-221(2)	50
H(40B)	5500(3)	2598(2)	-744(2)	50
H(2AA)	7515(3)	4137(2)	1205(2)	55
H(2AB)	7579(3)	5013(2)	2071(2)	55
H(3AA)	2506(3)	499(3)	4347(2)	49
H(3AB)	2369(3)	-367(3)	3451(2)	49
H(4AA)	4323(3)	5228(3)	3034(2)	58
H(4AB)	3171(3)	4426(3)	2488(2)	58
H(5AA)	2241(3)	2827(3)	219(2)	54
H(5AB)	2318(3)	3719(3)	1064(2)	54
H(6AA)	1342(3)	539(3)	3111(3)	88
H(6AB)	2261(3)	669(3)	2495(3)	88
H(6AC)	2398(3)	1536(3)	3393(3)	88
H(7AA)	1216(3)	2211(3)	1282(3)	88
H(7AB)	2255(3)	2724(3)	2083(3)	88
H(7AC)	2177(3)	1829(3)	1236(3)	88
H(8AA)	3266(4)	6041(3)	2517(3)	95
H(8AB)	3137(4)	5422(3)	1473(3)	95
H(8AC)	4288(4)	6223(3)	2018(3)	95
H(9AA)	8488(3)	5703(3)	941(3)	81
H(9AB)	7473(3)	6001(3)	1049(3)	81
H(9AC)	7409(3)	5127(3)	186(3)	81

Table E1. Crystal data and structure refinement for **34**.

Empirical formula	$C_{18}H_{38}B_2F_8O_4Ru$	
Formula weight	593.17	
Temperature	210(2) K	
Wavelength	0.71073 Å	
Crystal system	Orthorhombic	
Space group	$P2_12_12_1$	
Unit cell dimensions	a = 10.07260(10) Å	α= 90°
	b = 13.8284(2) Å	β= 90°
	c = 18.3629(2) Å	γ = 90°
Volume	2557.73(5) $Å^3$	
Z	4	
Density (calculated)	1.540 Mg/m^3	
Absorption coefficient	0.692 mm^{-1}	
F(000)	1216	
Crystal size	0.40 × 0.30 × 0.20 mm^3	
θ range for data collection	1.84 to 26.54°.	
Index ranges	$-12 \le h \le 12, -17 \le k \le 17, -19 \le l \le 22$	
Reflections collected	21529	
Independent reflections	5246 [R(int) = 0.0175]	
Absorption correction	SADABS	
Refinement method	Full-matrix least-squares on F^2	
Data / restraints / parameters	5245 / 0 / 451	
Goodness-of-fit on F^2	1.040	
Final R indices [$I>2\sigma(I)$] [a]	R1 = 0.0148, wR2 = 0.0383	
R indices (all data) [a]	R1 = 0.0152, wR2 = 0.0390	
Absolute structure parameter	-0.012(14)	
Extinction coefficient	0.0002(2)	
Largest diff. peak and hole	0.333 and -0.296 e.$Å^{-3}$	

[a] $R1 = \Sigma(\|Fo\| - \|Fc\|)/\Sigma|Fo|$; $wR2 = [\Sigma[w(Fo^2 - Fc^2)^2]/\Sigma[w(Fo^2)^2]]^{0.5}$

Table E2. Atomic coordinates ($\times 10^4$) and equivalent isotropic displacement parameters ($Å^2 \times 10^3$) for 34. U(eq) is defined as one third of the trace of the orthogonalized U_{ij} tensor.

	x	y	z	U(eq)
Ru(1)	7806(1)	-95(1)	1449(1)	20(1)
C(1)	7631(2)	1447(1)	1666(1)	24(1)
C(2)	7038(2)	1246(1)	977(1)	24(1)
C(3)	6063(2)	491(1)	928(1)	24(1)
C(4)	5637(1)	-12(1)	1566(1)	24(1)
C(5)	6239(1)	200(1)	2249(1)	24(1)
C(6)	7252(2)	926(1)	2306(1)	23(1)
C(7)	8708(2)	2206(1)	1723(1)	30(1)
C(8)	8095(2)	3191(1)	1924(1)	43(1)
C(9)	7472(2)	1794(1)	292(1)	33(1)
C(10)	8681(2)	1388(2)	-103(1)	40(1)
C(11)	5547(2)	188(1)	185(1)	29(1)
C(12)	4323(2)	767(2)	-50(1)	42(1)
C(13)	4546(2)	-774(1)	1518(1)	30(1)
C(14)	5010(2)	-1824(1)	1447(1)	40(1)
C(15)	5811(2)	-345(1)	2927(1)	29(1)
C(16)	4684(2)	198(2)	3312(1)	41(1)
C(17)	7919(2)	1120(1)	3035(1)	30(1)
C(18)	9091(2)	461(2)	3212(1)	38(1)
O(1)	9926(1)	12(1)	1364(1)	36(1)
O(2)	8149(1)	-981(1)	500(1)	35(1)
O(3)	8446(1)	-1396(1)	1960(1)	34(1)
B(1)	6583(2)	-3118(2)	-404(1)	34(1)
F(1)	6463(1)	-3397(1)	-1133(1)	41(1)
F(2)	7728(2)	-3492(1)	-112(1)	70(1)
F(3)	5515(1)	-3470(1)	-9(1)	65(1)
F(4)	6627(2)	-2123(1)	-357(1)	63(1)
B(2)	2401(2)	1871(2)	1658(1)	37(1)
F(5)	3743(1)	1833(1)	1552(1)	64(1)
F(6)	2023(2)	1380(1)	2281(1)	70(1)
F(7)	1730(1)	1451(1)	1071(1)	47(1)
F(8)	1995(1)	2837(1)	1708(1)	51(1)
O(4)	8356(3)	-3070(1)	1300(1)	70(1)

Table E3. Bond lengths [Å] and angles [°] for **34**.

Ru(1)-O(3)	2.1294(12)	C(5)-C(6)	1.435(2)
Ru(1)-O(1)	2.1462(11)	C(5)-C(15)	1.517(2)
Ru(1)-C(3)	2.1566(14)	C(6)-C(17)	1.523(2)
Ru(1)-O(2)	2.1590(12)	C(7)-C(8)	1.540(2)
Ru(1)-C(1)	2.1753(14)	C(9)-C(10)	1.525(3)
Ru(1)-C(6)	2.1859(13)	C(11)-C(12)	1.532(2)
Ru(1)-C(2)	2.1874(14)	C(13)-C(14)	1.531(2)
Ru(1)-C(5)	2.1940(14)	C(15)-C(16)	1.534(2)
Ru(1)-C(4)	2.1980(13)	C(17)-C(18)	1.527(3)
C(1)-C(2)	1.426(2)	B(1)-F(2)	1.373(3)
C(1)-C(6)	1.430(2)	B(1)-F(4)	1.379(2)
C(1)-C(7)	1.513(2)	B(1)-F(3)	1.385(2)
C(2)-C(3)	1.436(2)	B(1)-F(1)	1.398(2)
C(2)-C(9)	1.533(2)	B(2)-F(5)	1.367(3)
C(3)-C(4)	1.429(2)	B(2)-F(6)	1.384(3)
C(3)-C(11)	1.518(2)	B(2)-F(7)	1.397(2)
C(4)-C(5)	1.424(2)	B(2)-F(8)	1.399(2)
C(4)-C(13)	1.526(2)		

O(3)-Ru(1)-O(1)	77.78(5)	O(1)-Ru(1)-C(2)	105.36(6)
O(3)-Ru(1)-C(3)	139.42(6)	C(3)-Ru(1)-C(2)	38.60(6)
O(1)-Ru(1)-C(3)	138.73(6)	O(2)-Ru(1)-C(2)	102.58(5)
O(3)-Ru(1)-O(2)	80.10(5)	C(1)-Ru(1)-C(2)	38.15(6)
O(1)-Ru(1)-O(2)	79.66(5)	C(6)-Ru(1)-C(2)	69.38(5)
C(3)-Ru(1)-O(2)	89.15(5)	O(3)-Ru(1)-C(5)	94.56(5)
O(3)-Ru(1)-C(1)	140.49(6)	O(1)-Ru(1)-C(5)	138.72(5)
O(1)-Ru(1)-C(1)	91.54(6)	C(3)-Ru(1)-C(5)	69.05(6)
C(3)-Ru(1)-C(1)	69.36(6)	O(2)-Ru(1)-C(5)	139.59(5)
O(2)-Ru(1)-C(1)	135.80(5)	C(1)-Ru(1)-C(5)	68.73(6)
O(3)-Ru(1)-C(6)	107.78(5)	C(6)-Ru(1)-C(5)	38.25(6)
O(1)-Ru(1)-C(6)	105.19(6)	C(2)-Ru(1)-C(5)	81.59(6)
C(3)-Ru(1)-C(6)	82.49(6)	O(3)-Ru(1)-C(4)	107.59(5)
O(2)-Ru(1)-C(6)	171.34(5)	O(1)-Ru(1)-C(4)	172.94(5)
C(1)-Ru(1)-C(6)	38.28(5)	C(3)-Ru(1)-C(4)	38.29(6)
O(3)-Ru(1)-C(2)	176.14(6)	O(2)-Ru(1)-C(4)	105.54(5)

C(1)-Ru(1)-C(4)	81.40(6)	C(1)-C(6)-Ru(1)	70.46(8)
C(6)-Ru(1)-C(4)	69.04(6)	C(5)-C(6)-Ru(1)	71.18(8)
C(2)-Ru(1)-C(4)	69.10(6)	C(17)-C(6)-Ru(1)	129.39(11)
C(5)-Ru(1)-C(4)	37.83(5)	C(1)-C(7)-C(8)	110.05(15)
C(2)-C(1)-C(6)	121.27(13)	C(10)-C(9)-C(2)	115.87(14)
C(2)-C(1)-C(7)	119.82(13)	C(3)-C(11)-C(12)	112.60(14)
C(6)-C(1)-C(7)	118.89(14)	C(4)-C(13)-C(14)	116.10(14)
C(2)-C(1)-Ru(1)	71.38(8)	C(5)-C(15)-C(16)	110.20(14)
C(6)-C(1)-Ru(1)	71.26(8)	C(6)-C(17)-C(18)	115.01(14)
C(7)-C(1)-Ru(1)	129.36(11)	F(2)-B(1)-F(4)	108.9(2)
C(1)-C(2)-C(3)	118.93(13)	F(2)-B(1)-F(3)	108.4(2)
C(1)-C(2)-C(9)	120.84(14)	F(4)-B(1)-F(3)	110.1(2)
C(3)-C(2)-C(9)	120.18(14)	F(2)-B(1)-F(1)	110.0(2)
C(1)-C(2)-Ru(1)	70.47(8)	F(4)-B(1)-F(1)	109.8(2)
C(3)-C(2)-Ru(1)	69.54(8)	F(3)-B(1)-F(1)	109.68(15)
C(9)-C(2)-Ru(1)	130.06(11)	F(5)-B(2)-F(6)	111.7(2)
C(4)-C(3)-C(2)	120.50(13)	F(5)-B(2)-F(7)	110.6(2)
C(4)-C(3)-C(11)	119.96(14)	F(6)-B(2)-F(7)	107.5(2)
C(2)-C(3)-C(11)	119.44(14)	F(5)-B(2)-F(8)	109.6(2)
C(4)-C(3)-Ru(1)	72.42(8)	F(6)-B(2)-F(8)	109.4(2)
C(2)-C(3)-Ru(1)	71.86(8)	F(7)-B(2)-F(8)	107.9(2)
C(11)-C(3)-Ru(1)	125.00(10)		
C(5)-C(4)-C(3)	119.64(13)		
C(5)-C(4)-C(13)	120.01(13)		
C(3)-C(4)-C(13)	120.35(14)		
C(5)-C(4)-Ru(1)	70.94(8)		
C(3)-C(4)-Ru(1)	69.28(8)		
C(13)-C(4)-Ru(1)	132.41(11)		
C(4)-C(5)-C(6)	120.70(13)		
C(4)-C(5)-C(15)	119.95(13)		
C(6)-C(5)-C(15)	119.35(13)		
C(4)-C(5)-Ru(1)	71.24(8)		
C(6)-C(5)-Ru(1)	70.57(8)		
C(15)-C(5)-Ru(1)	131.41(11)		
C(1)-C(6)-C(5)	118.84(13)		
C(1)-C(6)-C(17)	121.09(14)		
C(5)-C(6)-C(17)	120.06(13)		

Table E4. Anisotropic displacement parameters ($Å^2 \times 10^3$)for 34. The anisotropic displacement factor exponent takes the form: $-2\pi^2[h^2a^{*2}U_{11} + ... + 2 h k a^* b^* U_{12}]$

	U_{11}	U_{22}	U_{33}	U_{23}	U_{13}	U_{12}
Ru(1)	22(1)	17(1)	20(1)	-1(1)	0(1)	1(1)
C(1)	28(1)	19(1)	25(1)	-2(1)	4(1)	3(1)
C(2)	28(1)	20(1)	24(1)	1(1)	0(1)	6(1)
C(3)	25(1)	23(1)	23(1)	-2(1)	-2(1)	6(1)
C(4)	21(1)	24(1)	27(1)	1(1)	1(1)	4(1)
C(5)	25(1)	21(1)	24(1)	0(1)	2(1)	3(1)
C(6)	27(1)	21(1)	21(1)	-3(1)	1(1)	4(1)
C(7)	34(1)	25(1)	31(1)	-2(1)	5(1)	-5(1)
C(8)	60(1)	23(1)	46(1)	-4(1)	8(1)	-2(1)
C(9)	43(1)	29(1)	26(1)	6(1)	1(1)	1(1)
C(10)	51(1)	44(1)	27(1)	6(1)	10(1)	0(1)
C(11)	32(1)	32(1)	24(1)	-3(1)	-5(1)	7(1)
C(12)	41(1)	54(1)	32(1)	-4(1)	-10(1)	16(1)
C(13)	26(1)	33(1)	31(1)	-2(1)	0(1)	-4(1)
C(14)	41(1)	31(1)	49(1)	-6(1)	1(1)	-7(1)
C(15)	34(1)	28(1)	26(1)	2(1)	2(1)	-2(1)
C(16)	40(1)	50(1)	34(1)	-1(1)	11(1)	0(1)
C(17)	36(1)	30(1)	23(1)	-4(1)	-1(1)	-5(1)
C(18)	37(1)	49(1)	28(1)	0(1)	-9(1)	0(1)
O(1)	25(1)	24(1)	59(1)	-7(1)	4(1)	2(1)
O(2)	31(1)	39(1)	36(1)	-16(1)	-1(1)	4(1)
O(3)	44(1)	24(1)	33(1)	4(1)	1(1)	6(1)
B(1)	32(1)	38(1)	33(1)	-11(1)	0(1)	-8(1)
F(1)	50(1)	42(1)	32(1)	-9(1)	0(1)	-12(1)
F(2)	60(1)	102(1)	48(1)	-16(1)	-10(1)	33(1)
F(3)	54(1)	100(1)	42(1)	-17(1)	10(1)	-36(1)
F(4)	96(1)	40(1)	53(1)	-14(1)	-18(1)	-13(1)
B(2)	36(1)	37(1)	39(1)	-5(1)	6(1)	-2(1)
F(5)	36(1)	83(1)	74(1)	-11(1)	1(1)	5(1)
F(6)	94(1)	68(1)	47(1)	11(1)	12(1)	-1(1)
F(7)	48(1)	45(1)	49(1)	-13(1)	4(1)	-10(1)
F(8)	62(1)	38(1)	53(1)	-13(1)	6(1)	-1(1)
O(4)	122(2)	40(1)	49(1)	-2(1)	-10(1)	13(1)

Table E5. Hydrogen coordinates ($\times 10^4$) and isotropic displacement parameters ($Å^2 \times 10^3$) for **34**.

	x	y	z	U(eq)
H(7A)	9142(23)	2242(16)	1270(13)	42(6)
H(7B)	9295(25)	2017(16)	2079(13)	45(6)
H(8A)	7498(23)	3385(16)	1570(13)	42(6)
H(8B)	7621(20)	3163(13)	2379(11)	30(5)
H(8C)	8714(28)	3654(20)	1934(14)	61(7)
H(9A)	6705(21)	1768(15)	-44(11)	32(5)
H(9B)	7637(22)	2443(16)	431(11)	39(5)
H(10A)	8492(28)	765(20)	-251(14)	58(7)
H(10B)	9511(28)	1500(18)	199(14)	58(7)
H(10C)	8811(25)	1774(18)	-512(14)	52(7)
H(11A)	6238(19)	260(14)	-216(10)	31(5)
H(11B)	5330(19)	-476(15)	205(10)	25(5)
H(12A)	4459(26)	1480(19)	-77(14)	57(7)
H(12B)	3624(26)	666(17)	249(13)	48(7)
H(12C)	4055(25)	537(18)	-513(15)	59(7)
H(13A)	4018(19)	-692(14)	1922(11)	24(4)
H(13B)	3977(21)	-626(15)	1113(11)	32(5)
H(14A)	5558(27)	-1987(18)	1846(14)	51(7)
H(14B)	4252(24)	-2262(16)	1394(13)	45(6)
H(14C)	5414(24)	-1954(17)	1018(14)	44(6)
H(15A)	6559(20)	-409(14)	3284(10)	30(5)
H(15B)	5490(20)	-977(15)	2800(10)	32(5)
H(16A)	4998(25)	833(18)	3476(14)	55(7)
H(16B)	4418(26)	-190(19)	3739(15)	65(7)
H(16C)	3892(26)	258(19)	2996(14)	61(7)
H(17A)	7277(21)	1078(13)	3400(11)	32(5)
H(17B)	8181(20)	1755(15)	3065(10)	30(5)
H(18A)	9436(22)	614(15)	3690(12)	39(5)
H(18B)	8833(26)	-216(21)	3239(14)	59(7)
H(18C)	9723(28)	504(20)	2847(15)	64(8)
H(1A)	10331(28)	-413(20)	1390(17)	59(8)
H(1B)	10351(26)	475(19)	1298(14)	50(7)

H(2A)	7651(29)	-1318(20)	299(15)	60(8)
H(2B)	8900(29)	-1102(19)	333(14)	52(7)
H(3A)	8436(27)	-1922(20)	1696(14)	54(7)
H(3B)	8221(27)	-1569(19)	2383(15)	56(7)
H(4A)	7969(51)	-3423(33)	1701(26)	145(17)
H(4B)	8041(47)	-3254(31)	911(24)	122(15)

Table F1. Crystal data and structure refinement for **35**.

Empirical formula	$C_{21}H_{39}Cl_2O_3PRu$	
Formula weight	542.46	
Temperature	210(2) K	
Wavelength	0.71073 Å	
Crystal system	Triclinic	
Space group	P-1	
Unit cell dimensions	a = 9.8280(10) Å	α= 71.768(4)°
	b = 10.2520(10) Å	β= 85.496(3)°
	c = 13.364(2) Å	γ = 68.6570(10)°
Volume	1190.3(2) $Å^3$	
Z	2	
Density (calculated)	1.514 Mg/m^3	
Absorption coefficient	0.969 mm^{-1}	
F(000)	564	
Crystal size	0.30 × 0.18 x 0.08 mm^3	
θ range for data collection	2.23 to 28.43°	
Index ranges	$-13 \le h \le 13, -13 \le k \le 13, -17 \le l \le 17$	
Reflections collected	14274	
Independent reflections	5358 [R(int) = 0.0229]	
Absorption correction	SADABS	
Max. and min. transmission	0.934773 and 0.760503	
Refinement method	Full-matrix least-squares on F^2	
Data / restraints / parameters	5358 / 0 / 410	
Goodness-of-fit on F^2	1.042	
Final R indices [$I>2\sigma(I)$] [a]	R1 = 0.0224, wR2 = 0.0603	
R indices (all data) [a]	R1 = 0.0247, wR2 = 0.0614	
Extinction coefficient	0.0030(6)	
Largest diff. peak and hole	0.558 and -0.689 $e.Å^{-3}$	

[a] $R1 = \Sigma(\|Fo\| - \|Fc\|)/\Sigma|Fo|$; $wR2 = [\Sigma[w(Fo^2 - Fc^2)^2]/\Sigma[w(Fo^2)^2]]^{0.5}$

Table F2. Atomic coordinates ($\times 10^4$) and equivalent isotropic displacement parameters ($Å^2 \times 10^3$) for **35**. U(eq) is defined as one third of the trace of the orthogonalized U_{ij} tensor.

	x	y	z	U(eq)
Ru(1)	1889(1)	356(1)	7381(1)	18(1)
Cl(1)	707(1)	-1126(1)	8649(1)	31(1)
Cl(2)	2400(1)	-1320(1)	6368(1)	33(1)
P(1)	3990(1)	-1205(1)	8323(1)	22(1)
C(1)	-137(2)	2313(2)	6562(1)	22(1)
C(2)	998(2)	2168(2)	5837(1)	21(1)
C(3)	2426(2)	2047(2)	6124(1)	22(1)
C(4)	2640(2)	2211(2)	7122(1)	22(1)
C(5)	1495(2)	2355(2)	7862(1)	22(1)
C(6)	137(2)	2328(2)	7594(1)	21(1)
C(7)	-1632(2)	2417(2)	6245(2)	29(1)
C(8)	-1850(2)	957(3)	6506(2)	37(1)
C(9)	702(2)	2096(2)	4770(1)	30(1)
C(10)	-1(3)	3625(3)	3984(2)	48(1)
C(11)	3681(2)	1742(2)	5390(2)	31(1)
C(12)	3694(3)	3045(3)	4459(2)	48(1)
C(13)	4075(2)	2286(2)	7385(2)	31(1)
C(14)	4212(3)	3766(3)	6833(2)	47(1)
C(15)	1717(2)	2517(2)	8922(1)	31(1)
C(16)	1501(3)	4087(3)	8871(2)	48(1)
C(17)	-1059(2)	2368(2)	8378(1)	28(1)
C(18)	-1997(3)	3919(2)	8382(2)	42(1)
O(1)	4383(1)	-784(1)	9292(1)	27(1)
C(19)	3569(3)	-1034(3)	10238(2)	35(1)
O(2)	5374(1)	-1188(1)	7631(1)	30(1)
C(20)	6837(2)	-2026(3)	8076(2)	39(1)
O(3)	4297(2)	-2887(1)	8929(1)	33(1)
C(21)	3924(3)	-3888(2)	8569(2)	41(1)

Table F3. Bond lengths [Å] and angles [°] for **35**.

Ru(1)-C(3)	2.193(2)	C(3)-C(4)	1.436(2)
Ru(1)-C(4)	2.202(2)	C(3)-C(11)	1.517(2)
Ru(1)-C(6)	2.209(2)	C(4)-C(5)	1.436(2)
Ru(1)-C(5)	2.228(2)	C(4)-C(13)	1.514(2)
Ru(1)-P(1)	2.2697(5)	C(5)-C(6)	1.421(2)
Ru(1)-C(2)	2.275(2)	C(5)-C(15)	1.518(2)
Ru(1)-C(1)	2.291(2)	C(6)-C(17)	1.510(2)
Ru(1)-Cl(2)	2.4002(5)	C(7)-C(8)	1.517(3)
Ru(1)-Cl(1)	2.4276(5)	C(9)-C(10)	1.527(3)
P(1)-O(3)	1.5838(13)	C(11)-C(12)	1.517(3)
P(1)-O(2)	1.5853(13)	C(13)-C(14)	1.516(3)
P(1)-O(1)	1.6010(12)	C(15)-C(16)	1.526(3)
C(1)-C(2)	1.416(2)	C(17)-C(18)	1.522(3)
C(1)-C(6)	1.432(2)	O(1)-C(19)	1.446(2)
C(1)-C(7)	1.519(2)	O(2)-C(20)	1.441(2)
C(2)-C(3)	1.434(2)	O(3)-C(21)	1.425(2)
C(2)-C(9)	1.507(2)		

C(3)-Ru(1)-C(4)	38.13(6)	C(6)-Ru(1)-C(1)	37.04(6)
C(3)-Ru(1)-C(6)	81.10(6)	C(5)-Ru(1)-C(1)	66.40(6)
C(4)-Ru(1)-C(6)	67.81(6)	P(1)-Ru(1)-C(1)	167.14(4)
C(3)-Ru(1)-C(5)	68.83(6)	C(2)-Ru(1)-C(1)	36.12(6)
C(4)-Ru(1)-C(5)	37.83(6)	C(3)-Ru(1)-Cl(2)	94.38(5)
C(6)-Ru(1)-C(5)	37.34(6)	C(4)-Ru(1)-Cl(2)	127.96(5)
C(3)-Ru(1)-P(1)	107.53(4)	C(6)-Ru(1)-Cl(2)	140.50(4)
C(4)-Ru(1)-P(1)	90.19(4)	C(5)-Ru(1)-Cl(2)	162.98(4)
C(6)-Ru(1)-P(1)	132.43(4)	P(1)-Ru(1)-Cl(2)	86.51(2)
C(5)-Ru(1)-P(1)	100.89(4)	C(2)-Ru(1)-Cl(2)	85.95(4)
C(3)-Ru(1)-C(2)	37.39(6)	C(1)-Ru(1)-Cl(2)	105.23(4)
C(4)-Ru(1)-C(2)	66.85(6)	C(3)-Ru(1)-Cl(1)	166.49(4)
C(6)-Ru(1)-C(2)	66.71(6)	C(4)-Ru(1)-Cl(1)	142.58(4)
C(5)-Ru(1)-C(2)	78.93(6)	C(6)-Ru(1)-Cl(1)	88.00(4)
P(1)-Ru(1)-C(2)	143.05(4)	C(5)-Ru(1)-Cl(1)	106.74(4)
C(3)-Ru(1)-C(1)	66.97(6)	P(1)-Ru(1)-Cl(1)	85.71(2)
C(4)-Ru(1)-C(1)	78.49(6)	C(2)-Ru(1)-Cl(1)	130.20(4)

C(1)-Ru(1)-Cl(1)	99.52(4)	C(15)-C(5)-Ru(1)	130.88(12)
Cl(2)-Ru(1)-Cl(1)	88.95(2)	C(5)-C(6)-C(1)	120.39(14)
O(3)-P(1)-O(2)	105.10(7)	C(5)-C(6)-C(17)	120.65(14)
O(3)-P(1)-O(1)	96.95(7)	C(1)-C(6)-C(17)	118.93(15)
O(2)-P(1)-O(1)	100.39(7)	C(5)-C(6)-Ru(1)	72.06(9)
O(3)-P(1)-Ru(1)	123.95(5)	C(1)-C(6)-Ru(1)	74.57(9)
O(2)-P(1)-Ru(1)	111.04(5)	C(17)-C(6)-Ru(1)	127.08(11)
O(1)-P(1)-Ru(1)	116.19(5)	C(8)-C(7)-C(1)	115.1(2)
C(2)-C(1)-C(6)	120.05(14)	C(2)-C(9)-C(10)	112.0(2)
C(2)-C(1)-C(7)	119.56(15)	C(12)-C(11)-C(3)	115.9(2)
C(6)-C(1)-C(7)	120.37(14)	C(4)-C(13)-C(14)	113.1(2)
C(2)-C(1)-Ru(1)	71.34(9)	C(5)-C(15)-C(16)	113.6(2)
C(6)-C(1)-Ru(1)	68.38(9)	C(6)-C(17)-C(18)	113.2(2)
C(7)-C(1)-Ru(1)	132.35(12)	C(19)-O(1)-P(1)	117.85(11)
C(1)-C(2)-C(3)	120.57(14)	C(20)-O(2)-P(1)	121.22(14)
C(1)-C(2)-C(9)	119.15(15)	C(21)-O(3)-P(1)	126.76(13)
C(3)-C(2)-C(9)	120.26(14)		
C(1)-C(2)-Ru(1)	72.55(9)		
C(3)-C(2)-Ru(1)	68.20(9)		
C(9)-C(2)-Ru(1)	131.07(12)		
C(2)-C(3)-C(4)	118.53(14)		
C(2)-C(3)-C(11)	120.58(15)		
C(4)-C(3)-C(11)	120.88(15)		
C(2)-C(3)-Ru(1)	74.41(9)		
C(4)-C(3)-Ru(1)	71.26(9)		
C(11)-C(3)-Ru(1)	124.93(12)		
C(3)-C(4)-C(5)	120.97(14)		
C(3)-C(4)-C(13)	119.67(15)		
C(5)-C(4)-C(13)	119.33(15)		
C(3)-C(4)-Ru(1)	70.60(9)		
C(5)-C(4)-Ru(1)	72.09(9)		
C(13)-C(4)-Ru(1)	132.33(12)		
C(6)-C(5)-C(4)	118.92(14)		
C(6)-C(5)-C(15)	119.80(15)		
C(4)-C(5)-C(15)	121.27(15)		
C(6)-C(5)-Ru(1)	70.61(9)		
C(4)-C(5)-Ru(1)	70.09(9)		

Table F4. Anisotropic displacement parameters ($Å^2 \times 10^3$)for 35. The anisotropic displacement factor exponent takes the form: $-2\pi^2[h^2a^{*2}U_{11} + ... + 2 h k a^* b^* U_{12}]$

	U11	U22	U33	U23	U13	U12
Ru(1)	17(1)	20(1)	18(1)	-5(1)	-1(1)	-7(1)
Cl(1)	31(1)	29(1)	31(1)	-3(1)	4(1)	-15(1)
Cl(2)	39(1)	29(1)	31(1)	-15(1)	-3(1)	-7(1)
P(1)	22(1)	20(1)	24(1)	-4(1)	-4(1)	-8(1)
C(1)	17(1)	22(1)	23(1)	-4(1)	-1(1)	-5(1)
C(2)	21(1)	21(1)	18(1)	-2(1)	-1(1)	-6(1)
C(3)	18(1)	22(1)	23(1)	-4(1)	2(1)	-6(1)
C(4)	20(1)	21(1)	25(1)	-4(1)	-2(1)	-9(1)
C(5)	25(1)	19(1)	22(1)	-5(1)	-1(1)	-8(1)
C(6)	22(1)	19(1)	22(1)	-6(1)	3(1)	-6(1)
C(7)	18(1)	37(1)	31(1)	-9(1)	-1(1)	-8(1)
C(8)	29(1)	48(1)	43(1)	-17(1)	-1(1)	-21(1)
C(9)	27(1)	39(1)	20(1)	-9(1)	0(1)	-9(1)
C(10)	45(1)	56(2)	27(1)	4(1)	-7(1)	-12(1)
C(11)	21(1)	36(1)	32(1)	-11(1)	8(1)	-8(1)
C(12)	45(1)	54(1)	38(1)	-5(1)	18(1)	-20(1)
C(13)	22(1)	31(1)	41(1)	-9(1)	-5(1)	-11(1)
C(14)	38(1)	38(1)	73(2)	-12(1)	-5(1)	-23(1)
C(15)	41(1)	32(1)	24(1)	-9(1)	-2(1)	-16(1)
C(16)	66(2)	40(1)	45(1)	-24(1)	-6(1)	-16(1)
C(17)	28(1)	29(1)	27(1)	-11(1)	9(1)	-11(1)
C(18)	36(1)	35(1)	56(1)	-22(1)	19(1)	-11(1)
O(1)	27(1)	30(1)	26(1)	-6(1)	-5(1)	-14(1)
C(19)	43(1)	41(1)	23(1)	-4(1)	-3(1)	-23(1)
O(2)	22(1)	29(1)	34(1)	-7(1)	0(1)	-4(1)
C(20)	22(1)	36(1)	52(1)	-13(1)	-3(1)	-2(1)
O(3)	38(1)	21(1)	39(1)	-2(1)	-14(1)	-12(1)
C(21)	45(1)	22(1)	56(1)	-10(1)	-16(1)	-9(1)

Table F5. Hydrogen coordinates ($\times 10^4$) and isotropic displacement parameters ($Å^2 \times 10^3$) for 35.

	x	y	z	U(eq)
H(7A)	-2386(25)	3080(25)	6576(17)	30(5)
H(7B)	-1817(29)	2884(29)	5501(22)	49(7)
H(8A)	-1863(27)	524(27)	7270(20)	40(6)
H(8B)	-1075(34)	246(34)	6248(23)	65(9)
H(8C)	-2733(31)	1108(30)	6152(20)	51(7)
H(9A)	59(26)	1524(26)	4862(18)	36(6)
H(9B)	1490(29)	1604(28)	4528(19)	39(6)
H(10A)	577(38)	4132(38)	3867(26)	69(10)
H(10B)	-144(40)	3487(40)	3396(31)	87(11)
H(10C)	-883(35)	4249(33)	4244(23)	62(8)
H(11A)	3675(27)	926(28)	5133(18)	43(6)
H(11B)	4625(30)	1365(29)	5795(20)	52(7)
H(12A)	4614(36)	2814(34)	4159(24)	63(9)
H(12B)	2941(44)	3274(42)	3913(31)	96(12)
H(12C)	3437(40)	3898(42)	4612(27)	84(11)
H(13A)	4811(28)	1602(27)	7204(18)	40(6)
H(13B)	4140(26)	2066(26)	8186(19)	40(6)
H(14A)	3392(35)	4510(35)	6886(23)	62(9)
H(14B)	5031(33)	3888(32)	7059(22)	58(8)
H(14C)	4338(40)	3890(41)	5994(31)	94(12)
H(15A)	2649(26)	1881(25)	9226(17)	32(6)
H(15B)	1069(27)	2186(27)	9421(19)	38(6)
H(16C)	2293(47)	4333(44)	8452(33)	105(14)
H(16A)	683(34)	4802(35)	8513(24)	59(8)
H(16B)	1491(40)	4143(40)	9527(31)	90(12)
H(17A)	-1672(24)	1912(24)	8195(16)	29(5)
H(17B)	-697(24)	1826(25)	9057(18)	30(5)
H(18A)	-2732(31)	3934(30)	8834(22)	48(7)
H(18B)	-1417(34)	4347(34)	8568(24)	65(9)
H(18C)	-2406(40)	4532(38)	7704(27)	79(10)
H(19A)	3677(24)	-478(24)	10624(17)	30(5)
H(19B)	3874(26)	-2015(29)	10602(19)	37(6)
H(19C)	2585(30)	-729(28)	10057(20)	43(7)

H(20A)	7126(34)	-1643(35)	8544(24)	68(9)
H(20B)	7454(38)	-1952(37)	7531(27)	77(10)
H(20C)	6970(37)	-2945(40)	8383(27)	78(10)
H(21A)	2981(32)	-3548(30)	8374(21)	49(7)
H(21B)	4250(34)	-4852(36)	9102(24)	67(9)
H(21C)	4406(41)	-4096(41)	8034(30)	84(12)

Table G1. Crystal data and structure refinement for 37.

Empirical formula	$C_{12}H_{36}Cl_2P_4Ru$	
Formula weight	476.26	
Temperature	210(2) K	
Wavelength	0.71073 Å	
Crystal system	Monoclinic	
Space group	P2/n	
Unit cell dimensions	a = 15.67730(10) Å	α= 90°
	b = 9.44760(10) Å	β= 111.5780(10)°
	c = 15.6812(2) Å	γ = 90°
Volume	2159.81(4) $Å^3$	
Z	4	
Density (calculated)	1.465 Mg/m^3	
Absorption coefficient	1.259 mm^{-1}	
F(000)	984	
Crystal size	0.40 × 0.28 × 0.09 mm^3	
θ range for data collection	1.40 to 26.47°	
Index ranges	$-19 \le h \le 19, -9 \le k \le 11, -19 \le l \le 19$	
Reflections collected	17943	
Independent reflections	4408 [R(int) = 0.0422]	
Absorption correction	SADABS	
Max. and min. transmission	1.0000 and 0.825625	
Refinement method	Full-matrix least-squares on F^2	
Data / restraints / parameters	4408 / 0 / 174	
Goodness-of-fit on F^2	1.051	
Final R indices [$I>2\sigma(I)$] [a]	R1 = 0.0231, wR2 = 0.0604	
R indices (all data) [a]	R1 = 0.0248, wR2 = 0.0614	
Largest diff. peak and hole	0.665 and -0.620 e.$Å^{-3}$	

[a] $R1 = \Sigma(\|Fo\| - \|Fc\|)/\Sigma|Fo|$; $wR2 = [\Sigma[w(Fo^2 - Fc^2)^2]/\Sigma[w(Fo^2)^2]]^{0.5}$

Table G2. Atomic coordinates ($\times 10^4$) and equivalent isotropic displacement parameters ($Å^2 \times 10^3$) for **37**. U(eq) is defined as one third of the trace of the orthogonalized U_{ij} tensor.

	x	y	z	U(eq)
Ru(1)	7500	9664(1)	2500	18(1)
Cl(1)	7260(1)	9650(1)	869(1)	31(1)
P(5)	6397(1)	7931(1)	2425(1)	26(1)
P(7)	6356(1)	11415(1)	2042(1)	25(1)
Ru(2)	2500	5045(1)	2500	20(1)
Cl(2)	838(1)	5045(1)	2073(1)	33(1)
P(6)	2164(1)	6776(1)	1340(1)	27(1)
P(8)	2573(1)	3307(1)	1454(1)	28(1)
C(8)	1346(2)	6261(4)	208(2)	43(1)
C(9)	3087(2)	7595(4)	1067(2)	40(1)
C(10)	3284(2)	1752(3)	1939(2)	40(1)
C(14)	3188(2)	3816(3)	704(2)	38(1)
C(16)	1524(3)	8329(3)	1464(2)	42(1)
C(17)	1529(2)	2490(4)	656(2)	44(1)
C(1A)	6802(3)	6375(3)	3158(2)	40(1)
C(2A)	6578(2)	12945(3)	1436(2)	39(1)
C(3A)	5986(2)	12247(4)	2900(2)	40(1)
C(4A)	5529(2)	8450(4)	2889(2)	39(1)
C(5A)	5277(2)	10923(4)	1134(2)	38(1)
C(6A)	5707(2)	7106(4)	1333(2)	41(1)

Table G3. Bond lengths [Å] and angles [°] for **37**.

Ru(1)-P(2)#1	2.3498(7)	Ru(2)-P(4)	2.3523(7)
Ru(1)-P(2)	2.3498(7)	Ru(2)-P(4)#2	2.3523(7)
Ru(1)-P(1)	2.3522(7)	Ru(2)-P(3)#2	2.3565(7)
Ru(1)-P(1)#1	2.3522(7)	Ru(2)-P(3)	2.3565(7)
Ru(1)-Cl(1)	2.4438(6)	Ru(2)-Cl(2)	2.4403(7)
Ru(1)-Cl(1)#1	2.4438(6)	Ru(2)-Cl(2)#2	2.4403(7)
P(1)-C(3)	1.830(3)	P(3)-C(9)	1.826(3)
P(1)-C(2)	1.831(3)	P(3)-C(7)	1.827(3)
P(1)-C(1)	1.830(3)	P(3)-C(8)	1.833(3)
P(2)-C(5)	1.826(3)	P(4)-C(12)	1.826(3)
P(2)-C(6)	1.826(3)	P(4)-C(10)	1.831(3)
P(2)-C(4)	1.832(3)	P(4)-C(11)	1.838(3)
P(2)#1-Ru(1)-P(2)	90.51(4)	C(5)-P(2)-C(4)	102.4(2)
P(2)#1-Ru(1)-P(1)	165.86(2)	C(6)-P(2)-C(4)	95.39(15)
P(2)-Ru(1)-P(1)	90.60(3)	C(5)-P(2)-Ru(1)	119.44(11)
P(2)#1-Ru(1)-P(1)#1	90.60(3)	C(6)-P(2)-Ru(1)	116.28(11)
P(2)-Ru(1)-P(1)#1	165.86(2)	C(4)-P(2)-Ru(1)	116.38(11)
P(1)-Ru(1)-P(1)#1	91.77(4)	P(4)-Ru(2)-P(4)#2	91.51(4)
P(2)#1-Ru(1)-Cl(1)	97.46(3)	P(4)-Ru(2)-P(3)#2	165.38(3)
P(2)-Ru(1)-Cl(1)	82.98(2)	P(4)#2-Ru(2)-P(3)#2	90.05(3)
P(1)-Ru(1)-Cl(1)	96.67(3)	P(4)-Ru(2)-P(3)	90.05(3)
P(1)#1-Ru(1)-Cl(1)	82.90(2)	P(4)#2-Ru(2)-P(3)	165.38(3)
P(2)#1-Ru(1)-Cl(1)#1	82.98(2)	P(3)#2-Ru(2)-P(3)	92.11(4)
P(2)-Ru(1)-Cl(1)#1	97.46(3)	P(4)-Ru(2)-Cl(2)	97.44(3)
P(1)-Ru(1)-Cl(1)#1	82.90(2)	P(4)#2-Ru(2)-Cl(2)	82.56(3)
P(1)#1-Ru(1)-Cl(1)#1	96.67(3)	P(3)#2-Ru(2)-Cl(2)	97.18(3)
Cl(1)-Ru(1)-Cl(1)#1	179.38(4)	P(3)-Ru(2)-Cl(2)	82.82(3)
C(3)-P(1)-C(2)	102.4(2)	P(4)-Ru(2)-Cl(2)#2	82.56(3)
C(3)-P(1)-C(1)	101.2(2)	P(4)#2-Ru(2)-Cl(2)#2	97.44(3)
C(2)-P(1)-C(1)	95.8(2)	P(3)#2-Ru(2)-Cl(2)#2	82.82(3)
C(3)-P(1)-Ru(1)	120.97(12)	P(3)-Ru(2)-Cl(2)#2	97.18(3)
C(2)-P(1)-Ru(1)	115.72(11)	Cl(2)-Ru(2)-Cl(2)#2	180.00(5)
C(1)-P(1)-Ru(1)	116.71(12)	C(9)-P(3)-C(7)	101.4(2)
C(5)-P(2)-C(6)	103.33(15)	C(9)-P(3)-C(8)	102.6(2)

C(7)-P(3)-C(8)	95.8(2)	C(12)-P(4)-C(11)	102.7(2)
C(9)-P(3)-Ru(2)	120.23(11)	C(10)-P(4)-C(11)	95.3(2)
C(7)-P(3)-Ru(2)	116.82(11)	C(12)-P(4)-Ru(2)	120.81(11)
C(8)-P(3)-Ru(2)	116.22(12)	C(10)-P(4)-Ru(2)	116.65(12)
C(12)-P(4)-C(10)	101.6(2)	C(11)-P(4)-Ru(2)	115.80(11)

Symmetry transformations used to generate equivalent atoms:

#1 -x+3/2,y,-z+1/2 #2 -x+1/2,y,-z+1/2

Table G4. Anisotropic displacement parameters ($Å^2 \times 10^3$)for 37. The anisotropic displacement factor exponent takes the form: $-2\pi^2[h^2a^{*2}U_{11} + ... + 2 h k a^* b^* U_{12}]$

	U_{11}	U_{22}	U_{33}	U_{23}	U_{13}	U_{12}
Ru(1)	22(1)	15(1)	19(1)	0	8(1)	0
Cl(1)	43(1)	31(1)	21(1)	1(1)	14(1)	7(1)
P(5)	29(1)	21(1)	28(1)	-1(1)	11(1)	-4(1)
P(7)	29(1)	20(1)	26(1)	-2(1)	9(1)	5(1)
Ru(2)	26(1)	15(1)	22(1)	0	11(1)	0
Cl(2)	28(1)	31(1)	41(1)	3(1)	15(1)	2(1)
P(6)	36(1)	22(1)	26(1)	5(1)	15(1)	3(1)
P(8)	33(1)	22(1)	31(1)	-5(1)	14(1)	0(1)
C(8)	48(2)	49(2)	26(1)	4(1)	7(1)	7(2)
C(9)	49(2)	36(2)	44(2)	10(2)	28(2)	-2(2)
C(10)	47(2)	23(2)	58(2)	-2(2)	29(2)	7(2)
C(14)	51(2)	34(2)	38(2)	-7(1)	27(2)	2(2)
C(16)	56(2)	28(2)	50(2)	8(2)	27(2)	15(2)
C(17)	46(2)	39(2)	44(2)	-16(2)	14(1)	-6(2)
C(1A)	53(2)	26(1)	41(2)	7(2)	18(1)	-5(2)
C(2A)	48(2)	26(1)	41(2)	7(1)	14(1)	8(1)
C(3A)	42(2)	40(2)	42(2)	-13(2)	21(1)	5(2)
C(4A)	37(2)	39(2)	47(2)	-3(2)	24(1)	-8(1)
C(5A)	33(2)	38(2)	34(2)	-4(1)	2(1)	5(1)
C(6A)	44(2)	33(2)	42(2)	-9(1)	9(1)	-10(2)

Table G5. Hydrogen coordinates ($\times 10^4$) and isotropic displacement parameters ($Å^2 \times 10^3$) for 37.

	x	y	z	U(eq)
H(8A)	819(2)	5807(4)	275(2)	65
H(8B)	1638(2)	5607(4)	-76(2)	65
H(8C)	1147(2)	7096(4)	-173(2)	65
H(9A)	3483(2)	6864(4)	983(2)	60
H(9B)	3441(2)	8213(4)	1566(2)	60
H(9C)	2827(2)	8143(4)	508(2)	60
H(10A)	3870(2)	2055(3)	2383(2)	60
H(10B)	3382(2)	1226(3)	1452(2)	60
H(10C)	2975(2)	1153(3)	2238(2)	60
H(14A)	3762(2)	4268(3)	1066(2)	57
H(14B)	2814(2)	4469(3)	239(2)	57
H(14C)	3310(2)	2978(3)	410(2)	57
H(16A)	1004(3)	8028(3)	1613(2)	64
H(16B)	1308(3)	8856(3)	894(2)	64
H(16C)	1921(3)	8926(3)	1952(2)	64
H(17A)	1089(2)	3222(4)	349(2)	66
H(17B)	1269(2)	1871(4)	990(2)	66
H(17C)	1675(2)	1944(4)	203(2)	66
H(1AA)	7184(3)	6675(3)	3772(2)	59
H(1AB)	7155(3)	5775(3)	2909(2)	59
H(1AC)	6279(3)	5850(3)	3183(2)	59
H(2AA)	6782(2)	12620(3)	956(2)	59
H(2AB)	7050(2)	13532(3)	1865(2)	59
H(2AC)	6019(2)	13492(3)	1166(2)	59
H(3AA)	6520(2)	12550(4)	3417(2)	60
H(3AB)	5638(2)	11572(4)	3106(2)	60
H(3AC)	5605(2)	13061(4)	2631(2)	60
H(4AA)	5825(2)	8907(4)	3478(2)	58
H(4AB)	5203(2)	7615(4)	2965(2)	58
H(4AC)	5099(2)	9101(4)	2469(2)	58
H(5AA)	5405(2)	10467(4)	639(2)	57
H(5AB)	4911(2)	11765(4)	903(2)	57
H(5AC)	4943(2)	10275(4)	1377(2)	57
H(6AA)	6105(2)	6786(4)	1023(2)	62
H(6AB)	5273(2)	7790(4)	951(2)	62
H(6AC)	5377(2)	6304(4)	1446(2)	62

Table H1. Crystal data and structure refinement for **52**.

Empirical formula	$C_{24}H_{24}Co_2O_7$	
Formula weight	542.29	
Temperature	210(2) K	
Wavelength	0.71073 Å	
Crystal system	Triclinic	
Space group	P-1	
Unit cell dimensions	a = 17.0510(10) Å	α= 112.590(10)°
	b = 17.1450(10) Å	β= 99.160(10)°
	c = 20.281(3) Å	γ = 110.620(10)°
Volume	4816.7(8) $Å^3$	
Z 8		
Density (calculated)	1.496 Mg/m^3	
Absorption coefficient	1.418 mm^{-1}	
F(000)	2224	
Crystal size	0.20 × 0.10 x 0.06 mm^3	
θ range for data collection	1.16 to 26.42°	
Index ranges	$-21 \le h \le 21, -21 \le k \le 21, -25 \le l \le 25$	
Reflections collected	49333	
Independent reflections	18151 [R(int) = 0.0661]	
Absorption correction	SADABS	
Max. and min. transmission	1.00 and 0.92	
Refinement method	Full-matrix least-squares on F^2	
Data / restraints / parameters	18151 / 0 / 1190	
Goodness-of-fit on F^2	1.064	
Final R indices [I>2σ(I)] [a]	R1 = 0.0520, wR2 = 0.0966	
R indices (all data) [a]	R1 = 0.1056, wR2 = 0.1167	
Extinction coefficient	0.00053(6)	
Largest diff. peak and hole	0.423 and -0.415 $e.Å^{-3}$	

[a] $R1 = \Sigma(||Fo| - |Fc||)/\Sigma|Fo|$; $wR2 = [\Sigma[w(Fo^2 - Fc^2)^2]/\Sigma[w(Fo^2)^2]]^{0.5}$

Table H2. Atomic coordinates ($\times 10^4$) and equivalent isotropic displacement parameters ($Å^2 \times 10^3$) for **52**. U(eq) is defined as one third of the trace of the orthogonalized U_{ij} tensor.

	x	y	z	U(eq)
Co(5)	-6287(1)	6805(1)	-821(1)	29(1)
Co(8)	-4644(1)	7560(1)	-272(1)	29(1)
O(1A)	-5622(2)	9046(2)	-546(2)	46(1)
C(1A)	-5374(3)	8509(3)	-1148(2)	28(1)
C(2A)	-4453(3)	9163(3)	-1090(3)	35(1)
C(3A)	-4193(3)	8728(3)	-1782(3)	35(1)
C(4A)	-4862(2)	8474(3)	-2513(3)	29(1)
C(5A)	-5781(3)	7766(3)	-2594(3)	32(1)
C(6A)	-6056(3)	8171(3)	-1915(3)	33(1)
C(7A)	-4599(3)	8160(4)	-3234(3)	41(1)
C(8A)	-3697(3)	8963(4)	-3094(3)	63(2)
C(9A)	-4502(4)	7250(4)	-3423(3)	68(2)
C(10A)	-5288(3)	8010(4)	-3908(3)	61(2)
C(11A)	-5391(2)	7677(3)	-1043(2)	27(1)
C(12A)	-5412(2)	6823(3)	-1355(2)	25(1)
C(13A)	-5395(2)	6076(3)	-2020(2)	25(1)
C(14A)	-4594(3)	6171(3)	-2149(3)	38(1)
C(15A)	-4579(3)	5476(4)	-2788(3)	44(1)
C(16A)	-5352(3)	4680(3)	-3295(3)	40(1)
C(17A)	-6145(3)	4573(3)	-3170(3)	41(1)
C(18A)	-6164(3)	5261(3)	-2539(3)	36(1)
C(19A)	-7315(3)	6335(3)	-1571(3)	39(1)
O(2A)	-7972(2)	6033(3)	-2031(2)	54(1)
C(20A)	-6496(3)	7600(4)	-54(3)	39(1)
O(3A)	-6630(2)	8100(3)	428(2)	57(1)
C(21A)	-6498(3)	5741(4)	-725(3)	35(1)
O(4A)	-6606(2)	5075(3)	-677(2)	52(1)
C(22A)	-4541(3)	6618(4)	-102(3)	40(1)
O(5A)	-4494(2)	6008(3)	-39(2)	62(1)
C(23A)	-4501(3)	8505(4)	628(3)	38(1)
O(6A)	-4418(2)	9101(3)	1183(2)	58(1)

C(24A)	-3553(3)	8089(4)	-308(3)	41(1)
O(7A)	-2850(2)	8404(3)	-323(2)	64(1)
Co(4)	2145(1)	5205(1)	4208(1)	32(1)
Co(7)	2291(1)	4228(1)	4804(1)	30(1)
O(1B)	347(2)	4345(2)	4867(2)	43(1)
C(1B)	268(3)	3744(3)	4098(3)	28(1)
C(2B)	-221(3)	2710(3)	3917(3)	29(1)
C(3B)	-477(3)	2005(3)	3085(3)	31(1)
C(4B)	-1013(3)	2205(3)	2542(3)	31(1)
C(5B)	-476(3)	3236(3)	2721(3)	34(1)
C(6B)	-267(3)	3930(3)	3549(3)	36(1)
C(7B)	-1338(3)	1453(3)	1690(3)	36(1)
C(8B)	-571(3)	1400(4)	1420(3)	58(2)
C(9B)	-1881(3)	1691(4)	1192(3)	64(2)
C(10B)	-1946(4)	468(4)	1574(3)	76(2)
C(11B)	1222(2)	4023(3)	4095(2)	25(1)
C(12B)	1754(2)	3824(3)	3714(2)	25(1)
C(13B)	1830(2)	3167(3)	3023(2)	25(1)
C(14B)	1686(3)	2259(3)	2901(3)	33(1)
C(15B)	1725(3)	1628(3)	2246(3)	38(1)
C(16B)	1931(3)	1899(4)	1714(3)	40(1)
C(17B)	2081(3)	2792(4)	1829(3)	37(1)
C(18B)	2040(3)	3430(3)	2483(3)	31(1)
C(19B)	3293(3)	5720(4)	4238(3)	43(1)
O(2B)	4007(2)	6017(3)	4248(2)	69(1)
C(20B)	1647(3)	5335(4)	3431(3)	42(1)
O(3B)	1341(3)	5420(3)	2939(2)	65(1)
C(21B)	2036(3)	6127(4)	4976(3)	41(1)
O(4B)	1992(2)	6706(3)	5457(2)	56(1)
C(22B)	1959(3)	3143(4)	4846(3)	37(1)
O(5B)	1786(2)	2453(3)	4880(2)	56(1)
C(23B)	2312(3)	5000(4)	5738(3)	42(1)
O(6B)	2320(3)	5482(3)	6305(2)	64(1)
C(24B)	3422(3)	4426(4)	4874(3)	52(2)
O(7B)	4112(3)	4507(4)	4883(3)	98(2)
Co(2)	-7275(1)	-530(1)	-4191(1)	27(1)

Co(6)	-7098(1)	580(1)	-4717(1)	27(1)
O(1C)	-5233(2)	-50(2)	-4375(2)	44(1)
C(1C)	-5229(3)	786(3)	-3808(2)	28(1)
C(2C)	-4790(3)	933(3)	-3029(3)	32(1)
C(3C)	-4554(3)	1899(3)	-2369(3)	31(1)
C(4C)	-3980(3)	2723(3)	-2482(3)	30(1)
C(5C)	-4490(3)	2586(3)	-3244(3)	32(1)
C(6C)	-4677(3)	1640(3)	-3893(3)	30(1)
C(7C)	-3643(3)	3721(3)	-1797(3)	41(1)
C(8C)	-3052(4)	3806(4)	-1092(3)	68(2)
C(9C)	-4406(3)	3932(4)	-1618(3)	68(2)
C(10C)	-3065(4)	4487(4)	-1963(3)	65(2)
C(11C)	-6192(2)	607(3)	-3944(2)	24(1)
C(12C)	-6751(2)	882(3)	-3636(2)	25(1)
C(13C)	-6855(2)	1531(3)	-2977(2)	26(1)
C(14C)	-6989(3)	1314(3)	-2395(3)	33(1)
C(15C)	-7072(3)	1940(3)	-1766(3)	35(1)
C(16C)	-7030(3)	2785(4)	-1694(3)	38(1)
C(17C)	-6894(3)	3006(4)	-2263(3)	42(1)
C(18C)	-6816(3)	2386(3)	-2900(3)	38(1)
C(19C)	-7226(3)	-1490(4)	-4957(3)	37(1)
O(2C)	-7193(2)	-2093(3)	-5430(2)	60(1)
C(20C)	-6994(3)	-827(3)	-3458(3)	36(1)
O(3C)	-6832(2)	-1026(3)	-2998(2)	60(1)
C(21C)	-8438(3)	-855(3)	-4295(3)	30(1)
O(4C)	-9149(2)	-996(2)	-4327(2)	47(1)
C(22C)	-8190(3)	570(3)	-4825(3)	36(1)
O(5C)	-8843(2)	605(3)	-4848(2)	60(1)
C(23C)	-6520(3)	1683(4)	-4713(3)	37(1)
O(6C)	-6178(2)	2366(3)	-4739(2)	57(1)
C(24C)	-7131(3)	-210(3)	-5643(3)	35(1)
O(7C)	-7159(2)	-712(3)	-6216(2)	61(1)
Co(1)	1052(1)	7865(1)	783(1)	28(1)
Co(3)	-509(1)	7504(1)	219(1)	28(1)
O(1D)	-554(2)	5441(2)	129(2)	39(1)
C(1D)	-365(2)	6140(3)	886(2)	25(1)

C(2D)	-1226(2)	5876(3)	1081(2)	29(1)
C(3D)	-1099(2)	6465(3)	1907(2)	29(1)
C(4D)	-387(3)	6433(3)	2453(2)	28(1)
C(5D)	483(2)	6749(3)	2276(2)	28(1)
C(6D)	339(3)	6124(3)	1446(3)	30(1)
C(7D)	-290(3)	6971(3)	3300(3)	34(1)
C(8D)	108(4)	8047(4)	3597(3)	56(2)
C(9D)	-1184(3)	6626(4)	3413(3)	70(2)
C(10D)	321(4)	6770(4)	3780(3)	60(2)
C(11D)	-36(2)	7095(3)	909(2)	23(1)
C(12D)	182(2)	8016(3)	1297(2)	24(1)
C(13D)	258(2)	8800(3)	2001(2)	24(1)
C(14D)	-505(3)	8875(3)	2104(3)	33(1)
C(15D)	-438(3)	9582(4)	2774(3)	42(1)
C(16D)	373(3)	10230(3)	3338(3)	37(1)
C(17D)	1133(3)	10167(3)	3237(3)	36(1)
C(18D)	1081(3)	9460(3)	2574(3)	29(1)
C(19D)	1173(3)	6985(3)	-5(3)	35(1)
O(2D)	1266(2)	6456(2)	-489(2)	54(1)
C(20D)	1946(3)	8074(3)	1535(3)	39(1)
O(3D)	2521(2)	8223(3)	2004(2)	65(1)
C(21D)	1572(3)	8981(4)	765(3)	39(1)
O(4D)	1878(2)	9680(3)	760(2)	59(1)
C(22D)	-638(3)	6681(4)	-722(3)	43(1)
O(5D)	-708(2)	6159(3)	-1311(2)	69(1)
C(23D)	-351(3)	8615(4)	236(3)	43(1)
O(6D)	-255(3)	9334(3)	296(3)	82(1)
C(24D)	-1656(3)	7081(4)	141(3)	40(1)
O(7D)	-2398(2)	6809(3)	57(2)	62(1)

Table H3. Bond lengths [Å] and angles [°] for **52**.

Molecule 1			
Co(5)-C(19A)	1.802(5)	C(5A)-C(6A)	1.518(6)
Co(5)-C(20A)	1.815(5)	C(7A)-C(10A)	1.523(7)
Co(5)-C(21A)	1.825(5)	C(7A)-C(9A)	1.532(7)
Co(5)-C(11A)	1.974(4)	C(7A)-C(8A)	1.553(6)
Co(5)-C(12A)	1.977(4)	C(11A)-C(12A)	1.338(6)
Co(5)-Co(8)	2.472(8)	C(12A)-C(13A)	1.473(6)
Co(8)-C(24A)	1.787(5)	C(13A)-C(18A)	1.385(6)
Co(8)-C(23A)	1.824(5)	C(13A)-C(14A)	1.397(5)
Co(8)-C(22A)	1.834(6)	C(14A)-C(15A)	1.395(6)
Co(8)-C(11A)	1.974(4)	C(15A)-C(16A)	1.371(6)
Co(8)-C(12A)	1.981(4)	C(16A)-C(17A)	1.377(6)
O(1A)-C(1A)	1.447(5)	C(17A)-C(18A)	1.382(6)
C(1A)-C(11A)	1.513(6)	C(19A)-O(2A)	1.132(5)
C(1A)-C(2A)	1.528(6)	C(20A)-O(3A)	1.145(5)
C(1A)-C(6A)	1.538(6)	C(21A)-O(4A)	1.136(5)
C(2A)-C(3A)	1.533(6)	C(22A)-O(5A)	1.128(6)
C(3A)-C(4A)	1.518(6)	C(23A)-O(6A)	1.137(5)
C(4A)-C(5A)	1.542(5)	C(24A)-O(7A)	1.140(5)
C(4A)-C(7A)	1.550(6)		
Molecule 2			
Co(4)-C(20B)	1.797(6)	C(1B)-C(6B)	1.526(6)
Co(4)-C(19B)	1.820(5)	C(1B)-C(2B)	1.528(6)
Co(4)-C(21B)	1.836(5)	C(1B)-C(11B)	1.529(5)
Co(4)-C(12B)	1.978(4)	C(2B)-C(3B)	1.525(6)
Co(4)-C(11B)	1.980(4)	C(3B)-C(4B)	1.534(6)
Co(4)-Co(7)	2.4666(9)	C(4B)-C(5B)	1.534(6)
Co(7)-C(22B)	1.785(5)	C(4B)-C(7B)	1.561(6)
Co(7)-C(24B)	1.808(5)	C(5B)-C(6B)	1.529(6)
Co(7)-C(23B)	1.834(5)	C(7B)-C(8B)	1.513(6)
Co(7)-C(11B)	1.959(4)	C(7B)-C(9B)	1.526(7)
Co(7)-C(12B)	1.984(4)	C(7B)-C(10B)	1.538(7)
O(1B)-C(1B)	1.453(5)	C(11B)-C(12B)	1.332(5)

C(12B)-C(13B)	1.482(6)	C(19B)-O(2B)	1.136(5)
C(13B)-C(18B)	1.387(6)	C(20B)-O(3B)	1.136(6)
C(13B)-C(14B)	1.399(6)	C(21B)-O(4B)	1.129(5)
C(14B)-C(15B)	1.384(6)	C(22B)-O(5B)	1.146(6)
C(15B)-C(16B)	1.377(7)	C(23B)-O(6B)	1.124(6)
C(16B)-C(17B)	1.376(6)	C(24B)-O(7B)	1.132(5)
C(17B)-C(18B)	1.388(6)		
Molecule 3			
Co(2)-C(20C)	1.796(5)	C(5C)-C(6C)	1.525(6)
Co(2)-C(21C)	1.812(4)	C(7C)-C(9C)	1.530(6)
Co(2)-C(19C)	1.818(5)	C(7C)-C(10C)	1.531(7)
Co(2)-C(11C)	1.970(4)	C(7C)-C(8C)	1.535(7)
Co(2)-C(12C)	1.996(4)	C(11C)-C(12C)	1.342(5)
Co(2)-Co(6)	2.4711(9)	C(12C)-C(13C)	1.460(6)
Co(6)-C(23C)	1.794(5)	C(13C)-C(18C)	1.390(6)
Co(6)-C(24C)	1.823(5)	C(13C)-C(14C)	1.395(6)
Co(6)-C(22C)	1.833(5)	C(14C)-C(15C)	1.383(6)
Co(6)-C(12C)	1.980(4)	C(15C)-C(16C)	1.374(6)
Co(6)-C(11C)	1.992(4)	C(16C)-C(17C)	1.373(7)
O(1C)-C(1C)	1.450(5)	C(17C)-C(18C)	1.384(6)
C(1C)-C(11C)	1.517(5)	C(19C)-O(2C)	1.137(5)
C(1C)-C(2C)	1.518(6)	C(20C)-O(3C)	1.137(6)
C(1C)-C(6C)	1.529(6)	C(21C)-O(4C)	1.136(4)
C(2C)-C(3C)	1.533(6)	C(22C)-O(5C)	1.130(5)
C(3C)-C(4C)	1.535(6)	C(23C)-O(6C)	1.136(5)
C(4C)-C(5C)	1.532(6)	C(24C)-O(7C)	1.130(5)
C(4C)-C(7C)	1.553(6)		
Molecule 4			
Co(1)-C(20D)	1.798(5)	Co(3)-C(22D)	1.807(5)
Co(1)-C(21D)	1.821(6)	Co(3)-C(23D)	1.814(6)
Co(1)-C(19D)	1.828(5)	Co(3)-C(11D)	1.971(4)
Co(1)-C(12D)	1.977(4)	Co(3)-C(12D)	1.977(4)
Co(1)-C(11D)	1.983(4)	O(1D)-C(1D)	1.433(5)
Co(1)-Co(3)	2.4703(8)	C(1D)-C(11D)	1.512(6)
Co(3)-C(24D)	1.786(5)	C(1D)-C(6D)	1.532(6)

C(1D)-C(2D)	1.540(5)	C(13D)-C(18D)	1.397(6)
C(2D)-C(3D)	1.518(6)	C(14D)-C(15D)	1.383(6)
C(3D)-C(4D)	1.538(6)	C(15D)-C(16D)	1.376(6)
C(4D)-C(5D)	1.541(5)	C(16D)-C(17D)	1.378(6)
C(4D)-C(7D)	1.554(6)	C(17D)-C(18D)	1.386(6)
C(5D)-C(6D)	1.529(6)	C(19D)-O(2D)	1.131(5)
C(7D)-C(9D)	1.520(6)	C(20D)-O(3D)	1.127(5)
C(7D)-C(10D)	1.528(7)	C(21D)-O(4D)	1.131(6)
C(7D)-C(8D)	1.537(6)	C(22D)-O(5D)	1.140(6)
C(11D)-C(12D)	1.337(6)	C(23D)-O(6D)	1.140(6)
C(12D)-C(13D)	1.485(6)	C(24D)-O(7D)	1.142(5)
C(13D)-C(14D)	1.392(5)		

Molecule 1

C(19A)-Co(5)-C(20A)	98.3(2)	C(23A)-Co(8)-C(12A)	140.8(2)
C(19A)-Co(5)-C(21A)	98.1(2)	C(22A)-Co(8)-C(12A)	100.7(2)
C(20A)-Co(5)-C(21A)	108.0(2)	C(11A)-Co(8)-C(12A)	39.5(2)
C(19A)-Co(5)-C(11A)	104.1(2)	C(24A)-Co(8)-Co(5)	152.3(2)
C(20A)-Co(5)-C(11A)	103.1(2)	C(23A)-Co(8)-Co(5)	98.21(13)
C(21A)-Co(5)-C(11A)	138.4(2)	C(22A)-Co(8)-Co(5)	98.05(14)
C(19A)-Co(5)-C(12A)	103.2(2)	C(11A)-Co(8)-Co(5)	51.24(12)
C(20A)-Co(5)-C(12A)	140.5(2)	C(12A)-Co(8)-Co(5)	51.27(11)
C(21A)-Co(5)-C(12A)	101.4(2)	O(1A)-C(1A)-C(11A)	106.8(3)
C(11A)-Co(5)-C(12A)	39.6(2)	O(1A)-C(1A)-C(2A)	108.4(3)
C(19A)-Co(5)-Co(8)	152.9(2)	C(11A)-C(1A)-C(2A)	112.9(3)
C(20A)-Co(5)-Co(8)	98.57(14)	O(1A)-C(1A)-C(6A)	108.5(3)
C(21A)-Co(5)-Co(8)	96.70(13)	C(11A)-C(1A)-C(6A)	111.0(4)
C(11A)-Co(5)-Co(8)	51.24(12)	C(2A)-C(1A)-C(6A)	109.2(4)
C(12A)-Co(5)-Co(8)	51.43(12)	C(1A)-C(2A)-C(3A)	113.0(4)
C(24A)-Co(8)-C(23A)	98.5(2)	C(4A)-C(3A)-C(2A)	111.6(3)
C(24A)-Co(8)-C(22A)	97.5(2)	C(3A)-C(4A)-C(5A)	107.7(4)
C(23A)-Co(8)-C(22A)	108.4(2)	C(3A)-C(4A)-C(7A)	116.0(3)
C(24A)-Co(8)-C(11A)	103.1(2)	C(5A)-C(4A)-C(7A)	114.3(4)
C(23A)-Co(8)-C(11A)	103.9(2)	C(6A)-C(5A)-C(4A)	111.7(4)
C(22A)-Co(8)-C(11A)	138.4(2)	C(5A)-C(6A)-C(1A)	114.0(3)
C(24A)-Co(8)-C(12A)	103.2(2)	C(10A)-C(7A)-C(9A)	109.8(5)

C(10A)-C(7A)-C(8A)	107.3(4)	Co(5)-C(12A)-Co(8)	77.3(2)
C(9A)-C(7A)-C(8A)	109.1(4)	C(18A)-C(13A)-C(14A)	117.6(4)
C(10A)-C(7A)-C(4A)	110.4(4)	C(18A)-C(13A)-C(12A)	121.8(4)
C(9A)-C(7A)-C(4A)	111.3(4)	C(14A)-C(13A)-C(12A)	120.6(4)
C(8A)-C(7A)-C(4A)	108.8(4)	C(15A)-C(14A)-C(13A)	120.7(4)
C(12A)-C(11A)-C(1A)	146.9(4)	C(16A)-C(15A)-C(14A)	120.4(4)
C(12A)-C(11A)-Co(8)	70.5(3)	C(15A)-C(16A)-C(17A)	119.5(4)
C(1A)-C(11A)-Co(8)	133.5(3)	C(16A)-C(17A)-C(18A)	120.4(4)
C(12A)-C(11A)-Co(5)	70.3(3)	C(13A)-C(18A)-C(17A)	121.4(4)
C(1A)-C(11A)-Co(5)	129.8(3)	O(2A)-C(19A)-Co(5)	178.3(5)
Co(8)-C(11A)-Co(5)	77.5(2)	O(3A)-C(20A)-Co(5)	179.7(6)
C(11A)-C(12A)-C(13A)	146.9(4)	O(4A)-C(21A)-Co(5)	177.4(4)
C(11A)-C(12A)-Co(5)	70.1(2)	O(5A)-C(22A)-Co(8)	176.2(5)
C(13A)-C(12A)-Co(5)	131.9(3)	O(6A)-C(23A)-Co(8)	178.9(5)
C(11A)-C(12A)-Co(8)	69.9(3)	O(7A)-C(24A)-Co(8)	177.4(5)
C(13A)-C(12A)-Co(8)	132.2(3)		

Molecule 2

C(20B)-Co(4)-C(19B)	97.5(2)	C(22B)-Co(7)-C(11B)	103.6(2)
C(20B)-Co(4)-C(21B)	98.2(2)	C(24B)-Co(7)-C(11B)	139.5(2)
C(19B)-Co(4)-C(21B)	106.6(2)	C(23B)-Co(7)-C(11B)	103.8(2)
C(20B)-Co(4)-C(12B)	101.2(2)	C(22B)-Co(7)-C(12B)	104.1(2)
C(19B)-Co(4)-C(12B)	104.5(2)	C(24B)-Co(7)-C(12B)	101.4(2)
C(21B)-Co(4)-C(12B)	140.5(2)	C(23B)-Co(7)-C(12B)	140.0(2)
C(20B)-Co(4)-C(11B)	104.1(2)	C(11B)-Co(7)-C(12B)	39.5(2)
C(19B)-Co(4)-C(11B)	140.6(2)	C(22B)-Co(7)-Co(4)	153.3(2)
C(21B)-Co(4)-C(11B)	102.5(2)	C(24B)-Co(7)-Co(4)	99.6(2)
C(12B)-Co(4)-C(11B)	39.3(2)	C(23B)-Co(7)-Co(4)	96.4(2)
C(20B)-Co(4)-Co(7)	151.6(2)	C(11B)-Co(7)-Co(4)	51.60(12)
C(19B)-Co(4)-Co(7)	97.5(2)	C(12B)-Co(7)-Co(4)	51.38(12)
C(21B)-Co(4)-Co(7)	100.4(2)	O(1B)-C(1B)-C(6B)	108.8(3)
C(12B)-Co(4)-Co(7)	51.61(13)	O(1B)-C(1B)-C(2B)	108.5(3)
C(11B)-Co(4)-Co(7)	50.85(12)	C(6B)-C(1B)-C(2B)	109.7(4)
C(22B)-Co(7)-C(24B)	95.4(2)	O(1B)-C(1B)-C(11B)	105.6(3)
C(22B)-Co(7)-C(23B)	99.7(2)	C(6B)-C(1B)-C(11B)	111.6(4)
C(24B)-Co(7)-C(23B)	107.9(2)	C(2B)-C(1B)-C(11B)	112.4(3)

C(3B)-C(2B)-C(1B)	113.5(4)	C(11B)-C(12B)-Co(4)	70.4(3)
C(2B)-C(3B)-C(4B)	112.5(4)	C(13B)-C(12B)-Co(4)	132.8(3)
C(3B)-C(4B)-C(5B)	108.4(3)	C(11B)-C(12B)-Co(7)	69.2(3)
C(3B)-C(4B)-C(7B)	113.4(4)	C(13B)-C(12B)-Co(7)	131.3(3)
C(5B)-C(4B)-C(7B)	115.1(4)	Co(4)-C(12B)-Co(7)	77.0(2)
C(6B)-C(5B)-C(4B)	111.5(4)	C(18B)-C(13B)-C(14B)	118.4(4)
C(1B)-C(6B)-C(5B)	111.7(4)	C(18B)-C(13B)-C(12B)	121.2(4)
C(8B)-C(7B)-C(9B)	108.4(4)	C(14B)-C(13B)-C(12B)	120.3(4)
C(8B)-C(7B)-C(10B)	108.4(4)	C(15B)-C(14B)-C(13B)	120.9(4)
C(9B)-C(7B)-C(10B)	107.6(4)	C(16B)-C(15B)-C(14B)	119.9(5)
C(8B)-C(7B)-C(4B)	112.3(4)	C(17B)-C(16B)-C(15B)	119.8(4)
C(9B)-C(7B)-C(4B)	110.1(4)	C(16B)-C(17B)-C(18B)	120.7(5)
C(10B)-C(7B)-C(4B)	109.9(4)	C(17B)-C(18B)-C(13B)	120.2(4)
C(12B)-C(11B)-C(1B)	146.8(4)	O(2B)-C(19B)-Co(4)	178.1(5)
C(12B)-C(11B)-Co(7)	71.3(2)	O(3B)-C(20B)-Co(4)	179.2(4)
C(1B)-C(11B)-Co(7)	131.4(3)	O(4B)-C(21B)-Co(4)	178.2(4)
C(12B)-C(11B)-Co(4)	70.3(2)	O(5B)-C(22B)-Co(7)	176.8(4)
C(1B)-C(11B)-Co(4)	131.6(3)	O(6B)-C(23B)-Co(7)	178.8(5)
Co(7)-C(11B)-Co(4)	77.54(14)	O(7B)-C(24B)-Co(7)	176.4(6)
C(11B)-C(12B)-C(13B)	147.2(4)		

Molecule 3

C(20C)-Co(2)-C(21C)	98.5(2)	C(12C)-Co(2)-Co(6)	51.29(12)
C(20C)-Co(2)-C(19C)	97.1(2)	C(23C)-Co(6)-C(24C)	98.1(2)
C(21C)-Co(2)-C(19C)	107.8(2)	C(23C)-Co(6)-C(22C)	97.4(2)
C(20C)-Co(2)-C(11C)	103.9(2)	C(24C)-Co(6)-C(22C)	108.0(2)
C(21C)-Co(2)-C(11C)	137.8(2)	C(23C)-Co(6)-C(12C)	105.2(2)
C(19C)-Co(2)-C(11C)	104.4(2)	C(24C)-Co(6)-C(12C)	142.1(2)
C(20C)-Co(2)-C(12C)	103.6(2)	C(22C)-Co(6)-C(12C)	98.2(2)
C(21C)-Co(2)-C(12C)	100.7(2)	C(23C)-Co(6)-C(11C)	103.1(2)
C(19C)-Co(2)-C(12C)	141.7(2)	C(24C)-Co(6)-C(11C)	106.5(2)
C(11C)-Co(2)-C(12C)	39.56(15)	C(22C)-Co(6)-C(11C)	136.5(2)
C(20C)-Co(2)-Co(6)	153.27(15)	C(12C)-Co(6)-C(11C)	39.5(2)
C(21C)-Co(2)-Co(6)	95.72(14)	C(23C)-Co(6)-Co(2)	153.29(15)
C(19C)-Co(2)-Co(6)	100.0(2)	C(24C)-Co(6)-Co(2)	96.3(2)
C(11C)-Co(2)-Co(6)	51.81(12)	C(22C)-Co(6)-Co(2)	99.36(15)

C(12C)-Co(6)-Co(2)	51.86(12)	C(12C)-C(11C)-Co(6)	69.8(2)
C(11C)-Co(6)-Co(2)	51.00(11)	C(1C)-C(11C)-Co(6)	134.6(3)
O(1C)-C(1C)-C(11C)	107.2(3)	Co(2)-C(11C)-Co(6)	77.18(14)
O(1C)-C(1C)-C(2C)	108.2(3)	C(11C)-C(12C)-C(13C)	147.0(4)
C(11C)-C(1C)-C(2C)	111.8(3)	C(11C)-C(12C)-Co(6)	70.7(3)
O(1C)-C(1C)-C(6C)	108.5(3)	C(13C)-C(12C)-Co(6)	132.1(3)
C(11C)-C(1C)-C(6C)	111.9(4)	C(11C)-C(12C)-Co(2)	69.2(2)
C(2C)-C(1C)-C(6C)	109.1(3)	C(13C)-C(12C)-Co(2)	132.2(3)
C(1C)-C(2C)-C(3C)	114.6(4)	Co(6)-C(12C)-Co(2)	76.9(2)
C(2C)-C(3C)-C(4C)	112.0(4)	C(18C)-C(13C)-C(14C)	117.7(4)
C(5C)-C(4C)-C(3C)	107.6(3)	C(18C)-C(13C)-C(12C)	121.6(4)
C(5C)-C(4C)-C(7C)	115.0(4)	C(14C)-C(13C)-C(12C)	120.7(4)
C(3C)-C(4C)-C(7C)	114.4(4)	C(15C)-C(14C)-C(13C)	120.4(4)
C(6C)-C(5C)-C(4C)	110.8(4)	C(16C)-C(15C)-C(14C)	121.5(4)
C(1C)-C(6C)-C(5C)	113.4(4)	C(15C)-C(16C)-C(17C)	118.5(4)
C(9C)-C(7C)-C(10C)	107.7(5)	C(16C)-C(17C)-C(18C)	121.0(5)
C(9C)-C(7C)-C(8C)	109.4(4)	C(17C)-C(18C)-C(13C)	121.0(5)
C(10C)-C(7C)-C(8C)	107.0(4)	O(2C)-C(19C)-Co(2)	179.2(5)
C(9C)-C(7C)-C(4C)	112.5(4)	O(3C)-C(20C)-Co(2)	178.8(4)
C(10C)-C(7C)-C(4C)	110.1(4)	O(4C)-C(21C)-Co(2)	175.3(4)
C(8C)-C(7C)-C(4C)	109.8(4)	O(5C)-C(22C)-Co(6)	175.9(4)
C(12C)-C(11C)-C(1C)	144.8(4)	O(6C)-C(23C)-Co(6)	177.2(4)
C(12C)-C(11C)-Co(2)	71.3(2)	O(7C)-C(24C)-Co(6)	178.9(5)
C(1C)-C(11C)-Co(2)	131.1(3)		

Molecule 4

C(20D)-Co(1)-C(21D)	98.4(2)	C(20D)-Co(1)-Co(3)	151.68(15)
C(20D)-Co(1)-C(19D)	97.7(2)	C(21D)-Co(1)-Co(3)	96.88(15)
C(21D)-Co(1)-C(19D)	106.3(2)	C(19D)-Co(1)-Co(3)	100.71(14)
C(20D)-Co(1)-C(12D)	101.7(2)	C(12D)-Co(1)-Co(3)	51.35(12)
C(21D)-Co(1)-C(12D)	103.8(2)	C(11D)-Co(1)-Co(3)	51.13(12)
C(19D)-Co(1)-C(12D)	141.2(2)	C(24D)-Co(3)-C(22D)	98.7(2)
C(20D)-Co(1)-C(11D)	103.7(2)	C(24D)-Co(3)-C(23D)	96.9(2)
C(21D)-Co(1)-C(11D)	140.1(2)	C(22D)-Co(3)-C(23D)	108.4(2)
C(19D)-Co(1)-C(11D)	103.3(2)	C(24D)-Co(3)-C(11D)	102.5(2)
C(12D)-Co(1)-C(11D)	39.5(2)	C(22D)-Co(3)-C(11D)	105.9(2)

C(23D)-Co(3)-C(11D)	137.2(2)	C(8D)-C(7D)-C(4D)	111.7(4)
C(24D)-Co(3)-C(12D)	106.6(2)	C(12D)-C(11D)-C(1D)	147.7(4)
C(22D)-Co(3)-C(12D)	140.4(2)	C(12D)-C(11D)-Co(3)	70.4(3)
C(23D)-Co(3)-C(12D)	98.3(2)	C(1D)-C(11D)-Co(3)	131.0(3)
C(11D)-Co(3)-C(12D)	39.6(2)	C(12D)-C(11D)-Co(1)	70.0(2)
C(24D)-Co(3)-Co(1)	153.5(2)	C(1D)-C(11D)-Co(1)	132.0(3)
C(22D)-Co(3)-Co(1)	94.47(14)	Co(3)-C(11D)-Co(1)	77.3(2)
C(23D)-Co(3)-Co(1)	100.55(15)	C(11D)-C(12D)-C(13D)	147.3(4)
C(11D)-Co(3)-Co(1)	51.54(10)	C(11D)-C(12D)-Co(1)	70.5(2)
C(12D)-Co(3)-Co(1)	51.32(11)	C(13D)-C(12D)-Co(1)	132.1(3)
O(1D)-C(1D)-C(11D)	107.9(3)	C(11D)-C(12D)-Co(3)	70.0(3)
O(1D)-C(1D)-C(6D)	109.6(3)	C(13D)-C(12D)-Co(3)	131.2(3)
C(11D)-C(1D)-C(6D)	111.0(3)	Co(1)-C(12D)-Co(3)	77.3(2)
O(1D)-C(1D)-C(2D)	108.1(3)	C(14D)-C(13D)-C(18D)	118.8(4)
C(11D)-C(1D)-C(2D)	112.1(3)	C(14D)-C(13D)-C(12D)	119.8(4)
C(6D)-C(1D)-C(2D)	108.0(4)	C(18D)-C(13D)-C(12D)	121.5(3)
C(3D)-C(2D)-C(1D)	114.3(3)	C(15D)-C(14D)-C(13D)	119.7(4)
C(2D)-C(3D)-C(4D)	112.1(3)	C(16D)-C(15D)-C(14D)	121.4(4)
C(3D)-C(4D)-C(5D)	108.3(3)	C(15D)-C(16D)-C(17D)	119.3(4)
C(3D)-C(4D)-C(7D)	113.3(3)	C(16D)-C(17D)-C(18D)	120.4(4)
C(5D)-C(4D)-C(7D)	114.9(3)	C(17D)-C(18D)-C(13D)	120.5(4)
C(6D)-C(5D)-C(4D)	111.1(3)	O(2D)-C(19D)-Co(1)	178.4(4)
C(5D)-C(6D)-C(1D)	112.9(3)	O(3D)-C(20D)-Co(1)	178.2(5)
C(9D)-C(7D)-C(10D)	107.0(4)	O(4D)-C(21D)-Co(1)	178.1(4)
C(9D)-C(7D)-C(8D)	109.0(4)	O(5D)-C(22D)-Co(3)	178.9(4)
C(10D)-C(7D)-C(8D)	108.7(4)	O(6D)-C(23D)-Co(3)	175.3(5)
C(9D)-C(7D)-C(4D)	111.0(4)	O(7D)-C(24D)-Co(3)	176.6(4)
C(10D)-C(7D)-C(4D)	109.3(4)		

Table H4. Anisotropic displacement parameters ($Å^2 \times 10^3$)for **52**. The anisotropic displacement factor exponent takes the form: $-2\pi^2[h^2a^{*2}U_{11} + ... + 2 h k a^* b^* U_{12}]$

	U^{11}	U^{22}	U^{33}	U^{23}	U^{13}	U^{12}
Co(5)	25(1)	29(1)	29(1)	12(1)	10(1)	11(1)
Co(8)	25(1)	31(1)	23(1)	10(1)	6(1)	10(1)
O(1A)	71(2)	36(2)	43(2)	15(2)	32(2)	35(2)
C(1A)	36(2)	27(3)	25(3)	10(2)	16(2)	16(2)
C(2A)	36(2)	27(3)	31(3)	14(2)	5(2)	6(2)
C(3A)	28(2)	31(3)	36(3)	14(2)	12(2)	6(2)
C(4A)	30(2)	26(3)	35(3)	18(2)	13(2)	10(2)
C(5A)	35(2)	33(3)	30(3)	16(2)	9(2)	15(2)
C(6A)	36(2)	35(3)	39(3)	23(2)	17(2)	21(2)
C(7A)	54(3)	44(3)	35(3)	23(3)	22(3)	24(3)
C(8A)	62(3)	81(5)	63(4)	43(4)	41(3)	29(3)
C(9A)	112(5)	63(4)	63(4)	35(4)	56(4)	59(4)
C(10A)	67(3)	86(5)	39(4)	33(3)	24(3)	37(3)
C(11A)	21(2)	30(3)	20(2)	7(2)	7(2)	8(2)
C(12A)	18(2)	26(3)	22(2)	8(2)	3(2)	5(2)
C(13A)	28(2)	23(2)	27(3)	13(2)	8(2)	12(2)
C(14A)	32(2)	33(3)	37(3)	7(2)	9(2)	16(2)
C(15A)	47(3)	39(3)	45(3)	9(3)	21(3)	27(3)
C(16A)	54(3)	31(3)	30(3)	6(2)	12(2)	22(3)
C(17A)	40(3)	29(3)	33(3)	5(2)	2(2)	11(2)
C(18A)	34(2)	39(3)	25(3)	9(2)	8(2)	14(2)
C(19A)	37(3)	37(3)	47(3)	19(3)	20(3)	18(2)
O(2A)	35(2)	56(3)	50(2)	14(2)	-4(2)	17(2)
C(20A)	29(2)	42(3)	40(3)	16(3)	13(2)	12(2)
O(3A)	55(2)	57(3)	53(3)	13(2)	31(2)	28(2)
C(21A)	25(2)	40(3)	36(3)	17(3)	13(2)	11(2)
O(4A)	45(2)	41(2)	72(3)	31(2)	19(2)	16(2)
C(22A)	30(2)	39(3)	38(3)	13(3)	1(2)	12(2)
O(5A)	56(2)	49(3)	77(3)	34(2)	1(2)	26(2)
C(23A)	29(2)	48(3)	31(3)	17(3)	5(2)	13(2)
O(6A)	62(2)	56(3)	30(2)	1(2)	8(2)	25(2)

C(24A)	34(3)	45(3)	30(3)	8(2)	8(2)	15(2)
O(7A)	30(2)	81(3)	47(3)	15(2)	14(2)	8(2)
Co(4)	41(1)	24(1)	31(1)	12(1)	18(1)	14(1)
Co(7)	32(1)	29(1)	26(1)	11(1)	10(1)	12(1)
O(1B)	46(2)	47(2)	30(2)	7(2)	21(2)	24(2)
C(1B)	34(2)	32(3)	27(3)	12(2)	18(2)	21(2)
C(2B)	28(2)	31(3)	32(3)	17(2)	16(2)	13(2)
C(3B)	34(2)	23(3)	34(3)	14(2)	14(2)	11(2)
C(4B)	29(2)	37(3)	27(3)	14(2)	14(2)	16(2)
C(5B)	34(2)	41(3)	40(3)	25(3)	14(2)	23(2)
C(6B)	42(3)	37(3)	40(3)	19(3)	20(2)	26(2)
C(7B)	33(2)	40(3)	32(3)	12(2)	13(2)	18(2)
C(8B)	48(3)	72(4)	36(3)	4(3)	15(3)	30(3)
C(9B)	64(3)	88(5)	36(3)	18(3)	10(3)	48(4)
C(10B)	84(4)	46(4)	42(4)	7(3)	7(3)	-9(3)
C(11B)	30(2)	21(2)	20(2)	8(2)	9(2)	11(2)
C(12B)	29(2)	20(2)	26(3)	10(2)	9(2)	13(2)
C(13B)	22(2)	26(3)	25(2)	11(2)	8(2)	12(2)
C(14B)	40(2)	35(3)	32(3)	18(2)	18(2)	23(2)
C(15B)	52(3)	31(3)	40(3)	15(2)	25(3)	27(2)
C(16B)	45(3)	48(3)	33(3)	15(3)	23(2)	29(3)
C(17B)	44(3)	44(3)	32(3)	21(3)	19(2)	23(3)
C(18B)	35(2)	31(3)	30(3)	15(2)	13(2)	16(2)
C(19B)	60(3)	32(3)	36(3)	13(2)	23(3)	20(3)
O(2B)	53(2)	69(3)	81(3)	36(3)	41(2)	15(2)
C(20B)	69(3)	36(3)	36(3)	19(3)	29(3)	31(3)
O(3B)	113(3)	69(3)	51(3)	41(2)	39(3)	62(3)
C(21B)	49(3)	31(3)	39(3)	19(3)	16(3)	10(2)
O(4B)	76(2)	40(2)	54(3)	12(2)	39(2)	31(2)
C(22B)	45(3)	42(3)	27(3)	16(3)	14(2)	23(3)
O(5B)	75(2)	43(2)	54(3)	30(2)	18(2)	24(2)
C(23B)	51(3)	35(3)	38(3)	17(3)	15(3)	18(3)
O(6B)	96(3)	57(3)	31(2)	10(2)	21(2)	39(2)
C(24B)	33(3)	61(4)	48(4)	23(3)	5(3)	14(3)
O(7B)	48(2)	127(5)	133(5)	72(4)	37(3)	40(3)
Co(2)	32(1)	25(1)	25(1)	13(1)	10(1)	12(1)

Co(6)	32(1)	27(1)	21(1)	12(1)	7(1)	11(1)
O(1C)	41(2)	39(2)	44(2)	4(2)	16(2)	26(2)
C(1C)	32(2)	27(3)	24(3)	8(2)	15(2)	15(2)
C(2C)	31(2)	30(3)	33(3)	13(2)	10(2)	14(2)
C(3C)	25(2)	39(3)	26(3)	16(2)	7(2)	13(2)
C(4C)	26(2)	29(3)	30(3)	10(2)	10(2)	12(2)
C(5C)	35(2)	32(3)	32(3)	19(2)	12(2)	10(2)
C(6C)	28(2)	39(3)	25(3)	17(2)	11(2)	14(2)
C(7C)	41(3)	31(3)	36(3)	9(2)	12(2)	10(2)
C(8C)	73(4)	54(4)	34(4)	8(3)	-5(3)	10(3)
C(9C)	57(3)	42(4)	70(5)	-4(3)	23(3)	19(3)
C(10C)	70(4)	36(4)	58(4)	16(3)	16(3)	2(3)
C(11C)	26(2)	23(2)	22(2)	11(2)	7(2)	9(2)
C(12C)	27(2)	25(3)	21(2)	12(2)	6(2)	10(2)
C(13C)	19(2)	29(3)	26(3)	11(2)	7(2)	11(2)
C(14C)	41(2)	30(3)	29(3)	15(2)	10(2)	17(2)
C(15C)	44(3)	40(3)	21(3)	14(2)	13(2)	20(2)
C(16C)	38(2)	43(3)	30(3)	9(2)	15(2)	23(2)
C(17C)	63(3)	42(3)	41(3)	20(3)	31(3)	37(3)
C(18C)	56(3)	41(3)	40(3)	26(3)	27(3)	33(3)
C(19C)	46(3)	32(3)	40(3)	20(3)	20(2)	21(2)
O(2C)	81(3)	36(2)	66(3)	18(2)	46(2)	28(2)
C(20C)	41(3)	29(3)	39(3)	16(2)	15(2)	17(2)
O(3C)	76(3)	71(3)	59(3)	48(3)	22(2)	43(2)
C(21C)	38(2)	28(3)	26(3)	16(2)	13(2)	12(2)
O(4C)	42(2)	53(2)	59(3)	33(2)	30(2)	21(2)
C(22C)	39(3)	38(3)	34(3)	23(2)	6(2)	16(2)
O(5C)	50(2)	79(3)	80(3)	52(3)	27(2)	41(2)
C(23C)	47(3)	31(3)	24(3)	12(2)	7(2)	13(2)
O(6C)	74(2)	39(2)	54(3)	28(2)	21(2)	15(2)
C(24C)	44(3)	37(3)	24(3)	16(2)	9(2)	18(2)
O(7C)	88(3)	60(3)	34(2)	15(2)	24(2)	41(2)
Co(1)	25(1)	30(1)	26(1)	11(1)	11(1)	13(1)
Co(3)	28(1)	32(1)	22(1)	12(1)	8(1)	15(1)
O(1D)	55(2)	23(2)	28(2)	4(2)	15(2)	16(2)
C(1D)	28(2)	22(2)	22(2)	6(2)	9(2)	12(2)

C(2D)	23(2)	23(3)	32(3)	11(2)	8(2)	6(2)
C(3D)	25(2)	28(3)	33(3)	13(2)	14(2)	10(2)
C(4D)	33(2)	24(3)	27(3)	13(2)	13(2)	10(2)
C(5D)	28(2)	30(3)	29(3)	16(2)	9(2)	14(2)
C(6D)	35(2)	31(3)	34(3)	17(2)	15(2)	21(2)
C(7D)	43(3)	31(3)	25(3)	12(2)	14(2)	15(2)
C(8D)	89(4)	43(4)	30(3)	13(3)	21(3)	27(3)
C(9D)	58(3)	89(5)	50(4)	26(4)	35(3)	20(3)
C(10D)	91(4)	68(4)	35(3)	28(3)	19(3)	48(4)
C(11D)	18(2)	29(3)	22(2)	12(2)	9(2)	9(2)
C(12D)	21(2)	29(3)	23(2)	14(2)	7(2)	11(2)
C(13D)	29(2)	21(2)	24(2)	10(2)	10(2)	13(2)
C(14D)	27(2)	32(3)	33(3)	9(2)	8(2)	14(2)
C(15D)	40(3)	46(3)	40(3)	13(3)	17(2)	27(3)
C(16D)	55(3)	30(3)	28(3)	10(2)	19(2)	24(2)
C(17D)	37(2)	31(3)	30(3)	11(2)	6(2)	13(2)
C(18D)	30(2)	29(3)	31(3)	16(2)	11(2)	14(2)
C(19D)	30(2)	31(3)	42(3)	18(3)	17(2)	10(2)
O(2D)	59(2)	40(2)	52(3)	9(2)	31(2)	22(2)
C(20D)	28(2)	44(3)	42(3)	15(3)	15(2)	19(2)
O(3D)	44(2)	82(3)	52(3)	15(2)	-3(2)	37(2)
C(21D)	37(3)	39(3)	34(3)	14(3)	12(2)	12(3)
O(4D)	61(2)	35(2)	73(3)	26(2)	26(2)	11(2)
C(22D)	40(3)	57(4)	32(3)	21(3)	9(2)	25(3)
O(5D)	72(2)	83(3)	31(2)	4(2)	12(2)	43(2)
C(23D)	48(3)	54(4)	42(3)	31(3)	19(3)	29(3)
O(6D)	118(3)	69(3)	102(4)	61(3)	51(3)	58(3)
C(24D)	41(3)	49(3)	28(3)	18(3)	7(2)	20(3)
O(7D)	29(2)	91(3)	63(3)	35(2)	15(2)	25(2)

Table H5. Hydrogen coordinates ($\times 10^4$) and isotropic displacement parameters ($Å^2 \times 10^3$) for **52**.

	x	y	z	U(eq)
H(1AA)	-5620(2)	9511(2)	-585(2)	69
H(2AA)	-4008(3)	9312(3)	-633(3)	42
H(2AB)	-4446(3)	9759(3)	-1037(3)	42
H(3AA)	-3603(3)	9180(3)	-1717(3)	42
H(3AB)	-4157(3)	8156(3)	-1817(3)	42
H(4AA)	-4910(2)	9060(3)	-2433(3)	35
H(5AA)	-6228(3)	7604(3)	-3056(3)	39
H(5AB)	-5758(3)	7183(3)	-2645(3)	39
H(6AA)	-6626(3)	7686(3)	-1979(3)	39
H(6AB)	-6151(3)	8707(3)	-1905(3)	39
H(8AA)	-3241(3)	9078(4)	-2667(3)	95
H(8AB)	-3758(3)	9537(4)	-2984(3)	95
H(8AC)	-3529(3)	8775(4)	-3544(3)	95
H(9AA)	-4063(4)	7350(4)	-2993(3)	102
H(9AB)	-4311(4)	7087(4)	-3862(3)	102
H(9AC)	-5071(4)	6738(4)	-3535(3)	102
H(10A)	-5347(3)	8587(4)	-3785(3)	92
H(10B)	-5858(3)	7498(4)	-4020(3)	92
H(10C)	-5098(3)	7848(4)	-4347(3)	92
H(14A)	-4059(3)	6710(3)	-1801(3)	45
H(15A)	-4037(3)	5554(4)	-2872(3)	53
H(16A)	-5341(3)	4211(3)	-3724(3)	49
H(17A)	-6677(3)	4029(3)	-3516(3)	49
H(18A)	-6710(3)	5174(3)	-2460(3)	43
H(1BA)	-157(2)	4221(2)	4899(2)	65
H(2BA)	160(3)	2581(3)	4234(3)	35
H(2BB)	-763(3)	2613(3)	4051(3)	35
H(3BA)	-832(3)	1363(3)	3001(3)	38
H(3BB)	65(3)	2031(3)	2970(3)	38
H(4BA)	-1555(3)	2166(3)	2674(3)	37
H(5BA)	83(3)	3316(3)	2620(3)	41

H(5BB)	-817(3)	3379(3)	2386(3)	41
H(6BA)	72(3)	4579(3)	3641(3)	43
H(6BB)	-827(3)	3872(3)	3642(3)	43
H(8BA)	-218(3)	1250(4)	1731(3)	88
H(8BB)	-201(3)	2006(4)	1460(3)	88
H(8BC)	-804(3)	911(4)	894(3)	88
H(9BA)	-2375(3)	1727(4)	1358(3)	95
H(9BB)	-2107(3)	1201(4)	668(3)	95
H(9BC)	-1504(3)	2296(4)	1234(3)	95
H(10D)	-2441(4)	489(4)	1745(3)	114
H(10E)	-1608(4)	283(4)	1863(3)	114
H(10F)	-2172(4)	10(4)	1039(3)	114
H(14B)	1561(3)	2077(3)	3269(3)	39
H(15B)	1610(3)	1014(3)	2164(3)	46
H(16B)	1971(3)	1476(4)	1274(3)	48
H(17B)	2211(3)	2972(4)	1461(3)	45
H(18B)	2156(3)	4042(3)	2560(3)	38
H(1CA)	-4713(2)	27(2)	-4316(2)	66
H(2CA)	-4245(3)	861(3)	-3022(3)	39
H(2CB)	-5192(3)	434(3)	-2947(3)	39
H(3CA)	-4230(3)	1956(3)	-1894(3)	37
H(3CB)	-5104(3)	1938(3)	-2323(3)	37
H(4CA)	-3442(3)	2645(3)	-2540(3)	35
H(5CA)	-5054(3)	2606(3)	-3228(3)	39
H(5CB)	-4138(3)	3103(3)	-3332(3)	39
H(6CA)	-4995(3)	1576(3)	-4373(3)	36
H(6CB)	-4109(3)	1639(3)	-3920(3)	36
H(8CA)	-2568(4)	3671(4)	-1205(3)	101
H(8CB)	-3406(4)	3356(4)	-949(3)	101
H(8CC)	-2809(4)	4444(4)	-676(3)	101
H(9CA)	-4784(3)	3456(4)	-1510(3)	103
H(9CB)	-4755(3)	3923(4)	-2050(3)	103
H(9CC)	-4164(3)	4553(4)	-1178(3)	103
H(10G)	-2574(4)	4370(4)	-2078(3)	98
H(10H)	-2833(4)	5104(4)	-1522(3)	98
H(10I)	-3423(4)	4473(4)	-2394(3)	98

H(14C)	-7022(3)	740(3)	-2430(3)	39
H(15C)	-7159(3)	1784(3)	-1378(3)	42
H(16C)	-7093(3)	3202(4)	-1266(3)	45
H(17C)	-6852(3)	3586(4)	-2219(3)	51
H(18C)	-6735(3)	2546(3)	-3288(3)	46
H(1DA)	-736(2)	4910(2)	104(2)	58
H(2DA)	-1660(2)	5950(3)	761(2)	34
H(2DB)	-1477(2)	5207(3)	956(2)	34
H(3DA)	-1667(2)	6227(3)	1991(2)	35
H(3DB)	-924(2)	7124(3)	2019(2)	35
H(4DA)	-590(3)	5759(3)	2322(2)	34
H(5DA)	698(2)	7410(3)	2380(2)	34
H(5DB)	940(2)	6714(3)	2608(2)	34
H(6DA)	154(3)	5470(3)	1353(3)	36
H(6DB)	905(3)	6339(3)	1355(3)	36
H(8DA)	680(4)	8272(4)	3527(3)	85
H(8DB)	189(4)	8361(4)	4132(3)	85
H(8DC)	-293(4)	8186(4)	3318(3)	85
H(9DA)	-1592(3)	6742(4)	3117(3)	105
H(9DB)	-1105(3)	6964(4)	3947(3)	105
H(9DC)	-1427(3)	5952(4)	3249(3)	105
H(10J)	901(4)	6982(4)	3723(3)	91
H(10K)	63(4)	6095(4)	3612(3)	91
H(10L)	385(4)	7107(4)	4310(3)	91
H(14D)	-1063(3)	8448(3)	1720(3)	40
H(15D)	-957(3)	9620(4)	2844(3)	50
H(16D)	408(3)	10710(3)	3788(3)	44
H(17D)	1690(3)	10607(3)	3619(3)	43
H(18D)	1603(3)	9424(3)	2509(3)	35

Appendix 2: Supplementary X-Ray Pictures and NMR Spectra

Figure

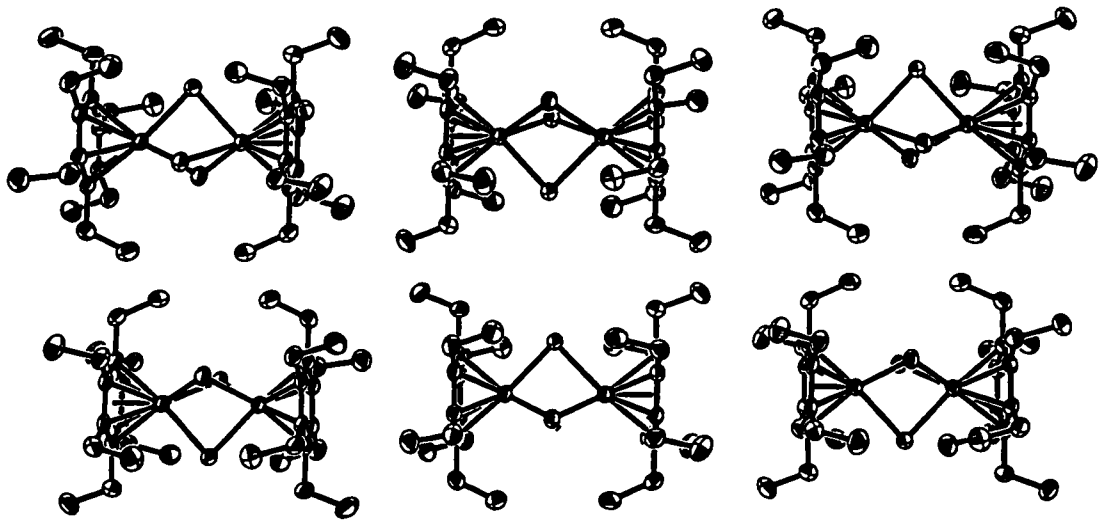

Figure A1. **Packing of the cations in $[(HEB)_2Ru_2(\mu\text{-}Cl)_3]^+$ $[C_5(CO_2Me)_5]^-$, 33, showing how the molecules pack to minimize contacts between distal ethyl groups.**

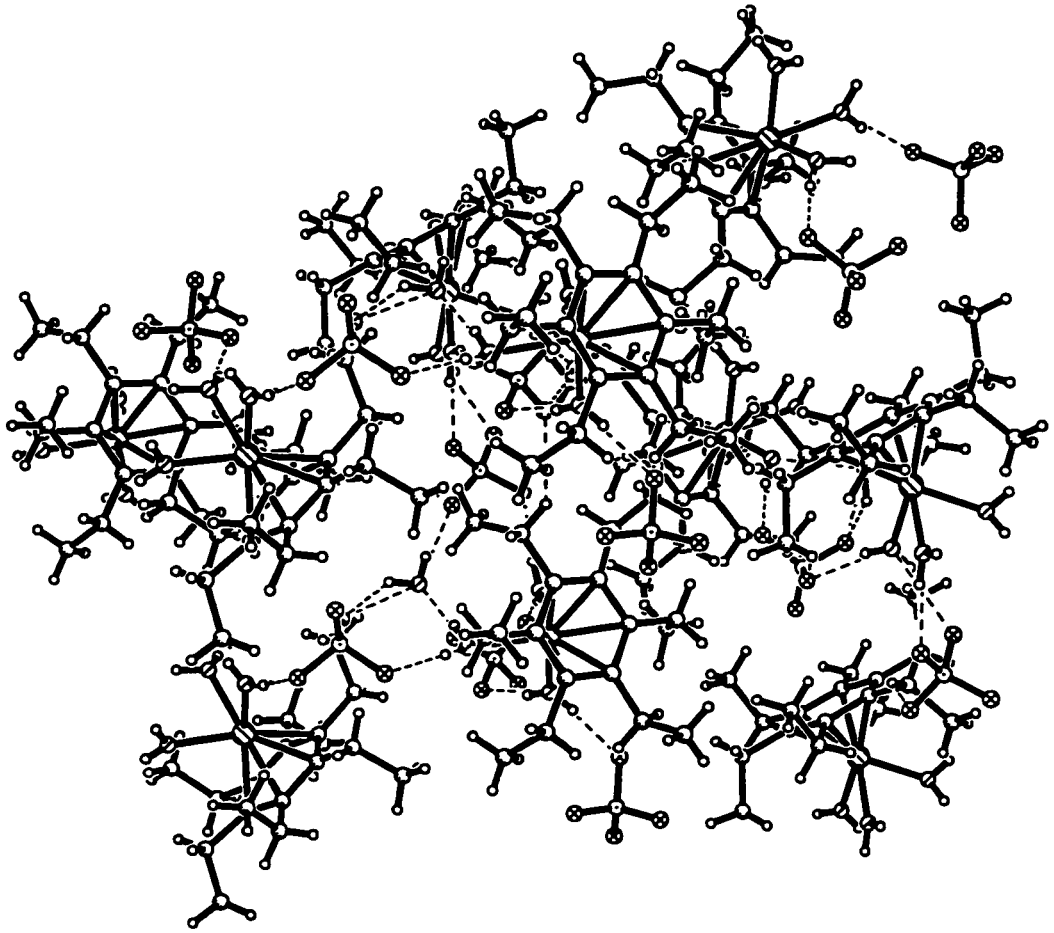

Figure A2. **Hydrogen bonding in 34, showing contacts between BF_4^- anions, lattice water molecules, and water ligands.**

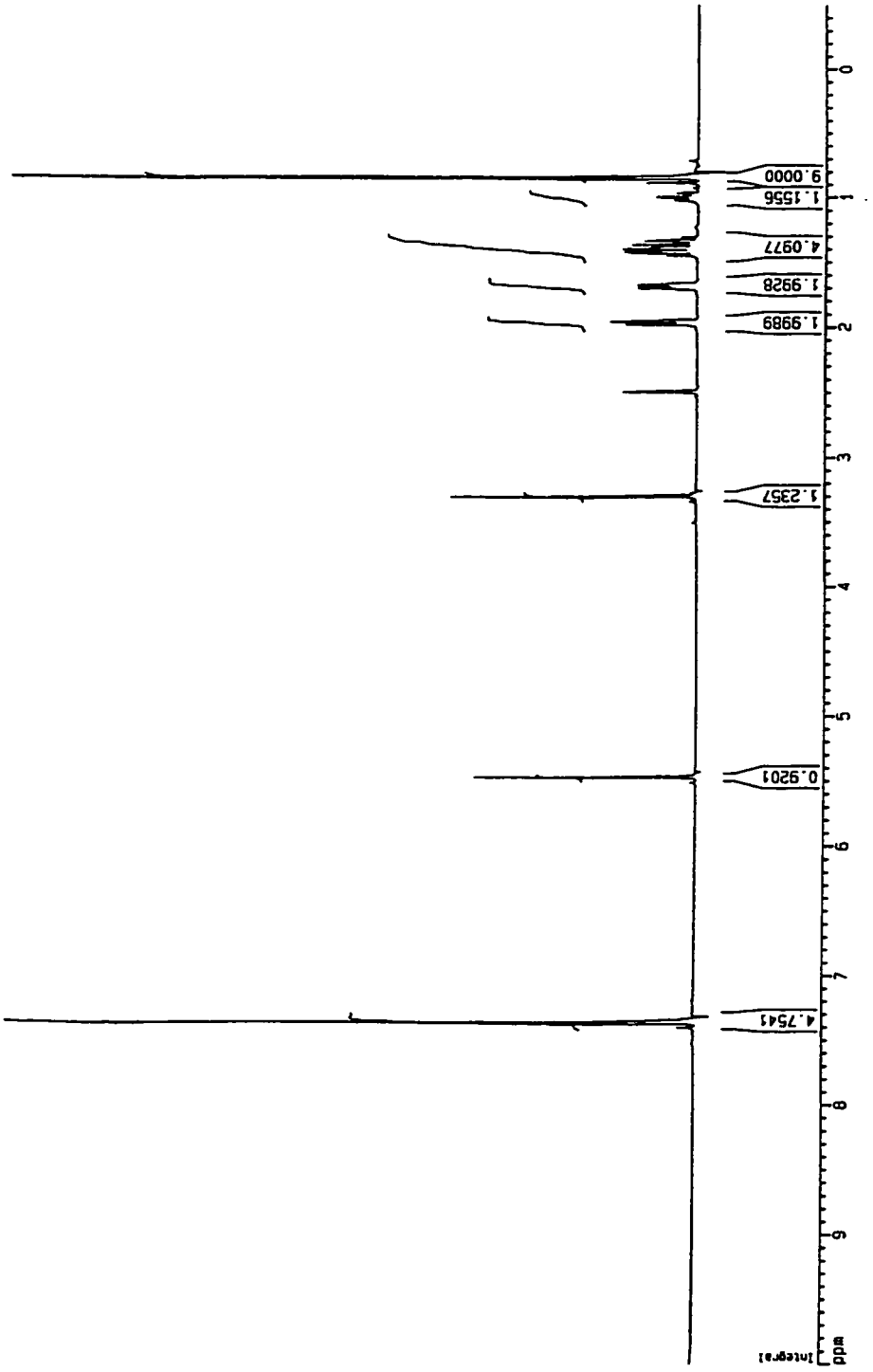

Figure A3. ^{1}H 500 MHz NMR spectrum for 51in DMSO-*d6*.

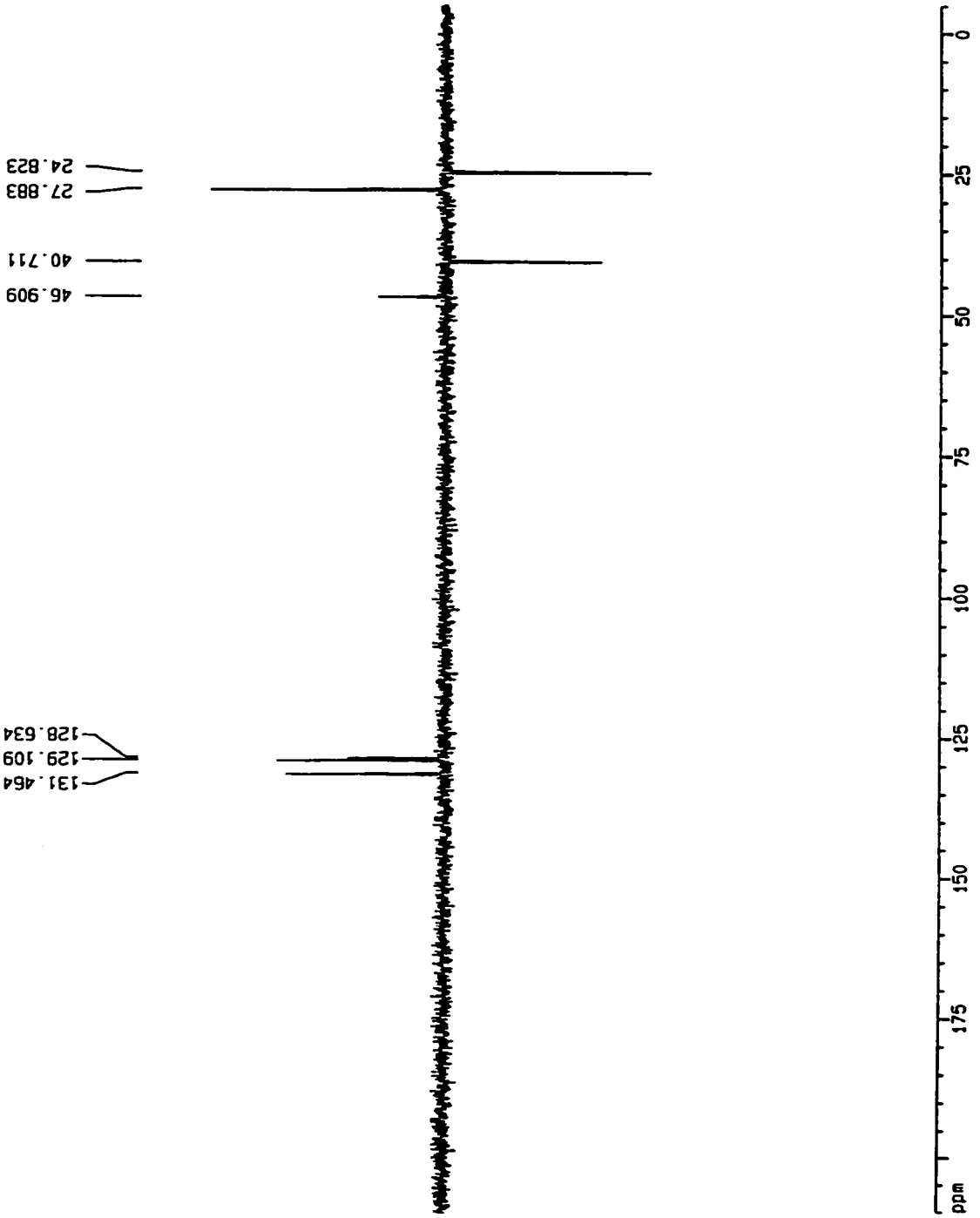

Figure A4. ^{13}C DEPT spectrum for 51 in DMSO-*d6*.

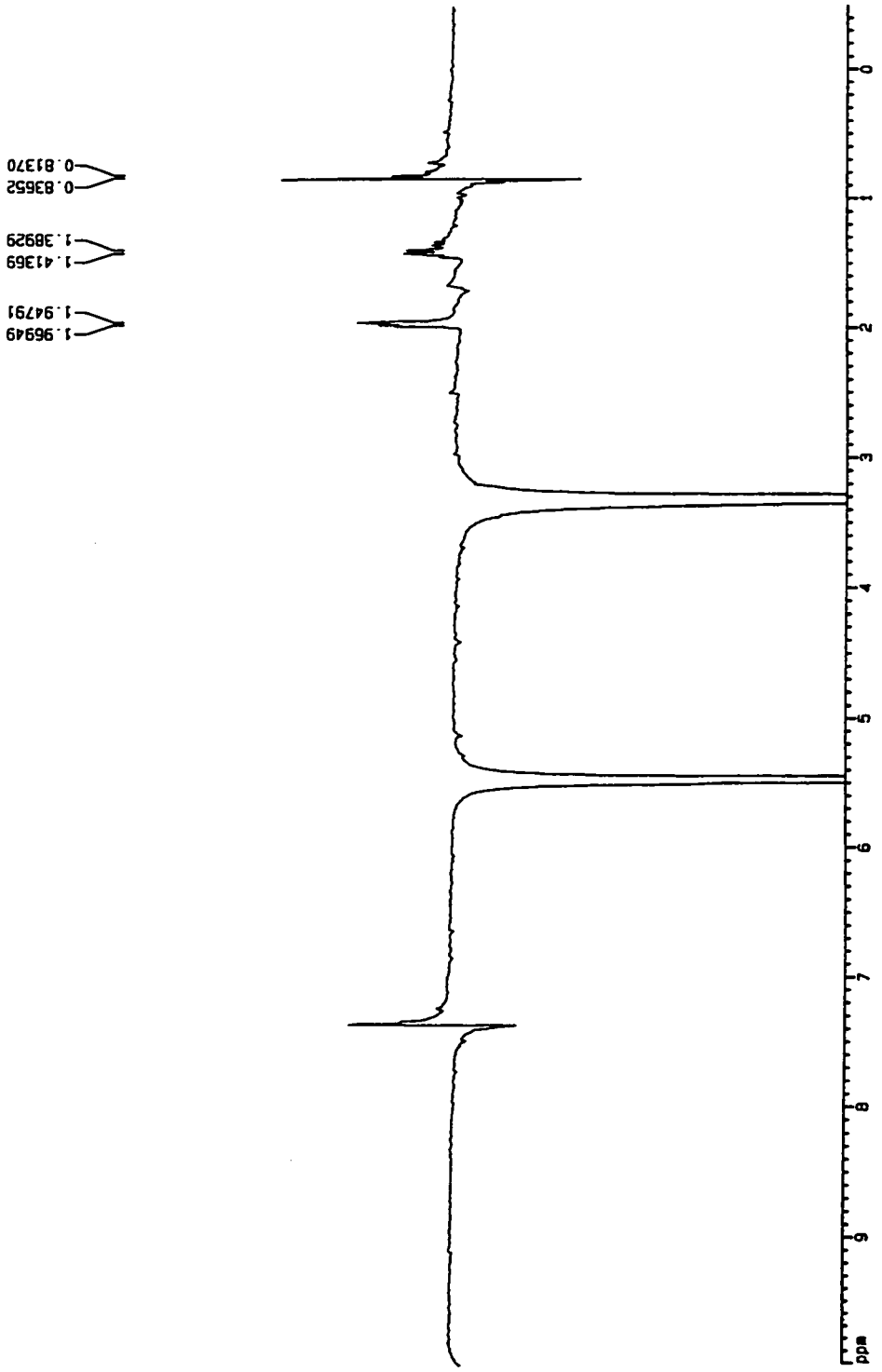

Figure A5. 500 MHz NOE difference experiment for 51.

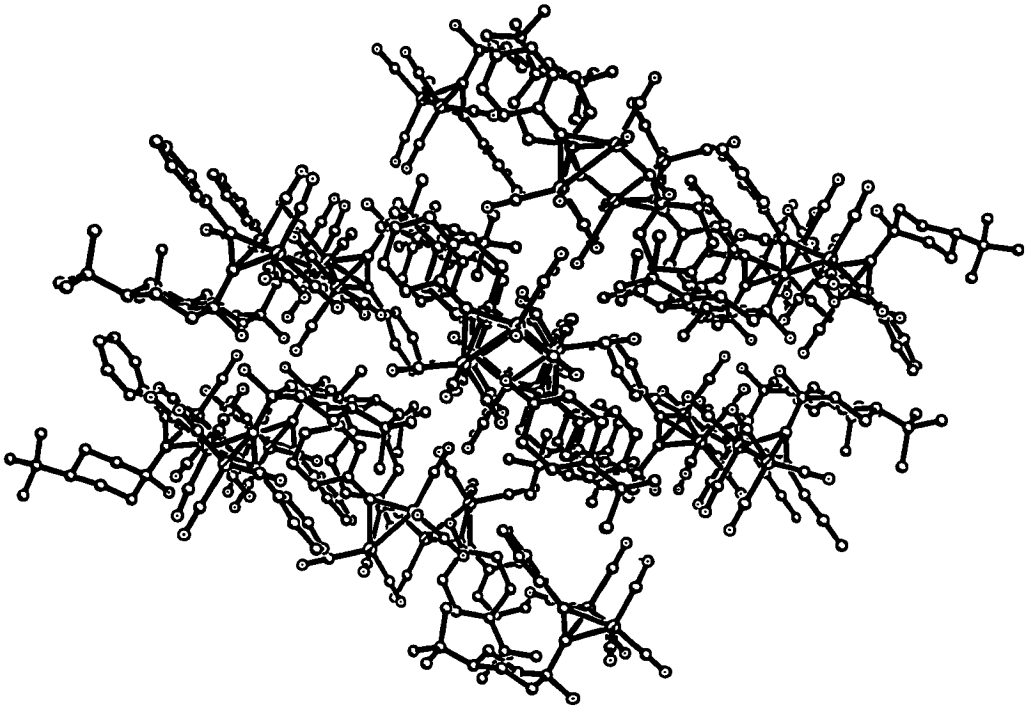

Figure A6. **Packing diagram for 52, showing stacking of the molecules, as viewed down the a axis.**